

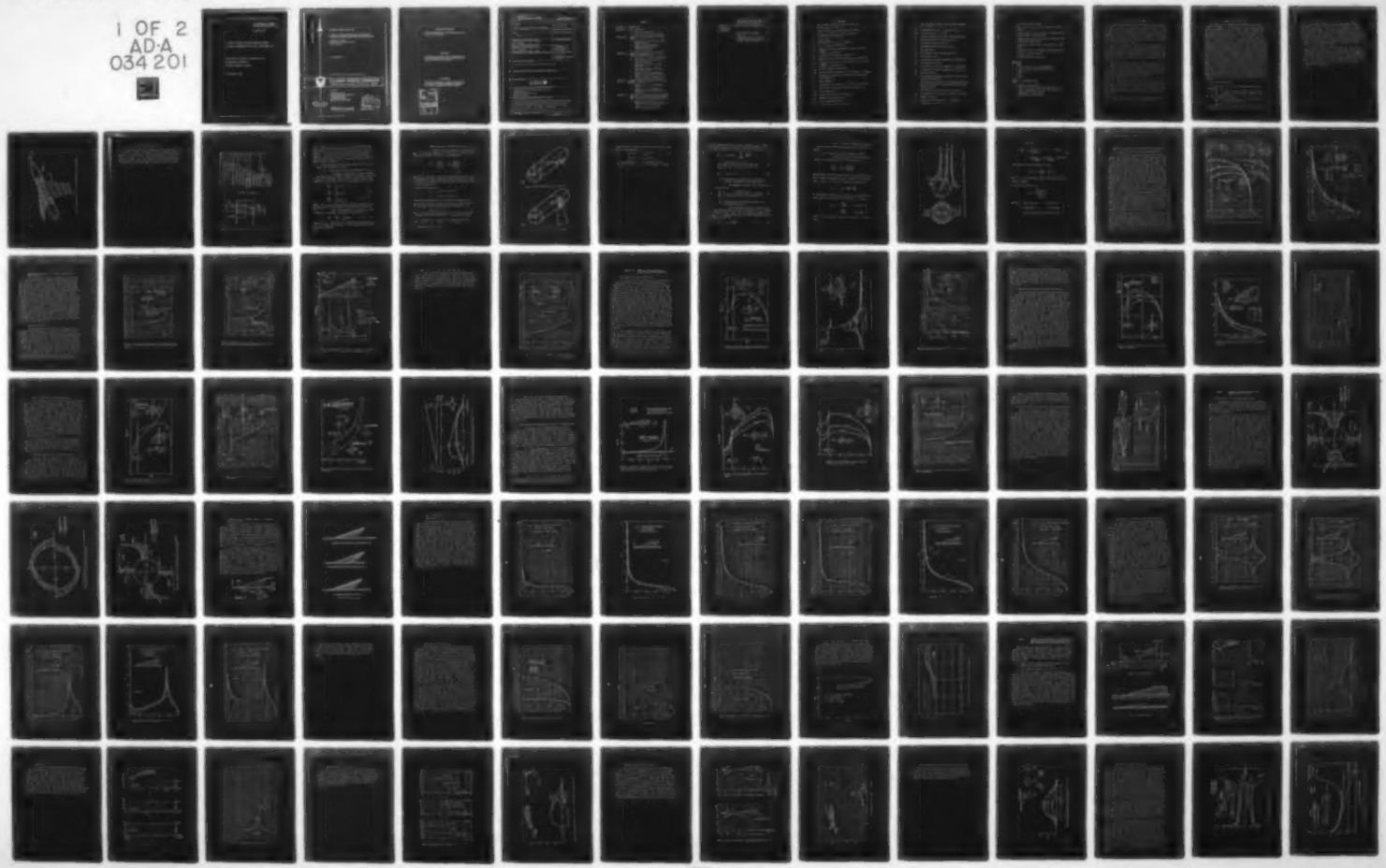
AD-A034 201 ARMY MISSILE RESEARCH DEVELOPMENT AND ENGINEERING LAB--ETC F/G 19/7
A STUDY OF VARIOUS SLENDER AND NON-SLENDER FIN-BODY COMBINATION--ETC(U)
NOV 76 N UCHIYAMA, Q M WU

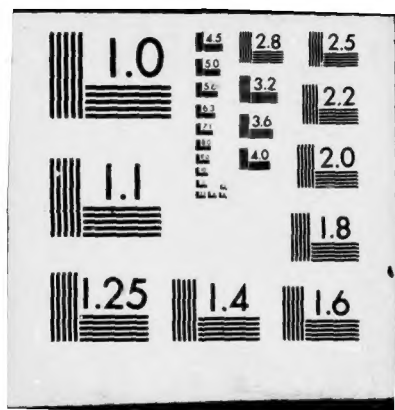
UNCLASSIFIED

RD-CR-76-5

NL

1 OF 2
ADA
034 201





U.S. DEPARTMENT OF COMMERCE
National Technical Information Service

AD-A034 201

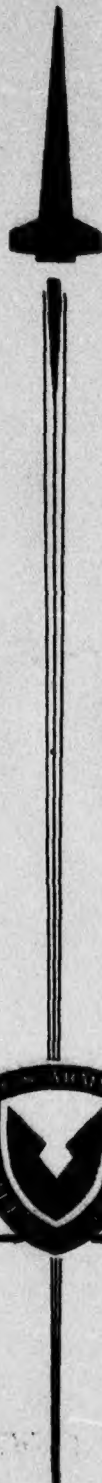
A STUDY OF VARIOUS SLENDER AND NON-SLENDER
FIN-BODY COMBINATIONS OF MISSILE CONFIGURATIONS

ARMY MISSILE RESEARCH, DEVELOPMENT AND
ENGINEERING LABORATORY
REDSTONE ARSENAL, ALABAMA

12 NOVEMBER 1976

ADA 034201

013024



TECHNICAL REPORT RD-CR-76-5

A STUDY OF VARIOUS SLENDER AND NON-SLENDER
FIN-BODY COMBINATIONS OF MISSILE CONFIGURATIONS

N. Uchiyama and J. M. Wu
The University of Tennessee Space Institute
Tullahoma, Tennessee

12 November 1976

APPROVED FOR PUBLIC RELEASE: DISTRIBUTION UNLIMITED.



U.S. ARMY MISSILE COMMAND
Redstone Arsenal, Alabama 35809

Prepared for:

Aeroballistics Directorate
US Army Missile Research, Development
and Engineering Laboratory
US Army Missile Command
Redstone Arsenal, Alabama 35809

REPRODUCED BY
**NATIONAL TECHNICAL
INFORMATION SERVICE**
U. S. DEPARTMENT OF COMMERCE
SPRINGFIELD, VA 22161

Drafts available to DDCI from the
permitted legible reproduction



DISPOSITION INSTRUCTIONS

**DESTROY THIS REPORT WHEN IT IS NO LONGER NEEDED. DO NOT
RETURN IT TO THE ORIGINATOR.**

DISCLAIMER

**THE FINDINGS IN THIS REPORT ARE NOT TO BE CONSTRUED AS AN
OFFICIAL DEPARTMENT OF THE ARMY POSITION UNLESS SO DESIG-
NATED BY OTHER AUTHORIZED DOCUMENTS.**

TRADE NAMES

**USE OF TRADE NAMES OR MANUFACTURERS IN THIS REPORT DOES
NOT CONSTITUTE AN OFFICIAL INDORSEMENT OR APPROVAL OF
THE USE OF SUCH COMMERCIAL HARDWARE OR SOFTWARE.**

ARMED FORCES	
DTB	DATA CENTER
DBR	DATA BROADCAST
MANUFACTURER	
DISTRIBUTOR	
DISTRIBUTOR/AVAILABILITY CODE	
AVAIL	DATA CENTER
A	

UNCLASSIFIED
SECURITY CLASSIFICATION OF THIS PAGE (When Data Entered)

REPORT DOCUMENTATION PAGE		READ INSTRUCTIONS BEFORE COMPLETING FORM
1. REPORT NUMBER RD-CR-76-5	2. GOVT ACCESSION NO.	3. RECIPIENT'S CATALOG NUMBER
4. TITLE (and Subtitle) A STUDY OF VARIOUS SLENDER AND NON-SLENDER FIN-BODY COMBINATIONS OF MISSILE CONFIGURATIONS		5. TYPE OF REPORT & PERIOD COVERED Technical Report
7. AUTHOR(s) N. Uchiyama and J. M. Wu		6. PERFORMING ORG. REPORT NUMBER
9. PERFORMING ORGANIZATION NAME AND ADDRESS Commander, US Army Missile Command Attn: DRSMI-RD Redstone Arsenal, Alabama 35809		10. PROGRAM ELEMENT, PROJECT, TASK AREA & WORK UNIT NUMBERS
11. CONTROLLING OFFICE NAME AND ADDRESS Commander, US Army Missile Command Attn: DRSMI-RPR Redstone Arsenal, Alabama 35809		12. REPORT DATE 12 November 1976
14. MONITORING AGENCY NAME & ADDRESS (if different from Controlling Office)		13. NUMBER OF PAGES 194
		15. SECURITY CLASS. (of this report) Unclassified
		15a. DECLASSIFICATION/DOWNGRADING SCHEDULE
16. DISTRIBUTION STATEMENT (of this Report) Approved for public release; distribution unlimited		
17. DISTRIBUTION STATEMENT (of the abstract entered in Block 20, if different from Report)		
18. SUPPLEMENTARY NOTES Reproduced from best available copy. 		
19. KEY WORDS (Continue on reverse side if necessary and identify by block number) Rectangular and Constant Chord Sweptback Fins Clipped Delta Fin Slender Fin-Body Combination Singularity Method		
20. ABSTRACT (Continue on reverse side if necessary and identify by block number) The aerodynamic loading on a number of rocket body-control surface combinations has been calculated using methods developed at the University of Tennessee Space Institute over the past five years. Variations in control surface planform, roll angle, control surface deflection or incorporation of elevons, are included. Compressibility is accounted for. Details of the digital computer program are included.		

CONTENTS

	Page
SECTION I. INTRODUCTION.....	1
SECTION II. BASIC ANALYSIS.....	2
1. Basic Consideration.....	2
2. Basic Equations and Coordinates	5
SECTION III. RESULTS AND DISCUSSIONS ON VARIOUS FINS.....	15
1. Rectangular and Constant Chord Sweptback Fins.....	15
2. Compressibility Effect on Pressure Coefficient of Rectangular Fins.....	18
3. Clipped Delta Fin.....	18
SECTION IV. RESULTS AND DISCUSSIONS ON VARIOUS FIN-BODY COMBINATIONS.....	24
1. Rectangular Fin-Body Combination	24
2. Constant Chord Sweptback Fin-Body Combination.....	28
3. Tapered, Sweptback Fin-Body Combination.....	32
4. Cruciform, Slender Delta Fin-Body Combination.....	32
5. Discussions on Compressible Effect of Fin-Body Combination..	37
6. Effect of Small Control Fin on Slender Fin-Body Combination....	42
SECTION V. KOERNER'S APPROACH COMPARED WITH OTHER METHODS AND DATA.....	44
1. Comparison with Slender-Body Theory.....	44
2. Comparisons with FLEXSTAB Singularity Distribution Method and Data.....	48
SECTION VI. COMPARISONS OF POTENTIAL FLOW THEORIES WITH DATA ON SLENDER CRUCIFORM CLIPPED DELTA FIN-BODY WITH ELEVON DEFLECTION	70
1. Results and Discussions on Various Effects of the Elevon Deflection on Fin-Body Combination	70
2. Comparison with Experimental Data.....	85

	Page
3. - Variation of Surface Pressure and Lift Coefficient with Free Stream Mach Number.....	92
SECTION VII. CONCLUSIONS AND RECOMMENDATIONS..	95
REFERENCES.....	96
APPENDICES.....	98
1. Determining Aerodynamic Matrices.....	98
2. Computer Program for Deter- mining Pressure Distribution on Fin-Body Combination.....	108

LIST OF SYMBOLS

- a Body radius, location of the fin corner in x-direction (see Figure 2).
- AR Aspect ratio of fin extended into the body.
- b Fin span, location of the fin corner in y-direction (see Figure 2).
- c Local chord.
- \bar{c} Reference chord $\left(= \frac{1}{S} \int_{-s}^s c^2(y) dy \right)$.
- C_L Lift coefficient based on S.
- $C_{L\alpha}$ Derivative of lift coefficient [lift curve slope;
 $= \left[\frac{\partial C_L}{\partial \alpha} \right]_\alpha = 0$] based on S.
- C_N Normal force coefficient based on S.
- C_n Spanwise normal force distribution (see Figure 34).
- $C_{N\alpha}$ Derivative of normal coefficient [normal force slope;
 $= \left[\frac{\partial C_N}{\partial \alpha} \right]_\alpha = 0$] based on S.
- C_p Surface pressure coefficient.
- ΔC_p Surface pressure difference $\left(= (C_p)_{\text{lower}} - (C_p)_{\text{upper}} \right)$
- d Fractional location of local panel in x-direction (see Figure 2).
- D Body diameter.
- e Location of local panel in y-direction (see Figure 2).
- h Half width of local fin panel (see Figure 3).
- $l(y)$ Local chord at y.
- LPC Local panel chord (see Figure 3).
- M Number of half body panels.
- M_∞ Free stream Mach number.
- n Total number of half fin panels.

- p** Total number of panels on fin-body combination
 $(= 2n + 2M)$.
- \bar{P}** Aerodynamic matrix ($= u/U_\infty$ per unit γ) .
- $\Delta p/q$** Load distribution ($= \Delta C_p$) .
- q** Strength of source per unit body surface area.
- \bar{Q}** Aerodynamic matrix (v/U_∞ per unit γ).
- r** Distance between two points.
- \bar{R}** Aerodynamic matrix (w/U_∞ per unit γ).
- s** Fin semi span.
- S** Fin surface area extended into body.
- ΔS** Local panel area.
- u** Perturbation velocity component in x-direction.
- U_∞** Free stream velocity.
- v** Perturbation velocity component in y-direction.
- w** Perturbation velocity component in z-direction.
- \vec{w}** Velocity vector.
- x** Body fixed x-coordinate parallel to free stream,
 positive downstream.
- y** Body fixed y-coordinate in the spanwise direction
 of a fin, positive in right hand side direction
 facing forward.
- z** Body fixed z-coordinate, positive upward.
- z_0** Fin location in z-direction mounted on the body.
- α** Angle of attack.
- β** Prandtl-Glauert parameter ($= \sqrt{1-M_\infty^2}$).
- γ** Circulation strength of fin vortex.

- Γ Circulation of fin vortex.
 δ Cant angle of fin, deflection angle of flap or elevon.
 θ Azimuth angle of body, positive counterclockwise facing forward (see Figure 4)
 $\bar{\theta}$ Azimuth angle of body, positive clockwise facing forward (see Figure 13b).
 λ Gradient of bound vortex, (see Figure 3), taper ratio.
 Λ Sweptback angle at specified chordwise position.
 ω Apparent angle of attack.
 ρ^* Distance between two points.

Subscripts

- b Body
 B Due to bound vortex (see Appendix 1).
 D Control point on panel (see Figure 3).
 e Elevon.
 f Fin.
 F Flap.
 $i, j, k,$
 $l, m, q,$
 v, μ } Local panel name.
 n Normal to body surface.
 P Due to port side vortex (see Appendix 1).
 S Due to starboard side vortex (see Appendix 1).
 t Tangential to body surface.
 V Bound vortex (see Figure 3).

SECTION I. INTRODUCTION

Aerodynamic performance of various kinds of fin-body combinations in inviscid, subsonic flow at small angles of attack can be analyzed by the "singularity method" (Refs. 1 and 5). Koerner's approach (Ref. 1) is followed in this analysis. In general, the singularity method has an advantage over the slender body theory in the sense of less restriction in the fin shape. By means of a modern high speed electronic computer, the pressure coefficient can be calculated rather simply.

The surface pressure distribution on the rectangular, the sweptback, and the tapered sweptback fins and fin-body combinations have been analyzed. The effect of compressibility is taken into account by Goethert's rule which showed very satisfactory with the experimental data up to a high subsonic free stream Mach number. For all of these no shock waves on fins and fin-body combinations are treated.

The present analysis has been extended to include the slender, cruciform, canted delta fin and fin-body combination and also includes the case of slender, cruciform, clipped delta fin-body combination geometry with a deflected small control fin. The results have been compared with the slender body theory (Ref. 2) and other singularity methods (Refs. 5 and 8).

The present method, with slight modification, can be applied also to a fin-body combination geometry of a fin with twist, camber, thickness, and arbitrary plan form. From the analytical study, it is also clear that a viscous flow study is needed in estimating the more accurate pressure distribution in the region of the fin-body junction as well as the fin tip, even at small angles of attack.

For more condensed contents of the present report and its interaction to the exhaust jet plume, see Ref. (12).

SECTION II. BASIC ANALYSIS

In estimating the aerodynamic performance on a fin-body combination geometry, the method based on slender body theory has been developed and easily applied. Very reasonable results have been obtained (see Ref. 2). The practical difficulty in applying the slender body theory is in its limitation to the very slender fin configuration (e.g., one needs to assume that $AR \ll 1$ theoretically, or $AR \approx 1$ even for a practical application to be held. On the other hand, the Prandtl's well-known "lifting line theory" has approximated very well the lift distribution for a rectangular fin with very large aspect ratio. The application to the other fin configurations (such as a finite AR fin) seems not that good as far as the accuracy is concerned for the surface pressure distribution. To overcome this deficiency, Lawrence (Ref. 4) has developed the approximate solution of the lifting line theory for low aspect ratio wings (including the rectangular shape) and delta fins with the aspect ratio from zero to four. However, the application of this technique to the fin-body combinations with the other fin configurations seems to be still in difficulty. A "singularity method" is a method of numerical analysis. From the study of literature, it can be said that such a numerical approach will provide the best estimation of the pressure distribution in nearly all the fin-body configurations with a good accuracy.

1. Basic Consideration

For simplicity, the following assumptions were made in this analysis, i.e.,

- (i) A steady, inviscid, uniform, subsonic free stream.
- (ii) A flat fin with a straight leading and trailing edge, and a streamwise fin tip.
- (iii) Fins are attached to a circular cylindrical body.
- (iv) A small angle of attack.

Based on the singularity method, constant strength vortex singularities are used to replace a lifting fin on a horizontal

plane. The image vortices are placed inside the body with respect to the body surface in order to compensate the body displacement effect. To obtain a good aerodynamic interaction for a fin-body geometry, the source-sink singularities are distributed on a body surface and the doublet singularities are distributed along the body axis. The doublet distribution gives the effect of a body inclination to a free stream. The iteration scheme is used so that all the simulated lifting surfaces can eventually satisfy the flow boundary conditions everywhere on the surface of the fin-body combination.

Figure 1 shows a schematic model of a basic fin-body combination for this analysis. A fin (or wing) has been divided to many panels and each one has been replaced by a horseshoe-type vortex which consists of three vortices (i.e., one bound vortex and two free vortices). The body has been divided also into many panels, each of which consists of a correct part of a body, and it has been replaced by a source or a sink at its surface. (Also, see Figure 51 in Appendix 1).

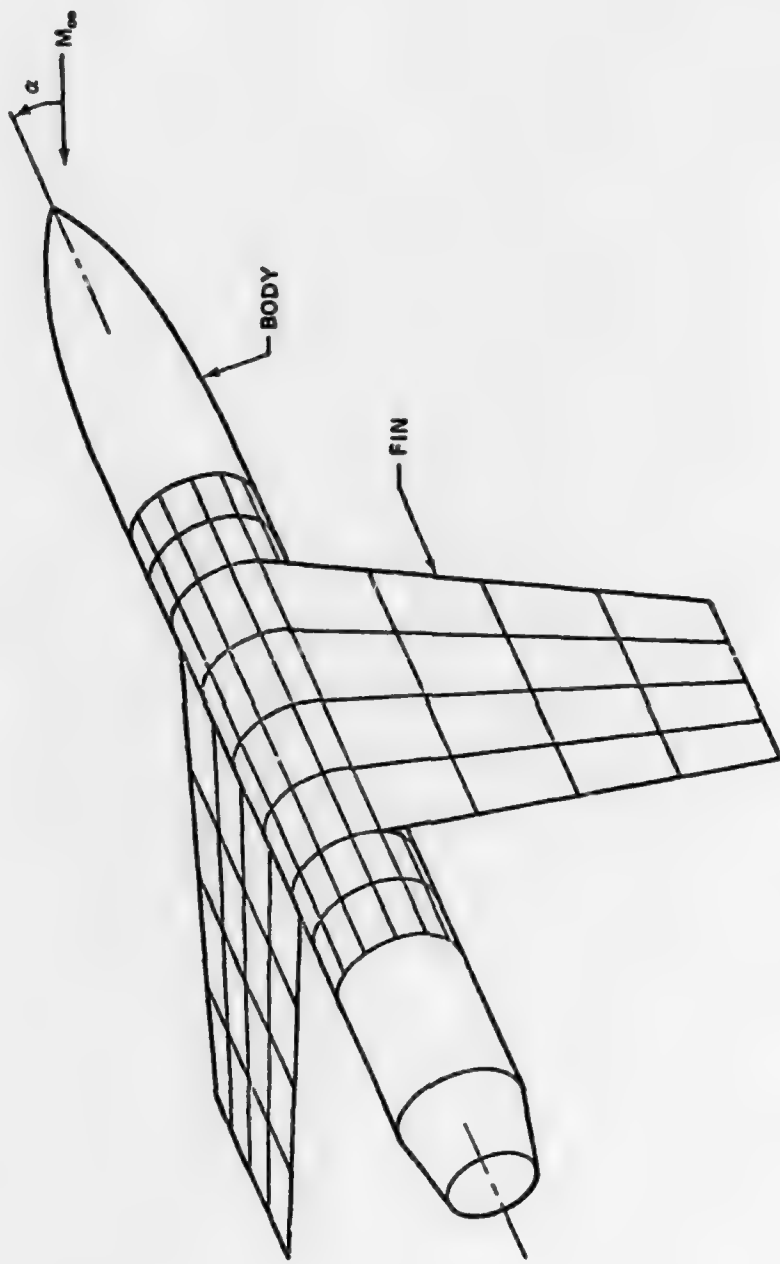


Figure 1. Schematic model of fin-body combination in present analysis.

2. Basic Equations and Coordinates

Figure 2 shows the coordinate of a fin part, which is divided by a number of trapezoidal panels which have the sides parallel to a free stream. Each panel has three vortices with a constant strength, i.e., one bound vortex, which is located at one quarter local panel chord length, and two free vortices which are located at local panel edges, parallel to the free stream.

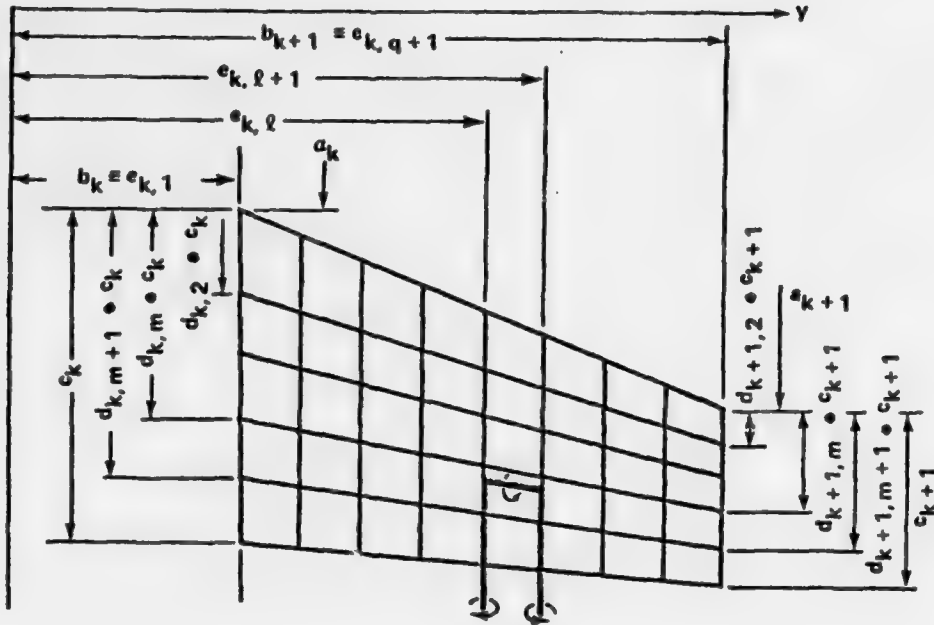


Figure 2. Fin panels [7]

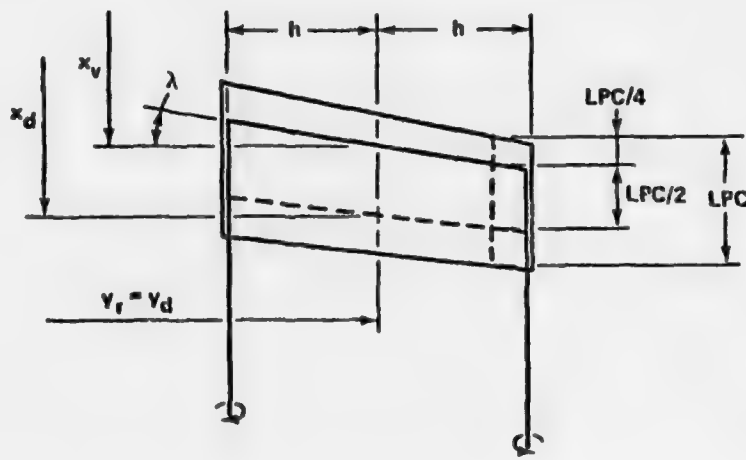


Figure 3. Location of horseshoe vortex and control point on panel [7].

The location of a control point at which the boundary condition will be satisfied is assumed at three-quarters of a local panel chord length in the center line of a local panel as shown in Figure 3. In addition to this, the Goethert compressible similarity rule has been employed to the present analysis, i.e., the coordinates normal to a free stream have been multiplied by Prandtl-Glauert Parameter β .

The following five steps are essential to the analysis. The steps were established by Ref. 1.

(i) Determining circulation distribution (γ_i) on a fin.

Normalized perturbation velocity components at any control point on panel i induced by any panel j which makes four discrete horseshoe vortices (two are from a pair of fins themselves, and two are from their body images) can be written as,

$$\begin{aligned} \frac{u_i}{U_\infty} &= \sum_{j=1}^n P_{ij} \gamma_j \\ \frac{v_i}{U_\infty} &= \sum_{j=1}^n Q_{ij} \gamma_j \\ \frac{w_i}{U_\infty} &= \sum_{j=1}^n R_{ij} \gamma_j \quad i = 1, n \end{aligned} \quad] \quad (1)$$

where: u_i , v_i , w_i are perturbation velocity components and P_{ij} , Q_{ij} and R_{ij} are the aerodynamic matrices given in Appendix 1.

The third equation as stated above is used for satisfying the boundary conditions of any panel, i.e.,

$$-\beta \omega_i = \frac{w_i}{U_\infty} = \sum_{j=1}^n R_{ij} \gamma_j \quad i = 1, n \quad (2)$$

where $\omega_i = \alpha_{fi}$. Equation 2 is n simultaneous linear equations with $n \times n$ constant coefficients. The γ_j can be solved by Gaussian elimination technique.

(ii) Determining Source Distribution (q_v) on the Body.

Induced velocity components at any point on panel v on the body surface due to the fin and its image vortices on the control point of panel j is expressible as,

$$\overset{+}{w}_v = \begin{pmatrix} u_{bv} \\ v_{bv} \\ w_{bv} \end{pmatrix} = \sum_{j=1}^n \begin{pmatrix} \bar{P}_{bvj} \\ \bar{Q}_{bvj} \\ \bar{R}_{bvj} \end{pmatrix} \gamma_j \quad (3)$$

$$v = 1, 2M$$

where \bar{P}_b , \bar{Q}_b , and \bar{R}_b are the same aerodynamic matrices as those in Equation (1), except taking the control points on the body, which are located at the center of local panels (see Figure 51 in Appendix 1), in the former case.

In cylindrical coordinates,

$$\begin{aligned} v_{nl} &= v_b \cos \theta + w_b \sin \theta \\ v_t &= -v_b \sin \theta + w_b \cos \theta \end{aligned} \quad (4)$$

Geometrical relationships are illustrated in Figures 4 and 5.

The resultant velocity component normal to the body surface due to the fin vortices and the sources must be vanished, i.e.,

$$v_{nl} + v_{n2} = 0 \quad (5)$$

where v_{n2} is the velocity component normal to the body surface due to the sources distributed on it, v_{n2} can be written as,

$$v_{n2} = \frac{q(x, \theta)}{2} + \int_{-\infty}^{\infty} \frac{q(x', \theta')}{4\pi} \frac{(1 - \cos(\theta - \theta')) a^2}{\rho^*} d\theta' dx' \quad (6)$$

in incompressible flow, where

$$\rho^* = (x - x')^2 + (y - y')^2 + (z - z')^2 \quad (7)$$

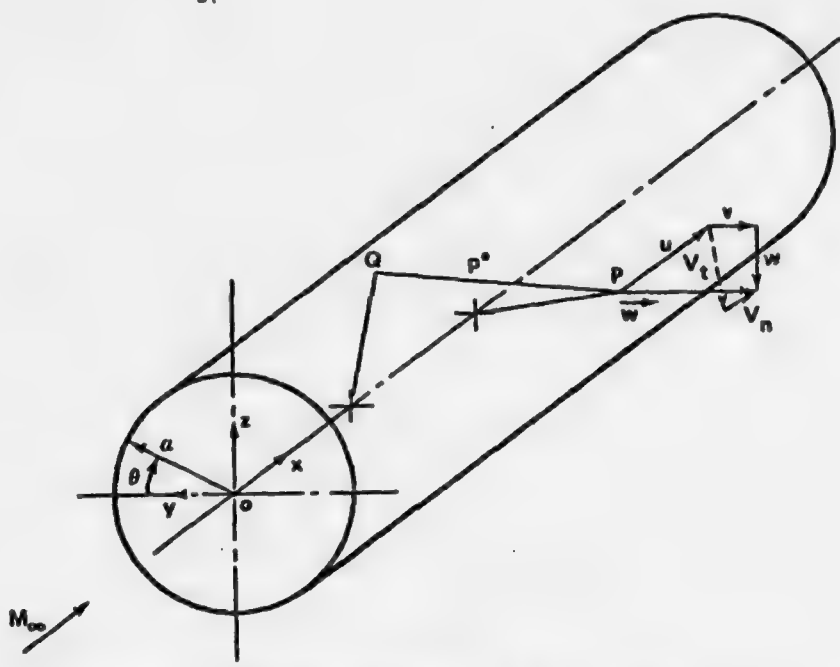


Figure 4. Induced velocity at P by a source Q [1].

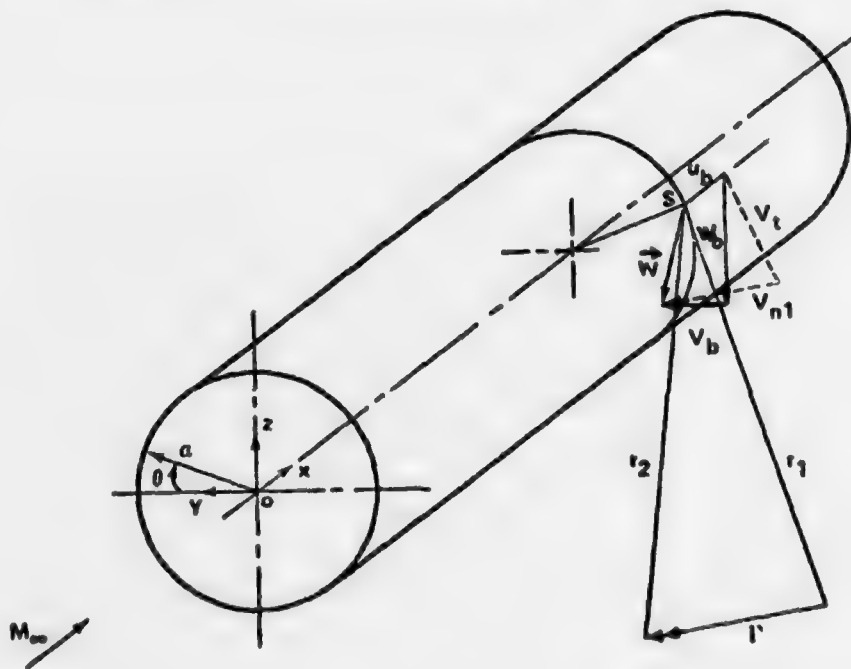


Figure 5. Induced velocity at S by a line vortex element Γ [1].

The integral equation (6) can be solved by the iteration scheme;
For the first approximation,

$$q_1(x, \theta) = -2 v_{nl}(x, \theta) \quad (8)$$

or,

$$q_2(x, \theta) = -2 v_{nl}(x, \theta) + \\ + \int_{-\infty}^{\infty} \int_0^{2\pi} \frac{v_{nl}(x', \theta')}{\pi} \frac{(1 - \cos(\theta - \theta')) a^2}{\rho^3} d\theta' dx' \quad (9)$$

The m^{th} approximation of the source strength q_v at a point v on a body surface which cancels the induced velocity v_{nl} in Equation (4) normal to a body surface can be written as

$$q_{m\mu} = -2 (v_{nl})_{m\mu} - \sum_{\substack{v=1 \\ v \neq \mu}}^{2M} \frac{q_{(m-1)v}}{2\pi} \frac{(1-\cos(\theta_\mu - \theta_v)) \beta a \Delta S_v}{[(x_\mu - x_v)^2 + \beta^2 \{1-\cos(\theta_\mu - \theta_v)\} a^2]^{3/2}} \quad (10)$$

and,

$$\Delta S_v = \beta a \Delta \theta \Delta x_v \quad (11)$$

(iii) Determining Downwash (w_{bu}) on Fin Due to Sources Distributed on the Body Surface

The downwash on panel μ due to source on panel v can be written as,

$$w_{bu} = \sum_{\substack{v=1 \\ v \neq \mu}}^{2M} \frac{q_v}{4\pi} \frac{\beta(z_o - z_v) \Delta S_v}{[(x_\mu - x_v)^2 + \beta^2 \{(y_\mu - y_v)^2 + (z_o - z_v)^2\}]^{3/2}} \quad (12)$$

(iv) Determining Circulation Distribution (γ_i) for Second Iteration

By the downwash obtained in Equation (12), the corresponding angle of attack is induced on a fin, which can be written as w_{bi}/U_∞ . Then, this term should be added to the original, i.e., geometrical angle of attack in Equation (2), thus ω_i must be written as,

$$-\omega_i = -\alpha_{fi} + \frac{w_{bi}}{U_\infty} \quad i = 1, n \quad (13)$$

After ω_i has been obtained on fin panels, the same procedure should be repeated until γ_i will not change greatly.

(v) In Case of Body with Angle of Attack.

Downwash on a fin due to the doublet along a body axis (as shown in Fig. 6) can be written as

$$\frac{w_f}{U_\infty} = \alpha_b a^2 \frac{y^2 - z_o^2}{(y^2 + z_o^2)^2} \quad (14)$$

This downwash has been assumed constant at any spanwise location, and it changes an apparent angle of attack (ω_i) as mentioned above. Thus, in this case, ω_i should be replaced by,

$$-\omega_i = -\alpha_{fi} + \frac{w_{bi}}{U_\infty} + \frac{w_{fi}}{U_\infty} \quad (15)$$

The aerodynamic performance coefficient can be computed in the usual manner for the pressure coefficient, C_p , on panel;

$$\left. \begin{aligned} C_{pj} &= \pm \frac{\Delta C_{pj}}{2} \dots \text{for fin,} \\ &= -\frac{2u_{bj}}{U_\infty} \dots \text{for body.} \end{aligned} \right\} \quad (16)$$

where "+" is for an upper surface of a fin and "-" is for a lower surface.

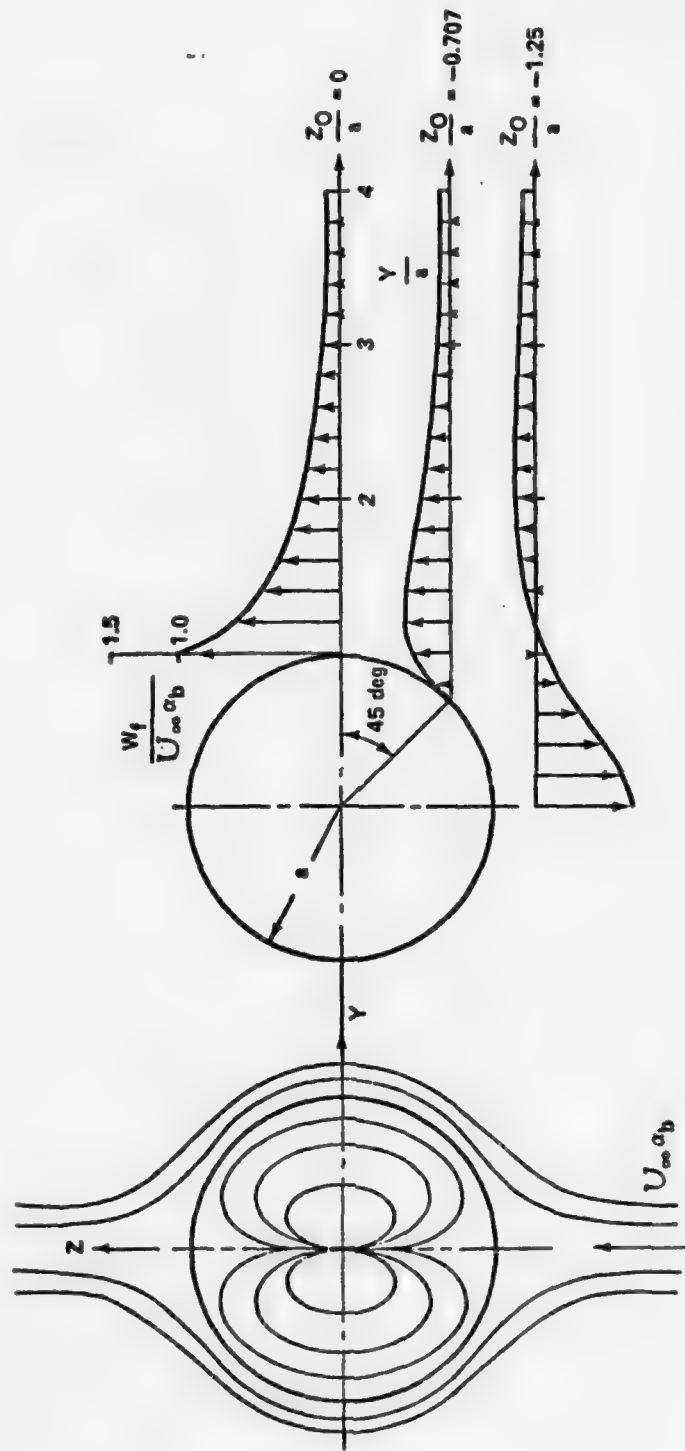


Figure 6. Velocity distribution on fin induced by the body angle of incidence [3].

For the load distribution, ΔC_p ,

$$\left. \begin{aligned} \Delta C_{pj} &= \frac{b \gamma_j}{\beta^2 (x_{dj} - x_{vj})} \dots \text{for fin,} \\ &= (C_{pj})_{\substack{\text{lower} \\ \text{surface}}} - (C_{pj})_{\substack{\text{upper} \\ \text{surface}}} \dots \text{for body.} \end{aligned} \right\} (17)$$

For the spanwise lift distribution, $C_L(y)$,

$$C_L(y) = \frac{2b}{\beta^2 l(y)} \sum_{i=1}^{n'} \gamma_i \quad (18)$$

where n' is a total number of panels along the chord $l(y)$ at a fixed y station.

For the lift coefficient, C_L ,

$$C_L = \frac{\sum_{j=1}^p C_{pj} \Delta S_j}{\sum_{j=1}^p \Delta S_j} \quad (19)$$

$$\left. \begin{aligned} \text{where } \Delta S_j &= 4\beta h_j (x_{dj} - x_{vj}) \dots \text{for the fin,} \\ &= \beta a \Delta \theta \Delta x_j \sin \theta_j \dots \text{for the body.} \end{aligned} \right\} (20)$$

(projected area on horizontal plane)

SECTION III. RESULTS AND DISCUSSIONS ON VARIOUS FINS.

1. Rectangular and Constant Chord Sweptback Fins.

As the first example by the singularity method, the spanwise lift distribution at $M_\infty = 0$ was computed for the fin with the three different leading edge sweptback angles, that is, zero (rectangular fin), 30 and 45 degrees. The aspect ratio of these fins is taken as all the same equals to six. The fin configuration and the computed results are shown in Fig. 7. This figure shows the spanwise lift distribution per unit angle of attack over the semi span of the fin. The half of the fin has been divided into the sixteen trapezoidal panels, i.e., four equidistantly in the chordwise direction, and four with cosine in the spanwise direction. The present calculations have been compared with those in Ref. (1), on which the present analysis was based. The results are shown in Fig. 7. It can be seen that there is little difference between them. As the ordinate in Fig. 7 is considered proportional to the circulation distribution per unit angle of attack over the semi-span of the fin (see curve A), i.e., the rectangular fin, is very close to the elliptics. With increasing the sweptback angles of a fin, the lift distribution around the center of the fin is decreasing, or the maximum point of the lift distribution moves to the fin tip, and thus the lift of the fin decreases accordingly. This means that the characteristics of the fin will be close to the one of the "delta" fin (compare it with Figs. 11 and 12).

The typical chordwise pressure distribution on a rectangular fin at the different spanwise positions is shown in Fig. 8. The same rectangular fin configuration as the one in Fig. 7 was used here. The pressure goes to infinity at the leading edge of the fin because of the "leading edge singularity" of the fin with zero thickness. It can be also seen that the Kutta's conditions at subsonic speed are certainly satisfied at the trailing edge of the fin.

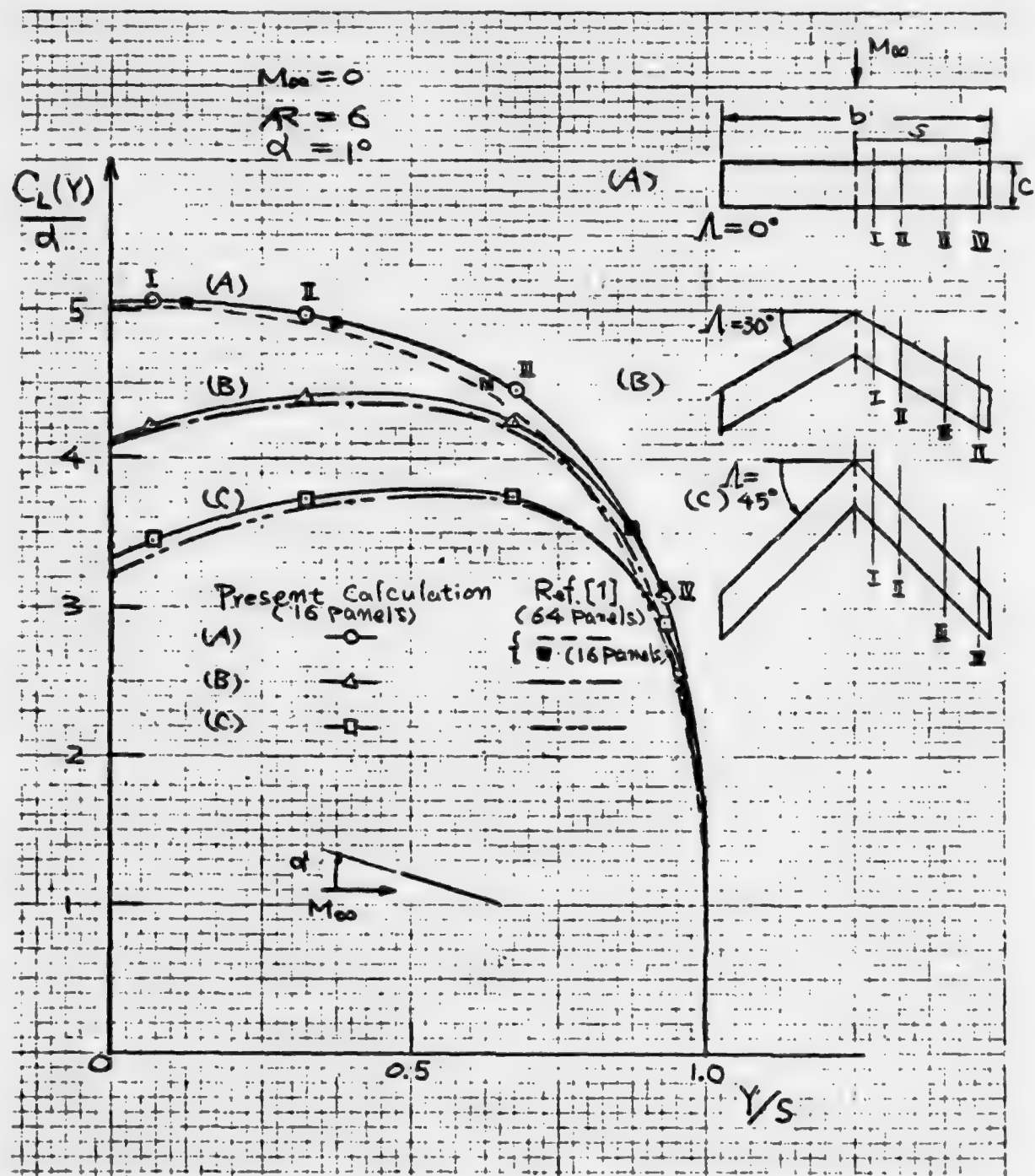


Figure 7. Spanwise lift distributions on constant chord sweptback fins.

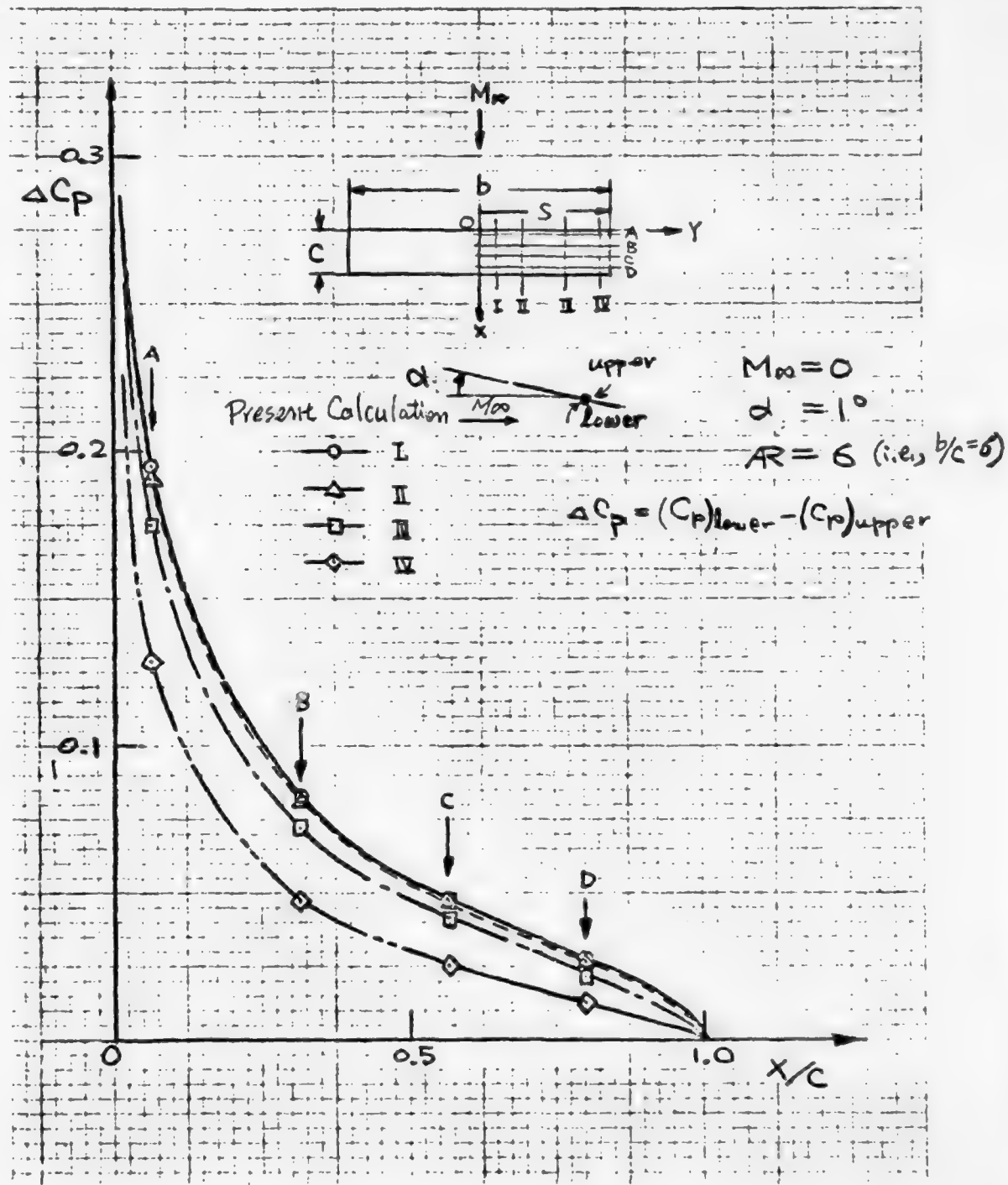


Figure 8. Chordwise pressure distribution on rec'angular fin.

2. Compressibility Effect on Pressure Coefficient of Rectangular Fin.

The variation of pressure coefficient with the free stream Mach number at one position on the rectangular fin is shown in Fig. 9. Goethert's rule was used for compensating the compressible effect in the present analysis as mentioned before. The computed results by using the other compressible similarity rules, such as Prandtl-Glauert and Kármán-Tsien rules, are also included in this figure for comparisons. The Cps corrected by using Prandtl-Glauert and Kármán-Tsien rules seem to be overestimated. The correction of compressibility based on Goethert's rule predicts satisfactorily well for a fin with low-aspect ratio up to a relatively high Mach number (for example, see Chapter 13 in Ref.(10)). With increase in the aspect ratio of a fin, the difference of the lift coefficients computed by using the Prandtl-Glauert and the Goethert rules becomes small. Fig. 10 shows the calculated example on the lift coefficient, for a rectangular fin with aspect ratio of twenty. It should be noted that both of the calculated results have little difference up to near a Mach number of 0.8.

3. Clipped Delta Fin.

The pressure distribution for a clipped delta fin configuration has been computed. The result is shown in Fig. 11. The solid lines indicate the chordwise pressure distribution along the corresponding chord lines, and the dotted lines indicate the spanwise pressure distribution along the one-quarter chordwise length of the local panel. As can be seen, the clipped fin tip effect shows up after the entire mid chord length or toward the trailing edge. It is relatively not affected in the front portion of the chord. The free stream Mach number for this computed case is 0.7, the leading edge sweptback angle is 77.2° , and the angle of attack is taken as one degree. From this figure, it can be seen that the aerodynamic characteristics of the clipped delta fin has the one combined with those of the sweptback and

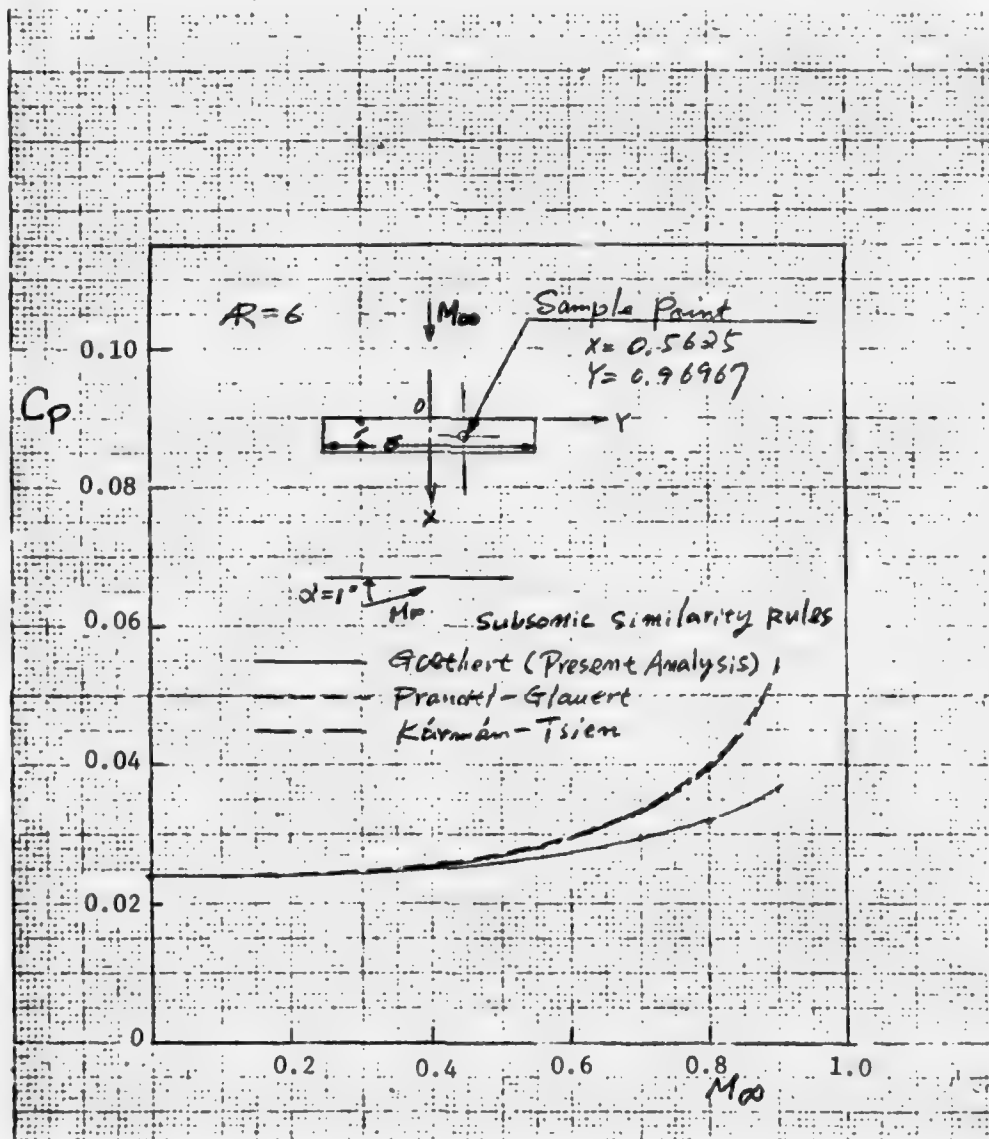


Figure 9. C_p at one point on rectangular fin changing with free stream Mach number computed by different subsonic compressible similarity rules.

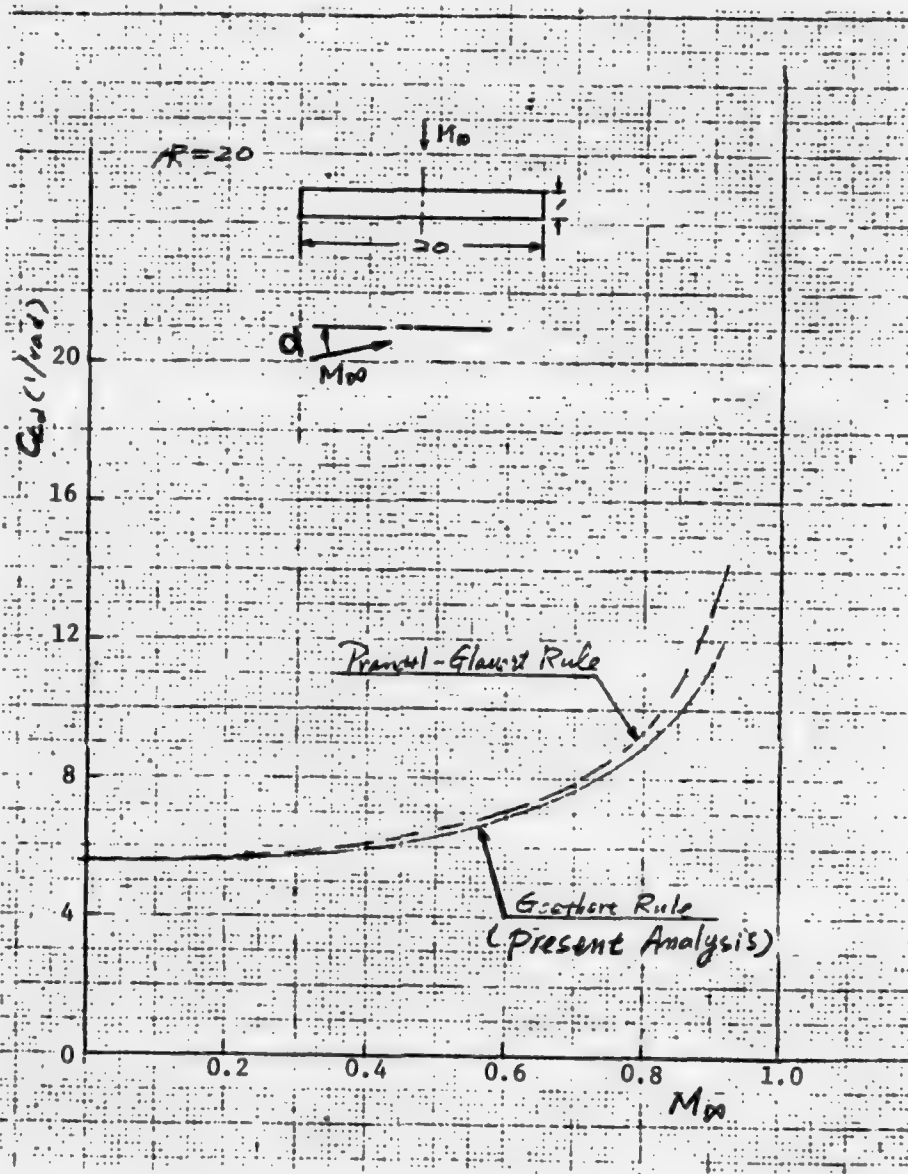


Figure 10. Comparison of lift coefficient of rectangular fin with large aspect ratio by two different similarity rules.

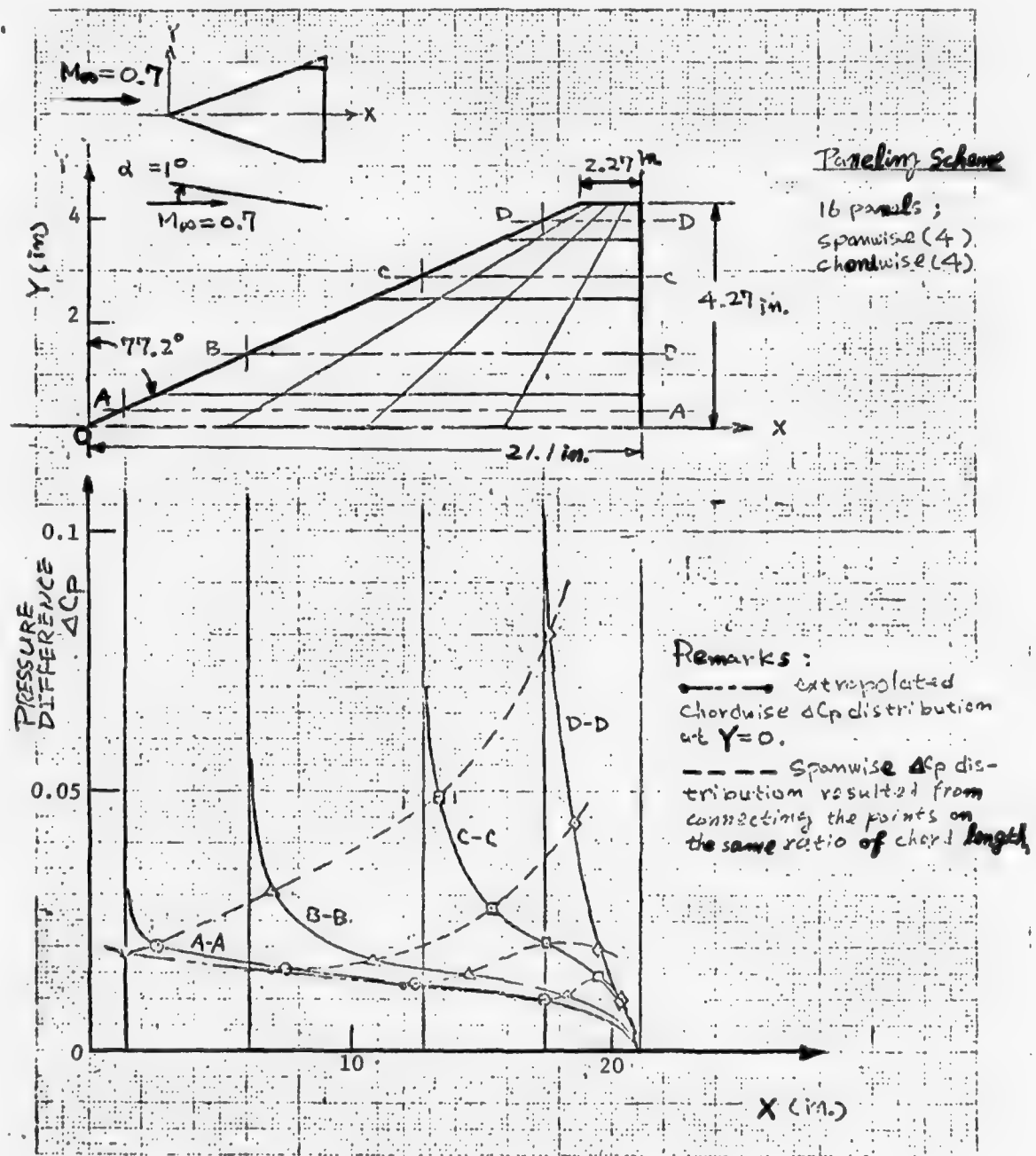


Figure 11. Pressure difference ($\Delta C_p = (C_p)_{lower} - (C_p)_{upper}$) of clipped delta fin with angle of attack of one degree and free stream Mach number of 0.7.

rectangular fins on the same fin (also see Fig. 12).

Fig. 12 shows the spanwise lift distribution, and that of the delta fin, the geometry of which is shown in Fig. 11, is also included in this figure for a comparison. Although the actual positions in the spanwise direction are slightly different in both cases, the decrease of the spanwise lift distribution caused by a clipping of the fin tip can be seen very clearly near the fin tip.

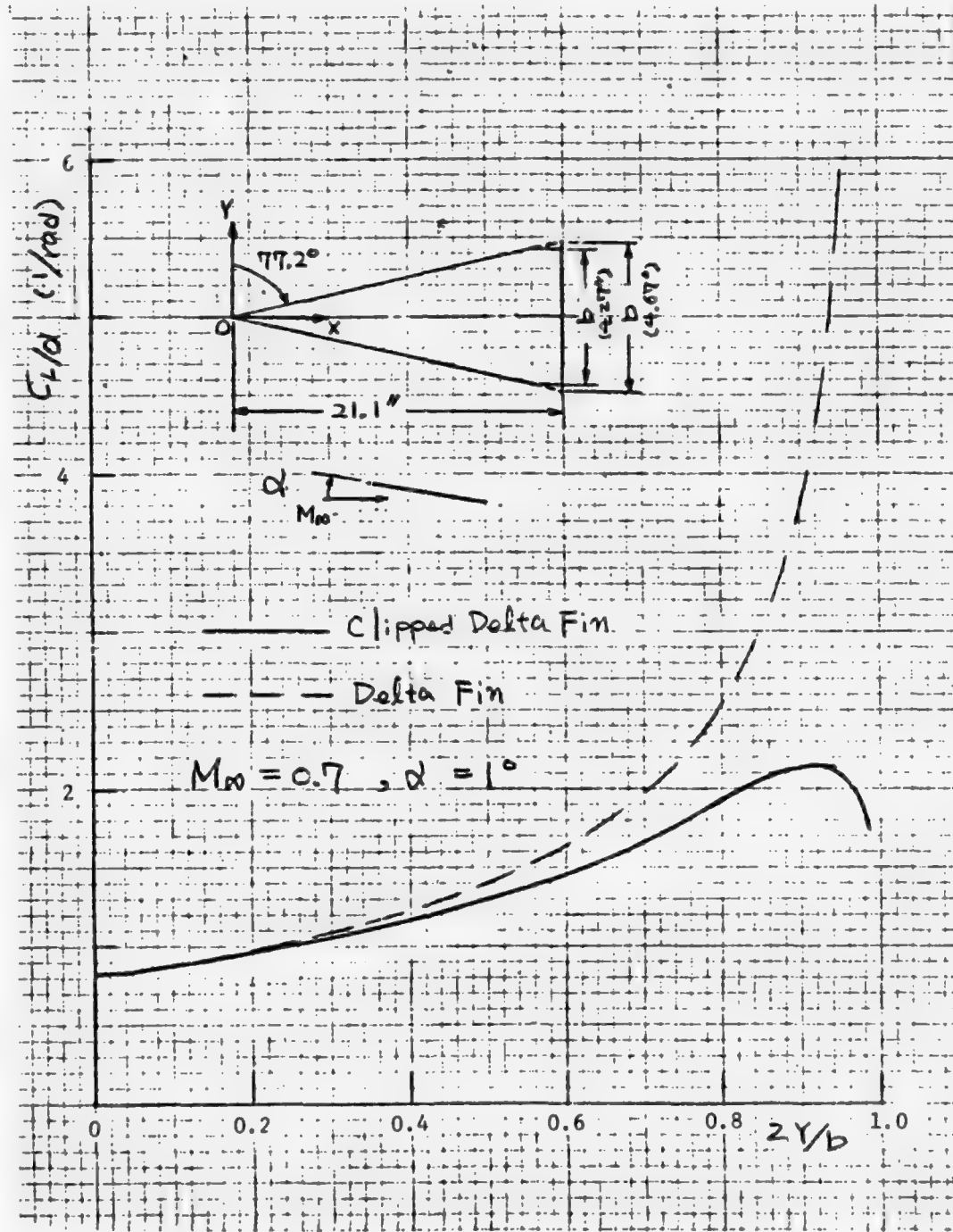


Figure 12. Spanwise lift distribution on clipped delta fin
 $(M_\infty = 0.7, \alpha = 1^\circ$; also, the delta fin's case is included).

SECTION IV. RESULTS AND DISCUSSIONS ON VARIOUS FIN-BODY COMBINATIONS.

1. Rectangular Fin-Body Combination.

The spanwise lift distributions have been calculated for a rectangular fin alone and a fin-body combination configuration at $M_\infty = 0$. They agree well with the original calculation of Koerner (Ref. 1) as shown in Fig. 13a. The discussion on the compressibility effect will be given later. The body treated has a zero angle of incidence, and a fin is canted by one degree (clearly, for a more cant fin, a simple linear multiplication of amplitude will yield a result). The presence of the body was simulated by image vortices of the fin and source-sink distributed on the body surface as discussed. The computed results for the fin-body interaction agreed well with a limited experimental data as shown in Fig. 13a, except in the region very close to the fin root. Koerner pointed out that this disagreement resulted from the presence of boundary layer in a real flow on the fin and the body (Ref. 1). This suggests that the viscous study is necessary in order to obtain a more accurate result in this small region. As it can be seen from Fig. 13a, the mutual interaction between the body and the fin is rather strong (comparing cases with and without the body presence).

The chordwise load distributions on the body in the same fin-body geometry as shown in Fig. 13a were computed at three different azimuthal positions. The results are shown in Fig. 13b. It can be seen that the influence of the fin on the body becomes stronger as closer to the fin root. It affects both the upstream and downstream flow beyond the fin location. The calculated chordwise lift distribution on the fin very close to the fin root is also included in Fig. 13b for a comparison.

Fig. 14 shows the chordwise load distribution on the rectangular fin-body combination, in which the fin is not canted,

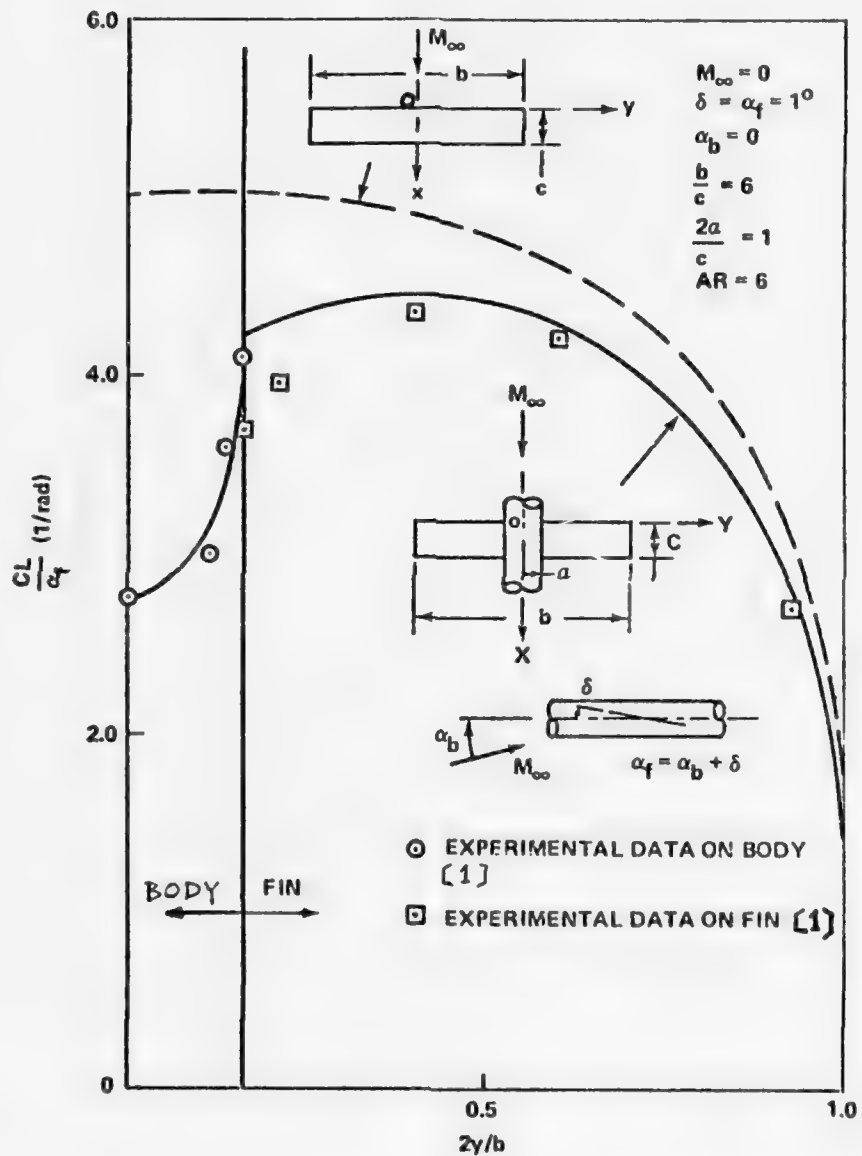


Figure 13a. Recalculated spanwise lift distribution of rectangular fin-body combination given by Korner [1].

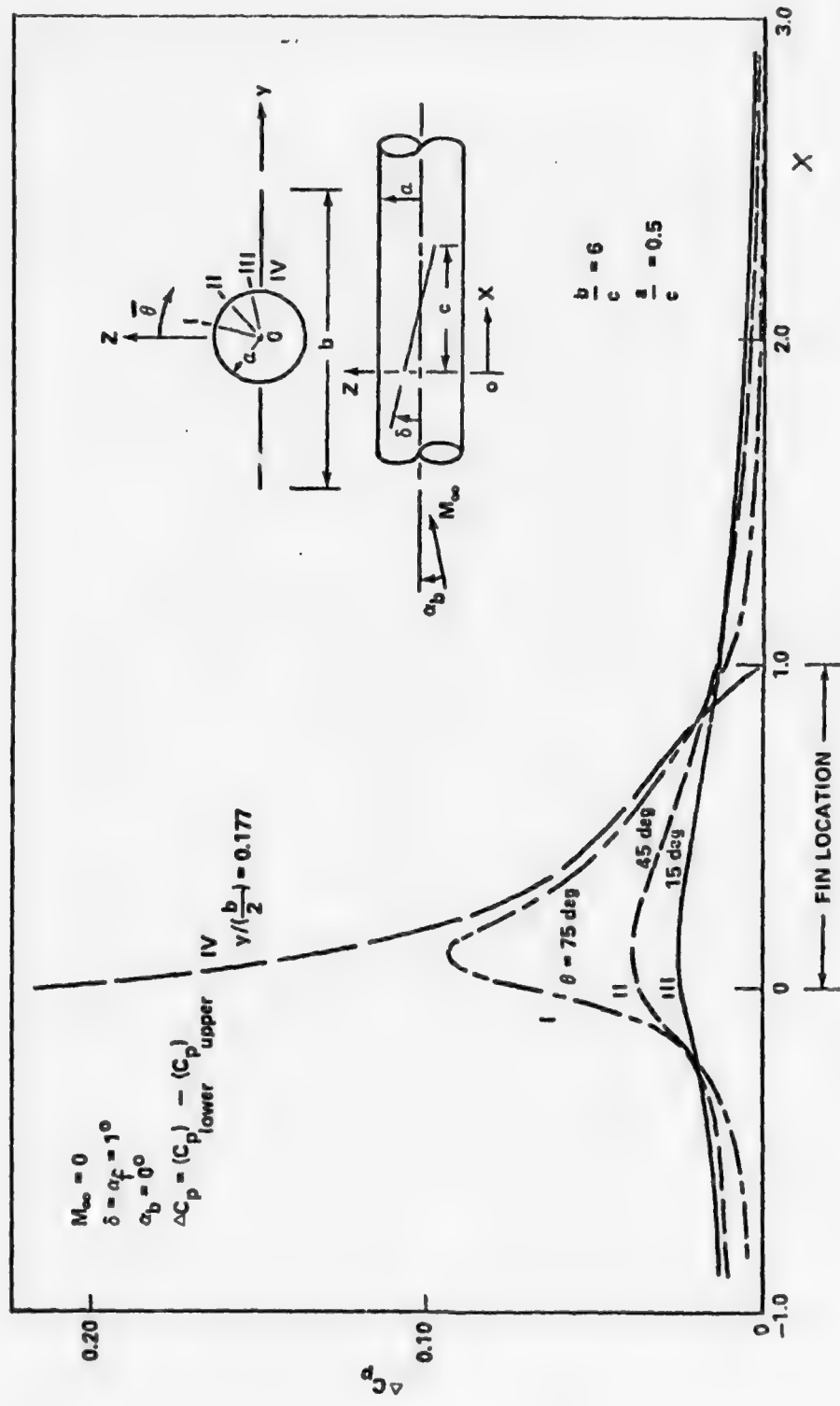


Figure 13b. Longitudinal pressure distribution of body with rectangular fin.

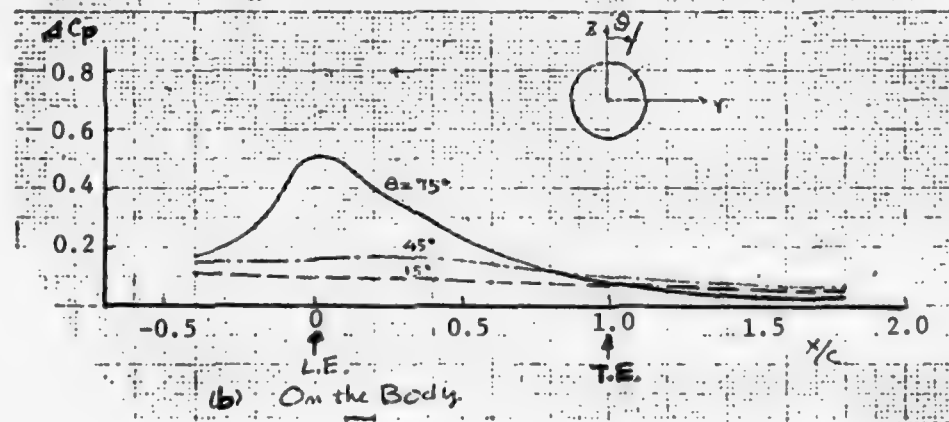
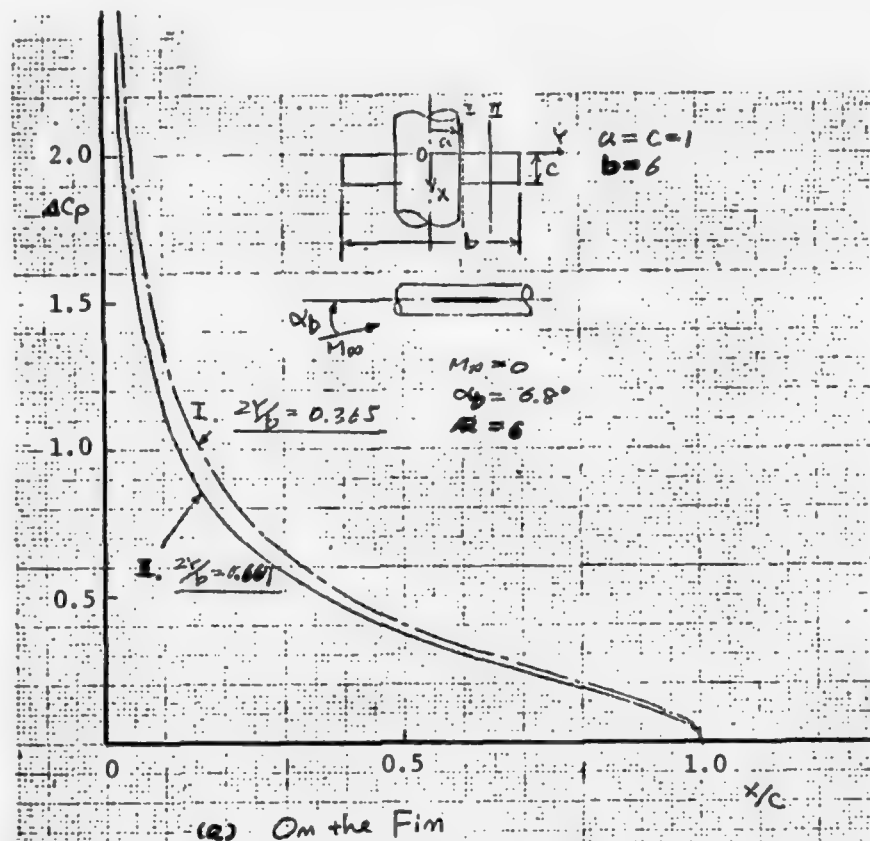


Figure 14. Longitudinal pressure distribution on rectangular fin-body combination ($\alpha_b = 6.8^\circ$, $M_\infty = 0$).

but the body has the angles of attack of 6.8 degrees. It can be seen, from Figs. 13 and 14, that the trend of the load distribution on both the body and the fin in the case of the angle of attack was very similar to the one in the cant fin case. Also, the strong effect of the fin on the body can be seen at the region on the body very close to the fin root from these figures.

2. Constant Chord Sweptback Fin-Body Combination.

The constant chord sweptback fin-body combination at $M_\infty = 0$ has been investigated here. The spanwise lift distributions are shown in Fig. 15. The sweptback angles are zero (i.e., rectangular fin, this is the same one as shown in Fig. 13), 30 and 45 degrees. The cant angle of the fins is one degree (again a simple linear multiplication to obtain a larger angle result) and the body has zero angle of attack. All three fins have the same aspect ratio of six. This figure can be contrasted to the case without a body as shown in Fig. 7. The maximum point of the spanwise lift distribution moves to the fin tip as the sweptback angle of a fin increases. The characteristics of a fin will be close to the one of the delta fin (see Figs. 17, 18, and 19a), as is more or less expected. Fig. 16a shows a calculated chordwise load distribution on the fin of a 45° sweptback fin-body combination. The variation of the load distribution which is rather small along the spanwise direction can be seen from this figure. There exists the maximum position of the semi-spanwise lift distribution. This can be calculated about 60% of the semi-span from the body axis, i.e., $2 y/b \approx 0.6$ from Fig. 15.

The corresponding longitudinal pressure distribution on the body is shown in Fig. 16b. The gradient of the pressure distribution curve was not so steep as the one in the rectangular fin case, as shown in Fig. 13b.

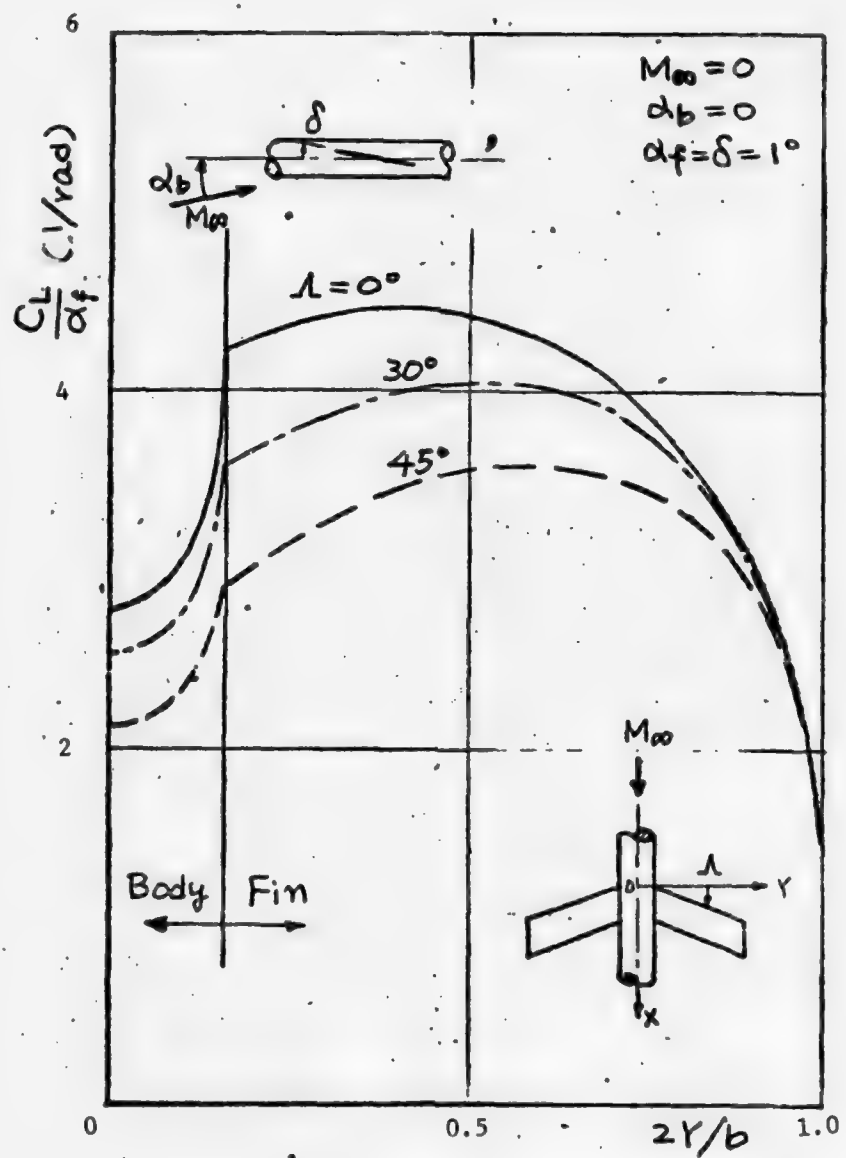


Figure 15. Spanwise lift distribution of constant chord sweptback fin-body combination.

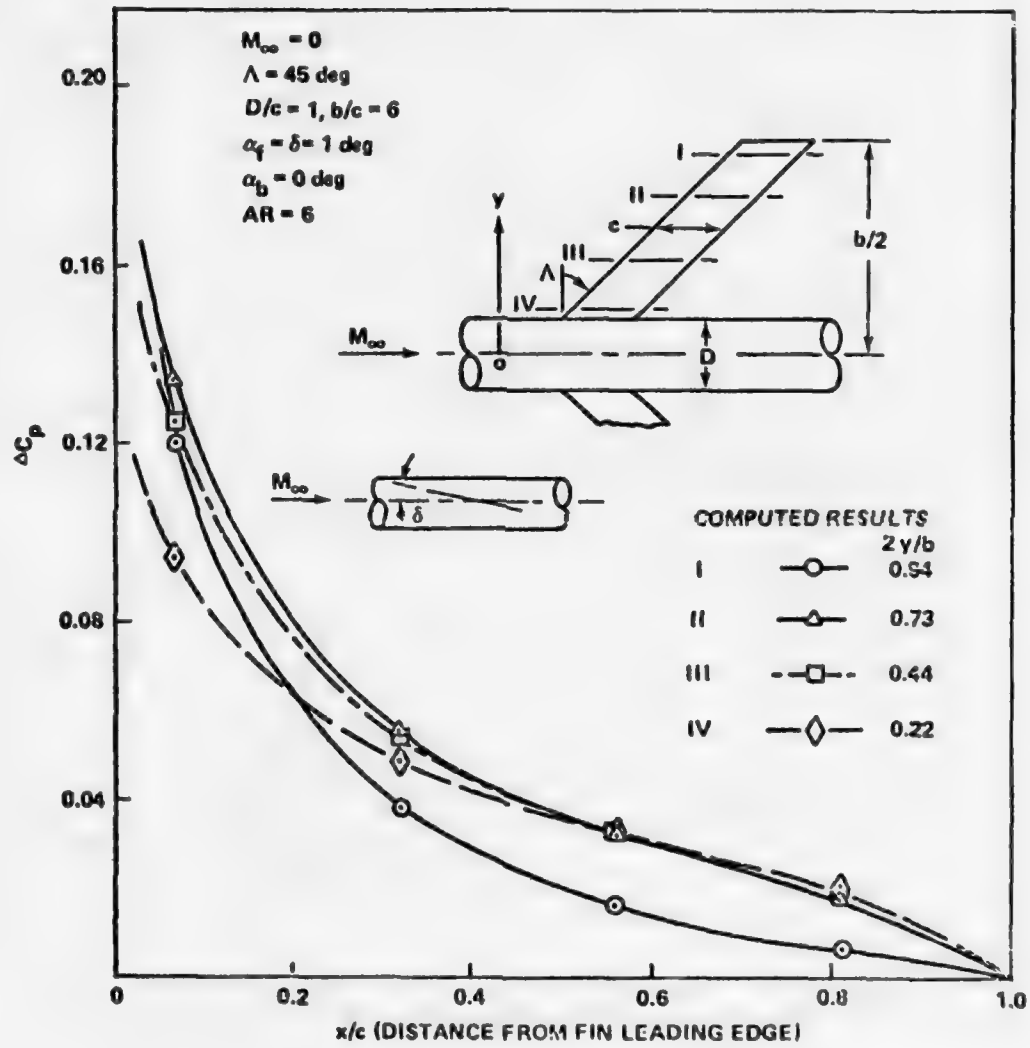


Figure 16a. Chordwise pressure distribution on 45° sweptback fin with body.

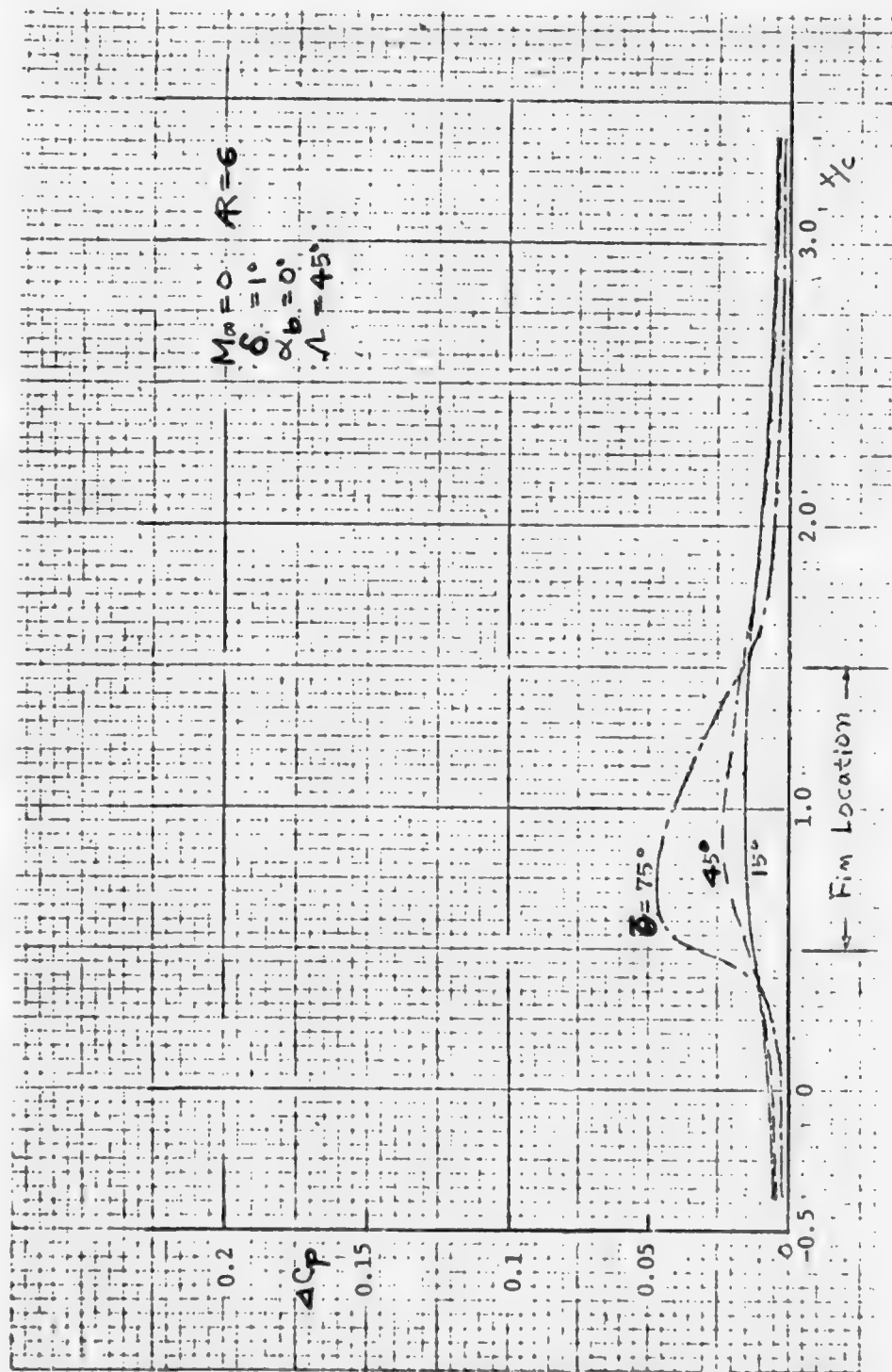


Figure 16b. Longitudinal pressure distribution on body.

3. Tapered, Sweptback Fin-Body Combination.

The sweptback fin-body combination, with two different taper ratio fins as used by Koerner (Ref. 1) has been investigated. Fig. 17 shows the computed spanwise lift distribution on such a geometry with a taper ratio $\lambda = l_a/l_i$ (where l_i is the maximum chord length through the body, and l_a is a fin tip chord length) of zero and one third. The sweptback angle for both cases was taken 30° at one quarter of the local chord length. The angle of incidence of the body was assumed one degree (again, for a larger angle case, a linear multiplication of amplitude is sufficient) and the fin was assumed with a zero cant angle. The lift distribution for $\lambda = 0$ agrees well with the characteristics of the delta fin-body combination, in spite of the fact that it is not quite a delta fin. Also, compare it with the result in Fig. 19a, a case of slender delta fin-body is shown although the fin configuration is not the same.

The spanwise lift distribution of the trapezoidal fin-body combination, the configuration of which is taken from Ref. (7), is shown in Fig. 18. The trend of the lift distribution curve has not much difference with the one in the case of $\lambda = 1/3$ as mentioned before, or the fin part of the clipped delta fin case as shown in Fig. 12.

4. Cruciform Slender Delta Fin-Body Combination.

Fig. 19a shows the spanwise lift distribution on three different cruciform fin-body combinations. In the case of the cruciform cant fin-body combination, a pair of horizontal fins is canted by three degrees so that it can rotate about the body axis (i.e., x-axis) to a negative direction in the sense of a commonly-accepted sign convention. The case of the fin only yielded the largest lift distribution as expected. The effect of the body can be seen clearly in this case also. The cant fin case showed the lowest lift distribution as expected (about this, for example, see Ref. (2)).

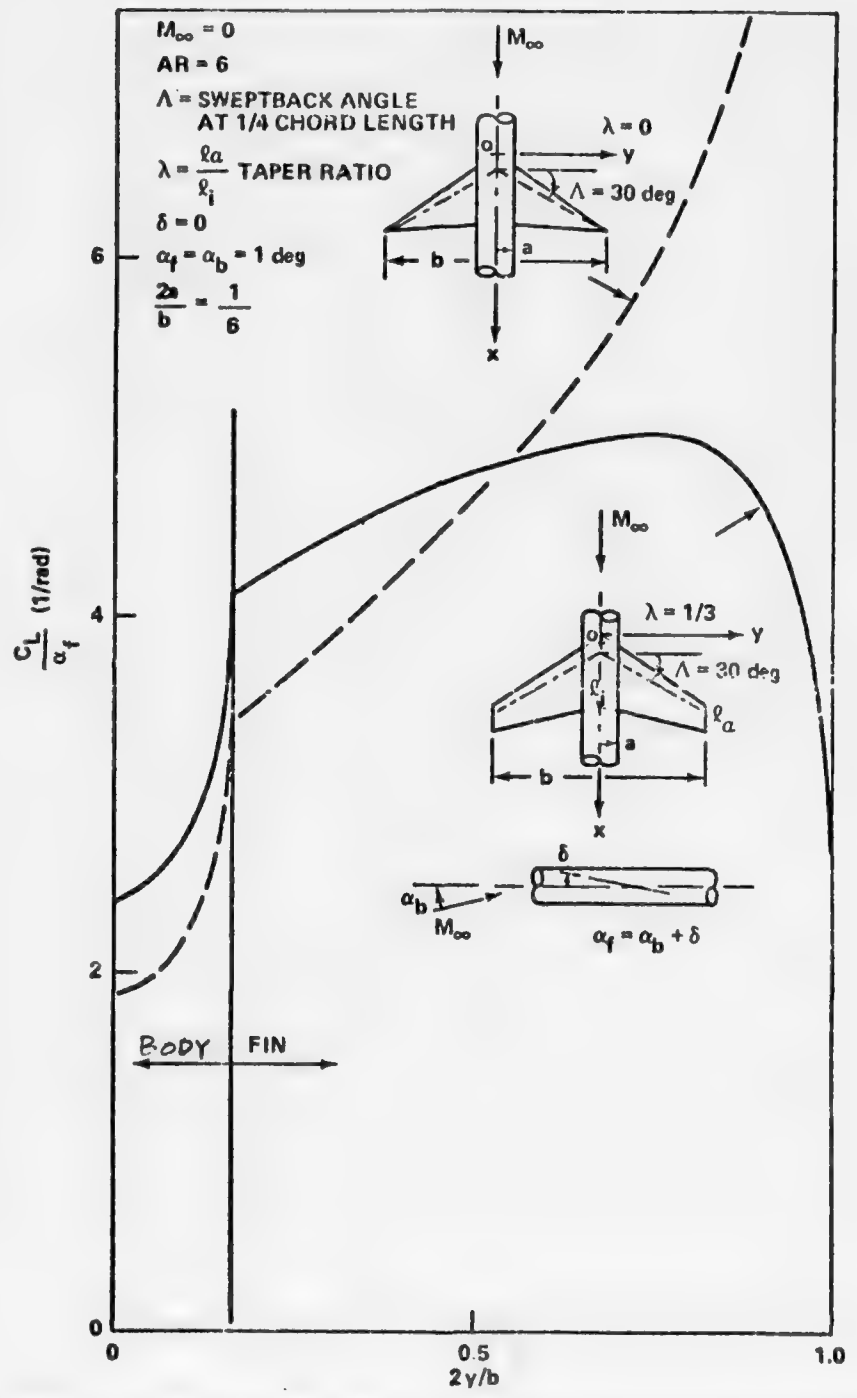


Figure 17. Recalculated spanwise lift distribution with different taper ratio fin given by Korner [3].

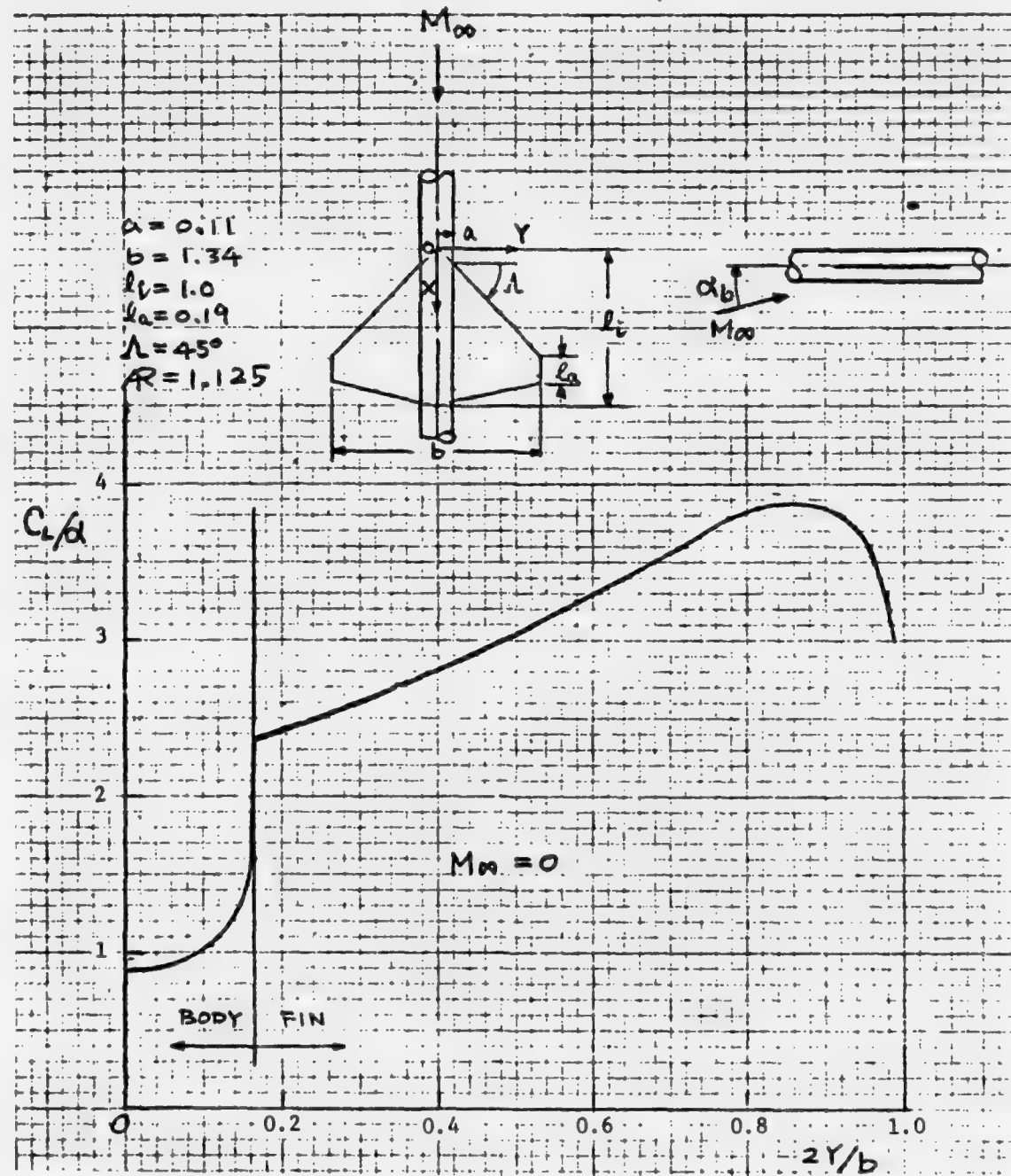


Figure 18. Spanwise lift distribution on trapezoidal fin-body combination.

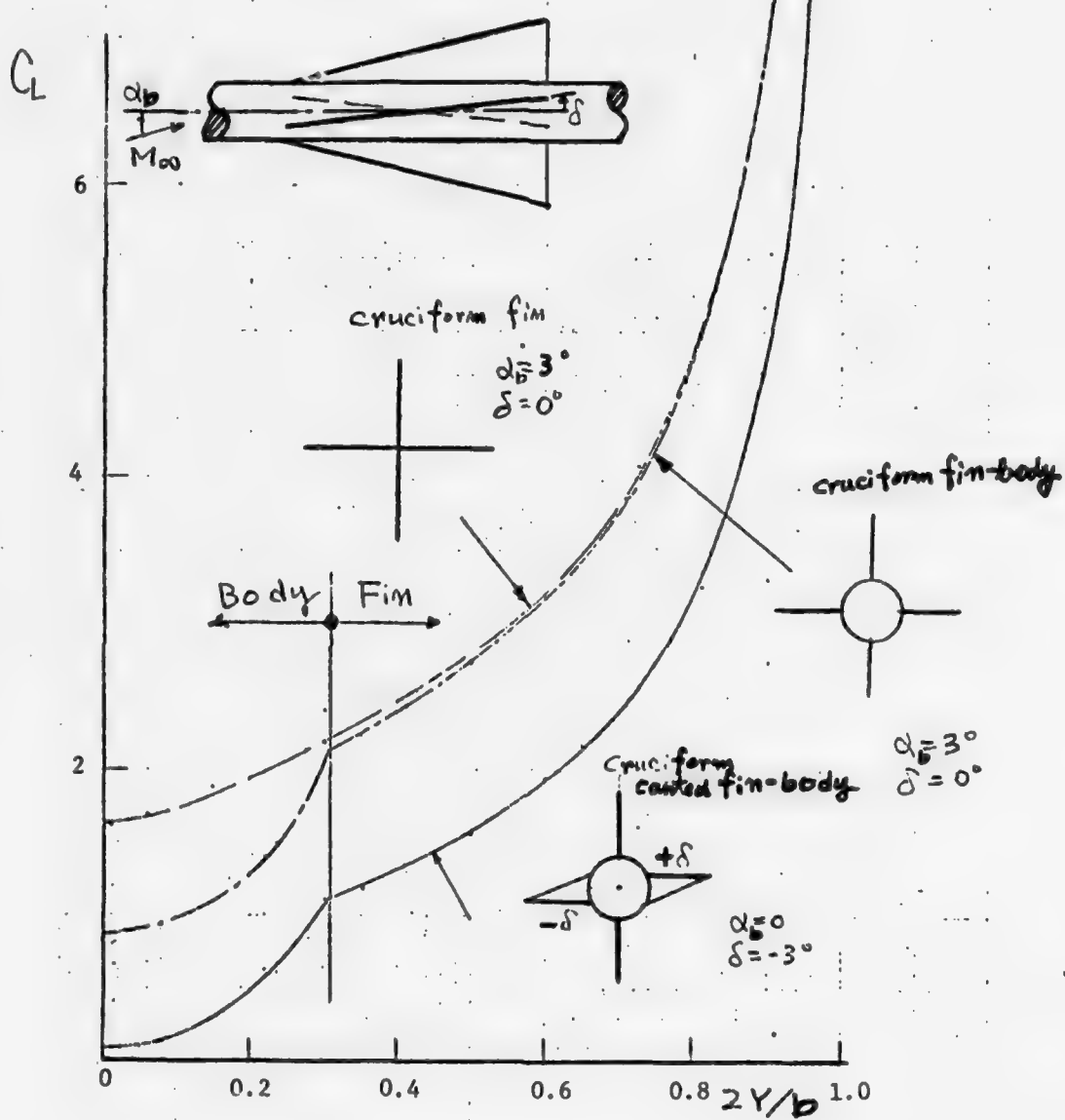


Figure 19a. Spanwise lift distribution on cruciform delta fin-body combination.

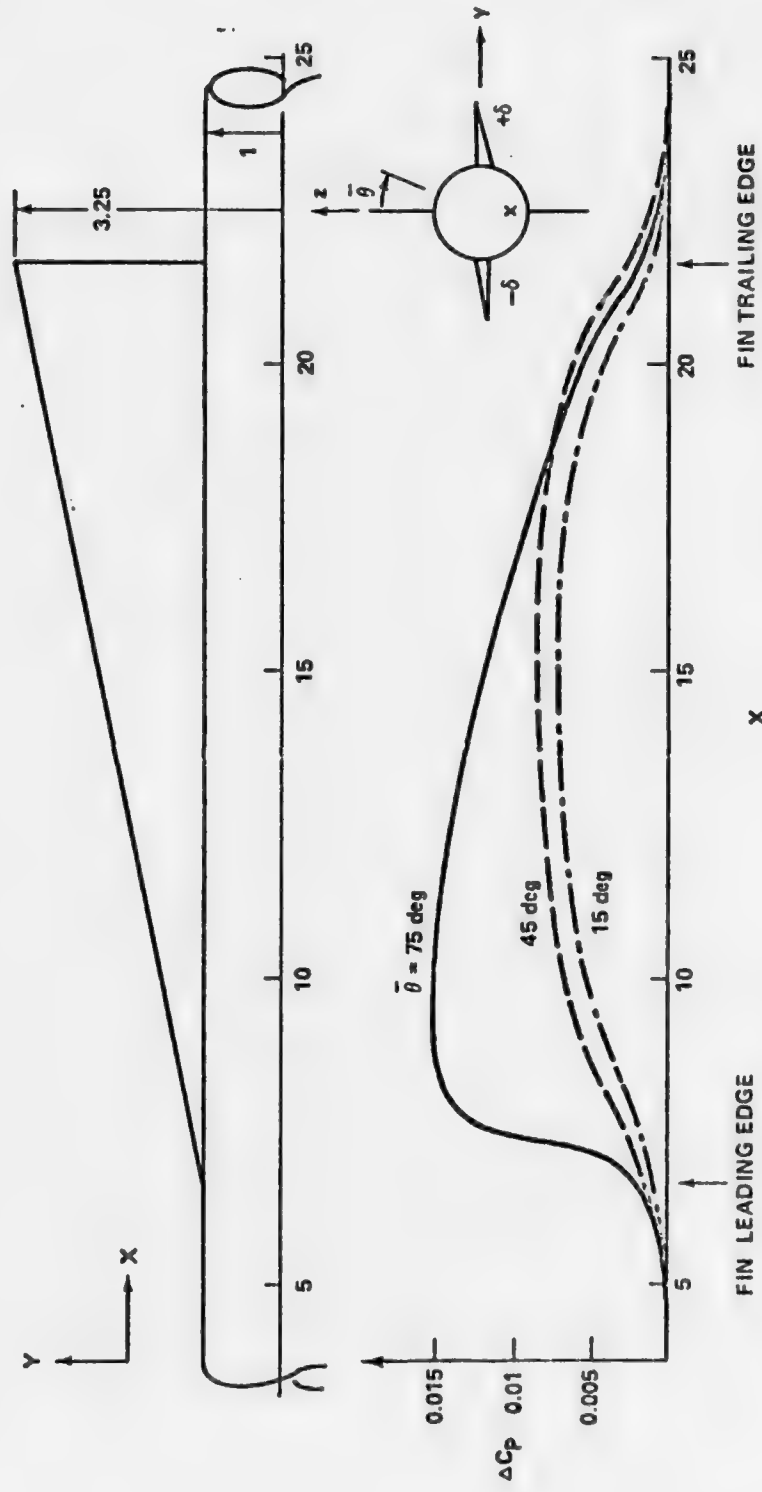


Figure 19b. Longitudinal pressure distribution on body with cruciform slender delta fin (horizontal fins are canted, $\delta = -3^\circ$).

Fig. 19b shows the calculated longitudinal pressure distribution on the body. It should be noted that the rate of perturbation pressure change is very sharp at the leading and the trailing edges with lower magnitude pressure as compared with the large aspect ratio fin case (see Fig. 13b). This is expected because the fin is slender so the influence of the fin on the body should be small. This result agrees well with the concept of the slender-body theory which states that the aerodynamic disturbance influences only in the cross plane to the free stream (see Ref. (2)).

5. Discussions on Compressibility Effect on Fin-Body Combination.

The effect of the compressibility on a lift coefficient of a cruciform slender delta fin-body combination is shown in Fig. 20. (Only the angle of attack influence is considered here for the sake of discussion.) The fin area extended through the body as shown on a dotted line was used as a reference area for the lift coefficient computation. In general, as mentioned before, the Prandtl-Glauert rule resulted in an over correction for such a small aspect ratio fin configuration (see Fig. 20).

It is more appropriate to use the Goethert's rule to calculate the compressibility effect in a fin-body combination geometry. For a slender fin-body combination case, after using the Goethert rule correction, the result (see Fig. 20) agreed very well with the result computed by the slender body theory. In view of a wider range of Mach number applicability of the slender body theory, such an agreement is not totally surprising. In the same figure, a result by Nielsen's estimation (Ref. 11) is also included for a comparison. For a non-slender fin case, the result by using Goethert's rule correction is shown in Figs. 21 and 22.

Fig. 23 shows the lift coefficient varying with the freestream Mach number on the non-slender rectangular fin-body combination. The configuration is given in Fig. 22. As it

$\alpha_b = 3 \text{ deg}$
 AR = 0.6
 S/a = 3.25

- (a) FIN EXTENDED THROUGH THE BODY
(BY SINGULARITY METHOD)
- (b) NIELSEN'S SLENDER BODY THEORY [11]

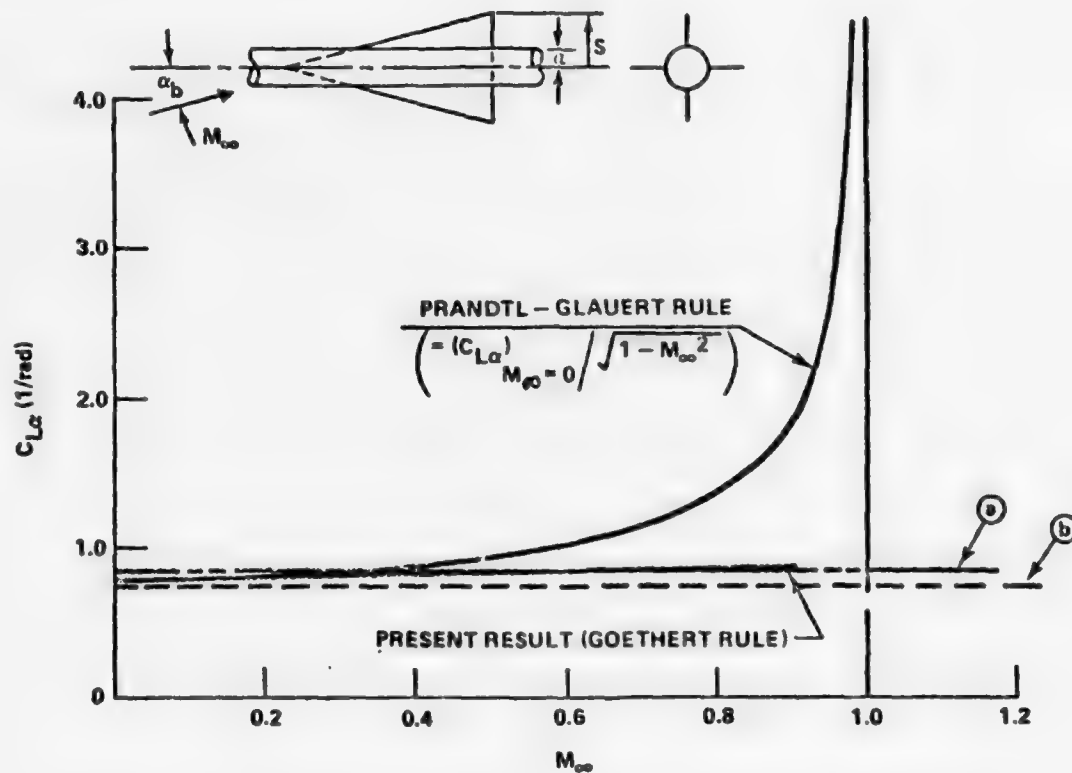


Figure 20. Comparison of subsonic similarity rules for cruciform slender delta fin-body combination at angle of incidence (also includes result from slender body theory).

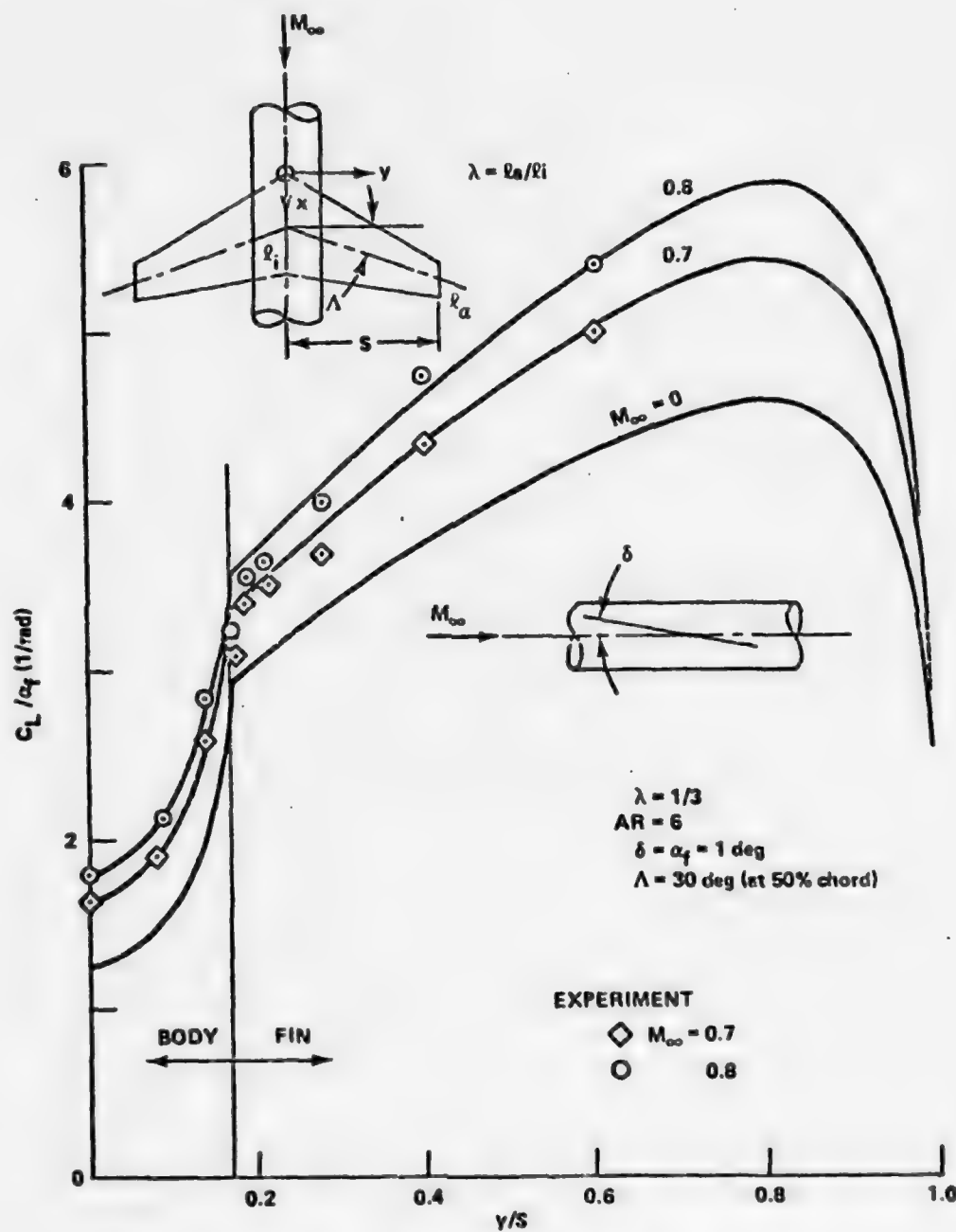


Figure 21. Local lift coefficient on fin body junction showing effect of Mach number change, -30° swept fin [43].

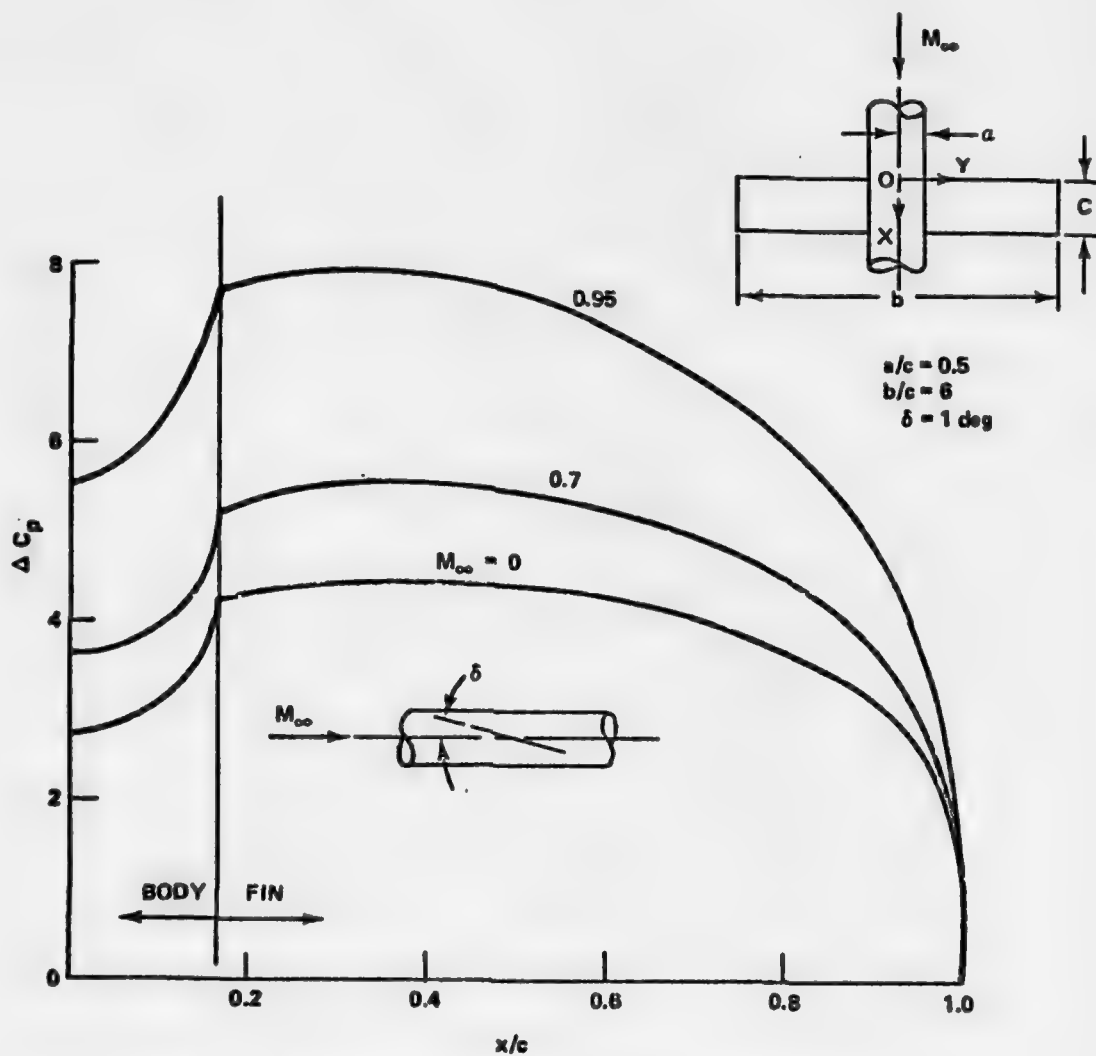


Figure 22. Load distribution on rectangular wing showing the effect of Mach number.

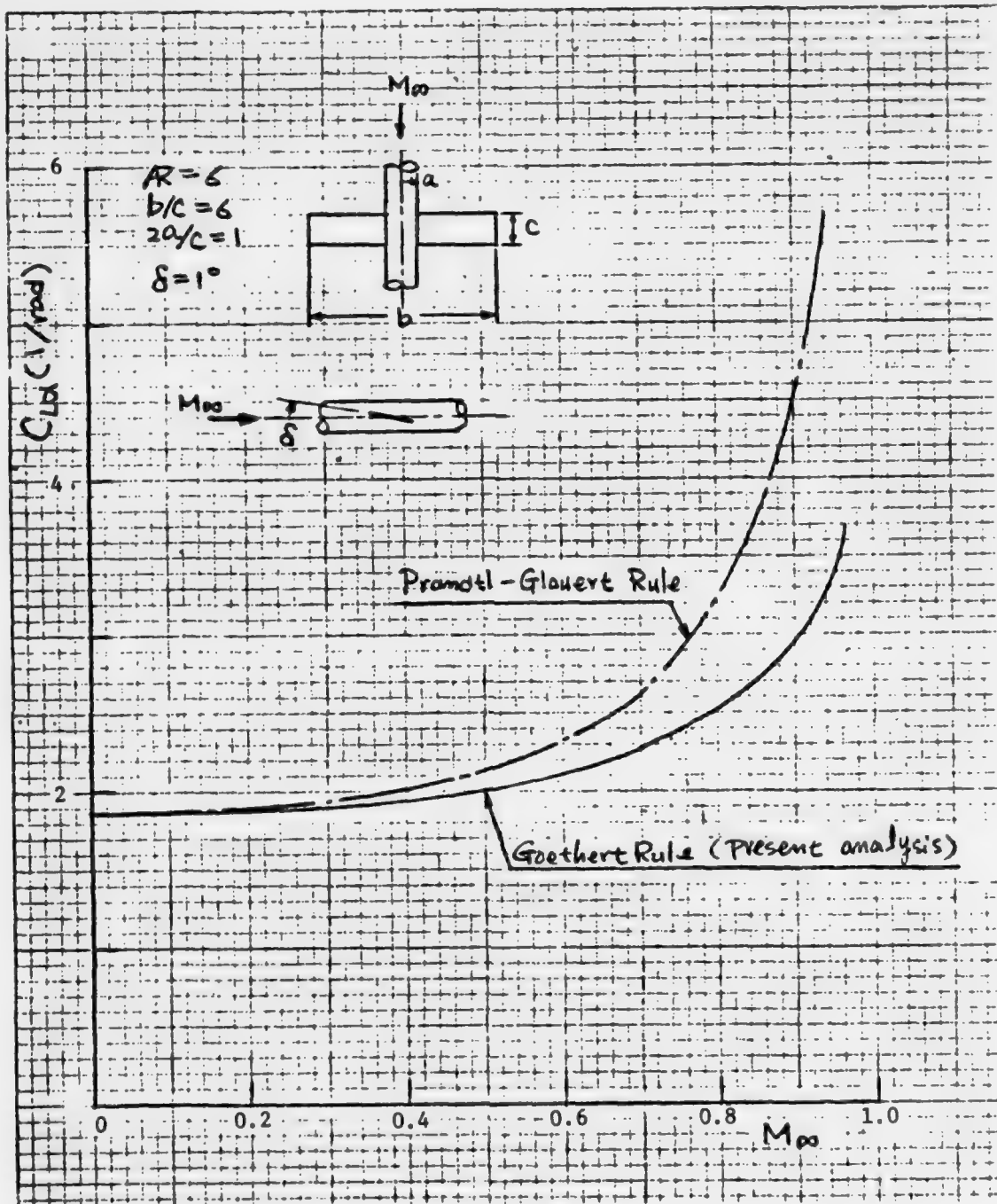


Figure 23. Comparison of subsonic similarity rules for non-slender rectangular fin-body combination.

can be seen very clearly from Figs. 20 and 23, the compressibility effect of lift coefficient on the slender fin-body combination is much more "blunt", or little change up to quite high subsonic speed than the one of the non-slender fin-body combination case.

6. Effect of Small Control Fin on Slender Fin-Body Combination.

One of the advantages of the singularity method is that the effect of a control fin can be computed very easily. The chordwise pressure distribution has been computed for the slender delta fin- (one part of which is used as the control fin) body combination at $M_\infty = 0$, and is given in Fig. 24. The hinge line of the control fin is assumed to be located at the three quarter local chord length of the delta fin. Angle of deflection of this fin is three degrees in the sense of the trailing edge of the control fin downwards. The main fin is assumed to position at zero angle of attack. Although such a computational configuration of the control fin position has not a great meaning in a practical application, yet the effect of its controllability can be seen very clearly. The hinge line can be considered as a singular point. And thus the local pressure goes to infinity. However, this is not a realistic case. The pressure at this point cannot be infinity because of the viscous effect in a real situation. It can be seen that the deflection of a control fin influences over the whole surface of the main fin. Such an influence is very strong near the fin tip. (Compare the present calculation with that in Ref. 9, for example.)

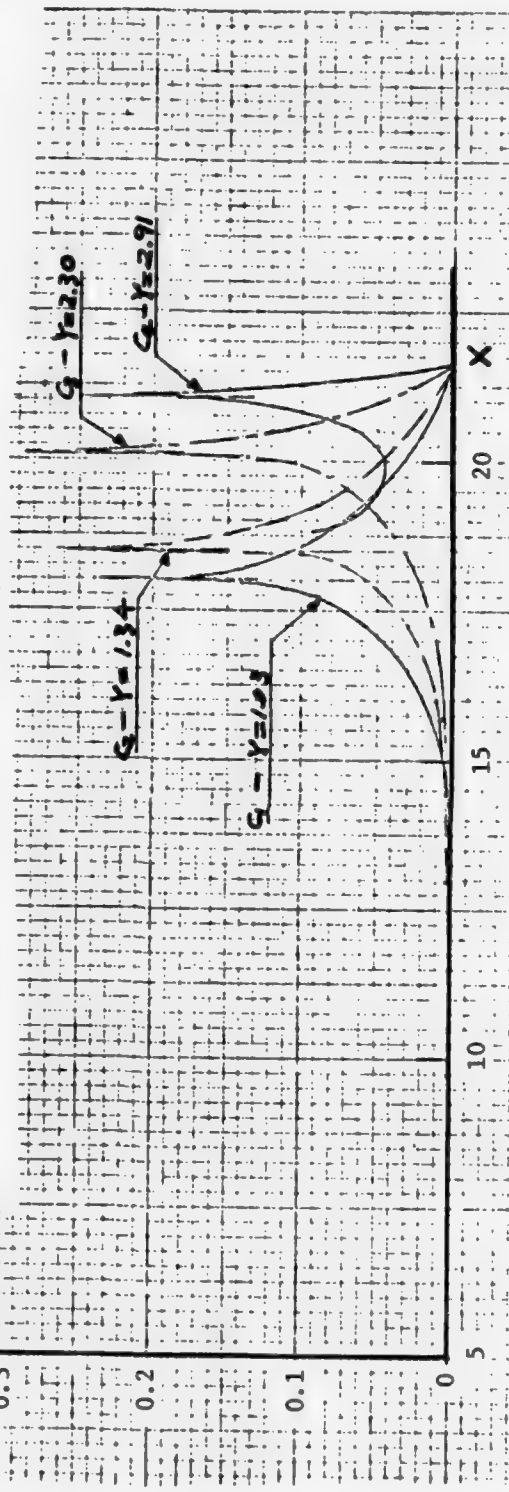
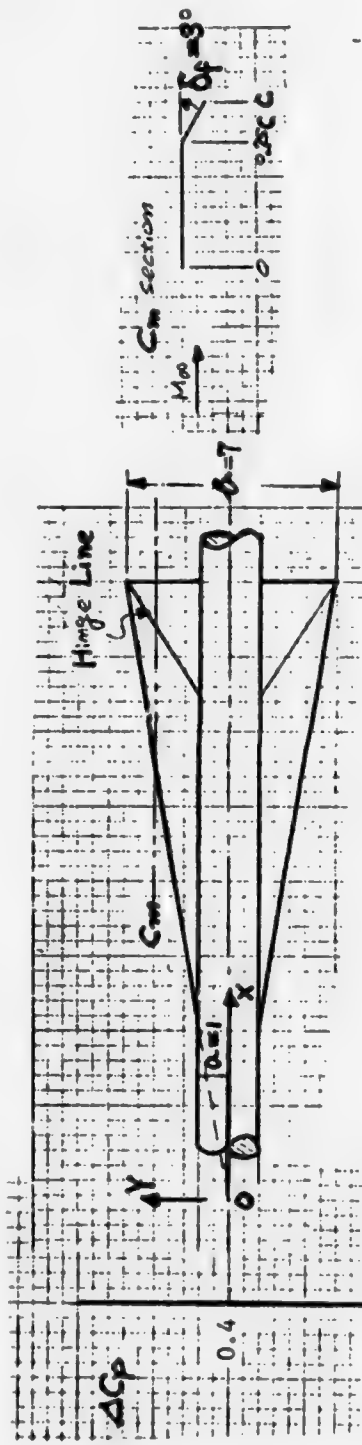


Figure 24. Chordwise pressure distribution due to small control fin
 $(M_{\infty} = 0, \delta_f = 3^\circ)$.

SECTION V. KOERNER'S APPROACH COMPARED WITH OTHER METHODS AND DATA.

1. Comparison with the Slender-Body Theory.

A comparison of computed results by the singularity method and the slender-body theory had been reported in the previous subsection. A surprisingly good agreement by both methods was obtained for the lift coefficient of a cruciform slender delta fin-body combination.

The pressure and the load distributions on a fin-body combination of the same computational model as used in the slender body theory example (see Ref. (2)) was calculated. The results are shown in Figs. 25 and 26. Fig. 25a shows the pressure distribution on one horizontal fin. It is worthwhile to note that the linearized C_p expression was used in the present analysis while the C_p expression in slender-body theory was considered up to the second order terms. The agreement of both methods is excellent. The pressure coefficient was computed azimuthally, at the six positions on the half body, and is shown in Fig. 25b. Note that the difference in the C_p expression is more sensitive on the fin than on the body. This means that the second order expression of the C_p is more important for such slender fin-body combination geometry even though its absolute value is small. Fig. 26 shows the load distribution on a horizontal and a vertical fin. It can be seen from Figs. 25 and 26 that the results of the present analysis and slender-body theory have agreed satisfactorily with each other. From these comparisons, it can be concluded that both methods will yield a similar result for a small aspect ratio fin-body combination geometry. This merely proves that the singularity method can be applied for fins with a wide range of aspect ratios and, therefore, is more versatile.

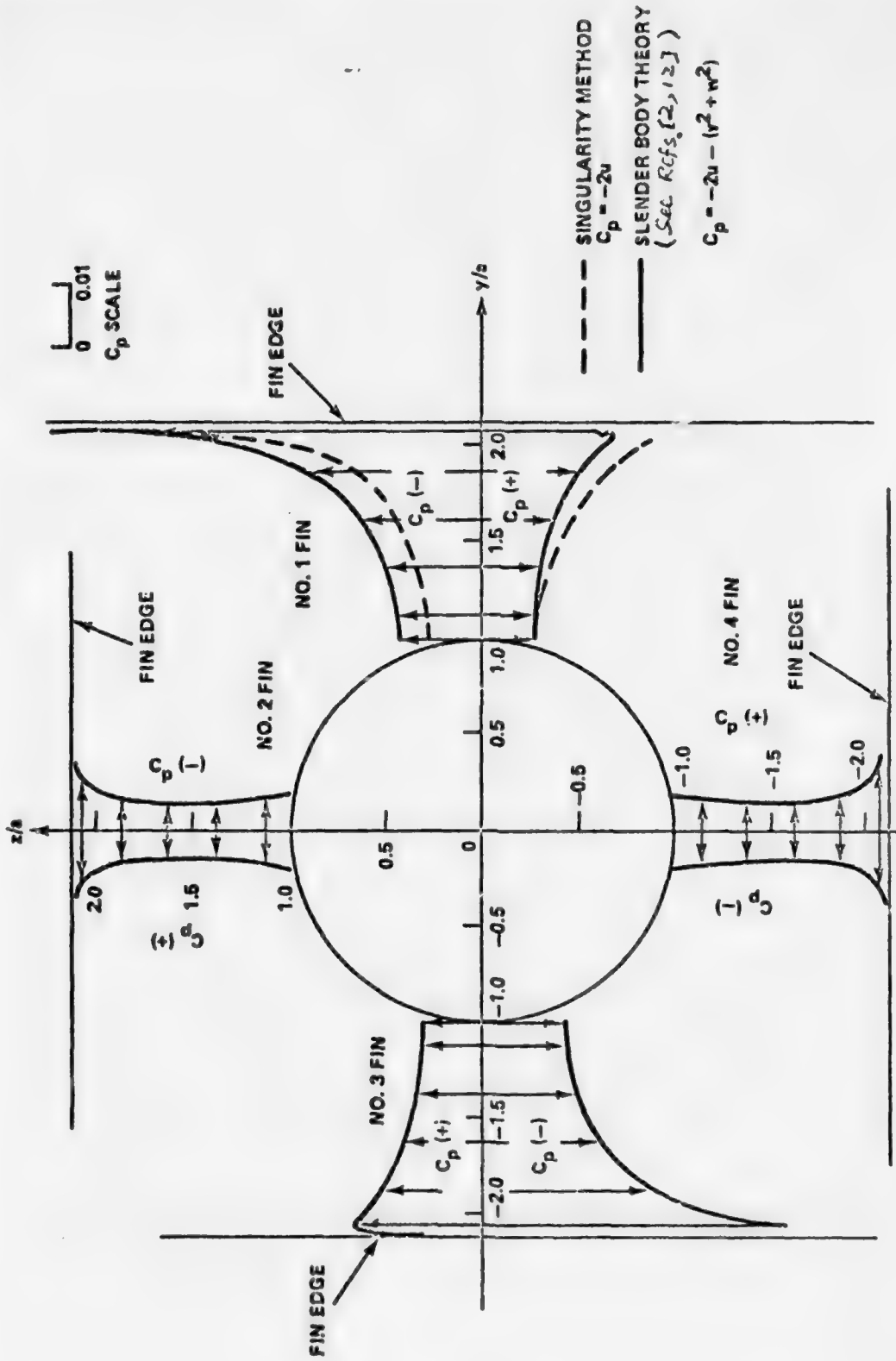


Figure 25a. Comparison with slender body theory, C_p distribution pattern on fins ($\delta = 3^\circ$, only horizontal fins are canted).

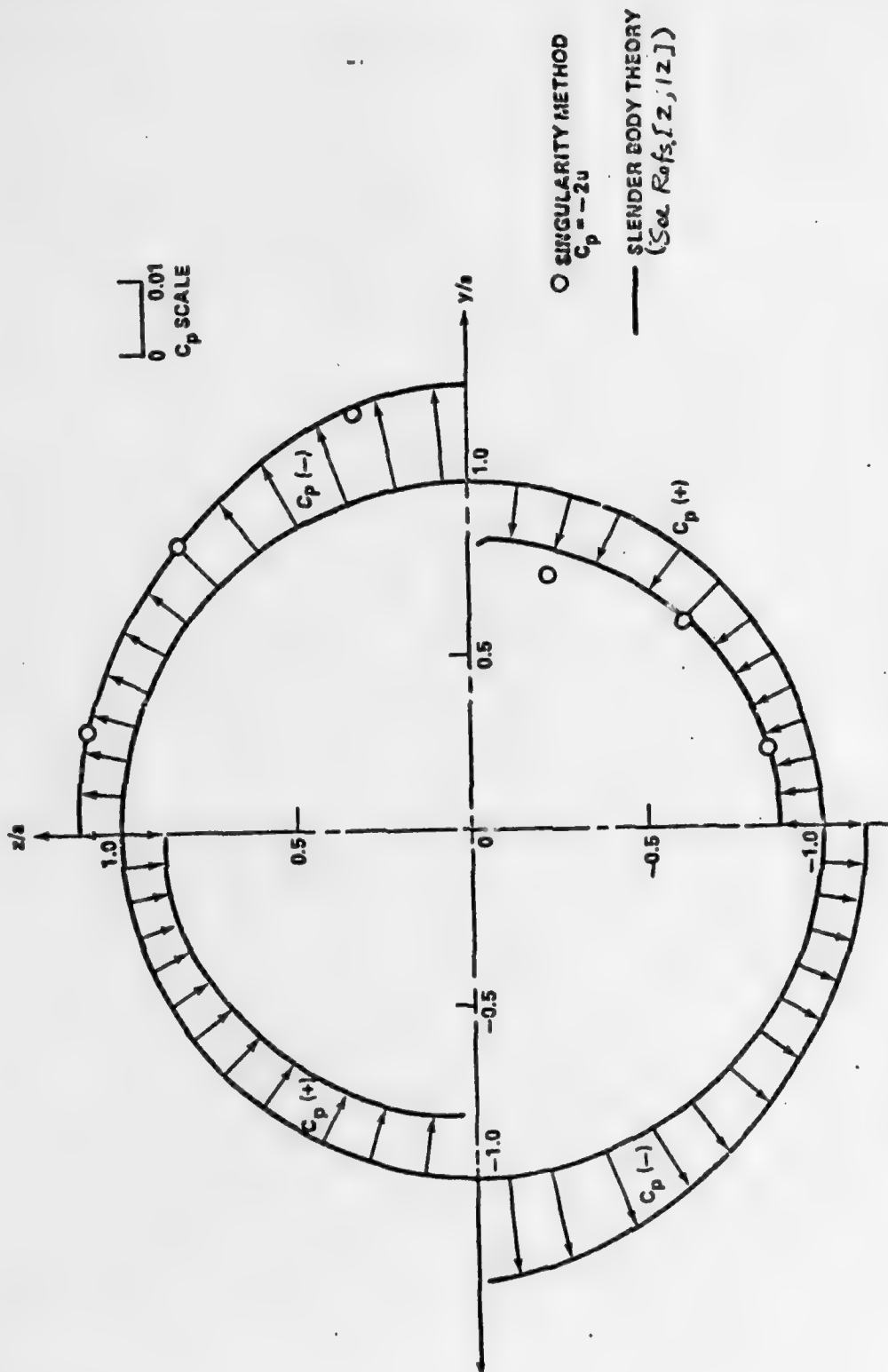


Figure 25b. Comparison with slender body theory on C_p distribution pattern on body ($-\delta = 3^\circ$, only horizontal fins are canted).

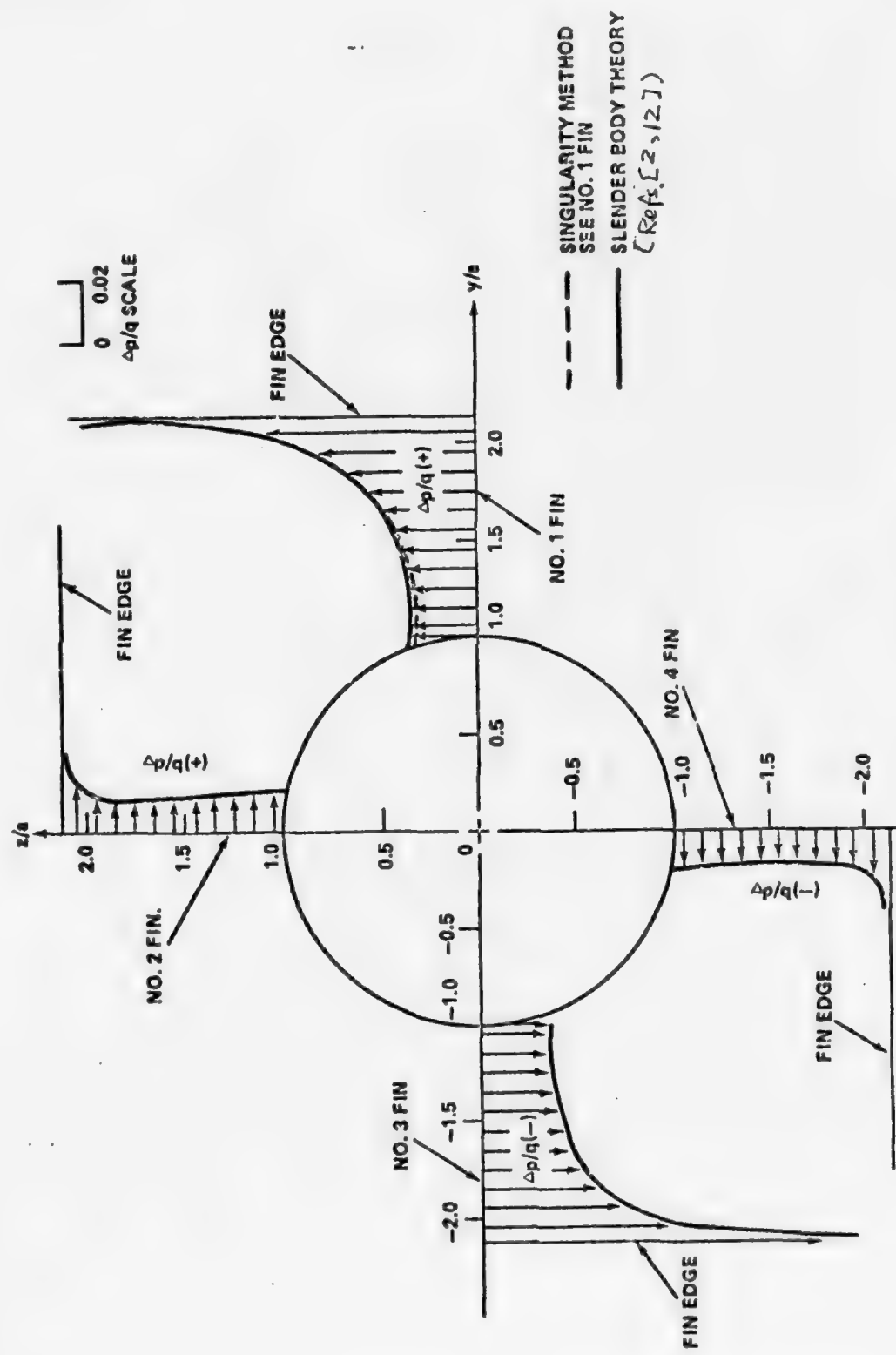


Figure 26. Comparison with slender body theory of load distribution pattern on fins ($-\delta = 3^\circ$, only horizontal fins are canted).

2. Comparisons with FLEXSTAB Singularity Distribution Method and Data.

FLEXSTAB's method (Ref. 8) has been applied to a wing-body combination of an aircraft flying at subsonic, transonic and supersonic speeds (Refs. 5 and 8). A comparison of computations based on the Koerner's scheme, as adapted in this analysis, was made to those configurations calculated based on FLEXSTAB's technique. The computational wing-body configuration which is taken from Ref. (8) is shown in Fig. 27, i.e., the aspect ratio of the wing is 1.65, taper ratio is 0.10, and sweptback angle of the leading edge is 71.2° , respectively.

The paneling scheme employed for the present calculations as well as those by the FLEXSTAB method are given in Fig. 28. The main difference of FLEXSTAB's method compared to the Koerner's technique is that the treatment on the "body" is different. FLEXSTAB's method treats the body by a number of discrete vortices distributed on the mean body surface. The main body surface is approximated by a number of rectangular strips with free streamwise surfaces (Ref. 5). In addition, FLEXSTAB's method was more complicated and allows one to take into account the thickness, the camber and the twist effects of a wing by a distribution of additional source-sink and vortex singularities.

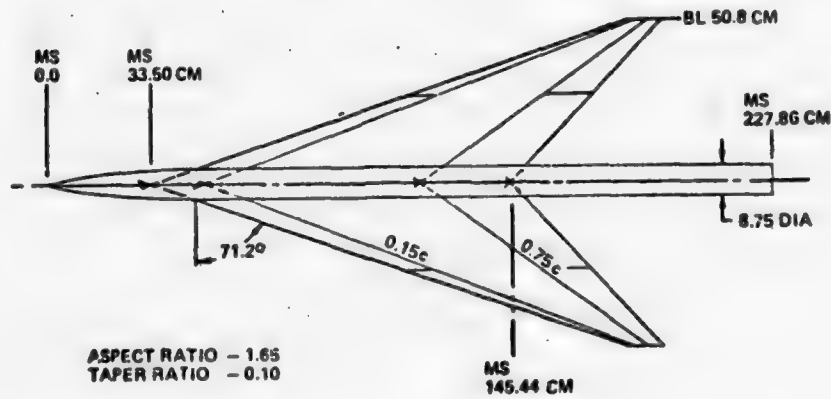
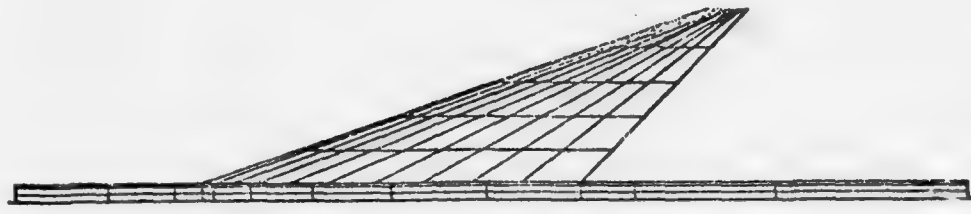


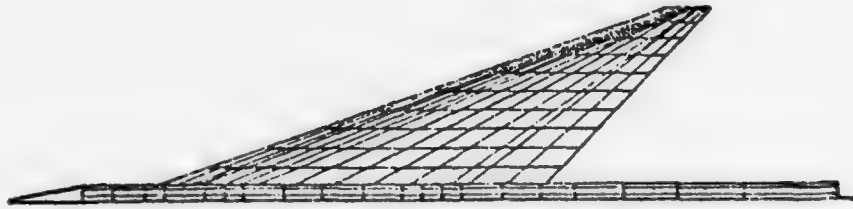
Figure 27. Computational wing-body configuration (Ref. [8]).



(a) PRESENT PANELING SCHEME (FOR ZERO DEFLECTED FLAP)



(b) PRESENT PANELING SCHEME (FOR A DEFLECTED FLAP)



(c) FLEXSTAB PANELING SCHEME. (Ref. 8)

Figure 28. Paneling schemes.

2.1 Effect of Angles of Attack on Chordwise Pressure Distribution.

The calculated chordwise pressure distribution on the wing is shown in Fig. 29, in which the angle of incidence of the body was taken two degrees, and the free-stream Mach number was 0.85. The computation was made at three different spanwise points. The agreement with FLEXSTAB's result was surprisingly good. The agreement with the experimental data was also satisfactorily good, except in the region very close to the wing leading edge, where a sudden pressure drop can be seen because of the local flow separation. The case of the angle of incidence of eight degrees is shown in Fig. 30. The agreement with FLEXSTAB's method was very good in this case also. The agreement with the experimental data was still very good at the region very close to the wing root although the small fluctuation of ΔC_p was caused by the present numerical calculation. However, the agreement with data was not so good from the leading edge to the mid-chord. The reason for this disagreement with data may be attributed to the flow separation from the sharp leading edge because of a considerably higher angle of incidence. A further study on such a situation is needed.

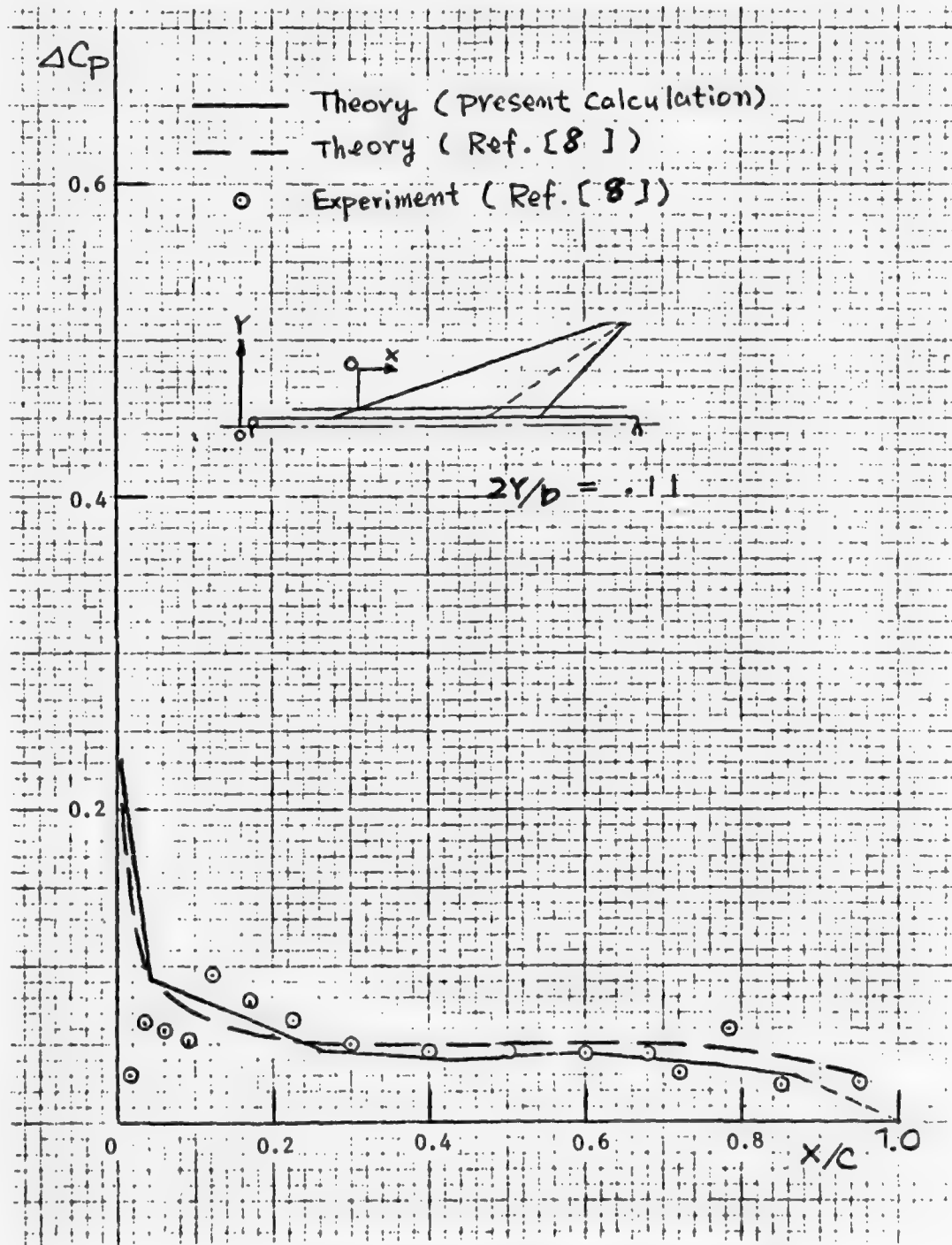


Figure 29a. Flat wing ($\alpha = 2^\circ$, $M_\infty = 0.85$).

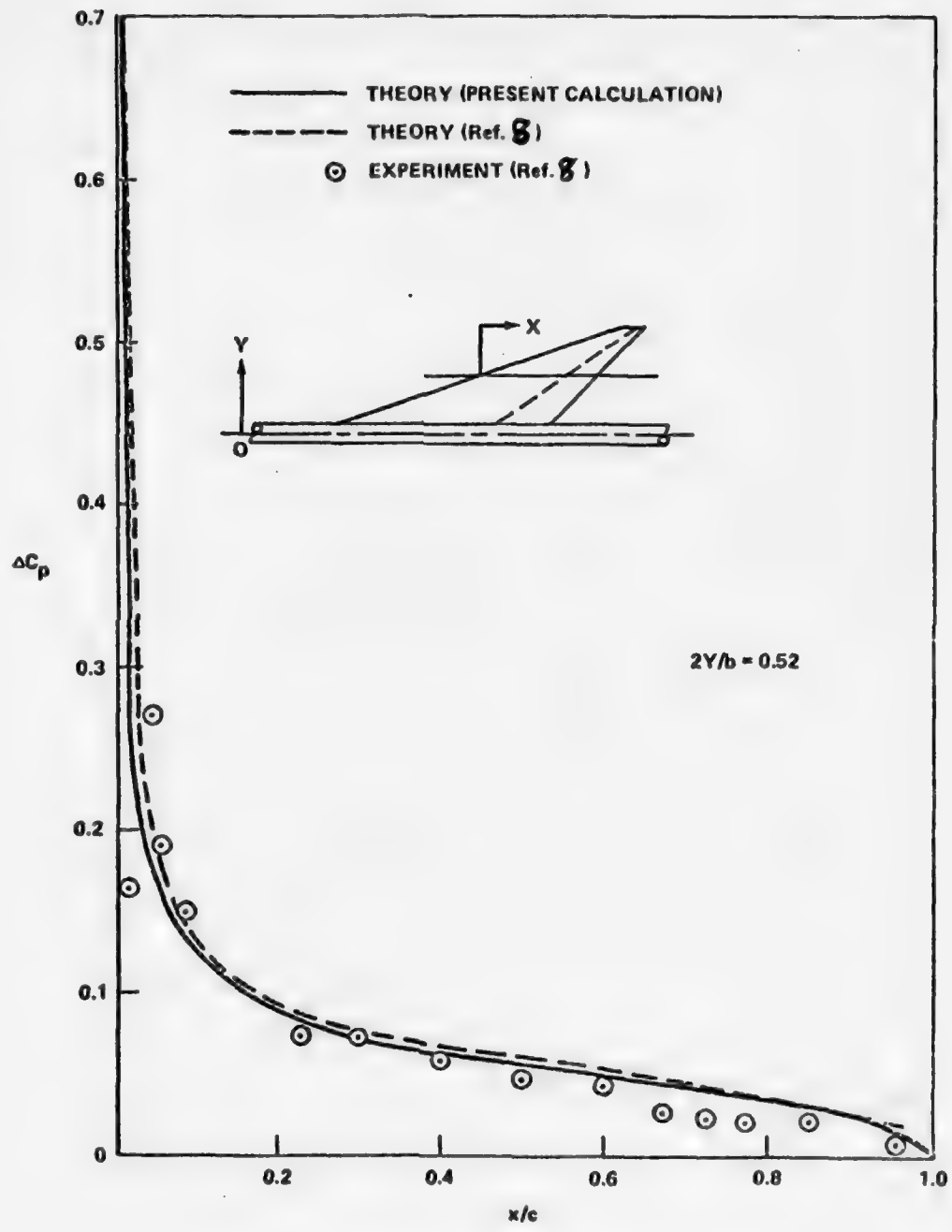


Figure 29b. Flat wing ($\alpha = 2^\circ$, $M_\infty = 0.85$).

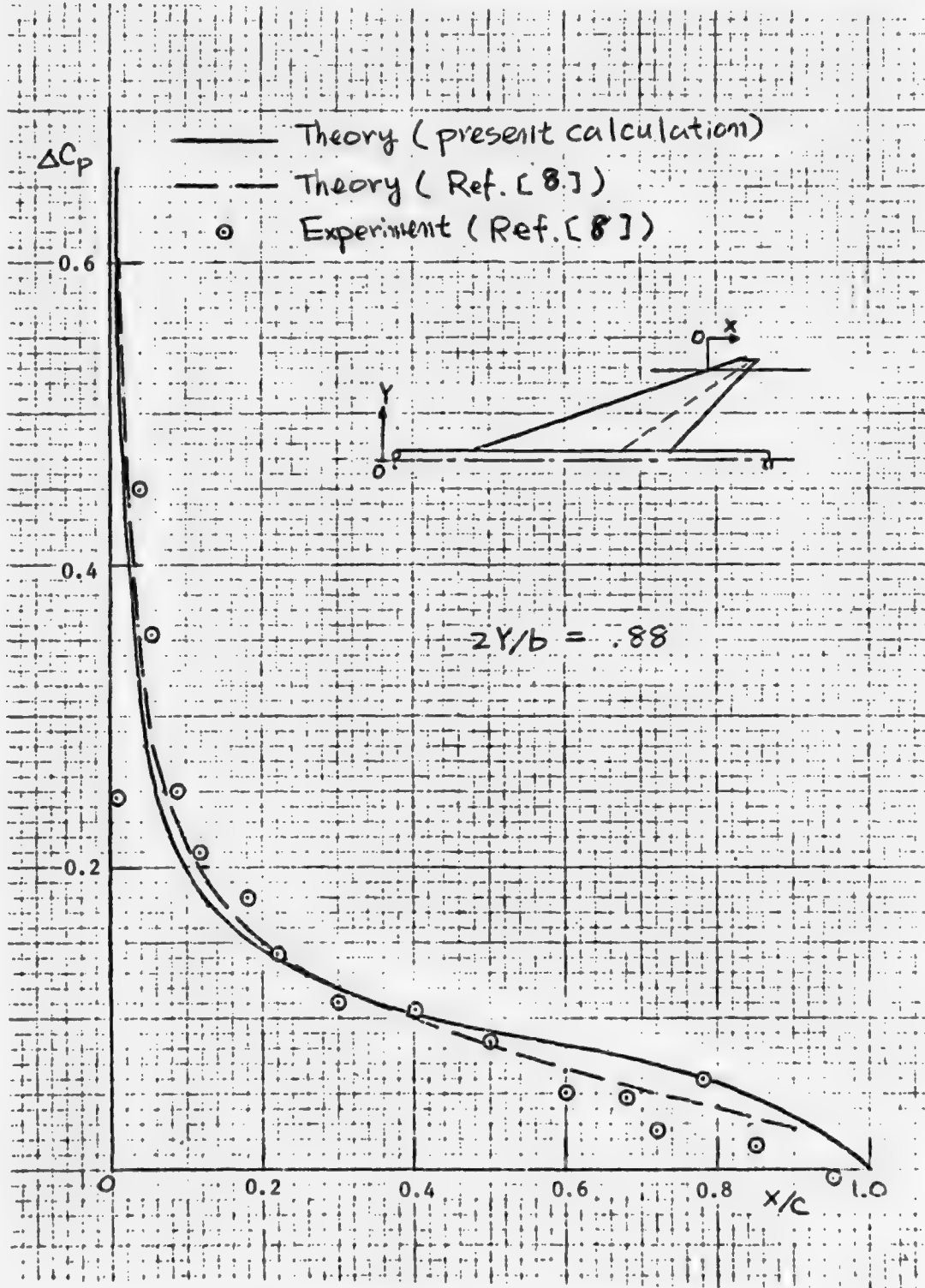


Figure 29c. Flat wing ($\alpha = 2^\circ$, $M_\infty = 0.85$).

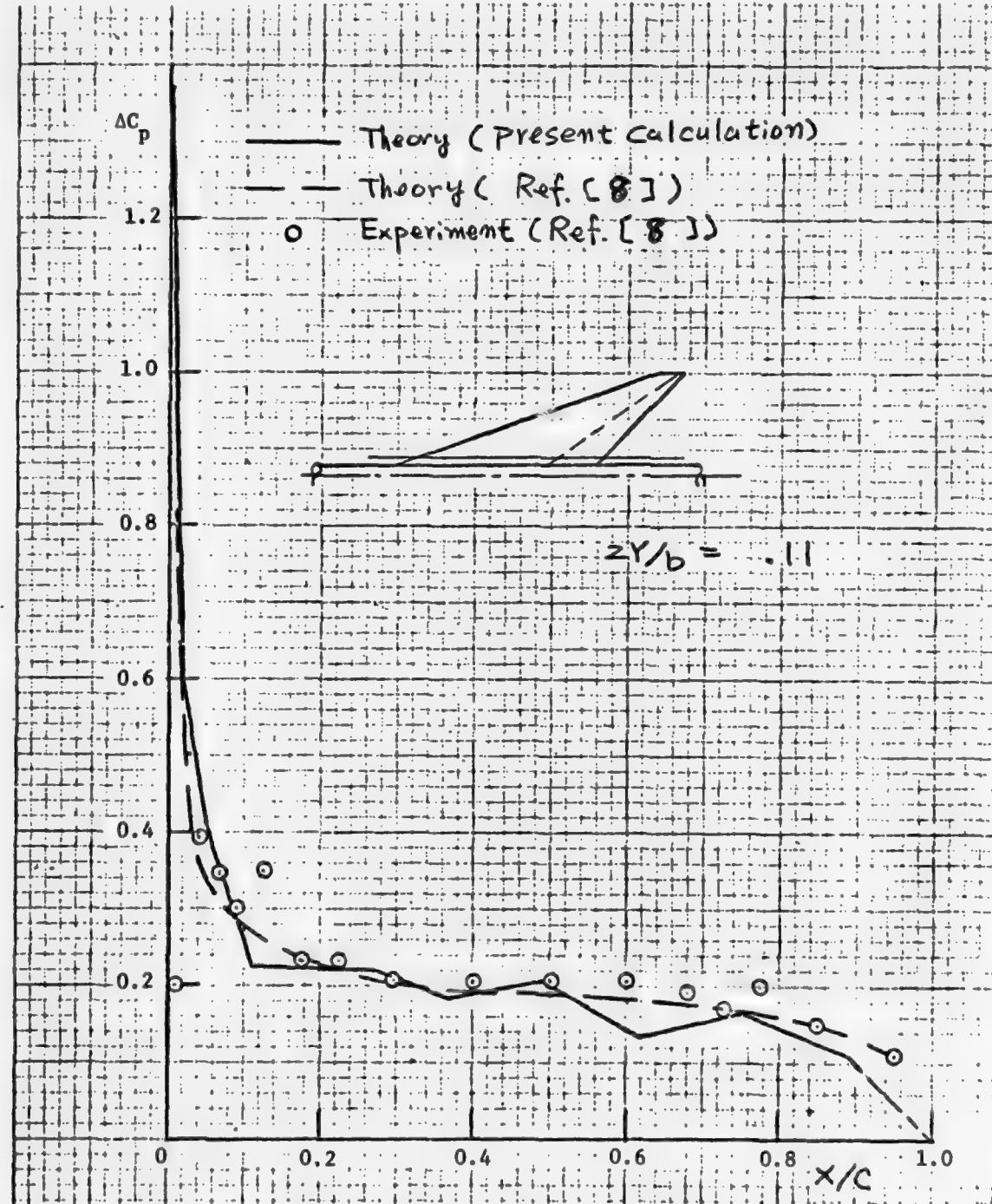


Figure 30a. Flat Plate ($\alpha = 8^\circ$, $M_\infty = 0.85$).

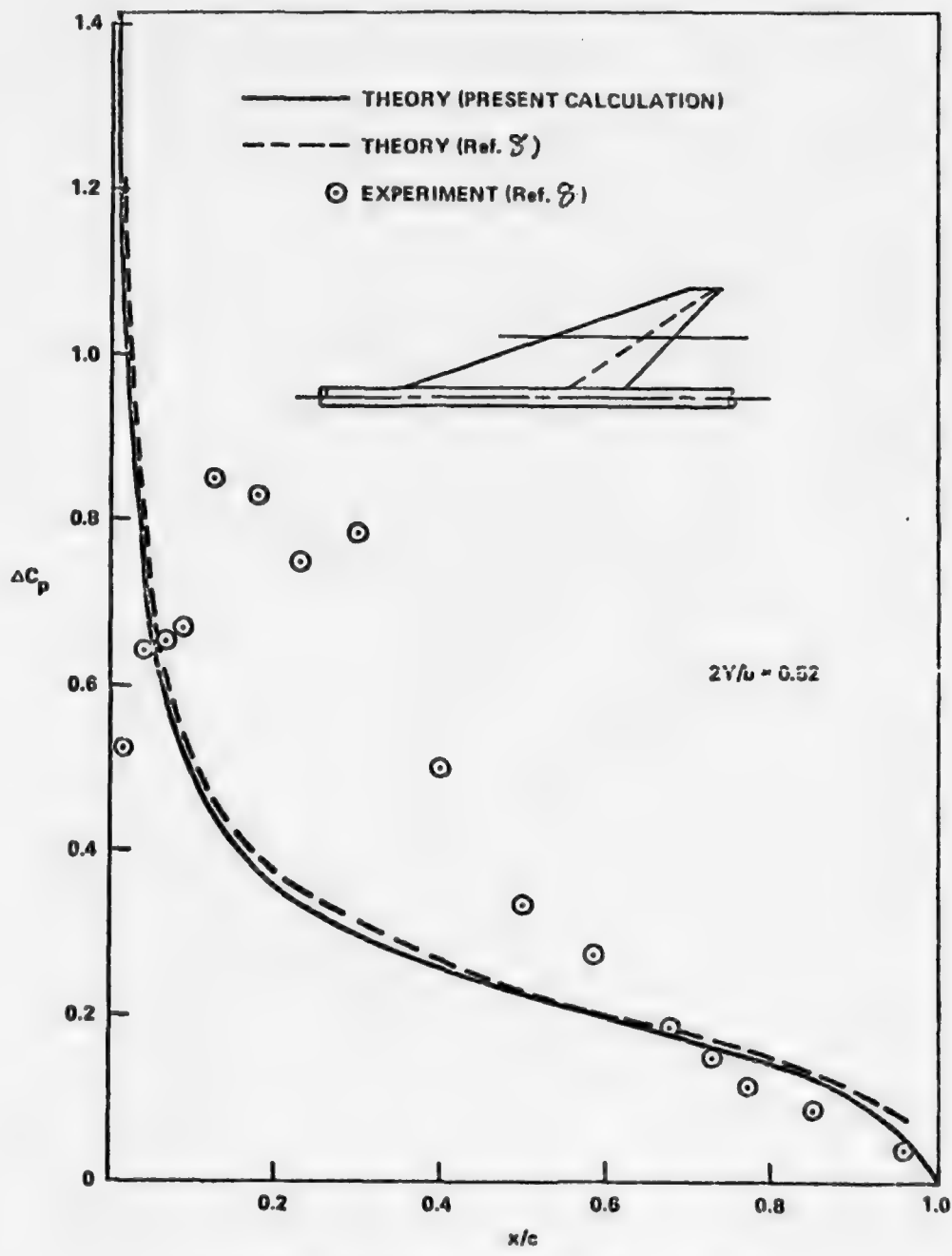


Figure 30b. Flat wing ($\alpha = 8^\circ$, $M_\infty = 0.85$).

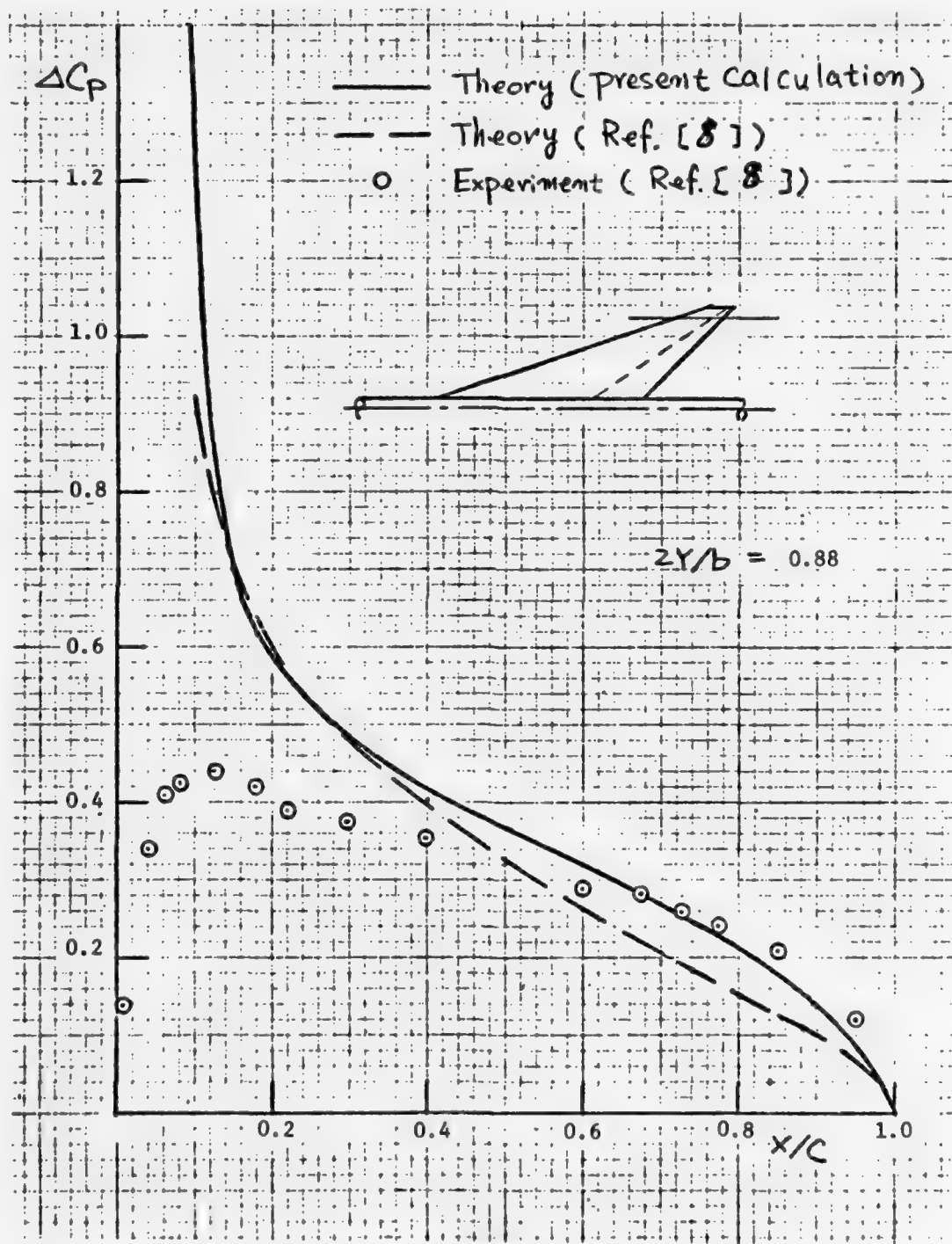


Figure 30c. Flat wing ($\alpha = 8^\circ$, $M_\infty = 0.85$).

2.2 Flap Effect on Chordwise Pressure Distribution.

A further comparison with the FLEXSTAB method was made on the effect of the flap of the wing. The calculated chordwise pressure distributions, based on both methods, are given in Figs. 31 to 33. In these cases, it is assumed that the wing has zero angle of attack and the flap angle is 8.3° . The following two examples (Figs. 31 and 32) show the chordwise C_p distribution on the upper and the lower surfaces of a wing and deflected flap at $M_\infty = 0.4$ and 0.85 , respectively. The calculated position is near the mid span. $\Delta C_p/2$ was taken for C_p in the present calculation (see Eq. 16). Fig. 31 shows the chordwise C_p distribution at $M_\infty = 0.4$. No correction about the round leading edge of a flat wing was made in the present analysis. Therefore, the C_p close to the leading edge of the wing has resulted in a rather poor agreement with those of the FLEXSTAB and experimental data. Except for this region of the wing, the agreement of the C_p distribution calculated by the present analysis compared favorably with data. The poor agreement with data near the flap hinge line is attributed to the local flow separation on the wing because of a considerably higher flap angle.

Fig. 32 shows the chordwise C_p distribution at $M_\infty = 0.85$. In this case, the values of C_p from Ref. (8) were replotted for eliminating the influence of the round leading edge of the wing at $\delta_F = 0^\circ$ as shown in this figure. The agreement of the present calculation with that of the FLEXSTAB was good, in general, over the whole surface of the wing, and with the experimental data, except the regions very close to the wing leading edge and the flap hinge line. The poor agreement with data near the flap hinge line is a result from the same reason as mentioned before. The variation of C_p with the free stream Mach number was very small in this type of body configuration.

The calculated chordwise pressure (ΔC_p) distribution at three different spanwise positions at $M_\infty = 0.85$ is shown in Fig. 33.

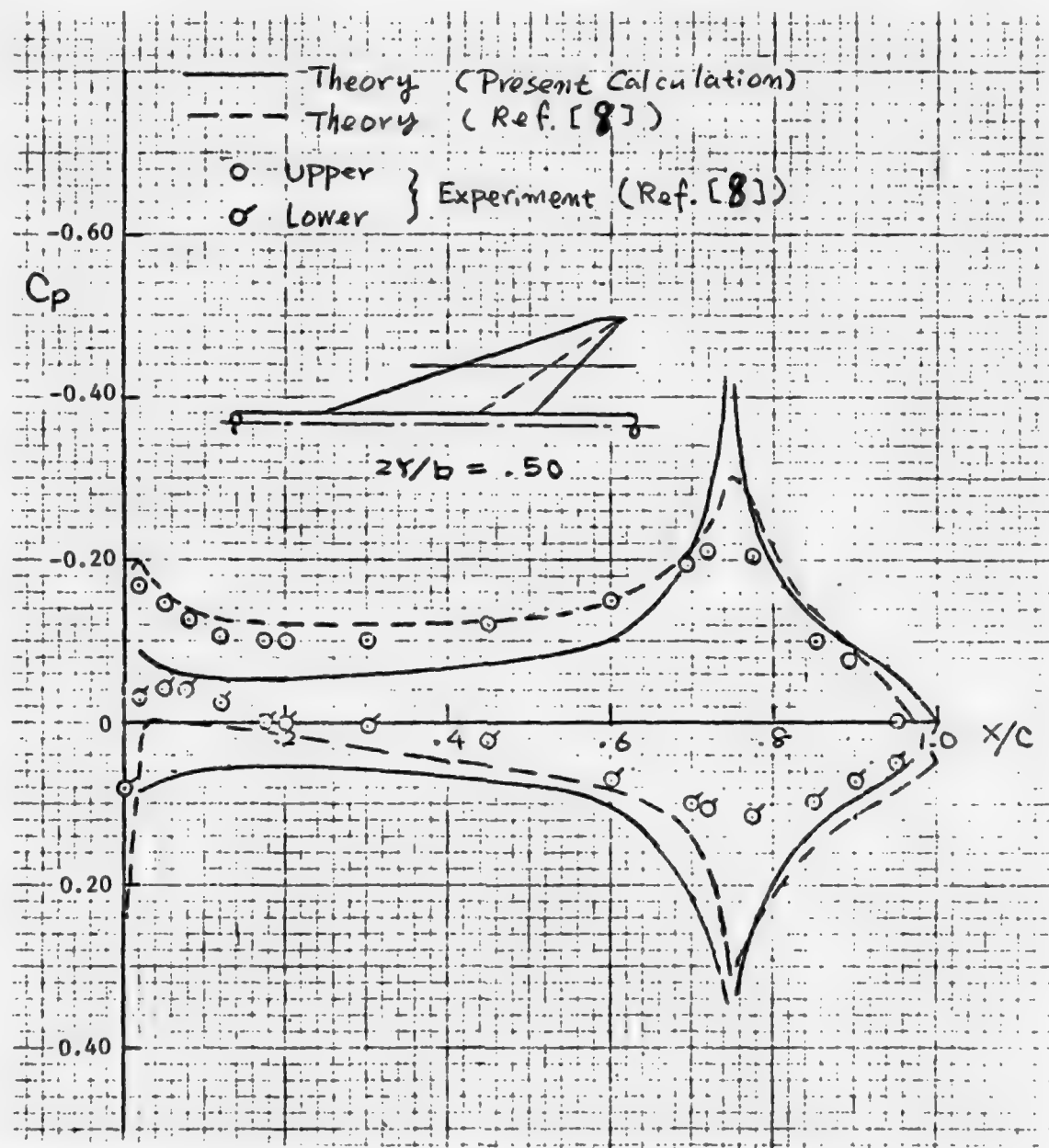


Figure 31. Surface pressure distribution of flat wing
 (trailing-edge $\delta_F = 8.3^\circ$, $\alpha = 0$, $M_\infty = 0.4$)

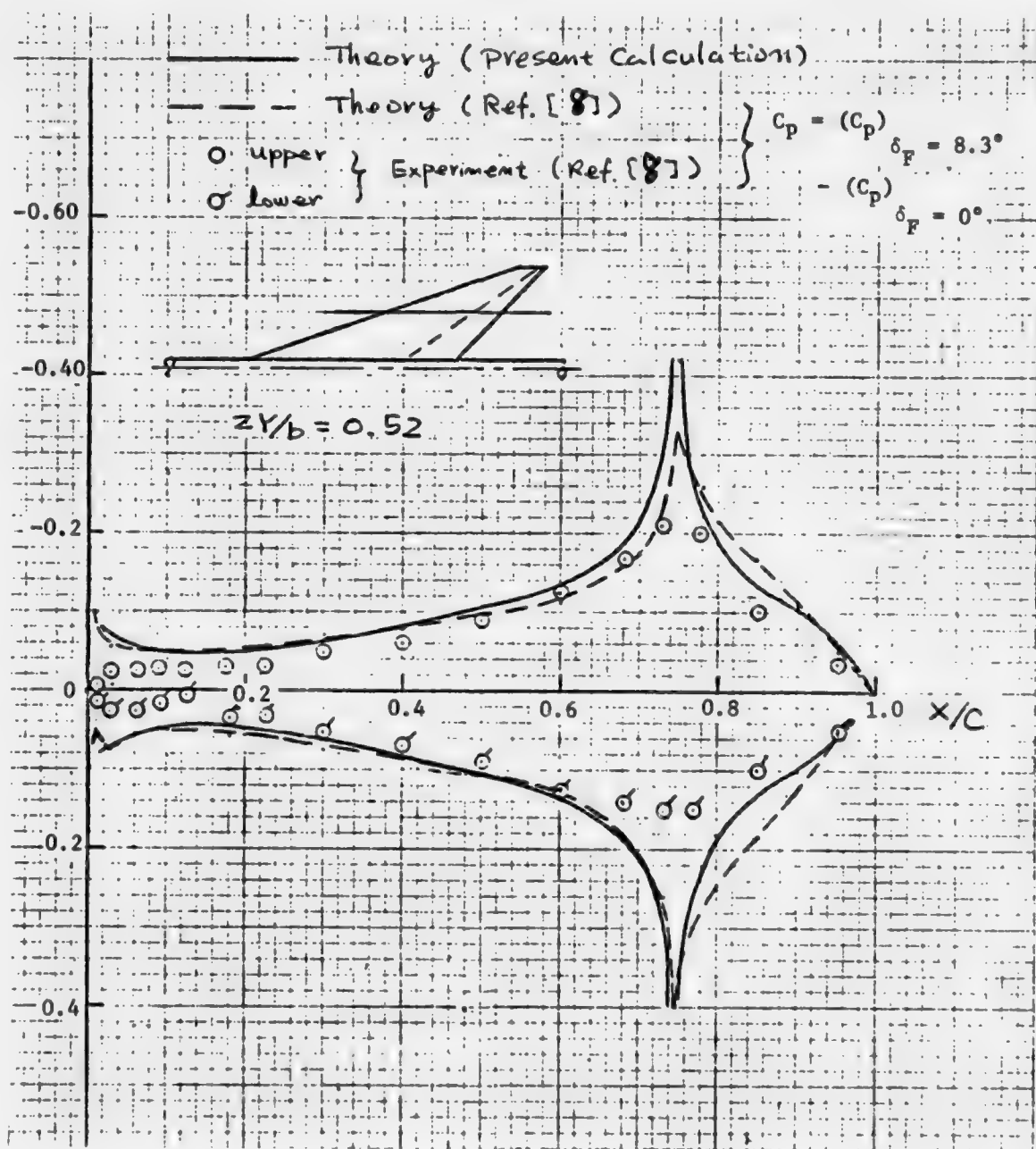


Figure 32. Surface pressure distribution of flat wing
(trailing-edge $\delta_F = 8.3^\circ$, $\alpha = 0$, $M_\infty = 0.85$).

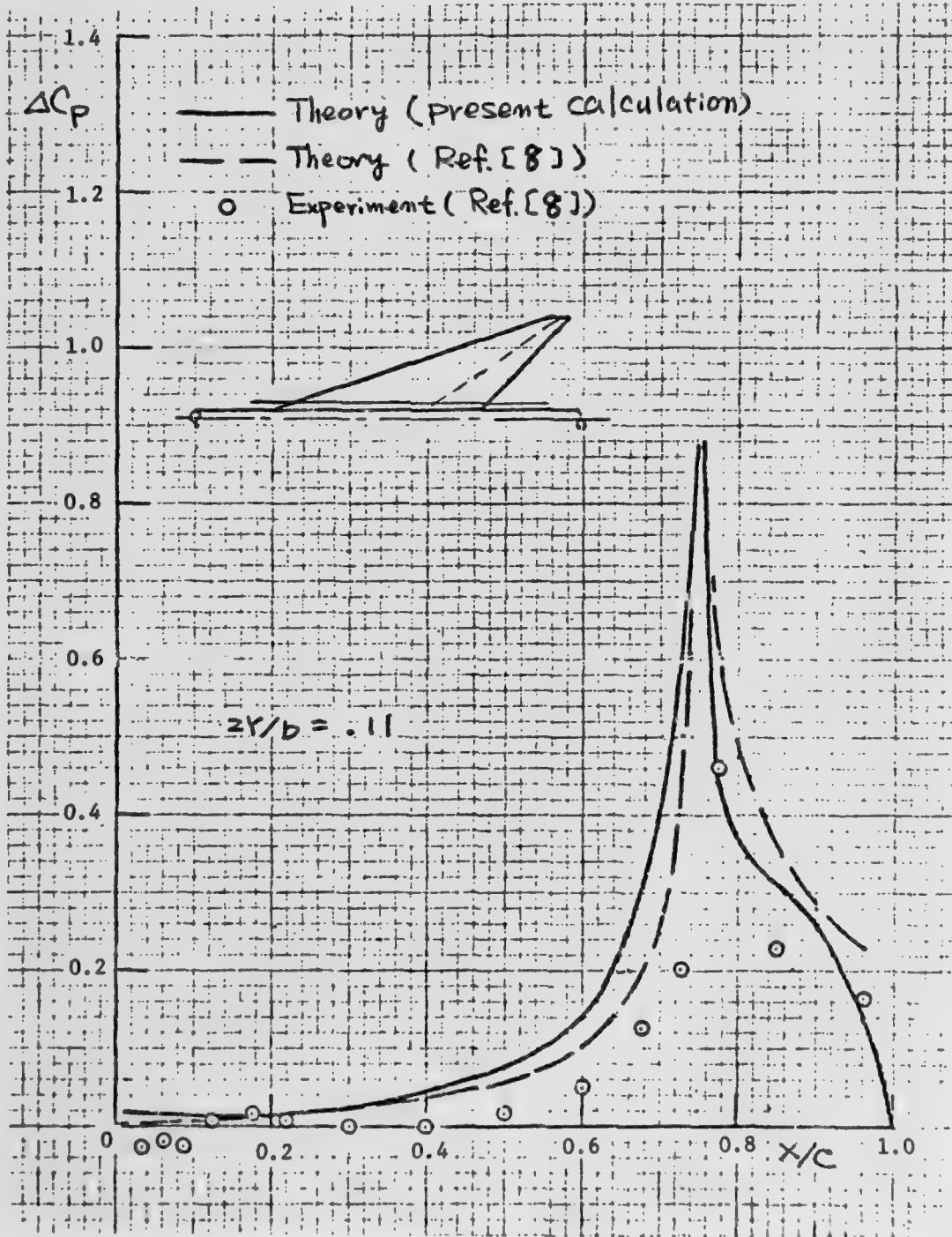


Figure 33a. Flat wing (trailing edge $\delta_F = 8.3^\circ$, $\alpha = 0$, $M_\infty = 0.85$).

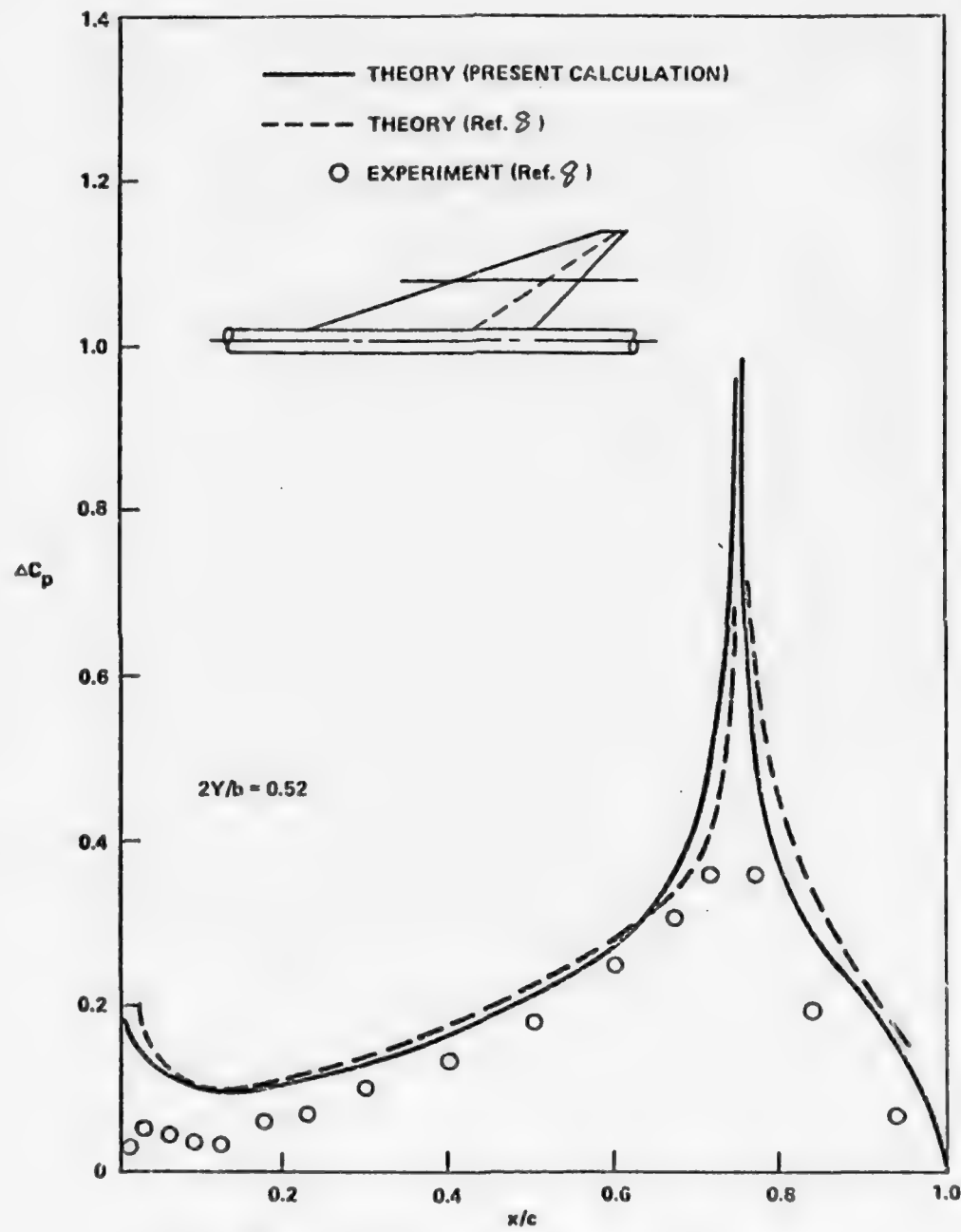


Figure 33b. Flat wing with deflected flap (trailing edge $\delta_F = 8.3^\circ$, $\alpha = 0^\circ$, $M_\infty = 0.85$).

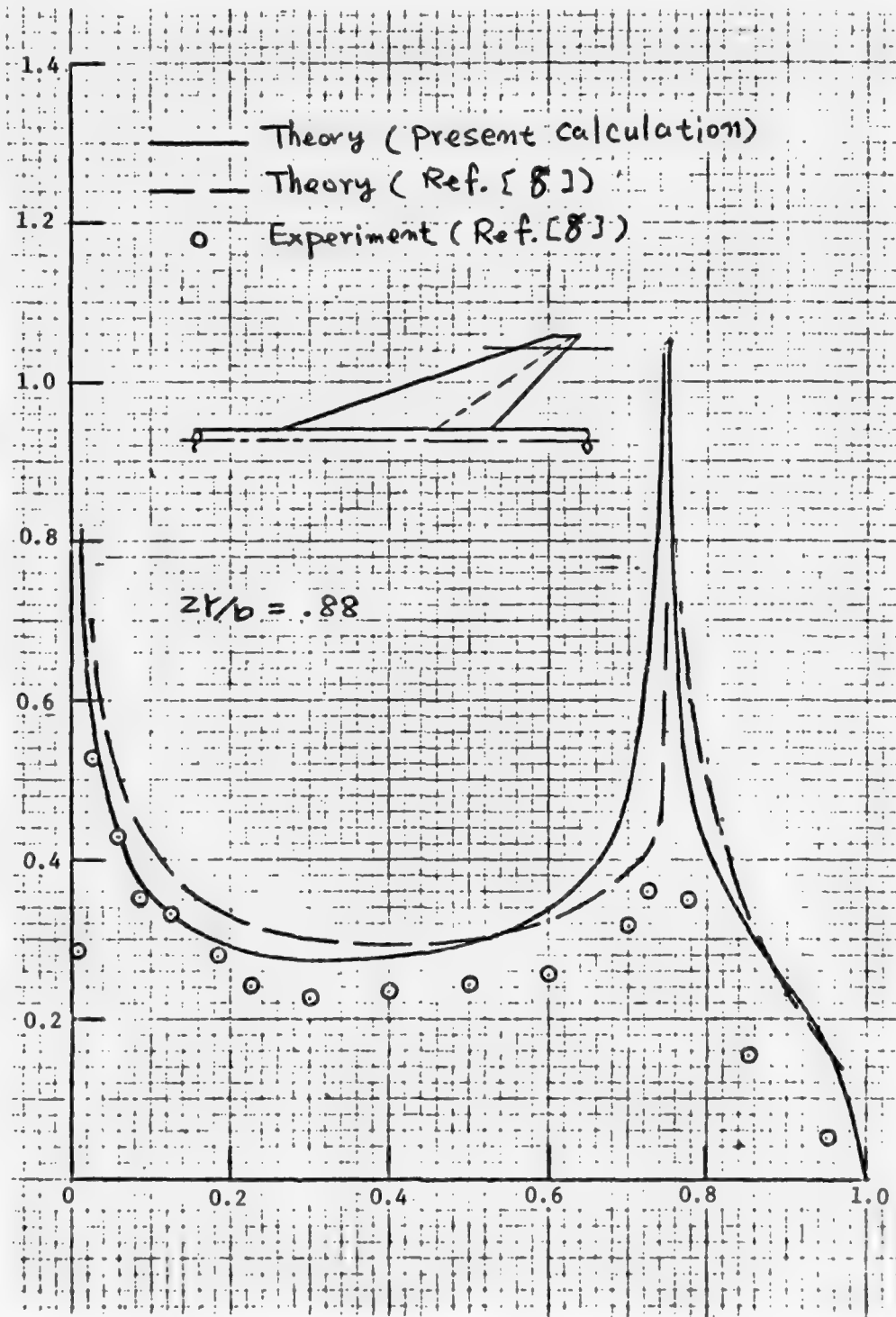


Figure 33c. Flat wing (trailing-edge $\delta_F = 8.3^\circ$, $\alpha = 0$, $M_\infty = 0.85$)

The agreement on both methods is good, however, the inviscid flow theory predicts a larger pressure difference than data indicated over the flap surface. Again, such a disagreement is probably attributed to the flow separation on the upper wing because of a considerably higher flap angle given in this example.

2.3 Spanwise Load Distribution.

The spanwise load (directly related to the lift) distribution was computed for two different angles of attack cases. And then they were compared with the results by the FLEXSTAB method. They are shown in Fig. 34 (for the chordwise pressure distributions, see Figs. 29 and 30). It was assumed that there is little difference between the lift and the normal force in this case, or, it is assumed negligibly small. In the case of the angles of attack of two degrees, the agreement of the present calculation with both the FLEXSTAB and data is satisfactorily good; this is apparent from Figs. 29a to c. On the other hand, the poor agreement with the experimental data occurred in the region from the mid span to the wing tip at the angles of attack of eight degrees. This can be also understood by looking back at Figs. 30b and c. The satisfactorily good agreement can be seen at the region below the mid span.

Figs. 35 and 36 show the spanwise load distribution in the case of a deflected flap at Mach number 0.4 and 0.85, respectively. Nonetheless, even with the large flap deflections, both the theoretical calculations were in good agreement with the experimental data. This means that the flap deflection does not influence the spanwise load distribution so much in this case as the angle of attack case did (see the case at $\alpha = 8^\circ$ in Fig. 34), because the part of the flap is small as compared with the total wing surface area. Little difference in the compressibility influence can be seen in this wing-body configuration (also, see Fig. 37 for the compressible effect to the normal force slope).

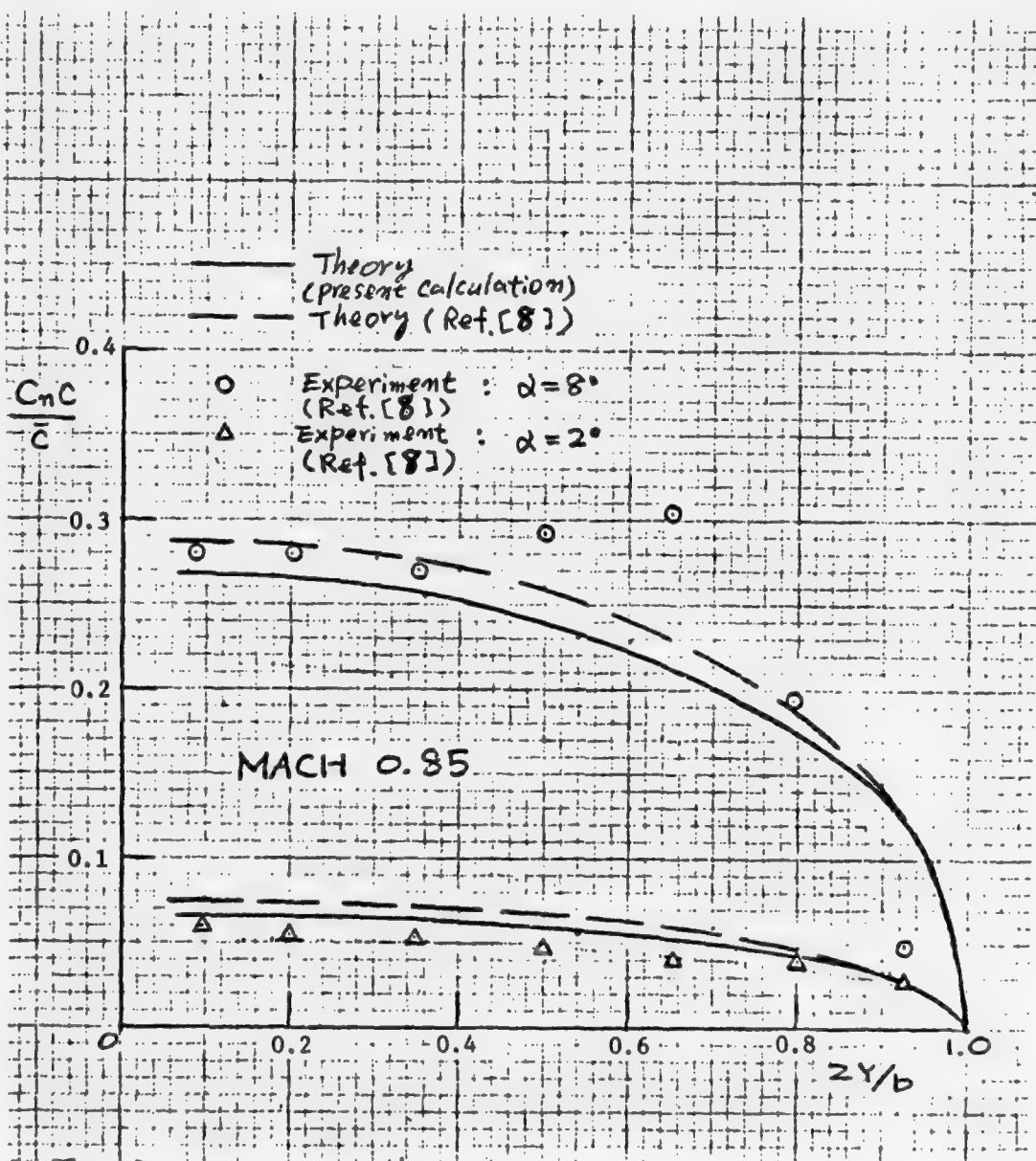


Figure 34. Spanwise load distribution ($M_\infty = 0.85$).

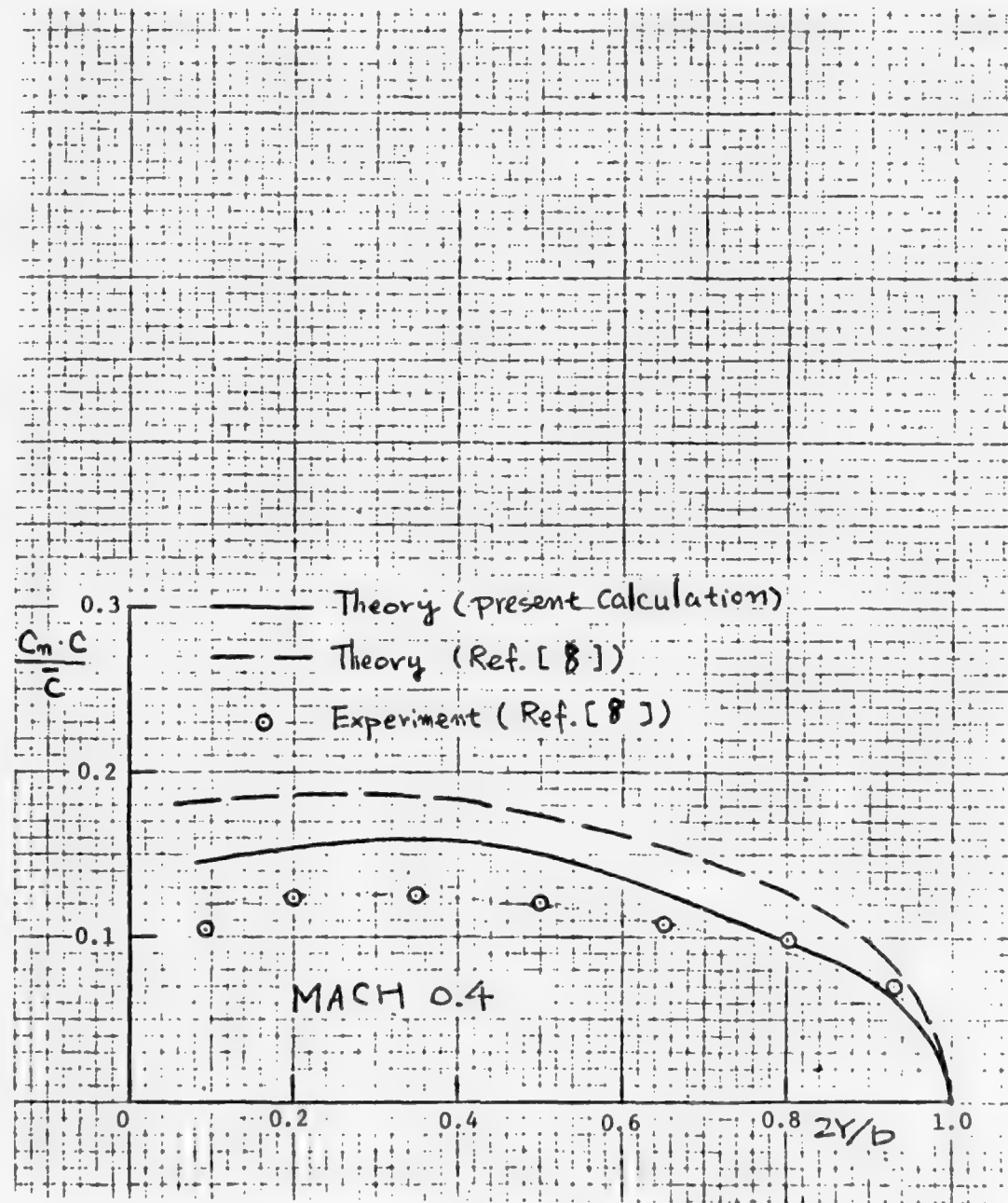


Figure 35. Spanwise load distribution (trailing-edge).

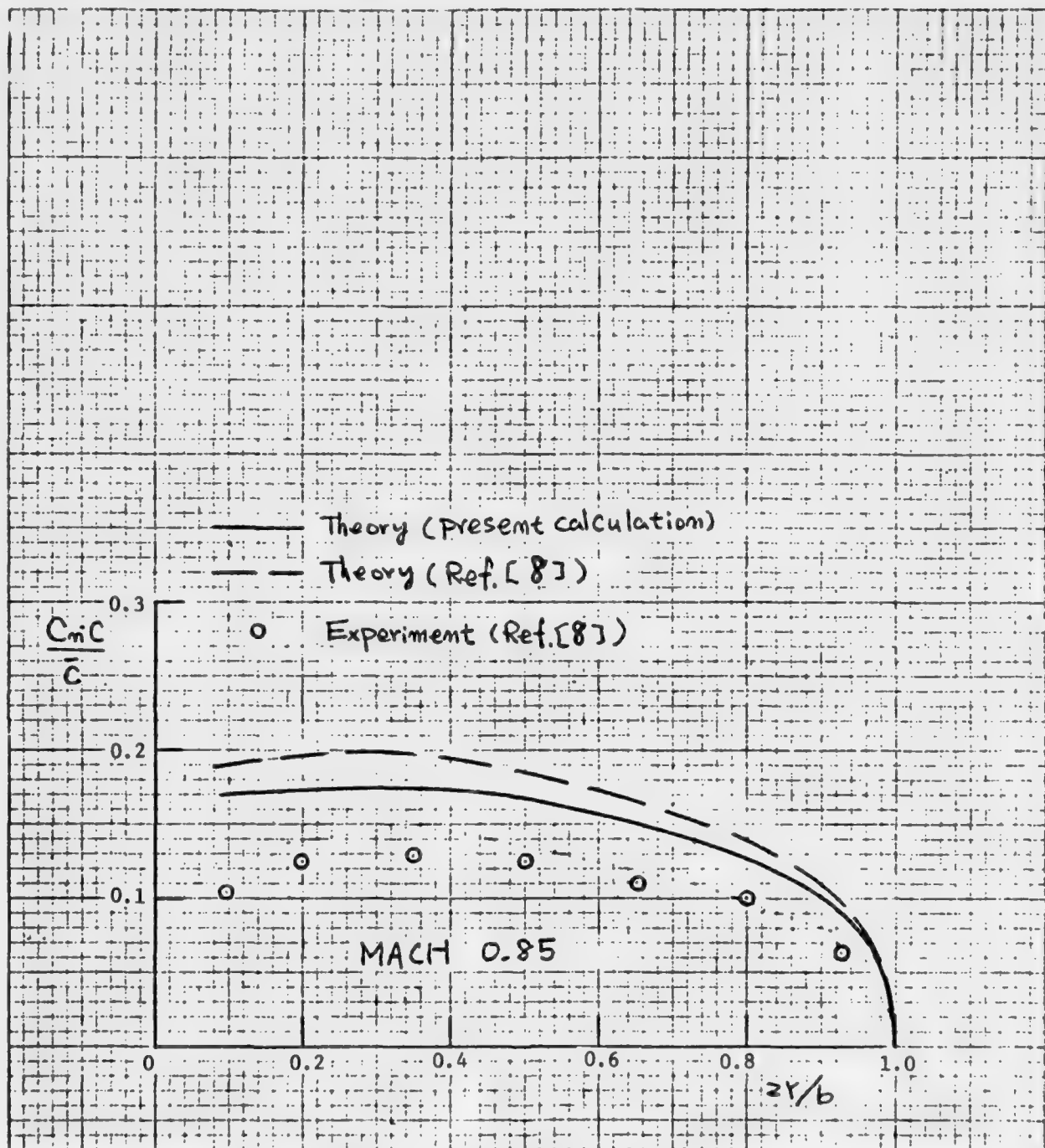


Figure 36. Spanwise lift distribution (trailing-edge $\delta_F = 8.3^\circ$, $a = 0$, $M_\infty = 0.85$).

2.4 Normal Force Coefficient of Wing-Body Combination.

Finally, the computed result on the normal force coefficient has been compared as shown in Fig. 37a. The agreement with the experiments is very good. The compressibility effect based on the Goethert's similarity rule is again proven to be very satisfactory. A further study based on Woodward's method (Ref. 6) to extend the computation into supersonic flow region has been undertaken currently. The computed result can be seen in Fig. 37b and this will be discussed in detail in our later publication (Ref. 13).

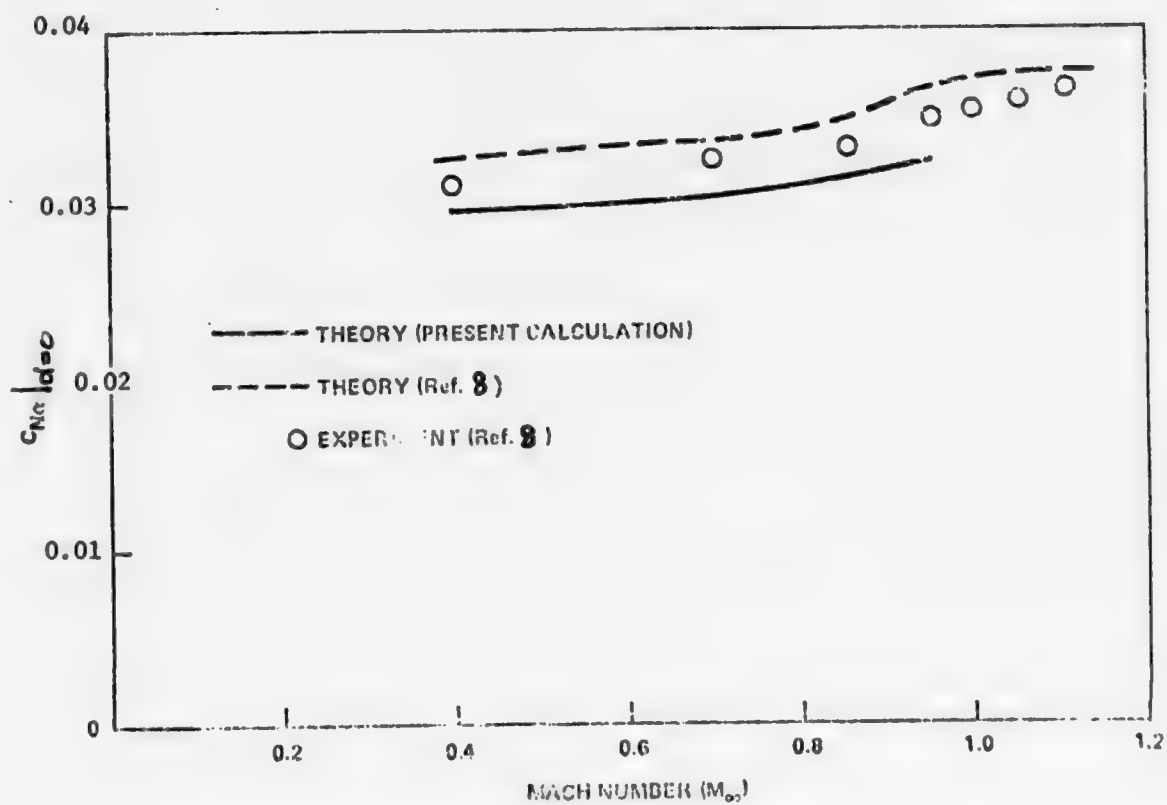


Figure 37a. Normal force coefficient.

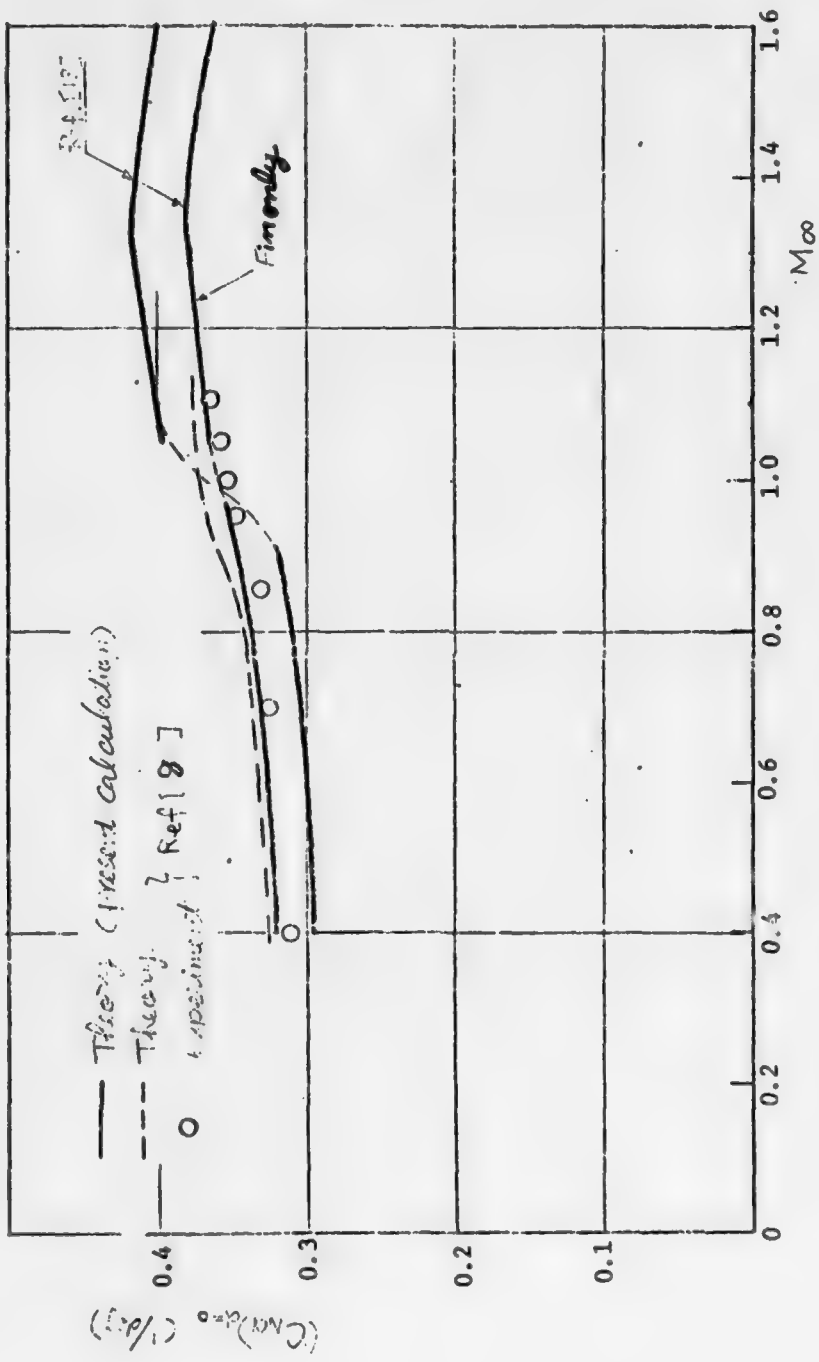


Figure 37b. Normal force slope of arrow fin-body combination.

SECTION VI. COMPARISONS OF POTENTIAL FLOW THEORIES WITH DATA ON CRUCIFORM SLENDER CLIPPED DELTA FIN-BODY COMBINATION WITH ELEVON DEFLECTION.

The computational model employed for a cruciform slender clipped delta fin-body combination is given in Fig. 38. Each fin has a small control fin called "eleven," and it is assumed that its hinge line is located near the trailing edge of the main fin as shown. Paneling scheme is shown in Fig. 39 for a deflected elevon.

1. Results and Discussions on Various Effects of Elevon Deflection on Fin-Body Combination.

1.1 Zero Elevon Deflection ($\alpha_b = 8.5^\circ$, $\delta_e = 0$).

The first calculation was made on the chordwise pressure distribution at three different spanwise positions. The angle of attack of the body is 8.5 degrees with zero elevon deflection, and the computed results are shown in Fig. 40a. The investigated Mach number was zero and 0.8, respectively. The variation of the chordwise pressure distribution at various different spanwise positions is given. It is found that the influence of the free stream Mach number is very small. Fig. 40b shows the longitudinal pressure distribution at three different azimuthal positions on the body corresponding to the fin in Fig. 40a. It can be seen that the trend of pressure distribution is very close to the one in Fig. 19b, i.e., the influence of fin on the body is strong in the fin location part on the body, and little influence from it outside of this region.

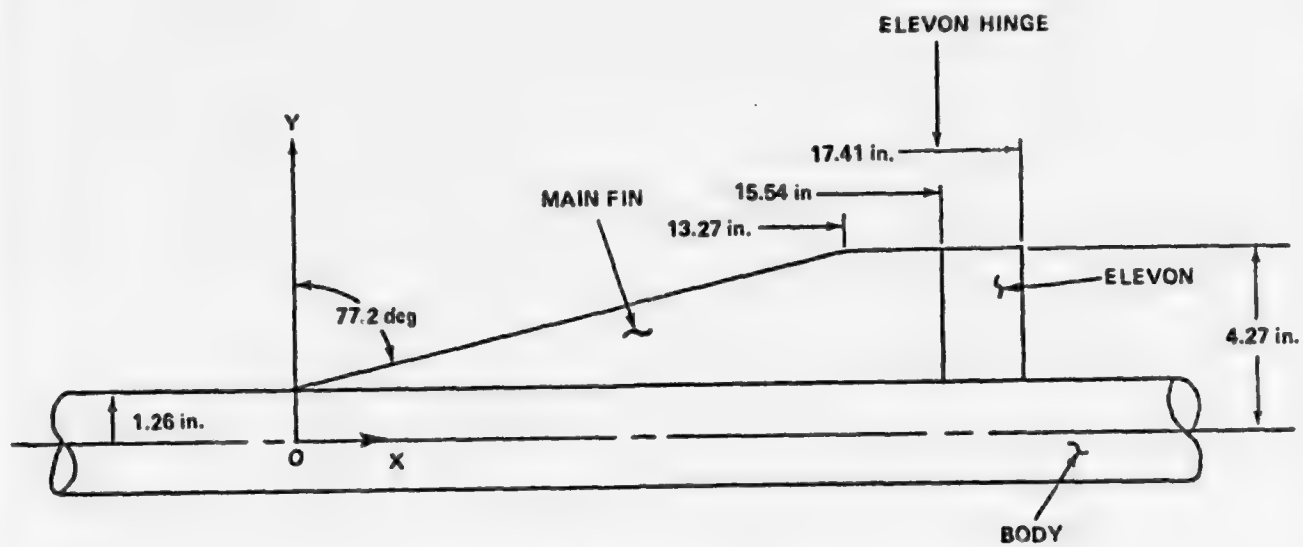


Figure 38. Fin-body geometry.

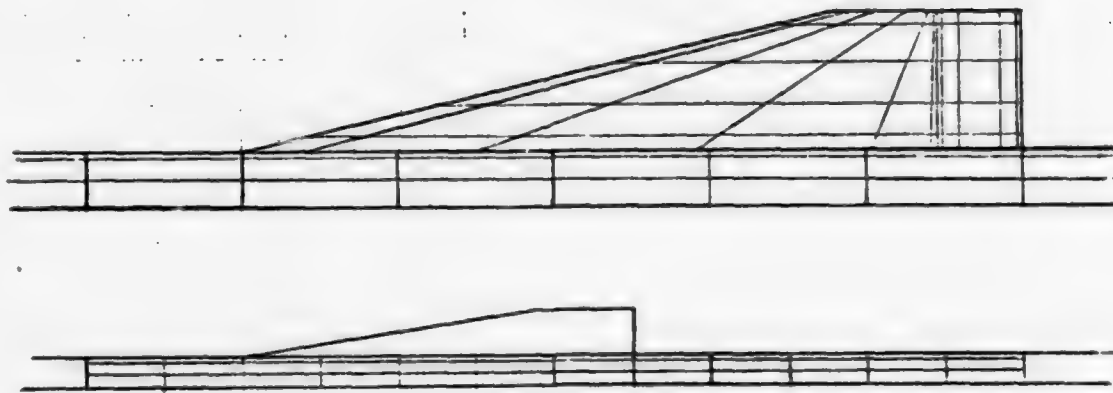


Figure 39. Paneling scheme.

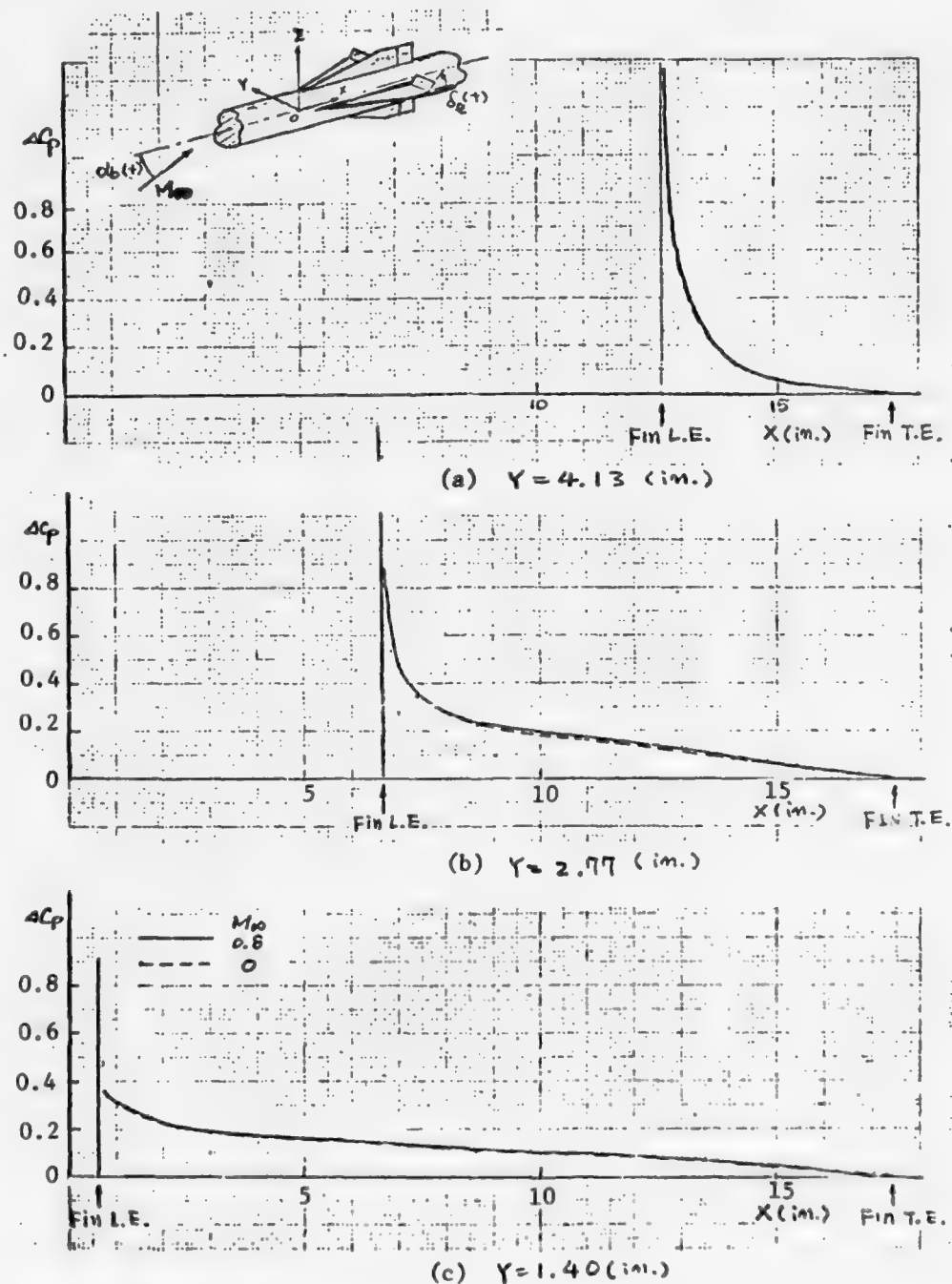


Figure 40a. Chordwise pressure distribution at three different spanwise positions on fin with zero deflected elevon of slender fin-body combination ($\alpha_b = 8.5^\circ$, $\delta_e = 0^\circ$, $M_\infty = 0$ and 0.8).

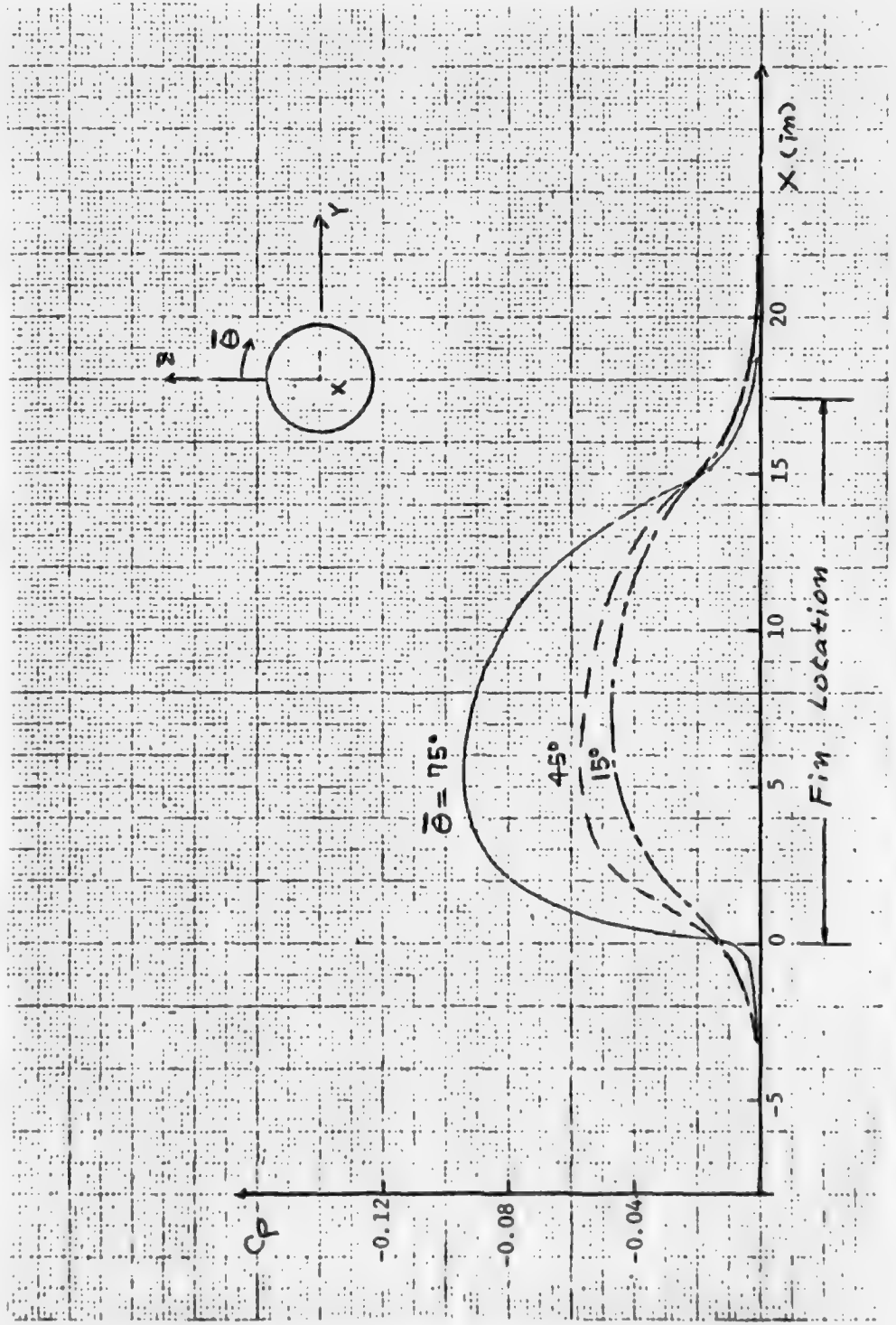
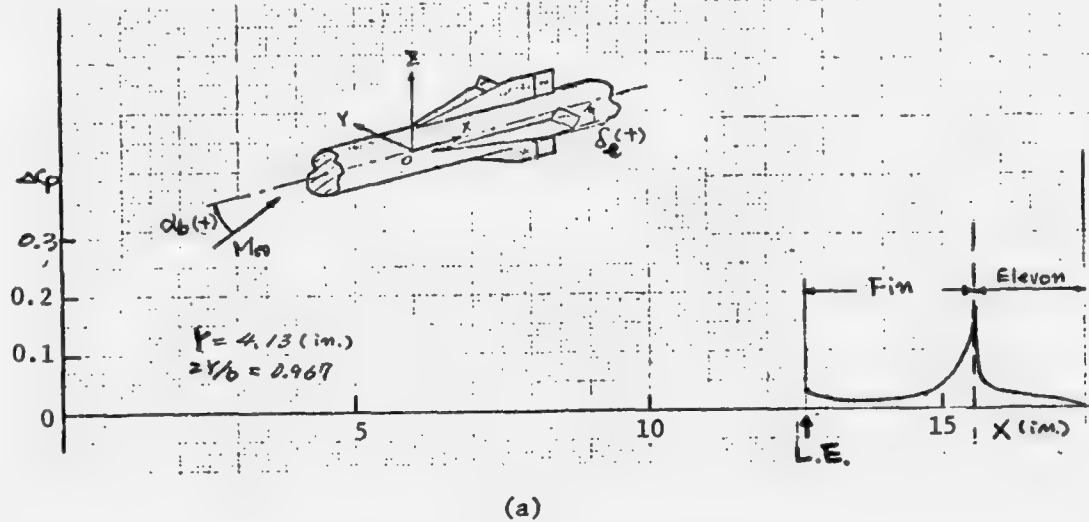


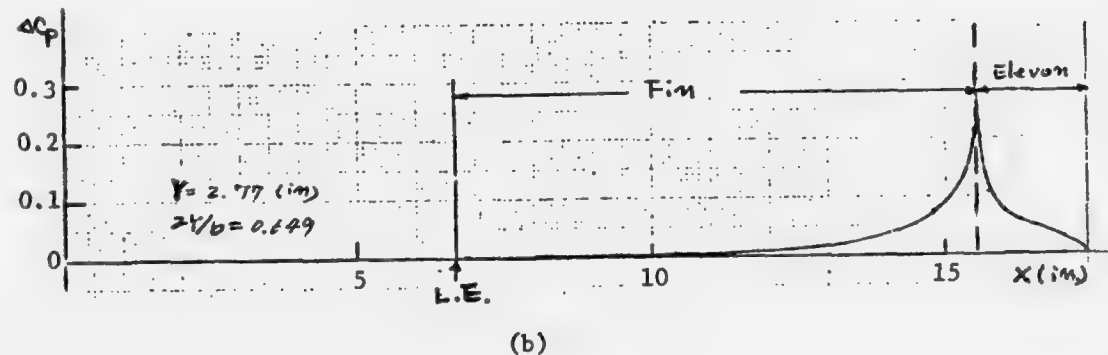
Figure 40b. Body longitudinal pressure distribution ($M_\infty = 0$, $\alpha_b = 8.5^\circ$).

1.2 Deflected Elevon ($\alpha_b = 0$, $\delta_e = 2^\circ$).

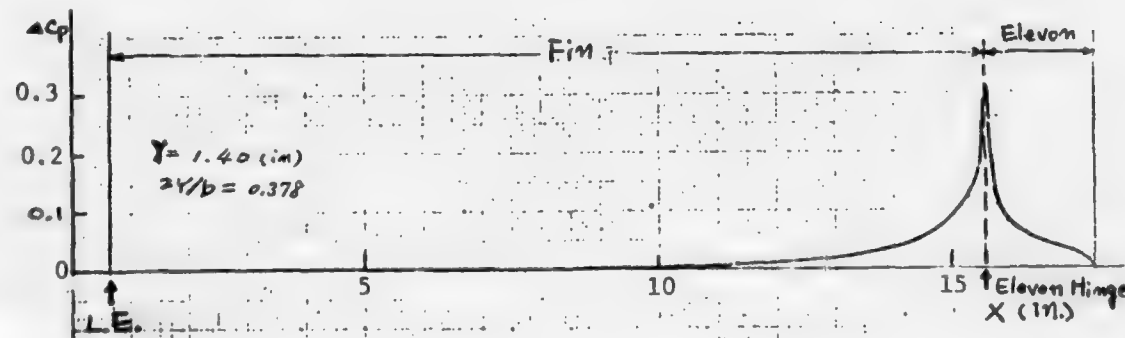
The effect of elevon deflection has been investigated next. The chordwise pressure distribution on the fin is shown in Fig. 41a. The angle of deflection of flap is two degrees, with the trailing edges of the elevons on both fins down symmetrically, with no angles of attack, and the free stream Mach number is zero, respectively. The influence of elevon on the main fin was very small in such small elevon deflection angles. However, such an influence will be rather strong as it is closer to the fin tip. The corresponding longitudinal pressure distribution on the body is shown in Fig. 41b. The influence of the elevon deflection on the body was very small in this case.



(a)



(b)



(c)

Figure 41a. Chordwise pressure distribution on fin with deflected elevon ($\delta_e = -2^\circ$, $\delta_b = 0$, $M_\infty = 0$).

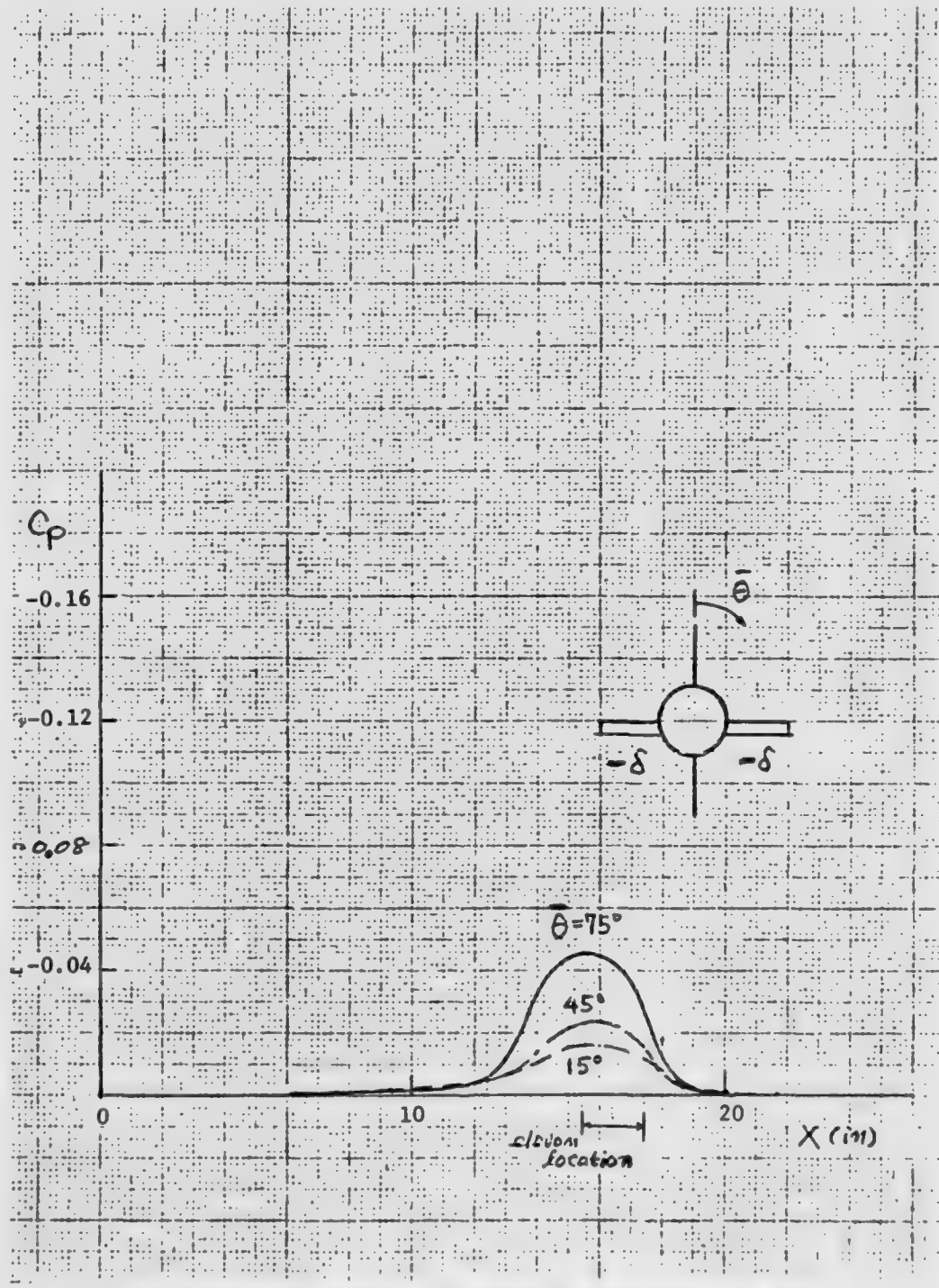
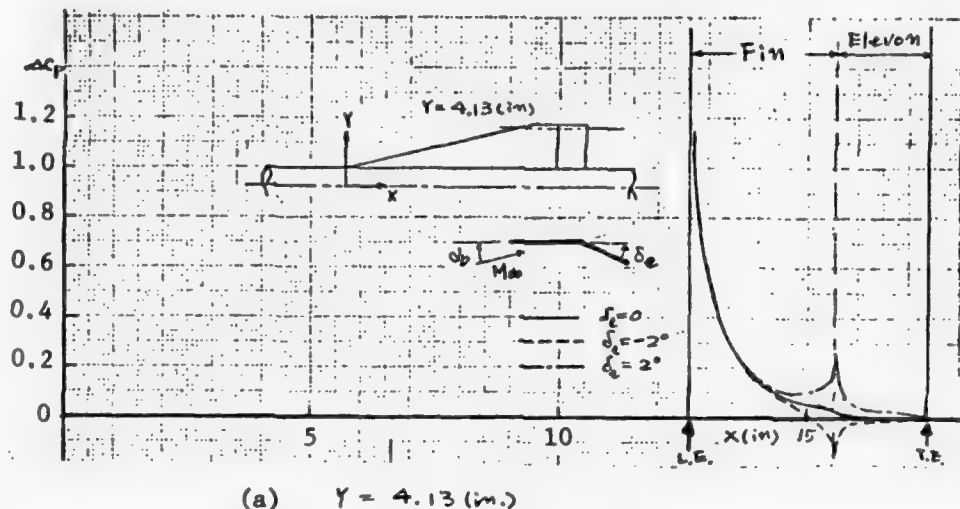


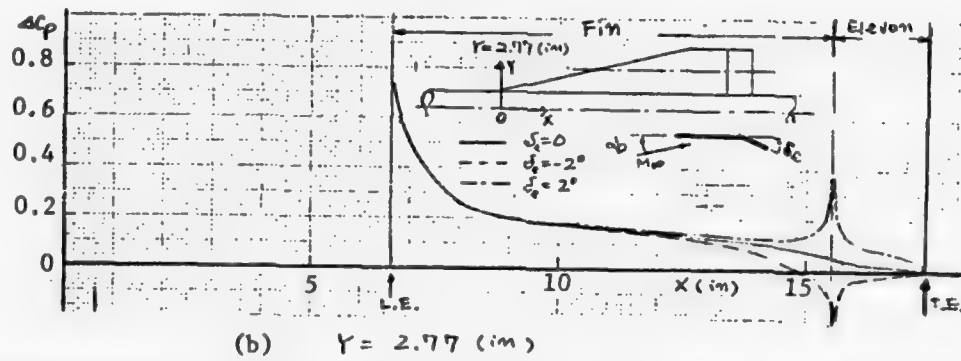
Figure 4lb. Longitudinal pressure distribution on body
 $(\delta_e = 2^\circ, \alpha_b = 0, M_\infty = 0)$.

1.3 Combined Effects ($\alpha_b = 8.5^\circ$, $\delta_e = 2^\circ$).

Fig. 42a shows the chordwise pressure distribution on a fin at an angle of attack of the body of 8.5° as well as the symmetrical elevon deflection of 2° or -2° , where the results of Figs. 40a and 41a were combined linearly. The corresponding longitudinal pressure distribution on the body is shown in Fig. 42b. This result was made also by the linear combination of the ones of Figs. 40b and 41b.



(a) $Y = 4.13$ (m.)



(b) $Y = 2.77$ (m.)

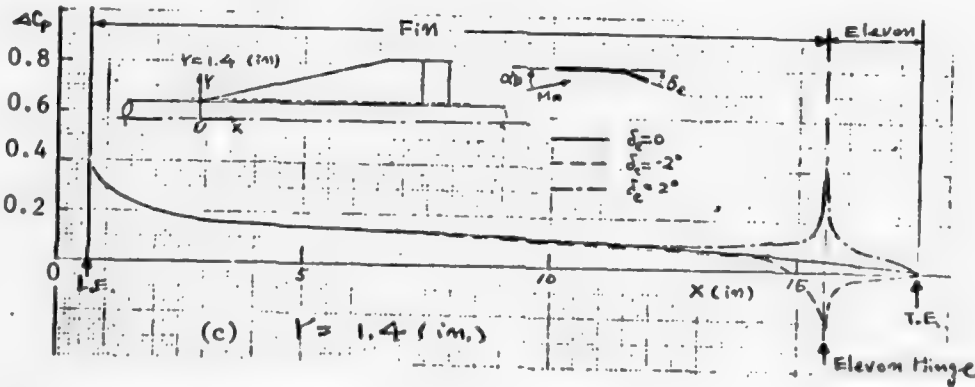


Figure 42a. Chordwise pressure distribution on fin with and without deflected elevon ($\delta_b = 8.5^\circ, M_\infty = 0$).

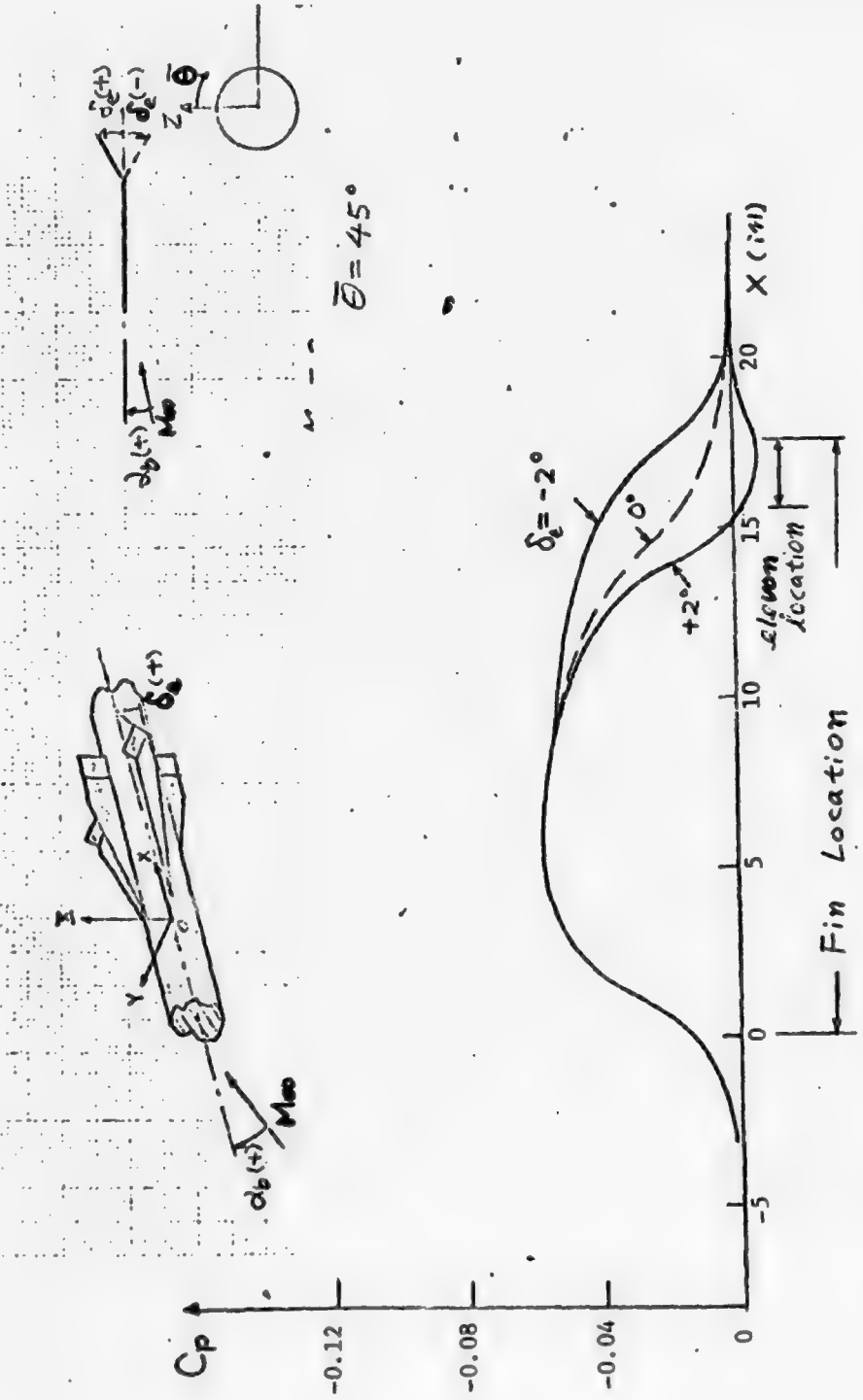


Figure 42b. Longitudinal body surface pressure distribution with and without elevon deflection ($M_\infty = 0, \alpha_b = 8.5^\circ$).

1.4 Asymmetrically Deflected Elevon.

The roll effect of the elevon was investigated on the cruciform fin-body combination at $M_\infty = 0$, and is shown in Fig. 43. The angle of deflection of a pair of horizontal elevons was taken as 2° asymmetrically in the negative direction of roll in sign convention. Fig. 43a(a) shows the load distribution on the horizontal fin, and Fig. 43a(b) shows the one on the vertical fin (i.e., no deflected elevon case), respectively. The influence of the elevon deflection on the vertical fin was not so large, but some amount of induced pressure difference (it acts as positive roll; see Ref. (2) for more details about this) can be seen from Fig. 43a(b). Fig. 43b shows the corresponding longitudinal C_p distribution on the body. The influence of the elevon deflection on the body was very small in this case.

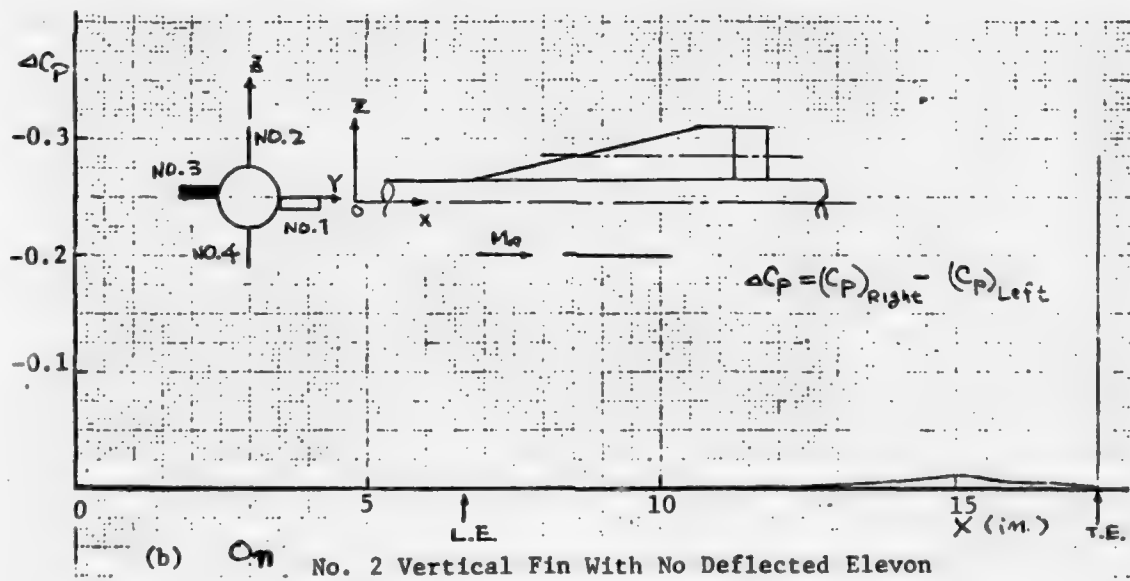
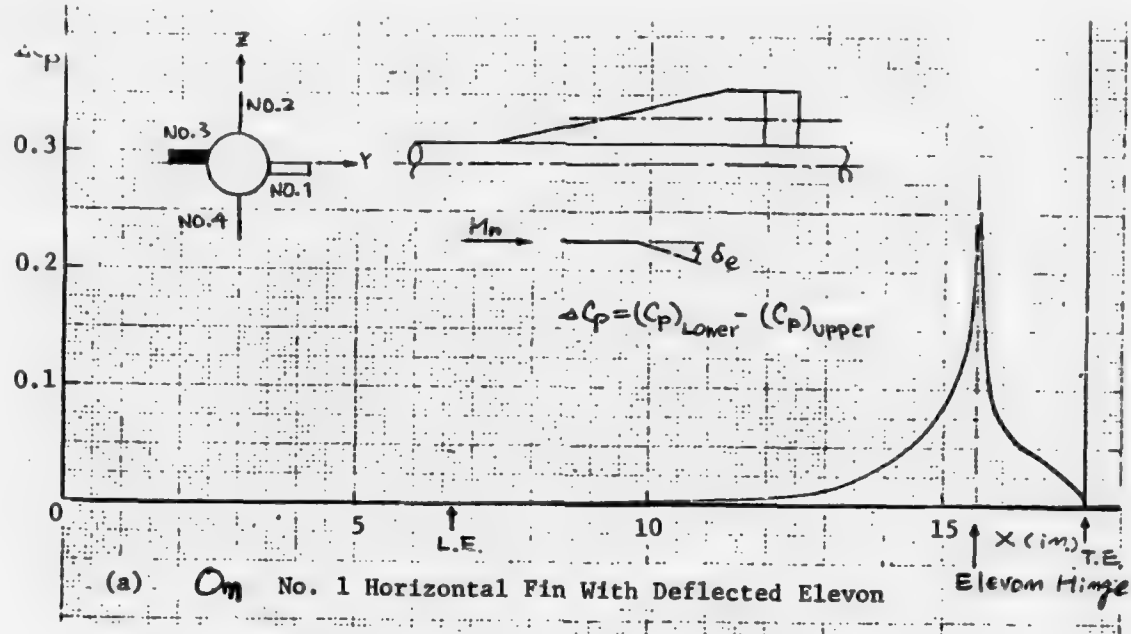


Figure 43a. Effect of antisymmetrically deflected horizontal elevon on fins
 $(\delta_e = \pm 2^\circ, M_\infty = 0)$.

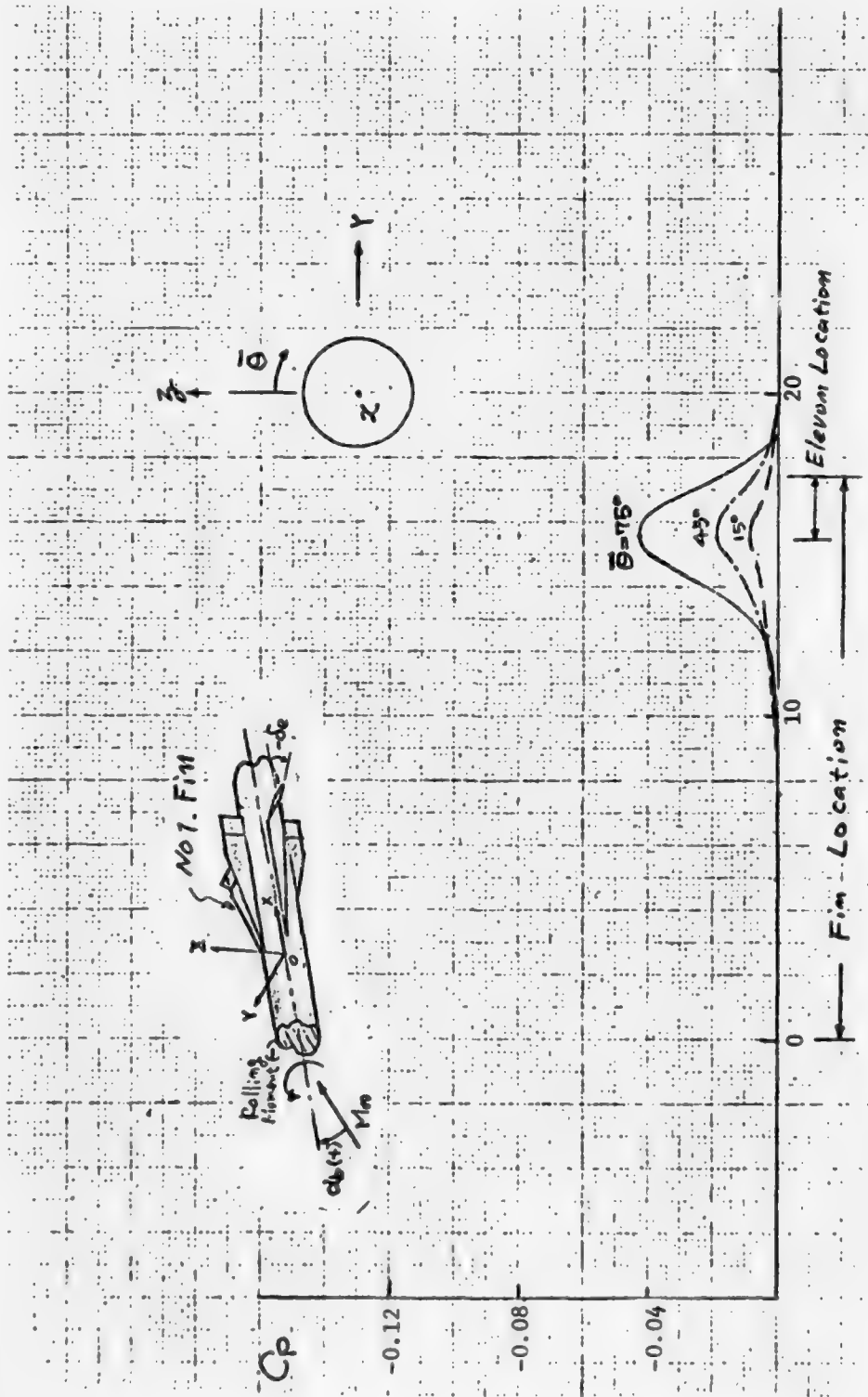


Figure 43b. C_p distribution on body with control fin deflection
 $(\delta_e = \pm 2^\circ, \alpha_b = 0, M_\infty = 0)$.

1.5 Fin-Body Combination with Angles of Attack and Yaw.

The pressure distribution on the body is shown in Fig. 44 for the fin-body combination at angles of incidence of 7.4° . This result was obtained from the linear summation of the ones of angles of attack of 6.8° and yaw angle of 2.8° based on the linearity of the basic equations (see Ref. (2)).

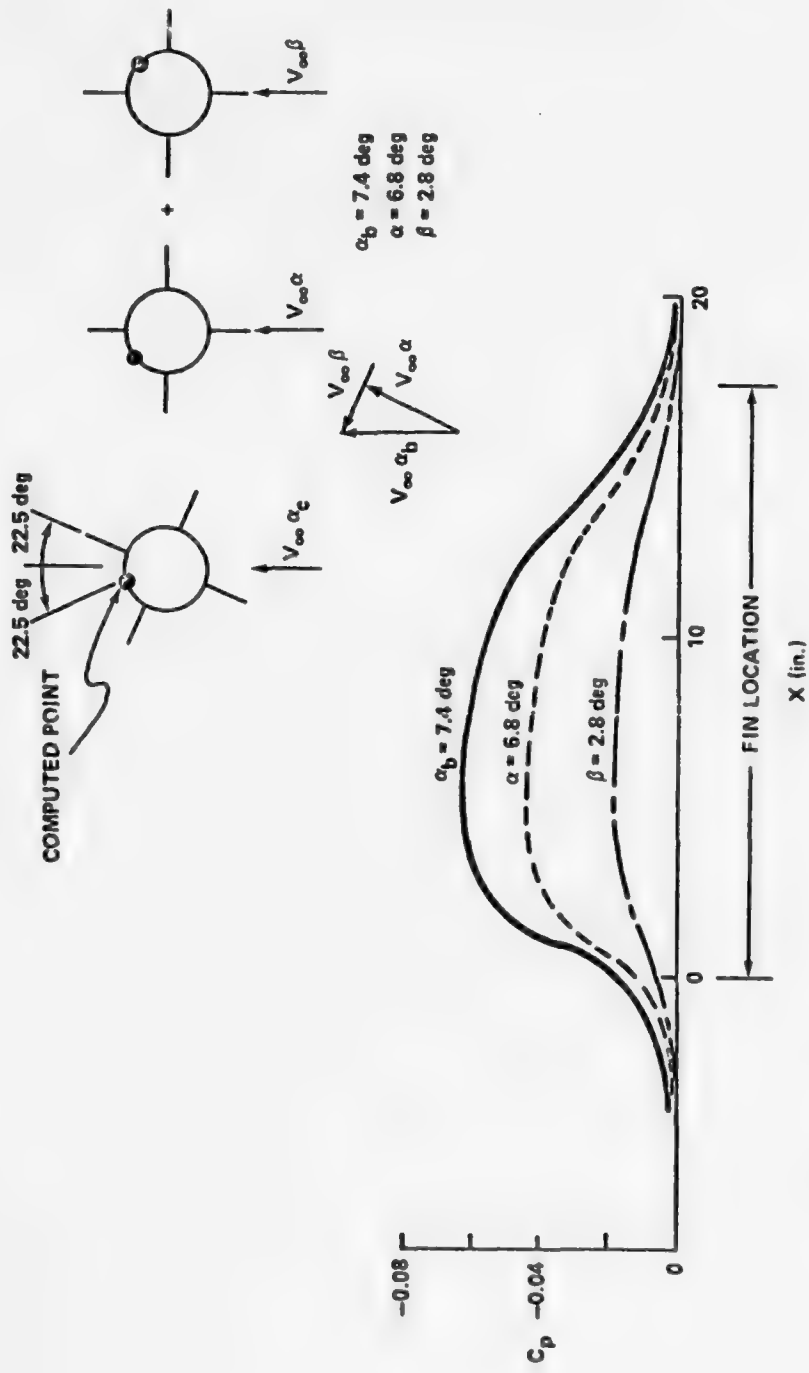


Figure 44. Longitudinal pressure distribution on body with angle of attack and yaw (0° elevon deflection angle).

2. Comparison with Experimental Data.

The angle of incidence of a body is taken at 8.54° with an elevon deflection angle of $\pm 30^\circ$, with which the body generates a counterclockwise roll facing to the upstream direction. The free stream Mach number is 1.62. With a proper sweptback, as in this example calculation, the leading edge of the fin is submerged in a subsonic stream. Because of the slenderness of the fin and its subsonic leading edge, one expects that a better agreement may be resulted by employing a slender body theory than the singularity distribution method. After a comparison with data, it indicates indeed that this is true. (The analysis at supersonic speeds by using "Singularity Method" similar to that at subsonic speeds is currently under investigation. The method employed is mainly as given in Ref. (6).)

Figs. 45a to f show the chordwise pressure distribution computed by singularity distribution and slender body theories, at different spanwise positions together with experimental measurements (MICOM). The agreement of the singularities distribution method by Koerner with the data was not bad in general over a fin surface even though the flow is supersonic. The pressure distribution on the elevon surface could not be compared because of a lack of the data on this part.

As is expected, the computed result by slender-body theory showed a better agreement with the data over a fin. This is especially so on the lower surface of the fin, however, it cannot calculate the effect of the elevon deflection, and a clipped tip effect. The Koerner's method estimated a rather large pressure distribution on the fin close to the hinge line of the elevon because of a very large elevon deflection angle. The large pressure increase is again attributed to the flow separation. This can be seen more clearly on the upper surface of the fin near the hinge line. The tip effect caused by the leading point P of the tip Mach cone may cause the pressure to increase. However, no correction has been made in the present analysis.

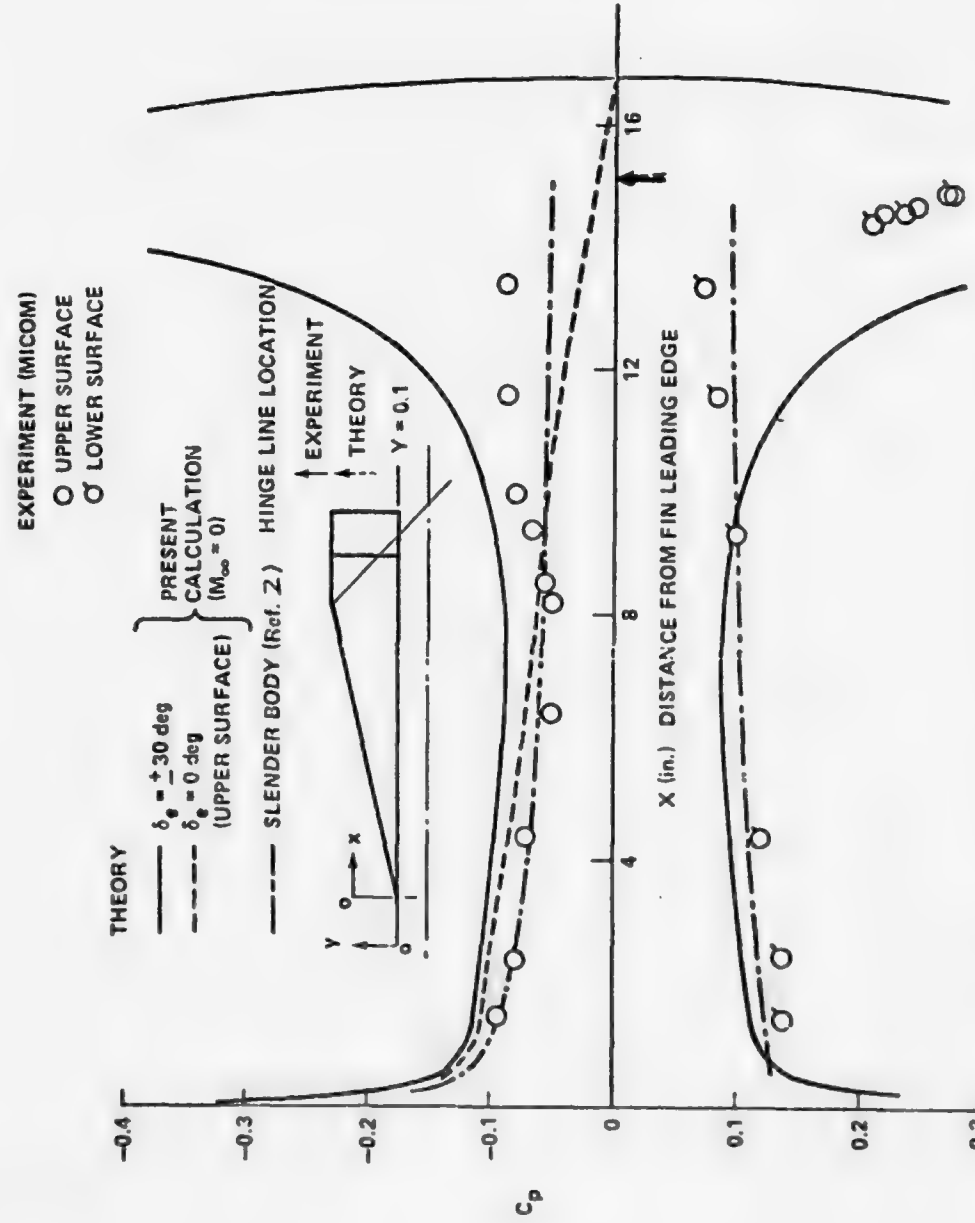


Figure 45a. Chordwise C_p distribution on fin: $M_\infty = 1.62$,
 $\alpha = 8.54^\circ$, $\delta_e = \pm 30^\circ$.

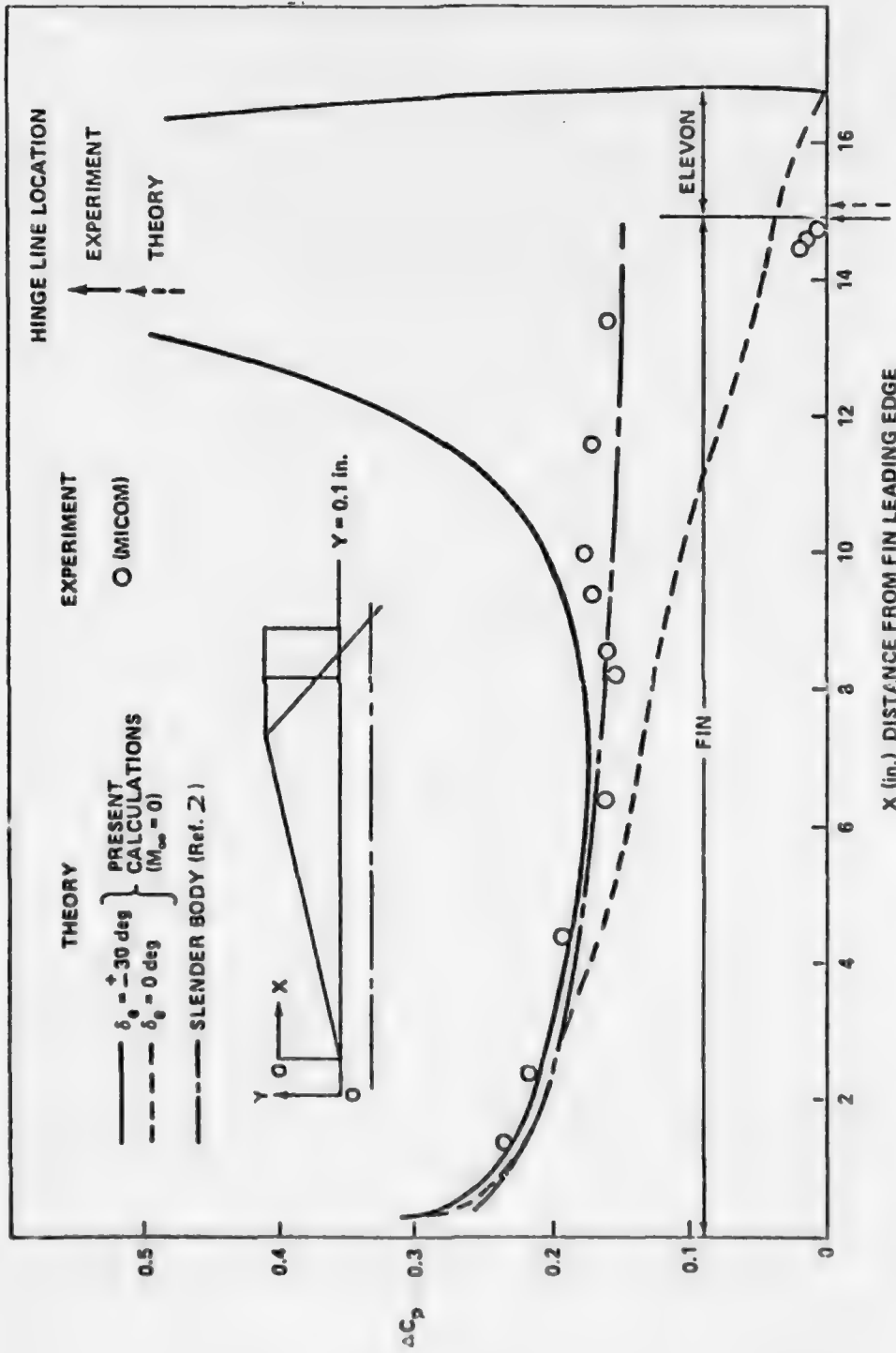


Figure 45b. Chordwise load distribution on fin ($M_{\infty} = 1.62$, $\alpha = 8.54^\circ$, $\delta_e = \pm 30^\circ$): $Y = 0.1$ in.

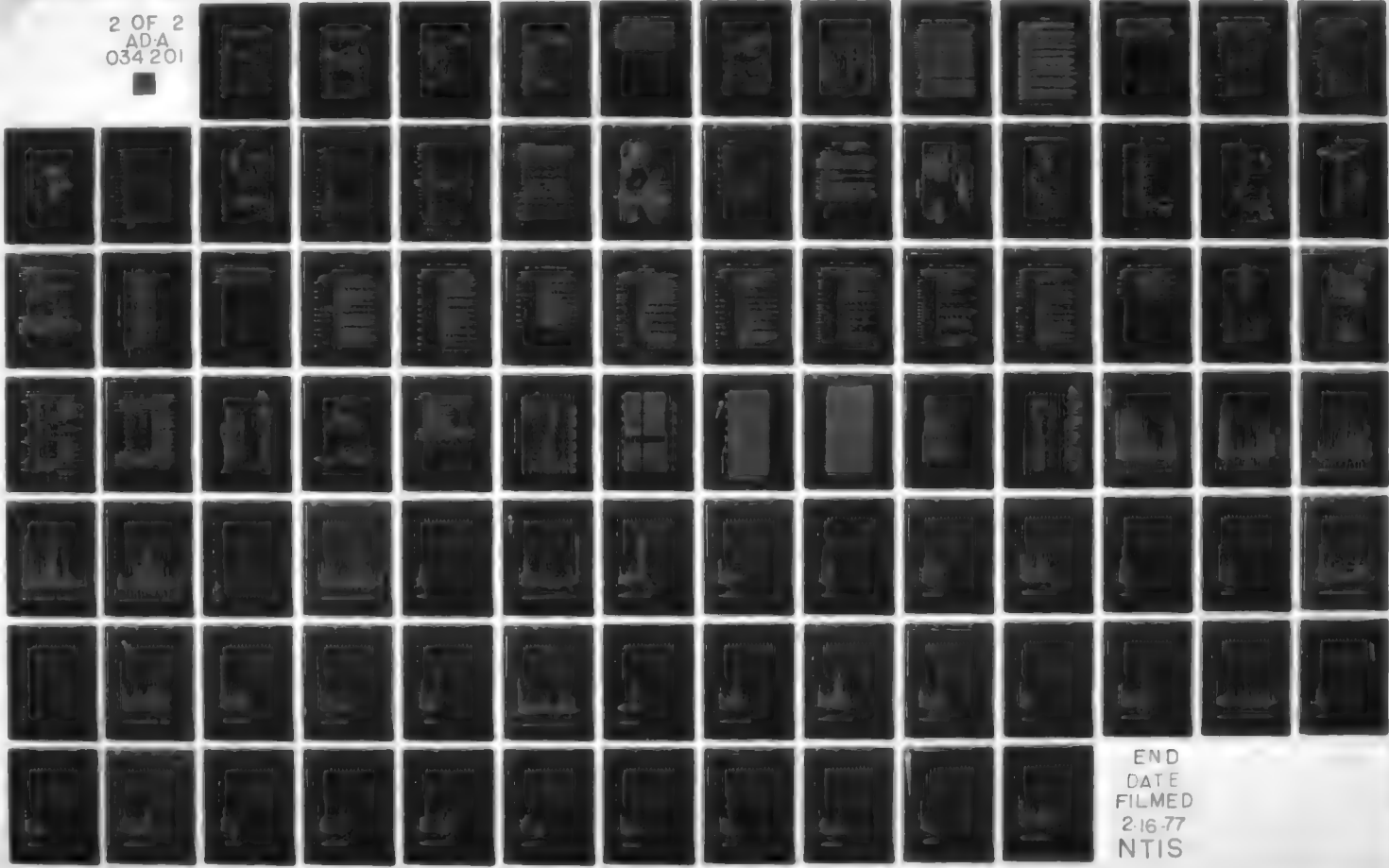
AD-A034 201 ARMY MISSILE RESEARCH DEVELOPMENT AND ENGINEERING LAB--ETC F/G 19/7
A STUDY OF VARIOUS SLENDER AND NON-SLENDER FIN-BODY COMBINATION--ETC(U)
NOV 76 N UCHIYAMA, J M WU

UNCLASSIFIED

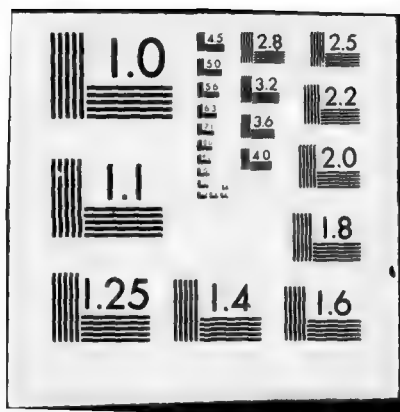
RD-CR-76-5

NL

2 OF 2
ADA
034 201



END
DATE
FILMED
2-16-77
NTIS



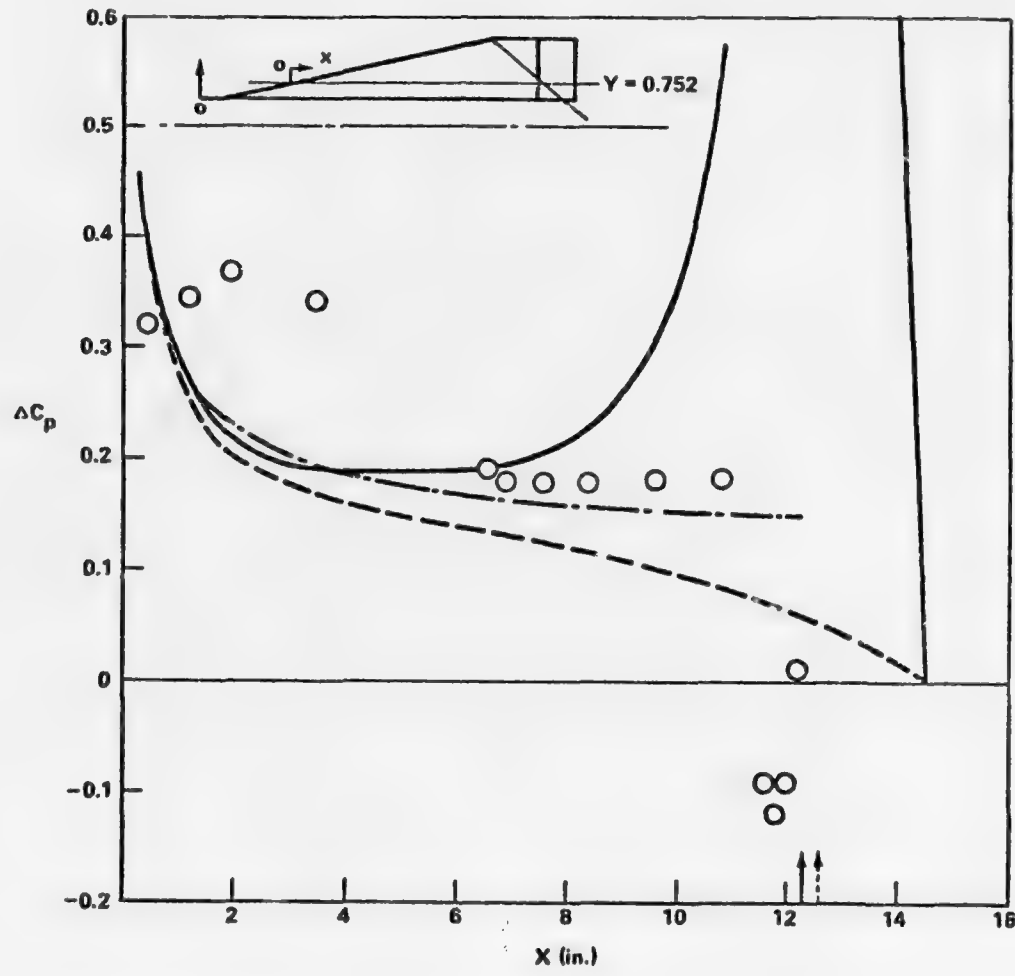


Figure 45c. Chordwise load distribution on fin for same conditions as Figure 69: $Y = 0.752$ in.

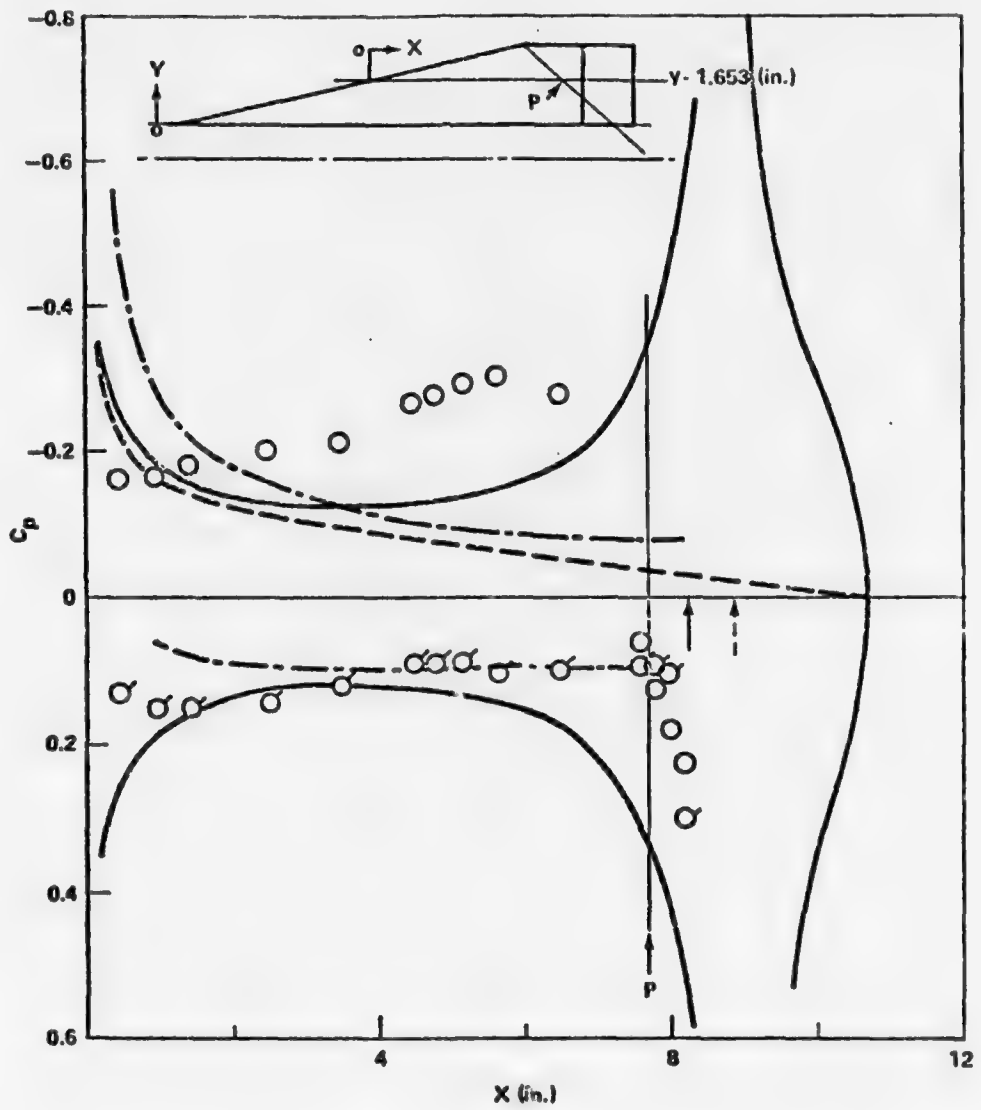


Figure 45d. Chordwise pressure distribution on fin for same conditions as Figure 69: $Y = 1.653$ in.

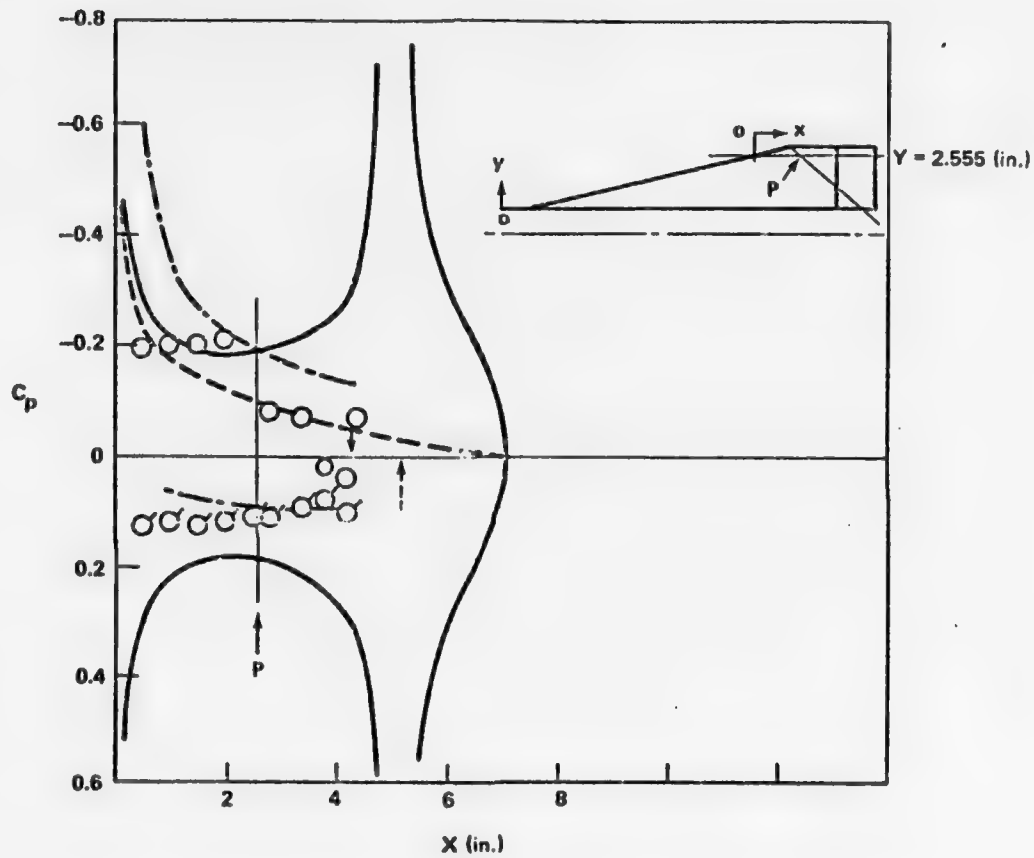


Figure 45e. Chordwise pressure distribution on fin for same conditions as Figure 69: $Y = 2.555$ in.

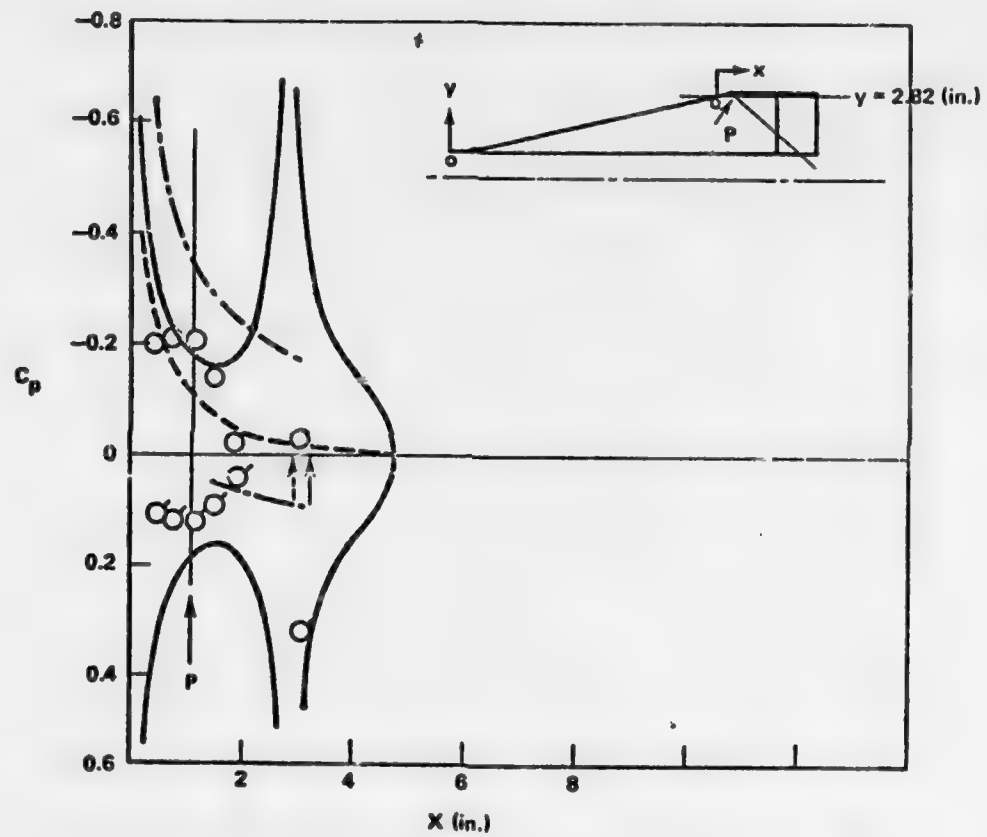


Figure 45f. Chordwise pressure distribution on fin for same conditions as Figure 69: $Y = 2.82$ in.

3. Variation of Surface Pressure and Lift Coefficient with Free Stream Mach Number.

Various compressibility corrections to the pressure coefficient of a sample point on the fin are shown in Fig. 46. The angle of attack of 8.5° was assumed in this case. The computed results used Prandtl-Glauert and Kármán-Tsien rules and showed an over-correction as discussed earlier. The total lift coefficient of this particular fin-body combination with zero elevon angle is shown in Fig. 47. The maximum body cross-section area was taken as the reference area for the lift coefficient calculation. The contribution of the body on the total lift coefficient is very small. Thus, as far as the total lift coefficient is concerned, the effect due to the body may be neglected.

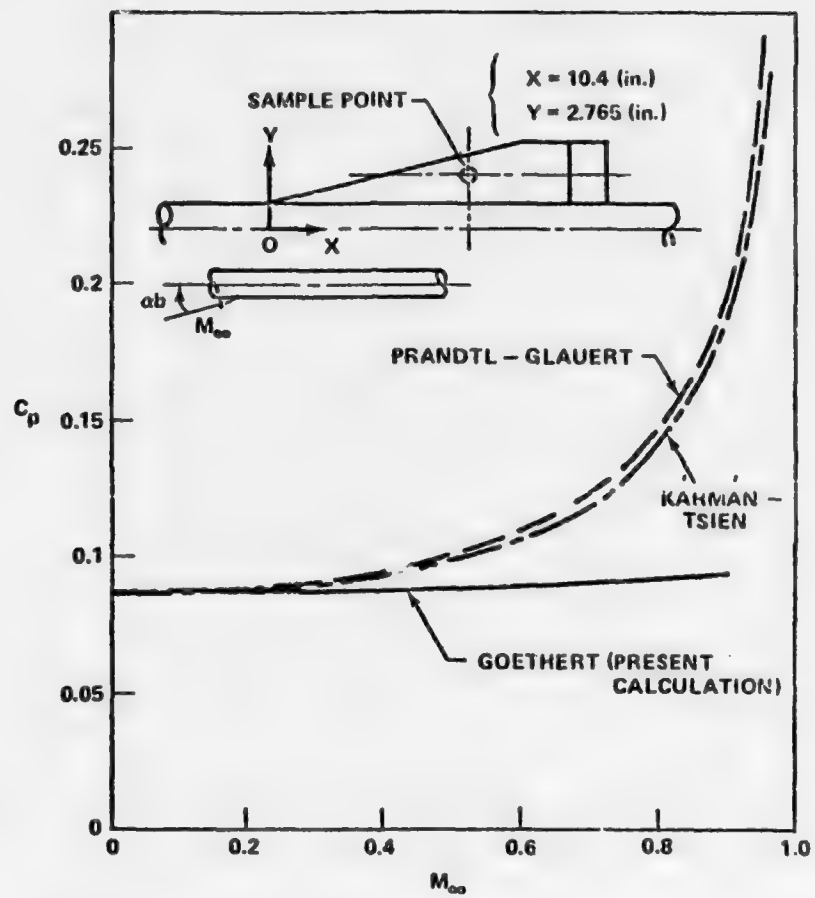


Figure 46. Comparison of compressibility effect of present result with other similarity rules ($\alpha_b = 8.5^\circ$).

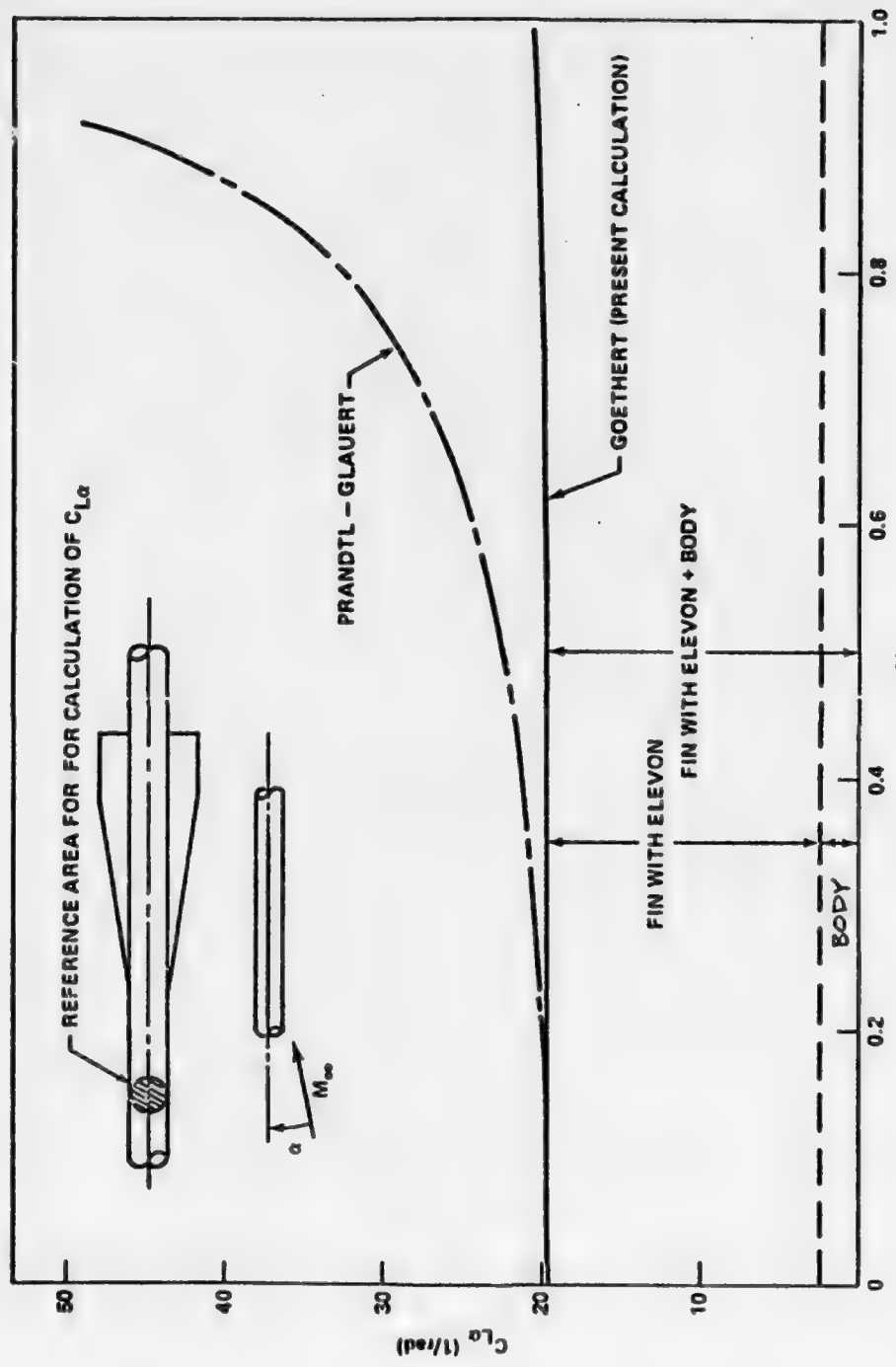


Figure 47. Variation of lift coefficient of fin-body combination with changing free-stream Mach number.

SECTION VII. CONCLUSIONS AND RECOMMENDATIONS.

The computational scheme for estimating the pressure distribution on a fin-body combination has been developed by the "Singularity Method" based on Ref. (1). The reasonable results were obtained over various kinds of fin-body configurations. The comparisons with the experimental data were generally good. Goethert's similarity rule predicted well the compressibility effect up to very high subsonic speed. This is not only for a moderately large aspect ratio fin but also to a slender fin-body combination at small angles of attack. The poor agreement of pressure distribution with the data appeared at a relatively high angle-of-attack (eight degrees in the present calculation) as reported in the other method. This seemed to be in the flow separation on the lifting surface due to high angles of attack, and thus further study on this will be needed. The calculated result by the slender-body theory (Ref. (2)) had a surprisingly good agreement with the experimental data for the slender fin-body combination even at supersonic speed as expected, except in the influence region of the fin tip, i.e., inside the tip Mach cone. The present analysis has coincided well with the slender-body theory, for slender fin-body configuration, and thus it may be said that the present analysis includes the slender-body theory at subsonic speed.

Although a flat plate fin case only has been investigated here, it is not too difficult to modify the present analysis so that it can be applied to include the cases of a fin with camber, twist, and thickness. Furthermore, the restriction of the straight leading and trailing edge is not so severe. Therefore, the present analysis can be applied to almost all the arbitrary plan formed fin-body combinations with a slight modification to the program.

REFERENCES

1. Koerner, H., Berechnung der Potential Theoretischen Strömung um Flügel-Rumpf-Kombinationen und Vergleich mit Messungen, Zeitschrift Für Flugwissenschaften, 20 Jahrgang, Heft 9, September, 1972.
2. Uchiyama, N. and Wu, J. M., "Inviscid Flow Analysis on Body of Revolution with Slender Cruciform Canted Delta Fins at Small Angle of Incidence," Technical Report RD-75-32, U. S. Army Missile Command, Redstone Arsenal, Alabama, March, 1975.
3. Koerner, H., Theoretische Parameteruntersuchungen an Flügel-Rumpf-Kombinationen, DLR-FB 72-63, 1972.
4. Lawrence, H. R., The Lift Distribution on Low Aspect Ratio Wings at Subsonic Speeds, Journal of The Aeronautical Sciences, October, 1951.
5. Woodward, F. A., Analysis and Design of Wing-Body Combinations at Subsonic and Supersonic Speeds, J. Aircraft, Vol. 5, No. 6, Nov.-Dec., 1968.
6. Woodward, F. A., et al., Analysis and Design of Supersonic Wing-Body Combinations, Including Flow Properties in the Near Field---Part I: Theory and Application, The Boeing Company, Renton, Washington, N67-34997, August, 1967. (Also NASA CR-73106)
LaRowe, E., et al. ---Part II: Digital Computer Program Description, N67-34994, August, 1967. (Also NASA CR-73107.)
7. Hedman, S. G., Vortex Lattice Method for Calculating of Quasi Steady State Loadings on Thin Elastic Wings in Subsonic Flow, FFA Rep. 105, 1966.
8. Manro, M. E., Tinoco, E. N., Bobbitt, P. J., and Rogers, J. T., Comparisons of Theoretical and Experimental Pressure Distributions on an Arrow-Wing Configuration at Transonic Speeds, Aerodynamic Analyses Requiring Advanced Computers, Part II, Langley Research Center, Hampton, Virginia, NASA Sp-347, March, 1975.
9. Chipman, R. R., and Rauch, F. J., Analytical and Experimental Study of the Effects of Wing-Body Aerodynamic Interaction on Space Shuttle Subsonic Flutter, NASA CR-2488, January, 1975.
10. Shapiro, A. H., The Dynamics and Thermodynamics of Compressible Fluid Flow, Vol. 1, The Ronald Press Company, New York, 1953.
11. Nielsen, J. N., Missile Aerodynamics, McGraw-Hill Book Company, Inc., New York, 1960, p. 211.

12. Wu, J. M., Moulden, T. H., and Uchiyama, N., "Aerodynamic Performance of Missile Configurations at Transonic Speeds Including the Effects of a Jet Plume," Technical Report RD-76-23, U. S. Army Missile Command, Redstone Arsenal, Alabama, March, 1976.
13. Uchiyama, N., and Wu, J. M., "A Further Study on Slender and Non-Slender Fin-Body Combinations of Missile Configurations with Emphasis on Low Supersonic Flow," Technical Report (in preparation), U. S. Army Missile Command, Redstone Arsenal, Alabama, 1977.

APPENDIX I. DETERMINING AERODYNAMIC MATRICES.

1. Determining the positions of a horseshoe vortex and a control point on a fin

By using the coordinates as shown in Figs. 2 and 3, the positions of a horseshoe vortex (x_v , y_v , z_v) a control point (x_D , y_D , z_D) on a fin can be written as:

$$\begin{aligned}
 y_v &= y_D = (e_{k,\ell} + e_{k,\ell+1})/2 \\
 x_v &= a_k + c_k \cdot (3d_{k,m} + d_{k,m+1})/4 + (y_v - b_k) \cdot \tan \lambda \\
 z_v &= z_D = 0 \\
 x_D &= a_k + c_k \cdot (d_{k,m} + 3d_{k,m+1})/4 \\
 &\quad + \{ c_{k+1} \cdot (d_{k+1,m} + 3d_{k+1,m+1})/4 \\
 &\quad - c_k \cdot (d_{k,m} + 3d_{k,m+1})/4 + a_{k+1} - a_k \} \cdot \\
 &\quad (y_v - b_k)/(b_{k+1} - b_k)
 \end{aligned} \tag{21}$$

where,

$$\begin{aligned}
 \tan \lambda &= \{ c_{k+1} \cdot (3d_{k+1,m} + d_{k+1,m+1})/4 \\
 &\quad - c_k \cdot (3d_{k,m} + d_{k,m+1})/4 \\
 &\quad + a_{k+1} - a_k \} / (b_{k+1} - b_k)
 \end{aligned}$$

The half spanwise width of a horseshoe vortex is,

$$h = (e_{k,\ell+1} - e_{k,\ell})/2 \tag{22}$$

2. Velocity components induced by a horseshoe vortex

The vertically intercepted point $S(\xi, \beta\eta, \beta z_v)$ between a bound vortex line and any control point $P(x_D, \beta y_D, \beta z_D)$ as shown in Fig. 48 can be written as:

$$\left. \begin{aligned} \xi &= \frac{x_v + x_D \tan^2 \mu + \beta \cdot (y_D - y_v) \tan \mu}{\tan^2 \mu + 1} \\ \beta\eta &= \frac{\beta y_D + \beta y_v \tan^2 \mu + (x_D - x_v) \tan \mu}{\tan^2 \mu + 1} \end{aligned} \right\} \quad (23)$$

where,

$$\tan \mu = \tan \lambda / \beta$$

By using Biot-Savart law, the velocity (w_B) induced at P by a bound vortex ξ can be written as:

$$w_B = \frac{\Gamma (\cos \gamma + \cos \phi)}{4\pi \sqrt{A^2 + Z^2}}$$

where

$$\cos \gamma = \frac{QS}{QP} = \frac{\pm \sqrt{B^2 + C^2}}{\sqrt{A^2 + B^2 + C^2 + Z^2}}$$

$$\cos \gamma > 0 \text{ for } \eta > y_v - h$$

$$\cos \gamma < 0 \text{ for } \eta < y_v - h$$

$$\cos \phi = \frac{RS}{RP} = \frac{\pm \sqrt{D^2 + E^2}}{\sqrt{A^2 + D^2 + E^2 + Z^2}}$$

$$\cos \phi < 0 \text{ for } \eta > y_v + h$$

$$\cos \phi > 0 \text{ for } \eta < y_v + h$$

(24)

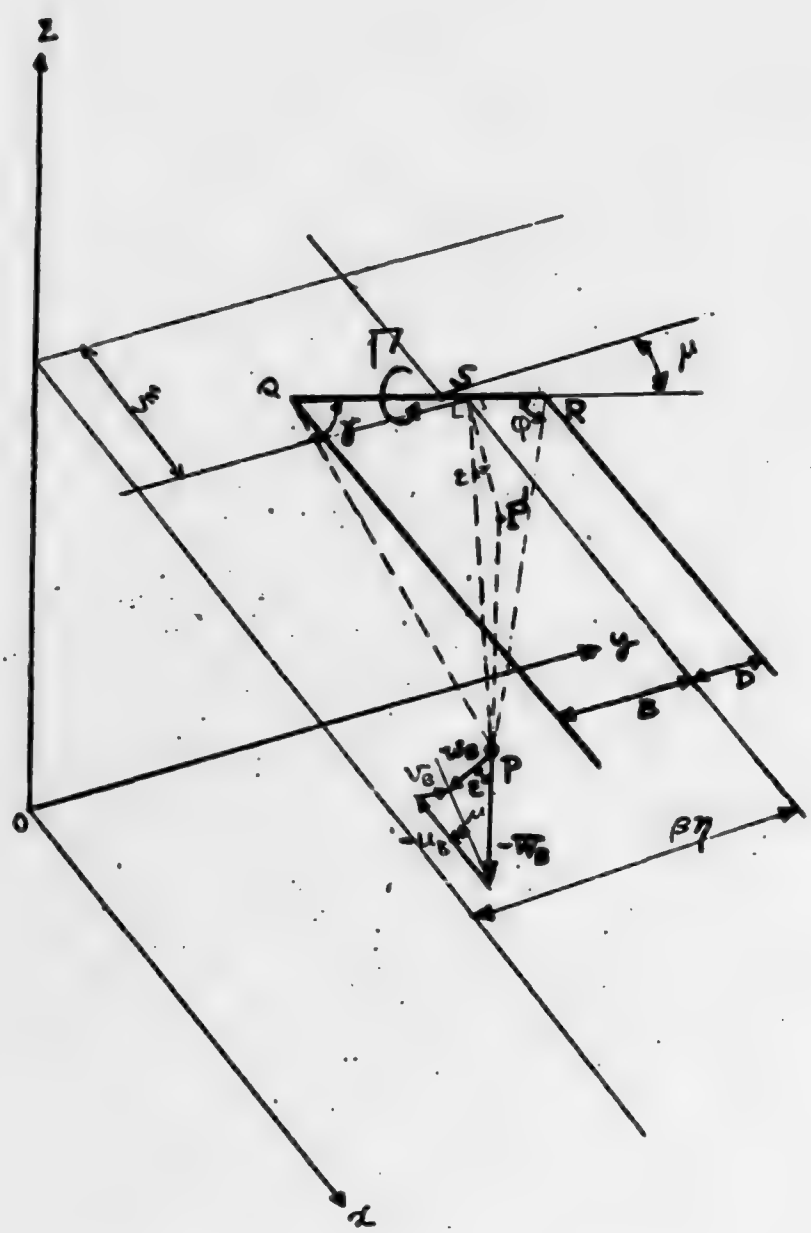


Figure 48. Induced velocity and its components due to a bound vortex.

and,

$$A^2 = (SP')^2 = (x_D - \xi)^2 + \beta^2 \cdot (\eta - y_D)^2$$

$$B = \beta \cdot (\eta - y_v + h)$$

$$C = \xi - x_v + \beta h \tan \mu$$

$$D = \beta \cdot (y_v + h - \eta)$$

$$E = x_v + \beta h \tan \mu - \xi$$

$$Z = \beta \cdot (z_v - z_D)$$

thus, the velocity components (u_B , v_B , w_B) of W_B can be written as:

$$u_B = - W_B \sin \epsilon \cos \mu$$

$$v_B = W_B \sin \epsilon \sin \mu$$

$$w_B = - W_B \cos \epsilon$$

where,

(25)

$$\sin \epsilon = \frac{Z}{\sqrt{A^2 + Z^2}}$$

$$\cos \epsilon = \frac{\pm A}{\sqrt{A^2 + Z^2}}$$

$\cos \epsilon > 0$ for $x_D > \xi$

$\cos \epsilon < 0$ for $x_D < \xi$

The velocity (W_p) induced at P due to a port free vortex as shown in Fig. 49 can be written as:

$$W_p = \frac{\Gamma}{4\pi} \cdot \frac{1 + \cos k}{\sqrt{G^2 + Z^2}}$$

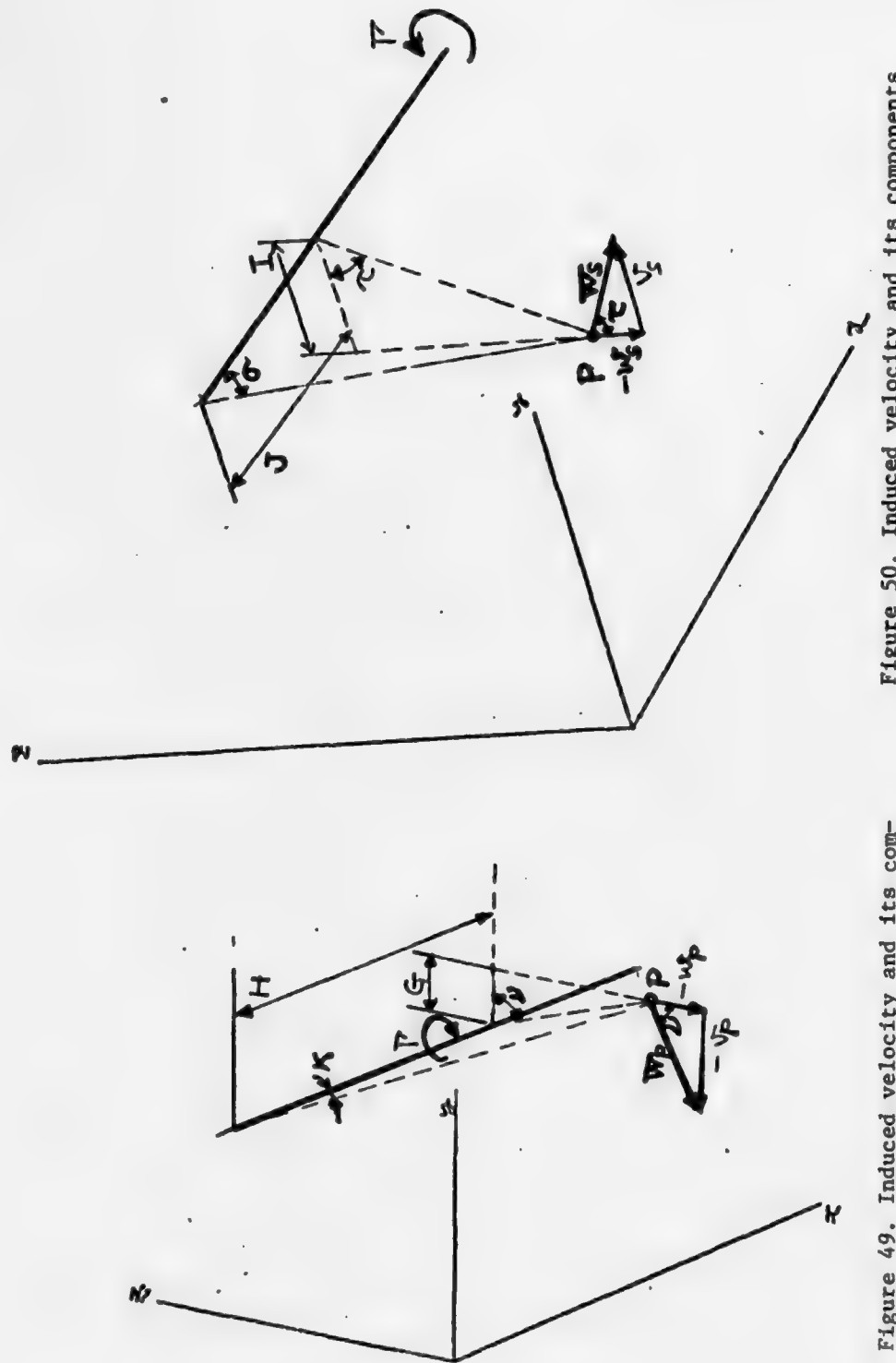


Figure 49. Induced velocity and its components due to a port free vortex.

Figure 50. Induced velocity and its components due to a starboard free vortex.

where

$$\cos k = \frac{H}{\sqrt{G^2 + H^2 + Z^2}} \quad (26)$$

$$G = \beta \cdot (y_D - y_v + h)$$

$$H = x_D - x_v + \beta h \tan \mu$$

thus, the velocity components (u_p , v_p , w_p) of w_p can be written as:

$$u_p = 0$$

$$v_p = -w_p \sin v$$

$$w_p = -w_p \cos v$$

where,

$$\sin v = \frac{Z}{\sqrt{G^2 + Z^2}}$$

$$\cos v = \frac{G}{\sqrt{G^2 + Z^2}} \quad (27)$$

Similarly, the velocity (w_s) induced at P due to a starboard free vortex as shown in Fig. 50 can be written as:

$$w_s = \frac{\Gamma}{4\pi} \frac{1 + \cos \sigma}{\sqrt{I^2 + Z^2}}$$

where,

$$\cos \sigma = \frac{J}{\sqrt{I^2 + J^2 + Z^2}} \quad (28)$$

$$I = \beta (y_v + h - y_D)$$

$$J = x_D - x_v - \beta h \tan \mu$$

thus, the velocity components (u_S , v_S , w_S) of W_S can be written as:

$$\begin{aligned} u_S &= 0 \\ v_S &= w_S \sin \tau \\ w_S &= w_S \cos \tau \end{aligned}$$

where,

(29)

$$\begin{aligned} \sin \tau &= \frac{z}{\sqrt{I^2 + z^2}} \\ \cos \tau &= \frac{I}{\sqrt{I^2 + z^2}} \end{aligned}$$

Therefore, the induced velocity components (u , v , w) due to a complete horseshoe vortex is considered as a linear summation of the three vortices mentioned above, and can be written as:

$$\begin{aligned} u &= u_B + u_P + u_S \\ v &= v_B + v_P + v_S \\ w &= w_B + w_P + w_S \end{aligned}$$

(30)

or,

$$\begin{aligned} u &= - \frac{\Gamma}{4\pi} \frac{\cos \gamma + \cos \phi}{A^2 + Z^2} Z \cos \mu = P\Gamma \\ v &= \frac{\Gamma}{4\pi} \left[\frac{\cos \gamma + \cos \phi}{A^2 + Z^2} \sin \mu - \frac{1 + \cos k}{G^2 + Z^2} \right. \\ &\quad \left. + \frac{\cos \sigma + 1}{I^2 + Z^2} \right] Z = Q\Gamma \\ w &= \frac{\Gamma}{4\pi} \left[\frac{\cos \gamma + \cos \phi}{A^2 + Z^2} \cdot A - \frac{1 + \cos k}{G^2 + Z^2} G \right. \\ &\quad \left. - \frac{\cos \sigma + 1}{I^2 + Z^2} I \right] = R\Gamma \end{aligned}$$

(31)

The first term in w ; - for $x_D > \xi$
+ for $x_C < \xi$

3. Aerodynamic Matrices.

For a planar fin-body configuration geometry, the effect of the horseshoe vortex on the opposite side's fin and the image vortex can be treated in the same way as that mentioned above. Thus, total velocity components at any control point induced by four horseshoe vortices (i.e., two on a pair of fins, and two inside a body) as shown in Fig. 51) can be written as:

$$\left. \begin{aligned} u_i &= \sum_{j=1}^n (P_{ij}^{(SS)} + P_{ij}^{(PS)} + P'_{ij}^{(SS)} + P'_{ij}^{(PS)}) \Gamma_j \\ v_i &= \sum_{j=1}^n (Q_{ij}^{(SS)} - Q_{ij}^{(PS)} - Q'_{ij}^{(SS)} + Q'_{ij}^{(PS)}) \Gamma_j \\ w_i &= \sum_{j=1}^n (\underbrace{R_{ij}^{(SS)} + R_{ij}^{(PS)}}_{\text{due to a pair of fins' vortices}} + \underbrace{R'_{ij}^{(SS)} - R'_{ij}^{(PS)}}_{\text{due to image vortices inside a body}}) \Gamma_j \end{aligned} \right\} \quad (32)$$

where, the superscript (SS) indicates that as well vortex as control point are situated on the starboard side (see Ref. (7)), and,

$$P_{ij}^{(PS)} = P_{ij}^{(SS)} \text{ etc., with } y_D \equiv -y_D, \text{ on the opposite fin}$$

$$P'_{ij}^{(PS)} = P'_{ij}^{(SS)} \text{ etc., with } y \equiv \frac{a^2}{y} \text{ for } 0 < y \leq a, \text{ inside a body}$$

It has been assumed, for simplicity, that the bound vortex of an image has the straight line instead of the actual curved line.

By the relation of,

$$\gamma = \frac{\Gamma}{6U_\infty}, \quad (33)$$

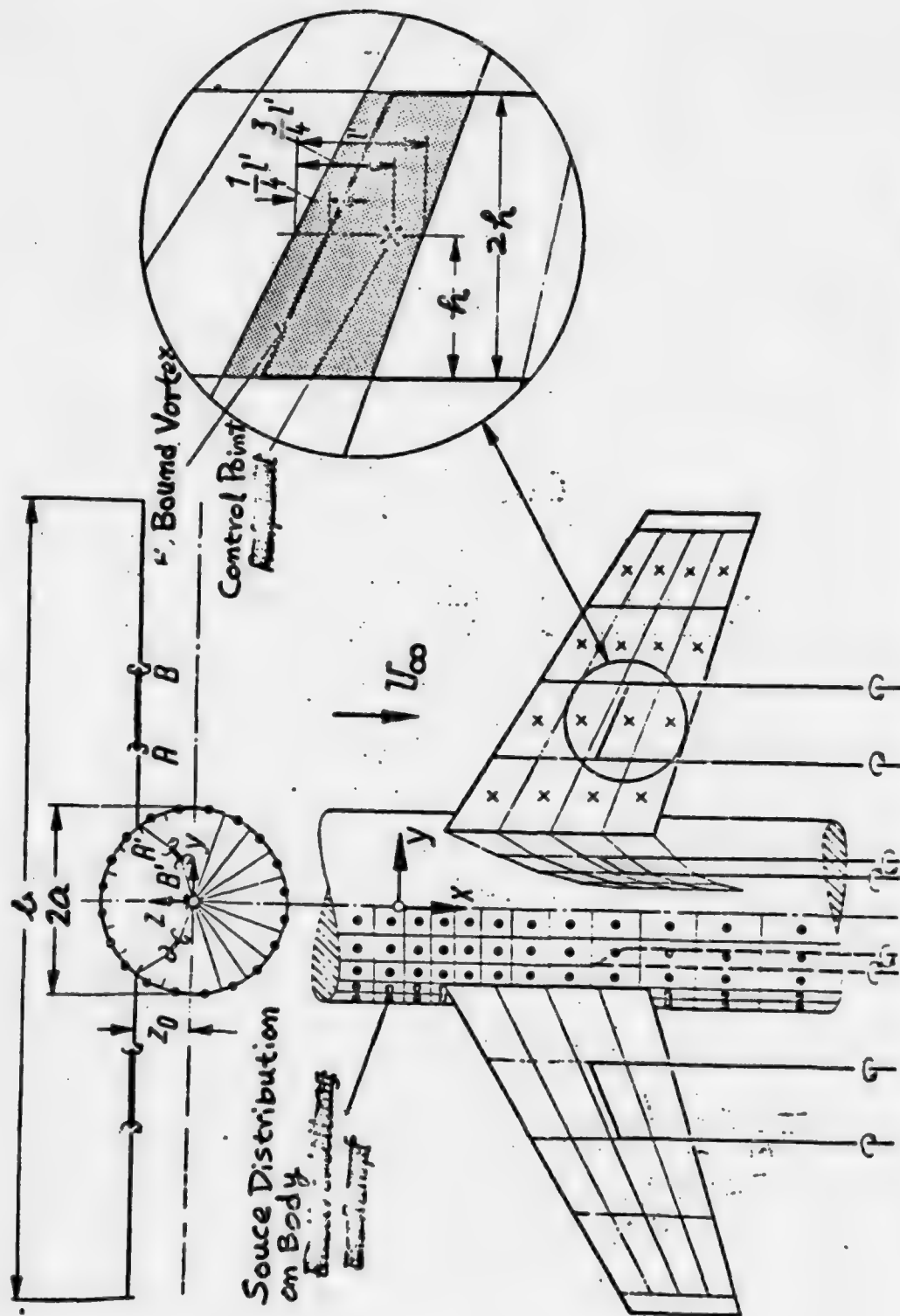


Figure 51. Illustration of wing-body combination with singularities (Refs. [1,3]).

Eq. (32) can be rewritten as:

$$\begin{aligned}\frac{u_i}{U_\infty} &= \sum_{j=1}^n \bar{P}_{ij} \gamma_j \\ \frac{v_i}{U_\infty} &= \sum_{j=1}^n \bar{Q}_{ij} \gamma_j \\ \frac{w_i}{U_\infty} &= \sum_{j=1}^n \bar{R}_{ij} \gamma_j\end{aligned}\quad (34)$$

where,

$$\bar{P}_{ij} = b \{ P_{ij}^{(SS)} + P_{ij}^{(PS)} + P'_{ij}^{(SS)} + P'_{ij}^{(PS)} \}$$

$$\bar{Q}_{ij} = b \{ Q_{ij}^{(SS)} - Q_{ij}^{(PS)} - Q'_{ij}^{(SS)} + Q'_{ij}^{(PS)} \}$$

$$\bar{R}_{ij} = b \{ R_{ij}^{(SS)} + R_{ij}^{(PS)} + R'_{ij}^{(SS)} - R'_{ij}^{(PS)} \}$$

APPENDIX 2. COMPUTER PROGRAM FOR
DETERMINING PRESSURE
DISTRIBUTION ON FIN-BODY
COMBINATION

2.1 Program Description

A computer program has been developed to calculate the pressure distribution and aerodynamic characteristics of fin and fin-body combination in subsonic flow. The program is written in FORTRAN IV, and designed for IBM 360 computer, however, it is easily adaptable to other computers with minor modifications.

2.2 Program Structure

The computer program consists of one main overlay program and thirty-one subroutines.

Main Program

The brief outline of the Main program is shown in Fig. 52. The iteration scheme is used only for a fin-body combination to solve a fin-body interaction result.

A considerably detailed expression of the Main program is shown in Fig. 53. The Main program controls almost all subroutines. The effect of the horizontal fin on the vertical fin is computed in the rear part of this Main program.

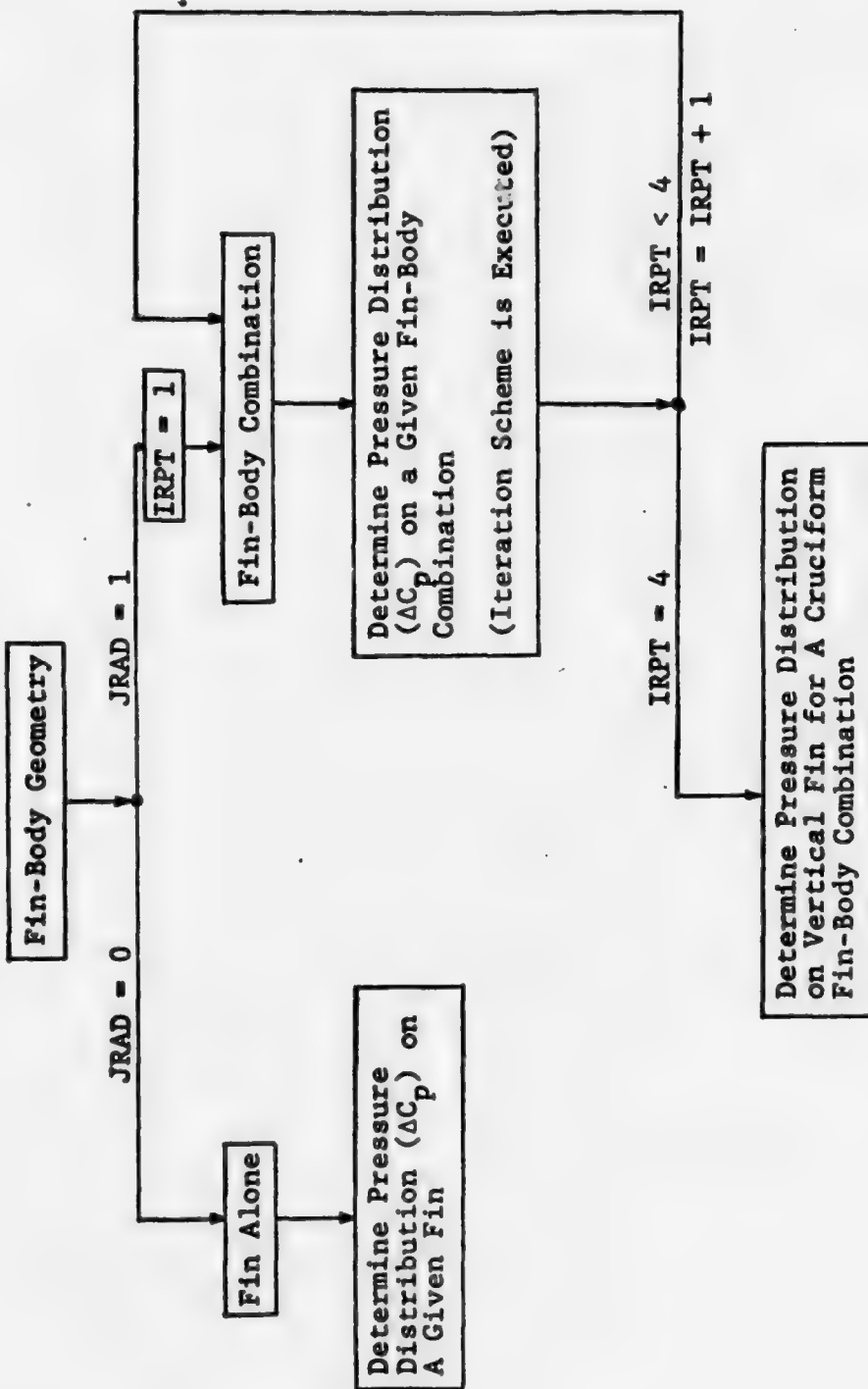


Figure 52. Outline of Main Program.

Aerodynamic Performance of Planar Fin or
Fin-Body Combination Must Be Computed at First.

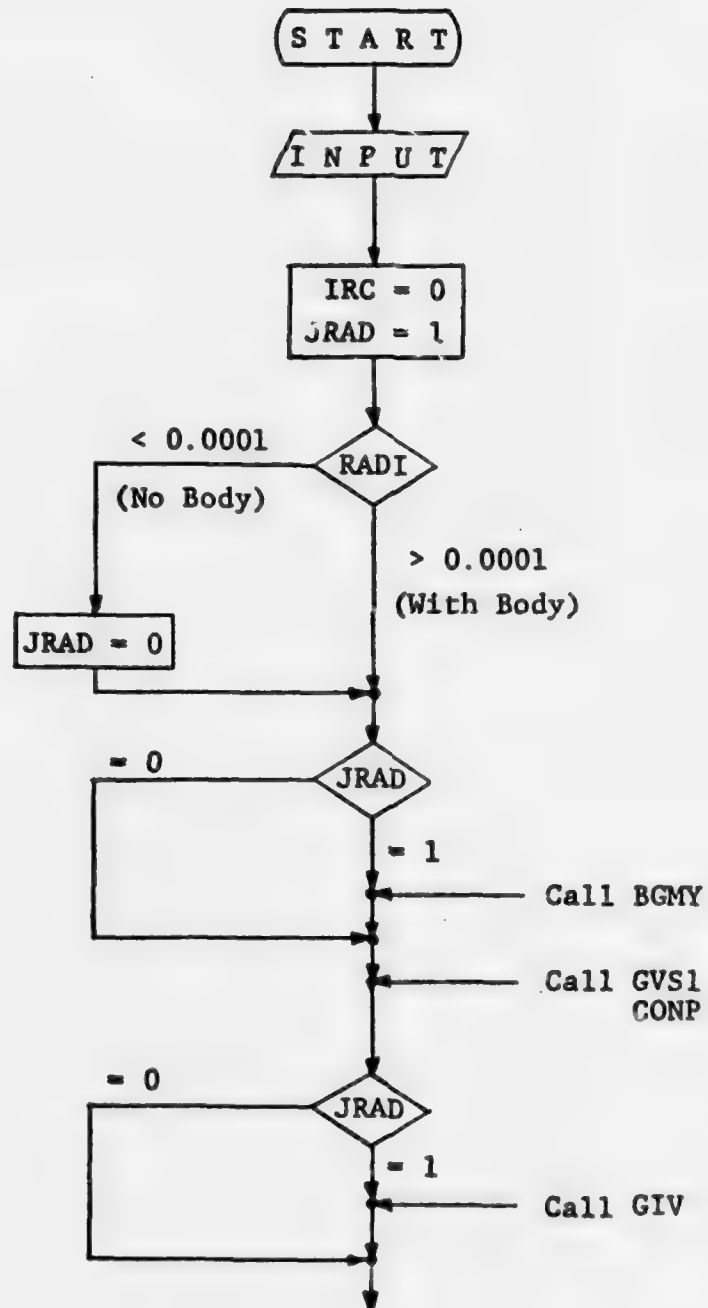


Figure 53. Flow Diagram for MAIN PROGRAM.

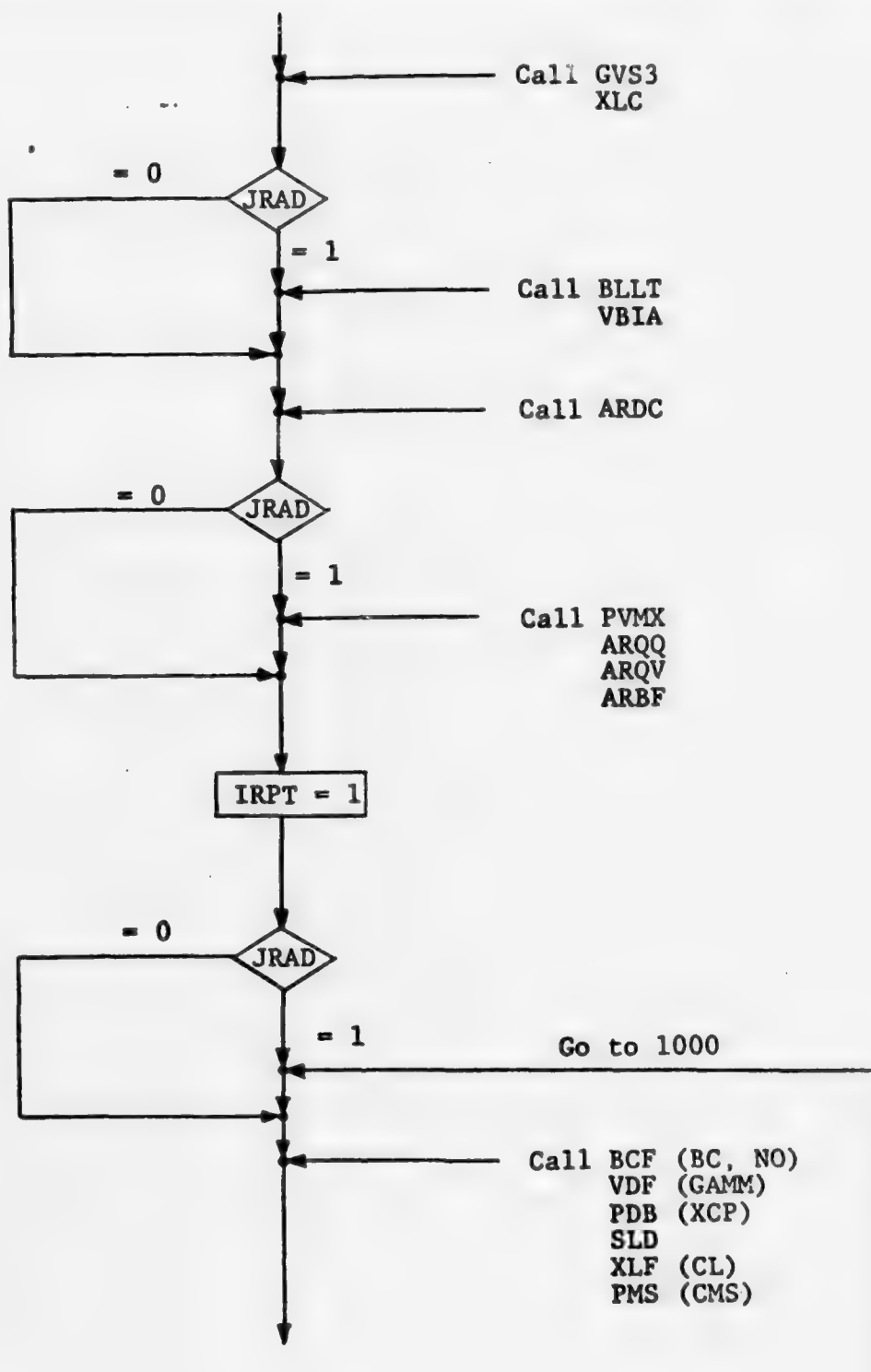


Figure 53. (Continued)

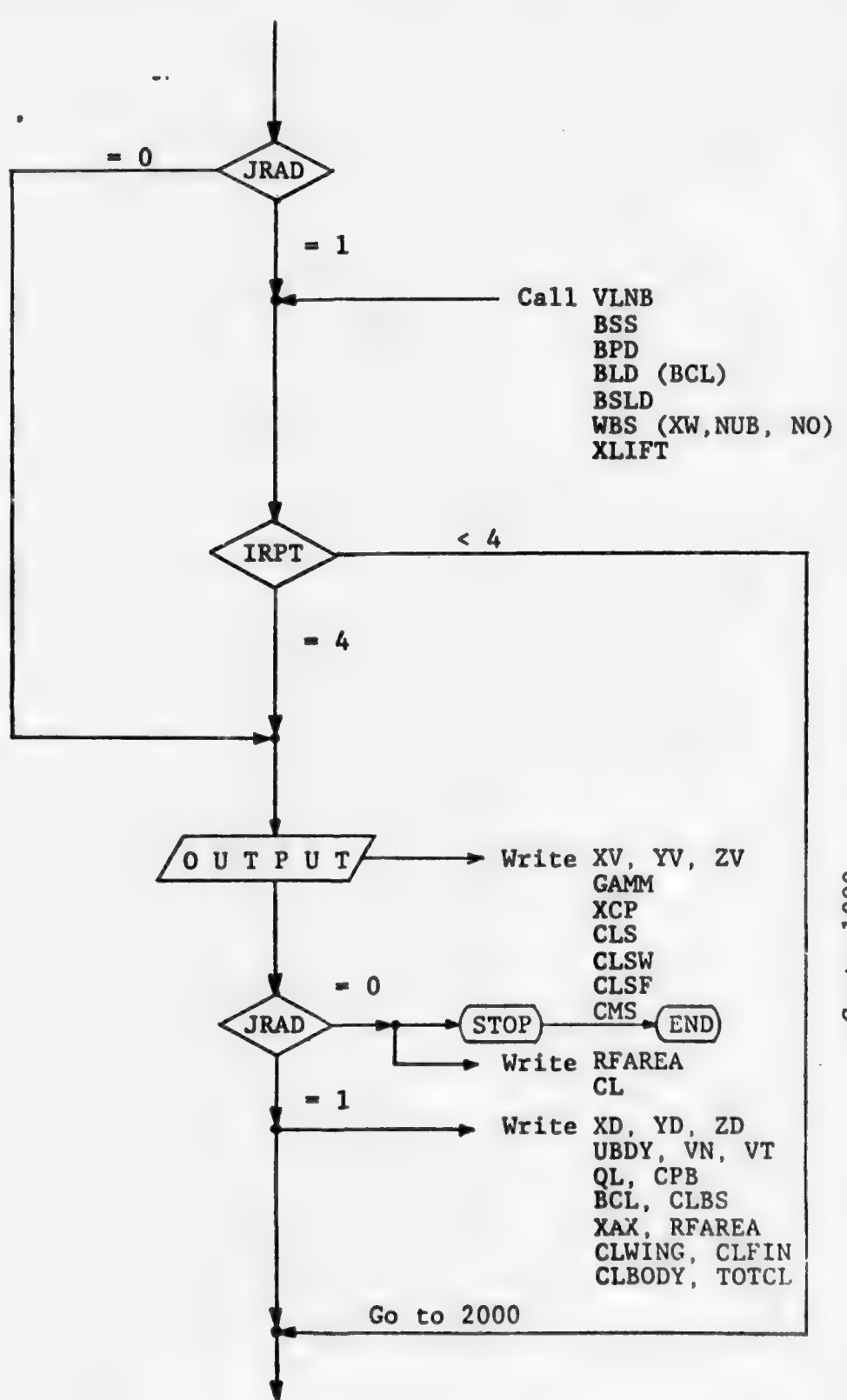
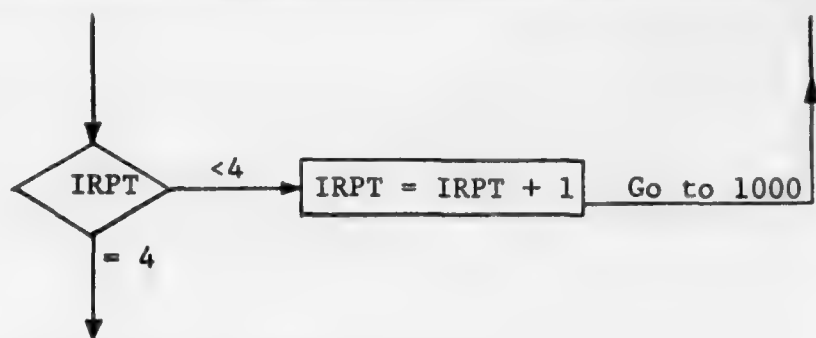


Figure 53. (Continued)



Computation for Aerodynamic Performance of
Planar Fin or Fin-Body Combination Terminates.
Subsequently, Effects of Horizontal Fin on
Vertical Fin is Computed.

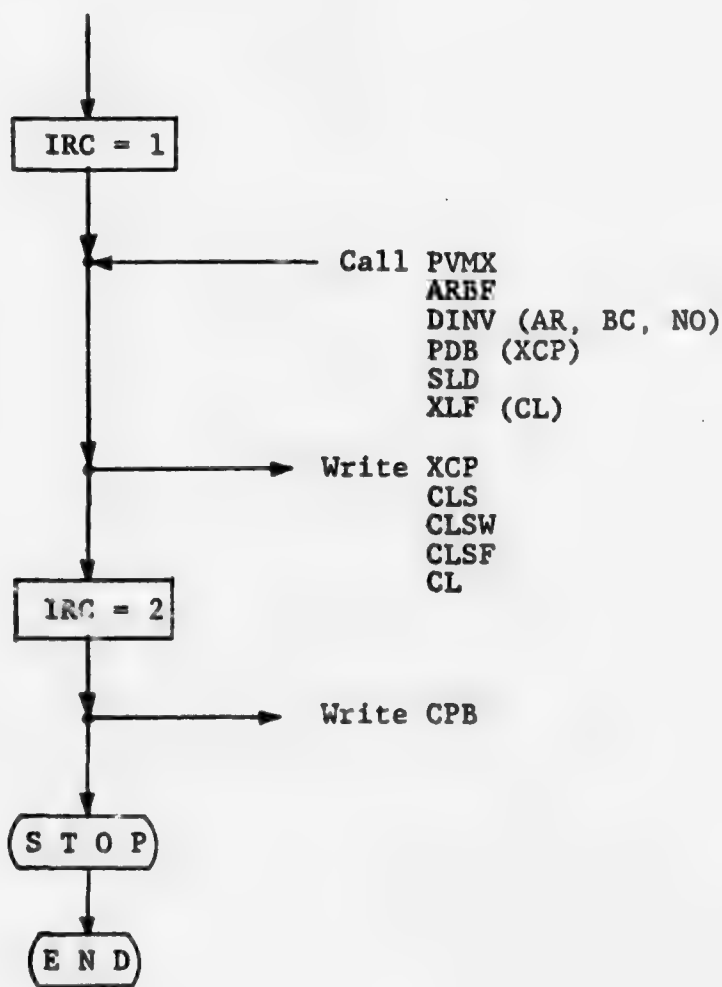


Figure 53. (Concluded)

Subprogram SUBROUTINE ARDC

In this subprogram, the aerodynamic matrices of a fin to fin will be computed. The subprograms PVB, PVP, and PVS are called here.

In this subprogram,

NN = 2, no body
= 4, with body (see Fig. 54)

AR (I,J) = SAR + ASYN * PAR + SIAR + ASYN * PIAR
where, I..... influenced panel
J..... influencing panel

SAR.... }
PAR.... } = WB + WP + WS } for NN = 1
SIAR.... } = 2
PIAR.... } = 3
= 4

(see Fig. 54)

ASYN.... = ASYW for main fin or wing
= ASYF for flap or elevon

Exchange of the Cards (except Data cards)

In the list of the subroutines BGMY and GVS1, the cosine paneling is shown. A few cards must be exchanged by the suitable ones when a user wants the equidistant paneling. They are shown in Table 1. A clear example of the spanwisely equidistant, chordwisely cosine paneling on a fin, and longitudinally cosine paneling on a body is shown in Figs. 28(a) and (b).

TABLE 1. EXCHANGE OF THE CARDS

SUBROUTINE	Line No.	Cosine Paneling	Equidistant Paneling
BGMY	0025 0029 C034	10 $XN(J1+1) = XN(J1) + ABS(X1-XP)*SIN(AZ1*J1)$ 20 $XN(NBF+J2+1) = XN(X1+ABS(X3-X1)*IT-COS(X2*X3)*IT)$ 30 $XN(NB1+J3) = XN(ABS(X3-X1)*(1.0-COS(AZ3*X3)))$	10 $XN(J1+1) = XN(J1) + ABS(X1-XP)/NBF$ 20 $XN(NBF+J2+1) = XN(NBF+J2) + ABS(X3-X1)/NBF$ 30 $XN(NB1+J3) = XN(NB1+J3-1) + ABS(XA-X1)/NBF$
GVS1	0017 0038 0056	 YF(JC+1)=Y1+(Y2-Y1)*(IT-COSTJC*IT/NTITZC) DK(K+1)=COS(THM*EXK) DK(K+1)=COS(THF*EXK) 	 YF(JC+1)=Y1+(Y2-Y1)*(IT-COSTJC*IT/NTITZC) DK(K+1)=DK(K)+1./N DK(K+1)=DK(K)+1./NFLP

2.3 List of Subprograms

All the subprogram SUBROUTINEs and their purposes are shown in Table 2. Most of them are controlled by the Main program.

2.4 List of Symbols

The symbols and their meanings used in the Main program and SUBROUTINEs are shown in Table 3.

TABLE 2
LISTS OF SUBPROGRAMS

NAME	PURPOSE
GVS 1	Defining location of control points on the fin, and half width of local bound vortex.
BGMY	Defining body control points (which also equals to location of body sources).
CONP	Naming location of total control points on fin-body combination.
GIV	Computing location and slope of body image vortex.
GVS 2 (SX, SY, TMU)	Computing interception at S. (See Fig. 48.)
PVB (UB, VB, WB)	Computing normalized perturbation velocity components induced by bound vortex.
PVP (UP, VP, WP)	Computing normalized perturbation velocity component induced by port free vortex.
PVS (US, VS, WS)	Computing perturbation velocity component induced by starboard free vortex.
BCF (XB, N3)	Defining initial angle of attack of fin, and induced angle of attack due to angle of incidence of body (when it is not zero) and distributed sources on body.
ARDC	Computing aerodynamic matrices of fin only.

Table 2. Lists of SUBPROGRAMS (Continued)

NAME	PURPOSE
VDF (GAMM)	Compute circulation strength (i.e., solve the simultaneous linear eqs.).
GVS 3	Computing local fin panel area, reference fin area, and reference chord.
XLC	Computing local chord of fin.
BLLT	Computing local chord length of fin provided that fin was extended into body.
DINV (D, E, N)	Solving the simultaneous linear equation.
PDB (XCP)	Computing pressure distribution (ΔC_p) on fin.
SLD	Computing spanwise lift distribution based on local fin chord.
XLF (CL)	Computing lift coefficient of fin based on reference area (RFAREA).
PMS (CMS)	Computing spanwise moment distribution around 25% local chord based on local chord CLL and XAX.
PVMX	Computing perturbation velocity component on body due to unit circulation of fin.
VLNB	Computing perturbation velocity components on body.
BPD	Computing pressure distribution (C_p) on body.
ARQQ	Computing pressure distribution on body due to unit source strength.

Table 2. Lists of SUBPROGRAMS (Continued)

NAME	PURPOSE
BLD (BCL)	Computing pressure distribution (ΔC_p) on body.
BSS	Computing source strength on body.
ARQV	Computing body source strength for m^{th} iteration.
WBS (XW, N1, N2)	Computing normalized downwash on fin induced by body source.
ARBF	Computing normalized downwash on fin induced by body unit source.
BSLD	Computing spanwise lift distribution on body based on local chord of fin, supposed to be extended into body.
VBIA	Computing angle of attack on fin induced by angle of incidence of body.
XLIFT	Computing lift coefficient of total fin-body combination.

TABLE 3
LIST OF SYMBOLS

*: Control parameter. Integer inside of () denotes dimensions.

SYMBOLS	MEANINGS
BD (56)	(Equivalent to XB in SUBPROGRAM BCF.) Apparent angle of attack of local panel.
XW (56)	Normalized component of induced velocity on local panel due to body source.
GAMM (55)	Circulation strength of local panel
XREF (10)	X-coordinate for 25% local chord of fin.
XCP (55)	Pressure difference (ΔC_p) on local panel of fin.
CMS (10)	Spanwise moment distribution around 25% local chord, based on local chord of fin.
BCL (36)	Pressure difference (ΔC_p) on body.
RADI	Radius of body (= constant in present analysis).
CPB (72)	Pressure coefficient (C_p) on body.
AR (56, 56)	Aerodynamic influence matrix for fin only.
AQ (72, 72)	Perturbation velocity component (x-direction) on body due to body source ($(C_p)_B =$ $-2(u + u_s)/\beta^2$, see SUBPROGRAM BPD).
ASV (72, 72)	$= \frac{1}{2\pi} \frac{[1 - \cos(\theta_\mu - \theta_\nu)] \beta a \Delta S_\nu}{[(x_\mu - x_\nu)^2 + \beta^2 (1 - \cos(\theta_\mu - \theta_\nu)) a^2]^{3/2}}$ (See Eq. (10).)

Table 3. "List of Symbols (Continued)

SYMBOLS	MEANINGS
AFN (72,55)	Coefficient for determining induced velocity (w-component) on fin due to unit source strength on body.
MB	Circumferential division number along half body.
NB	= NBF + NBM + NBB.
NUB	= NB x MB; total panel numbers on half body.
PSA (55)	Local panel area (includes compressible effect).
BREF (5)	Local chord of fin, provided extending into body.
XDV (55)	= XG - SV; 1/2 local panel chord through its center in present analysis.
YVI (55)	Y - location of center of bound vortex for body image.
WHI (55)	Half width of body image vortex.
TLMDI (55)	Slope (or gradient) of bound vortex of body image.
NBF, NBM, NBB	Longitudinal division numbers on body for forward (ahead of L. E. of fin location), middle (at fin location), and backward (aft of it), respectively.
FDL	See Fig. 56(a).
BDL	
ALFAB	Angle of attack of body (degrees).

Table 3. - List of Symbols (Continued)

SYMBOLS	MEANINGS
XBW (55)	Additive angle of attack of local panel of fin due to body angle of attack.
*JRAD	Control integer. See Figs. 52, 53.
AREAB (96)	Local panel area on body surface.
UBDY (72)	Induced velocity (u -component) at control point on body.
VN (72)	Induced velocity component normal to body surface due to circulation of fin.
QL (72)	Source strength per unit body surface area.
*ASYF	} Control variables. See 2.2 Input Data Cards.
*ASYW	
CLL (55)	Local chord length ($= XC3 - XC1$).
BCL	Load distribution on body.
M1	$= MB/2$.
NFLP	Chordwise division number for flap or elevon.
NT	$= N + NFLP$.
NW	$= M \times N$.
AFLAP	Flap or elevon deflection (degrees).
*IRPT	Control integer. (See Figs. 52, 53).
X1, Y1...X6, Y6	See Fig. 55(a).
M	Spanwise division number for main fin.
N	Chordwise division number for main fin.

Table 3. -List of Symbols (Continued)

SYMBOLS	MEANINGS
XM	Free stream Mach number.
ALFAF	Angle of attack for fin (degrees).
NO	M x NT (total panel number for half fin).
PI	Constant (= 3.14159).
BETA	= $\sqrt{1 - M_\infty^2}$
SPN	(= Y 2)
XC1 (55)	{ Location in x-direction of intercept points. See Fig. 55(c).
XC2 (5)	
XC3 (5)	
ABU (72,55)	
ABV (72,55)	Induced velocity components at control point on fin, due to circulation of fin.
ABW (72,55)	
XL (10)	XC2 - XC1. See Fig. 55(c).
NTOT	= NO + NUB, total panel number.
XG (55)	{ Location of control point on fin.
YG (55)	
ZG (55)	
XS (72)	Location of source distribution on body (= location of control point on body).
TS (127)	Angular position for source (thus, control point) on body (radian).

Table 3. -List of Symbols (Continued)

SYMBOLS	MEANINGS
XD (127)	
YD (127)	
ZD (127)	
XV (55), YV (55), ZV (55)	Location of control point of local panel of fin-body combination.
WH (55)	Location of middle of bound vortex on local panel of fin.
TLMD (55)	Half width of local panel on fin.
YF	Slope of local bound vortex. See Fig. 55(b).
RFAREA	
XAX	
DT	
*IRC	Y - location of local panel edges. See Fig. 55(b).
DX (96)	Reference area for C_L .
CLS (5)	Maximum chord length of fin, reference chord.
CLSW (5)	Circumferential length of local body panel.
CLSF (5)	Control integer. See Fig. 53.
CLBS (5)	Longitudinal length of local body panel.
	Spanwise lift distribution for wing + fin based on CLL.
	Spanwise lift distribution for wing, based on CLL.
	Spanwise lift distribution for fin, based on CLL.
	Spanwise lift distribution on body, based on BREF.

Table 3. List of Symbols (Continued)

SYMBOLS	MEANINGS
CLWING	C_L for wing or main fin, based on reference area (RFAREA)
CLFIN	C_L for flap or elevon, based on reference area (RFAREA).
CLBODY	C_L for body, based on RFAREA.
TOTCL	Total C_L ($= (C_L)_{wing} + (C_L)_{fin} + (C_L)_{body}$)

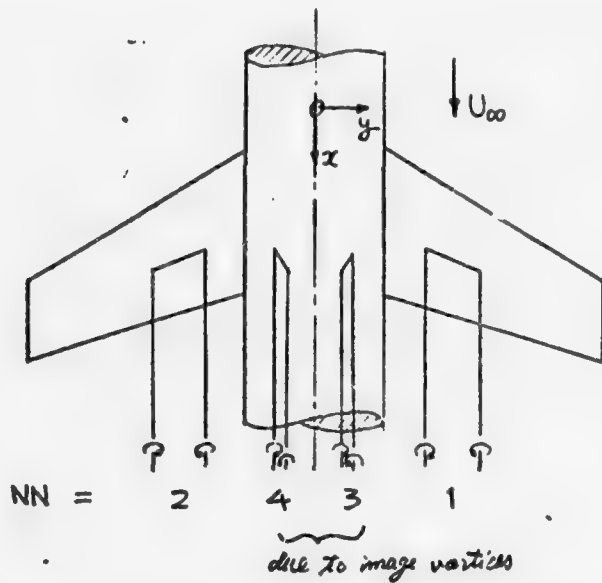


Figure 54. Fin vertices and its images.

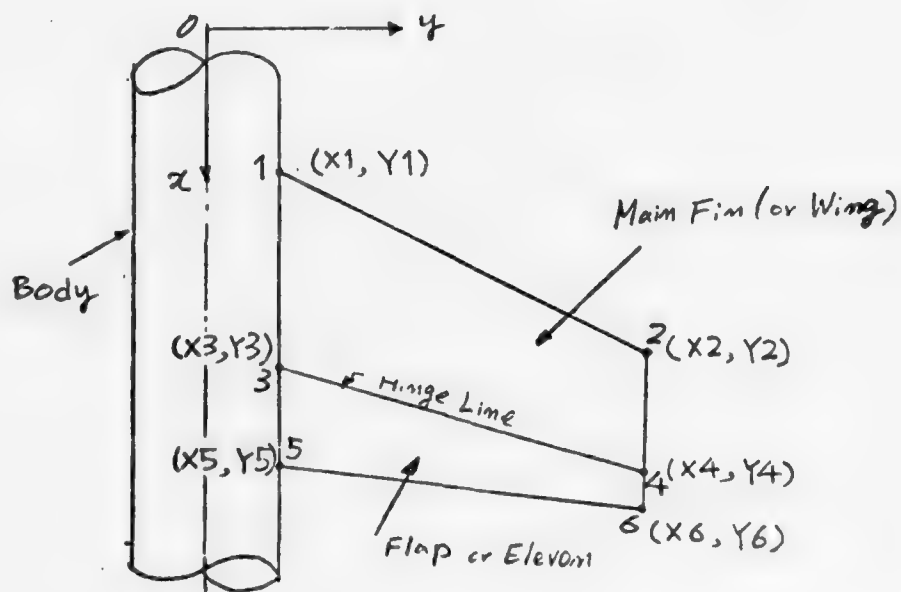


Figure 55a. Fin-body geometry coordinate input.

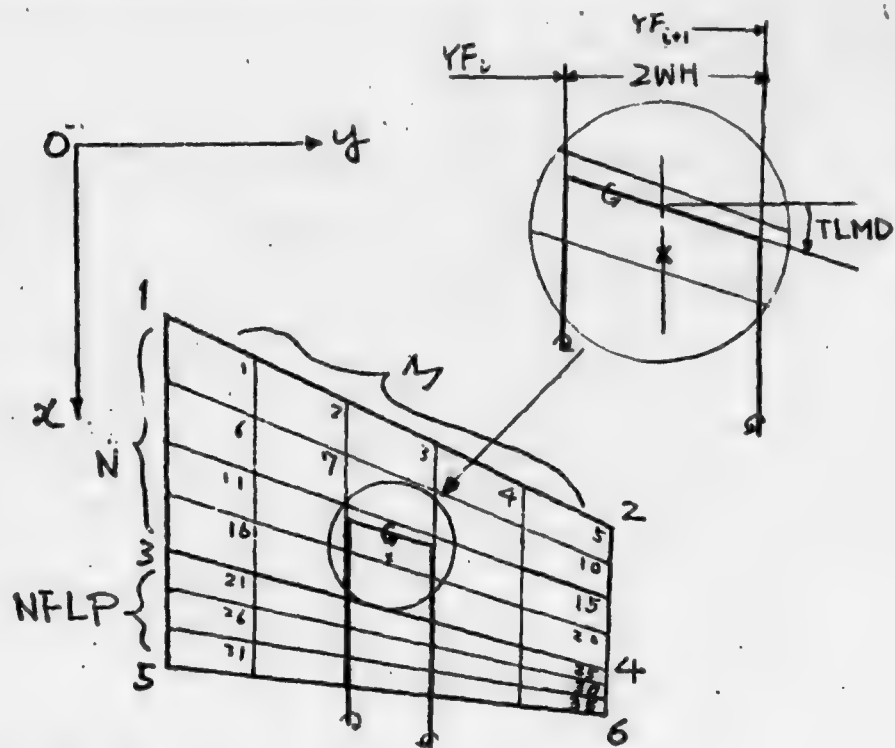


Figure 55b. Fin panel division number and named panels
(the above figure shows total 35 panels case).

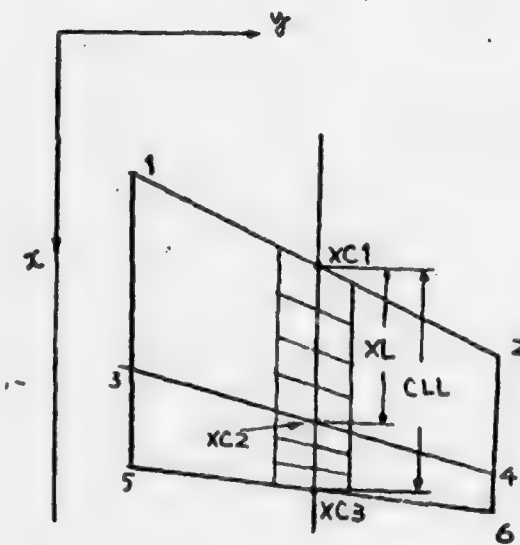


Figure 55c. Local chord definition.

2.5 INPUT DATA Cards

The fin-body geometry must be given by the 1st and 2nd cards.

	<u>Column</u>	<u>Symbols</u>	<u>Explanation</u>
<u>1st Card</u>	FORMAT (8F10.5)		
	1 - 10	X1	Coordinate of the corner
	11 - 20	Y1	points of main fin or wing.
	21 - 30	X2	(See Fig. 55(a).) If no
	31 - 40	Y2	flap nor elevon, X3, Y3, X4,
	41 - 50	X3 (or X5)	Y4 must be the same values
	51 - 60	Y3 (or Y5)	as X5, Y5, X6, Y6, respec-
	61 - 70	X4 (or X6)	tively.
	71 - 80	Y4 (or Y6)	
<u>2nd Card</u>	FORMAT (4F10.5)		
	1 - 10	X5	Coordinate of the corner
	11 - 20	Y5	points of a flap or an ele-
	21 - 30	X6	von.
	31 - 40	Y6	
Panel number of a fin must be given by the 3rd card.			
<u>3rd Card</u>	FORMAT (3I10)		
	1 - 10	M	Spanwise panel number of
			main fin. (See Fig. 55(b).)
	11 - 20	N	Chordwise panel number of
			main fin.
	21 - 30	NFLP	Chordwise panel number of
			flap or elevon.
M must be less than or equal to five. The sum of N and NFLP must be less than or equal to eleven.			
Panel number of a body must be given by the 4th card.			
<u>4th Card</u>	FORMAT (4I10, 2F10.5)		
	1 - 10	MB	Circumferential panel number. (See Fig. 56(a).)
	11 - 20	NBF	} Longitudinal panel number { for front part.
	21 - 30	NBM	
	31 - 40	NBB	
			{ for middle part. for aft part.

4th Card (Continued)

41 - 50	FDL	Front part length/(X3-X1).
51 - 60	BDL	Aft part length/(X3-X1).

MB must be six. Total sum of NBF, NBM, and NBB must be less than or equal to twelve.

Aerodynamic Input must be given by the 5th card.

5th Card FORMAT (6F10.5)

1 - 10	XM	Free stream Mach number. (See Fig. 57.)
11 - 20	ALFAF	Angle-of-attack of main fin or wing.
21 - 30	ALFAB	Body Angle-of-attack.
31 - 40	AFLAP	Angle-of-attack of flap or elevon.
41 - 50	ASYW	= 1. for symmetrical flow of main fin or wing; = -1. for asymmetrical flow of main fin or wing.
51 - 60	ASYF	= 1. for symmetrical flow of flap or elevon. = -1. for asymmetrical flow of flap or elevon.

XM must be less than 1.0. Only when ALFAB equals to zero, ASYW and/or ASYF can take -1.0. Nonetheless that ASYW and/or ASYF equal to 1.0 or -1.0, the same amount of angle-of-attack of a pair of fins must be taken, thus the case that the right hand side of a pair of fins has angle-of-attack of 5° , and the left has 3° , cannot be allowed.

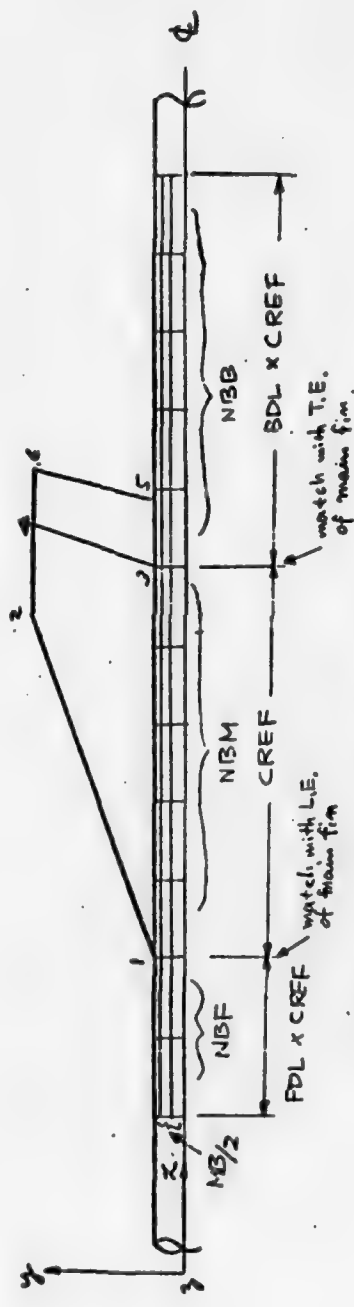


Figure 56a. Body paneling (for equidistance case).

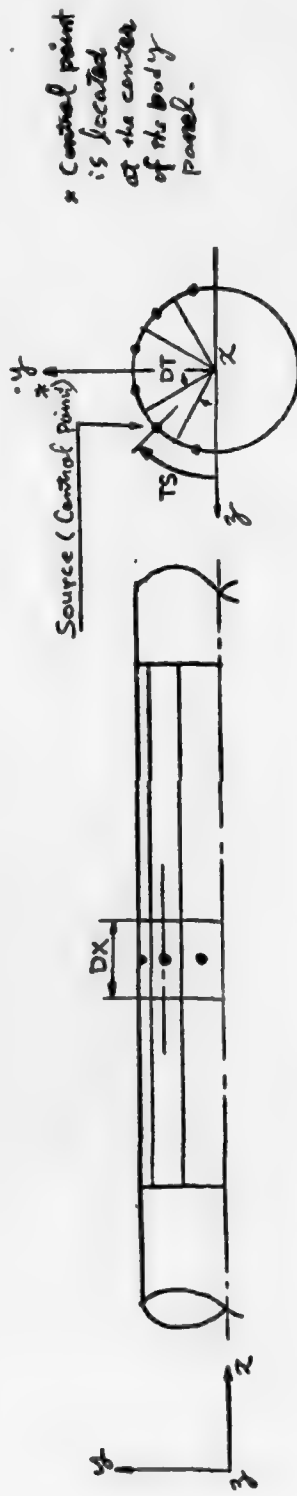


Figure 56b. Body paneling and body control point.

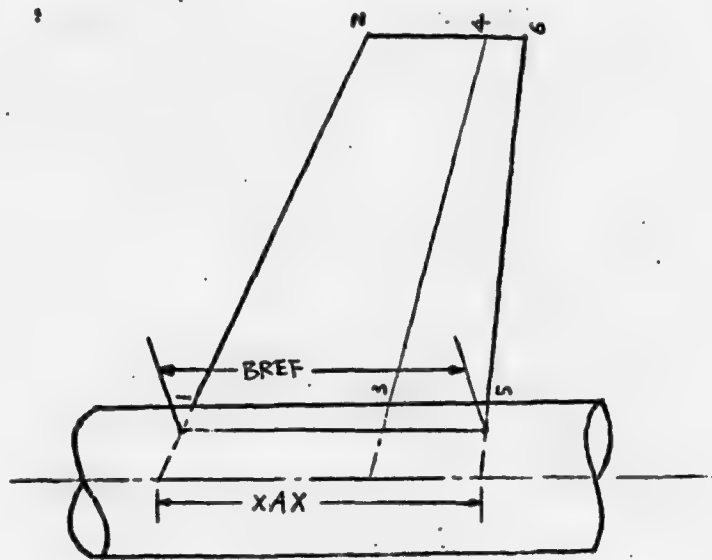


Figure 56c. Fin extended into body.

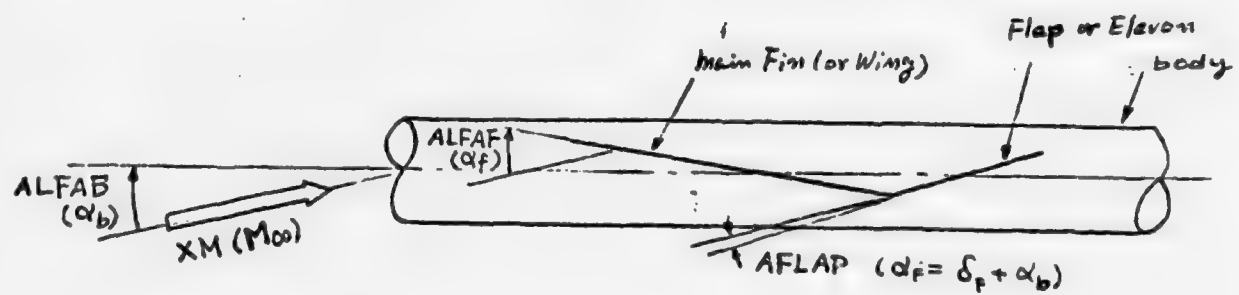


Figure 57. Aerodynamic input of fin-body combination

2.6 Program Output

One example of the computer print output is shown in
Table 4. The corresponding fin is the following:

Fin-body configuration..... cylindrical body with
rectangular fin

Fin aspect ratio..... 6

Maximum span/body diameter.. 6

Fin panel number..... 25

Body panel number..... 60

Total fin-body panel number. 85

Free stream Mach number.... 0.4

Angle of incidence of body.. +2($^{\circ}$)

No cant angle of fin, no flap

Remark: Note that WING CL, FIN CL, BODY CL, and TOTAL CL
in Output are half values of the correct ones, thus these values
have to be multiplied by two to obtain correct CL based on
reference area (also, see SUBROUTINE XLIFT). CL for fin only is
also in the same thing.

TABLE 4. EXAMPLE OF COMPUTER OUTPUT

----- COMPUTATION FOR SURFACE PRESSURE DISTRIBUTION ON FIN-BODY COMBINATION AT SUBSONIC SPEEDS

FIN-BODY GEOMETRY

<i>x₁</i>	<i>y₁</i>	<i>x₂</i>	<i>y₂</i>	<i>x₃</i>	<i>y₃</i>	<i>x₄</i>	<i>y₄</i>	<i>x₅</i>	<i>y₅</i>	<i>x₆</i>	<i>y₆</i>
0.0	0.500	0.0	5.000	1.0000	0.500	1.0000	3.000	1.0000	0.5000	1.0000	3.0000

FIN-BODY PANEL NUMBER

M = 5 N = 5 NFLP = 0 NW = 25 NO = 25

NB = 6 NBF = 3 NBH = 4 NBW = 3 NB = 10 NUB = 60

FDL = 0.50 BDL = 1.00 TOTAL PANEL = 85

MACH AU = 0.400 ANGLE OF INCIDENCE = 2.00 (DEG) FIN ANGLE OF ATTACK = 2.00 (DEG)
FLAP ANGLE OF ATTACK = 2.00 (DEG) FIN SYMMETRY = 1.00 FLAP SYMMETRY = 1.00

REFERENCE CHORD

ON BODY

BREF(1) = 0.10000E 01 0.10000E 01 0.10000E 01

ON FIN

XL(1)	=	0.10000E 01					
CLL(1)	=	0.10000E 01					
XC1(1)	=	0.0	0.0	0.0	0.0	0.0	0.0
XC2(1)	=	0.10000E 01					
XC3(1)	=	0.10000E 01					

ITERATION = 4

PRESSURE DISTRIBUTION ON PLANAR FIN

NO	XV	YV	ZV	XNR	YNR	GAMMA	XCP
1	0.12236E-01	0.61936E 00	0.0	0.12236E-01	0.20645E 00	0.37426E-02	0.10924E 01
2	-0.12236E-01	0.10512E 01	0.0	0.12236E-01	0.35041E 00	0.33271E-02	0.97112E 00
3	0.12236E-01	0.17500E 01	0.0	0.12236E-01	0.58333E 00	0.29734E-02	0.86789E 00
4	0.12236E-01	0.24488E 01	0.0	0.12236E-01	0.81626E 00	0.25238E-02	0.73666E 00
5	0.12236E-01	0.28806E 01	0.0	0.12236E-01	0.96021E 00	0.18182E-02	0.53070E 00
6	0.64453E-01	0.61936E 00	0.0	0.84453E-01	0.20645E 00	0.41028E-02	0.41265E 00
7	0.84453E-01	0.10512E 01	0.0	0.84453E-01	0.35041E 00	0.38394E-02	0.38615E 00
8	0.84453E-01	0.17500E 01	0.0	0.84453E-01	0.58333E 00	0.36458E-02	0.34657E 00
9	0.84453E-01	0.24488E 01	0.0	0.84453E-01	0.81626E 00	0.288804E-02	0.28970E 00
10	0.84453E-01	0.28806E 01	0.0	0.84453E-01	0.96021E 00	0.19053E-02	0.19163E 00
11	0.24488E 00	0.61936E 00	0.0	0.24488E 00	0.20645E 00	0.32314E-02	0.20867E 00
12	0.244649E 00	0.10512E 01	0.0	0.244649E 00	0.35041E 00	0.32413E-02	0.20930E 00
13	0.24629L 00	0.17500E 01	0.0	0.24629L 00	0.58333E 00	0.29380E-02	0.18972E 00
14	0.24629L 01	0.24488E 01	0.0	0.24629E 00	0.81626E 00	0.23750E-02	0.15336E 00
15	0.24629E 00	0.28806E 01	0.0	0.24629E 00	0.96021E 00	0.13974E-02	0.90236E-01
16	0.48191E 00	0.61936E 00	0.0	0.48191E 00	0.20645E 00	0.23247E-02	0.11913E 00
17	0.48191E 00	0.10512E 01	0.0	0.48191E 00	0.35041E 00	0.23842E-02	0.12218E 00
18	0.48191E 00	0.17500E 01	0.0	0.48191E 00	0.58333E 00	0.21855E-02	0.11200E 00
19	0.48191E 00	0.24488E 01	0.0	0.48191E 00	0.81626E 00	0.16992E-02	0.87076E-01
20	0.48191E 00	0.28806E 01	0.0	0.48191E 00	0.96021E 00	0.95491E-03	0.46935E-01
21	0.76824E 00	0.61936E 00	0.0	0.76824E 00	0.20645E 00	0.13344E-02	0.61689E-01
22	0.76824E 00	0.10512E 01	0.0	0.76824E 00	0.35041E 00	0.13941E-02	0.64449E-01
23	0.76824E 00	0.17500E 01	0.0	0.76824E 00	0.58333E 00	0.12829E-02	0.59308E-01
24	0.76824E 00	0.24488E 01	0.0	0.76824E 00	0.81626E 00	0.97063E-03	0.44872E-01
25	0.76824L 00	0.28806E 01	0.0	0.76824E 00	0.96021E 00	0.54850E-03	0.25357E-01

SPATIAL LIFT AND MOMENT DISTRIBUTION

	1	2	3	4	5
CLSL()	0.21051E 00	0.20266E 00	0.18322E 00	0.14927E 00	0.94633E-01
CLSh()	0.21051E 00	0.20266E 00	0.18322E 00	0.14927E 00	0.94633E-01
CLSF()	0.0	0.0	0.0	0.0	0.0
CMS()	-0.50055E-02	-0.23326E-02	-0.16661E-02	-0.26952E-02	-0.35314E-02

PRESSURE DISTRIBUTION ON BODY *****

NO	XD	YD	ZD	UBDY	VN	VT	AT	CPB
- 26	-0.37500E-00	-0.12941E-00	-0.48296E-00	-0.35355E-00	0.85831E-01	-0.21149E-02	-0.15401E-01	-0.28372E-01
- 27	-0.37500E-00	0.35355E-00	0.48296E-00	0.35355E-00	0.96993E-02	0.85046E-02	-0.80122E-02	-0.15984E-01
- 28	-0.37500E-00	0.48296E-00	0.12941E-00	0.12941E-00	0.51997E-02	-0.16680E-01	-0.92072E-02	-0.15564E-01
- 29	-0.37500E-00	0.48296E-00	-0.12941E-00	-0.12941E-00	-0.51996E-02	-0.46380E-02	-0.16680E-01	-0.15564E-01
- 30	-0.37500E-00	0.35355E-00	-0.35355E-00	-0.35355E-00	-0.96993E-02	-0.85046E-02	-0.80123E-02	0.15984E-01
- 31	-0.37500E-00	0.12941E-00	-0.48296E-00	-0.10009E-01	-0.10009E-01	-0.95831E-02	-0.21149E-02	0.15401E-01
- 32	-0.15849E-00	0.12941E-00	0.48296E-00	0.48296E-00	0.15468E-01	0.80508L-02	-0.14694E-02	-0.14110E-01
- 33	-0.15849E-00	0.35355E-00	0.35355E-00	0.35355E-00	0.18411E-01	0.94835E-02	-0.75085E-02	-0.17683E-01
- 34	-0.15849E-00	0.48296E-00	0.12941E-00	0.12941E-00	0.17453E-01	0.83411E-01	-0.28302E-01	-0.16749E-01
- 35	-0.15849E-00	0.48296E-00	-0.12941E-00	-0.12941E-00	-0.17453E-01	-0.83411E-02	-0.28303E-01	0.16749E-01
- 36	-0.15849E-00	0.35355E-00	-0.35355E-00	-0.35355E-00	-0.18411E-01	-0.94835E-02	-0.75085E-02	0.16749E-01
- 37	-0.15849E-00	0.12941E-00	-0.48296E-00	-0.48296E-00	-0.15468E-01	-0.80508E-02	-0.14694E-02	0.14110E-01
- 38	-0.33494E-01	0.12941E-00	0.48296E-00	0.48296E-00	0.18662E-01	0.60597E-02	-0.34533E-03	-0.10547E-01
- 39	-0.33494E-01	0.35355E-00	0.35355E-00	0.35355E-00	0.24991E-01	0.75131E-02	-0.36780E-02	-0.13989E-01
- 40	-0.33494E-01	0.48296E-00	0.12941E-00	0.12941E-00	0.45816E-01	0.95395E-02	-0.29323E-01	-0.19139E-01
- 41	-0.33494E-01	0.48296E-00	-0.12941E-00	-0.12941E-00	-0.45816E-01	-0.95395E-02	-0.29323E-01	0.19139E-01
- 42	-0.33494E-01	0.35355E-00	-0.35355E-00	-0.35355E-00	-0.24991E-01	-0.75132E-02	-0.36780E-02	0.13989E-01
- 43	-0.33494E-01	0.12941E-00	-0.48296E-00	-0.48296E-00	-0.18662E-01	-0.60597E-02	-0.34533E-03	0.10547E-01
- 44	0.30064E-01	0.12941E-00	0.48296E-00	0.48296E-00	0.24991E-01	0.43298E-02	0.55599E-03	-0.74660E-02
- 45	0.38664E-01	0.35355E-00	0.35355E-00	0.35355E-00	0.27780E-01	0.51514E-02	0.94633E-04	-0.95323E-02
- 46	0.32664E-01	0.48296E-00	0.12941E-00	0.12941E-00	0.62951E-01	0.51048L-02	-0.97593E-02	-0.10204E-01
- 47	0.36664E-01	0.48296E-00	-0.12941E-00	-0.12941E-00	-0.62951L-01	-0.51048L-02	-0.97594E-02	0.10204E-01
- 48	0.30064E-01	0.35355E-00	-0.35355E-00	-0.35355E-00	-0.27780E-01	-0.51514E-02	0.94610E-04	0.95323E-02
- 49	0.38664E-01	0.12941E-00	-0.48296E-00	-0.48296E-00	-0.24991E-01	-0.43298L-02	0.55599E-03	0.74660L-02
- 50	0.16451E-00	0.12941E-00	0.48296E-00	0.48296E-00	0.20892E-01	0.22249E-03	0.26448E-02	-0.60963E-04
- 51	0.18451E-00	0.35355E-00	0.35355E-00	0.35355E-00	0.26945E-01	0.50153E-03	0.88983E-02	0.12217E-02
- 52	0.18451E-00	0.48296E-00	0.12941E-00	0.12941E-00	-0.50302E-01	0.25648E-02	0.25084E-01	-0.53028E-02
- 53	0.16451E-00	0.48296E-00	-0.12941E-00	-0.12941E-00	-0.50302E-01	-0.25084E-02	-0.11293E-00	0.11293E-00

Reproduced from
best available copy.

56	0.18651E 99	0.35355E 99	-0.35355E 99	-0.26694E 00	-0.35355E 99	0.50155E -03	0.809983E -02	-0.12217E -02	0.55985E -01	
55	0.18451E 00	0.12941E 00	-0.48296E 00	-0.70892E -01	-0.22249E -03	0.60954E -04	0.36517E -01	-0.36517E -01	-0.33551E -01	
56	0.42510E 00	0.12941E 00	0.48296E 00	0.17429E -04	-0.55169E -02	0.56840E -02	0.10124E -01	-0.10124E -01	-0.33551E -01	
-	57	0.45510E 00	0.35355E 00	0.21237E -01	-0.63250E -02	0.19251E -01	0.12191E -01	-0.44352E -01	-0.44352E -01	
58	0.45510E 00	0.48296E 00	0.12941E 00	0.29278E -01	-0.41329E -02	0.37880E -01	0.63853E -02	-0.67407E -01	-0.67407E -01	
59	0.45510E 00	0.48296E 00	-0.12941E 00	-0.29278E -01	0.41328E -02	0.37881E -01	-0.83852E -02	0.67408E -01	-0.67408E -01	
-	60	0.45510E 00	0.35355E 00	-0.21237E -01	0.63250E -02	0.19251E -01	-0.12191E -01	0.44352E -01	-0.44352E -01	
61	0.45510E 00	0.12941E 00	-0.48296E 00	-0.17429E -01	0.55169E -02	0.56841E -02	-0.10124E -01	0.33551E -01	-0.33551E -01	
62	0.80666E 00	0.12941E 00	0.48296E 00	0.10614E -01	-0.77821E -02	0.73034E -02	0.14266E -01	-0.23002E -01	-0.23002E -01	
-	63	0.80666E 00	0.32355E 00	0.35355E 00	0.11376E -01	-0.75849E -02	0.23437E -01	0.14462E -01	-0.25599E -01	-0.25599E -01
64	0.80866E 00	0.48276E 00	0.12941E 00	0.15766E -01	-0.47142E -02	0.44033E -01	0.95206E -02	-0.32320E -01	-0.32320E -01	
65	0.60866E 00	0.48296E 00	-0.12941E 00	-0.13766E -01	0.47142E -02	0.44033E -01	-0.95206E -02	0.32320E -01	-0.32320E -01	
66	0.80866E 00	0.35355E 00	-0.35355E 00	-0.11376E -01	0.75849E -02	0.23437E -01	-0.14462E -01	0.25599E -01	-0.25599E -01	
67	0.80666E 00	0.12941E 00	-0.48296E 00	-0.19614E -01	0.77821E -02	0.73034E -02	-0.14266E -01	0.23002E -01	-0.23002E -01	
68	0.10675E 01	0.12941E 00	0.48296E 00	0.65682E -02	-0.71650E -02	0.74206E -02	0.14056E -01	-0.17224E -01	-0.17224E -01	
-	69	0.10675E 01	0.35355E 00	0.35355E 00	0.60243E -02	-0.64725E -02	0.23112E -01	-0.12935E -01	-0.16267E -01	-0.16267E -01
70	0.10675E 01	0.48296E 00	0.12941E 00	0.31645E -02	-0.32060E -02	0.39467E -01	0.65702E -02	-0.87982E -02	-0.87982E -02	
71	0.10675E 01	0.48296E 00	-0.12941E 00	-0.31644E -02	0.32060E -02	0.39467E -01	-0.65701E -02	0.87981E -02	-0.87981E -02	
72	0.10675E 01	0.35355E 00	-0.35355E 00	-0.60243E -02	0.64725E -02	0.23112E -01	-0.12935E -01	0.16267E -01	-0.16267E -01	
73	0.10675E 01	0.12941E 00	-0.48296E 00	-0.65682E -02	0.71650E -02	0.74207E -02	-0.14056E -01	0.17224E -01	-0.17224E -01	
74	0.10675E 01	0.12941E 00	0.48296E 00	0.49222E -02	-0.59164E -02	0.71552E -02	0.11474E -01	-0.12849E -01	-0.12849E -01	
-	75	0.10675E 01	0.35355E 00	0.35355E 00	0.33793E -02	-0.49144E -02	0.21759E -01	0.97065E -02	-0.10671E -01	-0.10671E -01
76	0.10675E 01	0.48296E 00	0.12941E 00	0.14309E -02	-0.20867E -02	0.35576E -01	0.42054E -02	-0.45456E -02	-0.45456E -02	
77	0.13170E 01	0.12941E 00	-0.48296E 00	-0.12941E 00	-0.14308E -02	0.20867E -02	0.35576E -01	-0.42054E -02	0.45455E -02	
-	78	0.13170E 01	0.35355E 00	-0.35355E 00	-0.33793E -02	0.49144E -02	0.21759E -01	-0.97065E -02	0.10671E -01	-0.10671E -01
79	0.13170E 01	0.12941E 00	-0.48296E 00	-0.49222E -02	0.59164E -02	0.71553E -02	-0.11474E -01	0.12849E -01	-0.12849E -01	
80	0.17500E 01	0.12941E 00	0.48296E 00	0.48296E 00	0.20246E -02	0.40373E -02	0.66695E -02	-0.78626E -02	-0.82437E -02	
-	81	0.17500E 01	0.35355E 00	0.35355E 00	0.15603E -02	-0.31336E -02	0.20025E -01	0.61627E -02	-0.62984E -02	-0.62984E -02
E2	0.17500E 01	0.48296E 00	0.12941E 00	0.60337E -03	-0.12206E -02	0.32404E -01	0.24246E -02	-0.24126E -02	-0.24126E -02	
83	0.17500E 01	0.48296E 00	-0.12941E 00	-0.60336E -03	0.12206E -02	0.32404E -01	-0.24245E -02	0.24126E -02	-0.24126E -02	
-	84	0.17500E 01	0.35355E 00	-0.35355E 00	-0.15603E -02	0.31336E -02	0.20025E -01	-0.61628E -02	0.62984E -02	-0.62984E -02
85	0.17500E 01	0.12941E 00	-0.48296E 00	-0.48296E 00	-0.20246E -02	0.40373E -02	0.66695E -02	-0.78626E -02	-0.82437E -02	

LOAD DISTRIBUTION ON BODY

1	0.56743E-01	2	0.56009E-01	3	0.31129E-01
4	0.64503E-01	5	0.81900E-01	6	0.85148E-01
7	0.69012E-01	8	0.99344E-01	9	0.20830E 00
10	0.59238E-01	11	0.92429E-01	12	0.26164E 00
13	0.73034E-01	14	0.11197E 00	15	0.22586E 00
16	0.67102E-01	17	0.88705E-01	18	0.13482E 00
19	0.46604E-01	20	0.51198E-01	21	0.64639E-01
22	0.34449E-01	23	0.32535E-01	24	0.17596E-01
25	0.25696E-01	26	0.21342E-01	27	0.90911E-02
28	0.16487E-01	29	0.12597E-01	30	0.48252E-02

SPANWISE LIFT DISTRIBUTION ON BODY

1 0.78256E-01 2 0.96747E-01 3 0.14851E 00.

MAX FIN CHORD = 1.0000 REFERENCE AREA = 0.600000E 01

WING CL = 0.72392E-01 FIN CL = 0.0 BODY CL = 0.79603E-02

TOTAL CL = 0.80352E-01

PRESSURE DISTRIBUTION ON VERTICAL FIN

LOAD DISTRIBUTION ON VERTICAL FIN

NO	XCP								
1	-0.48654E-02	2	-0.12267E-01	3	-0.99562E-02	4	-0.61927E-02	5	-0.36822E-02
6	-0.1024E-01	7	-0.78024E-02	8	-0.46928E-02	9	-0.27335E-02	10	-0.15389E-02
11	-0.14526E-01	12	-0.78556E-02	13	-0.35099E-02	14	-0.18359E-02	15	-0.96995E-03
16	-0.93121E-02	17	-0.59401E-02	18	-0.26508E-02	19	-0.13774E-02	20	-0.71187E-03
21	-0.67676E-02	22	-0.30359E-02	23	-0.18515E-02	24	-0.88402E-03	25	-0.46079E-03

SPANWISE LIFT DISTRIBUTION ON VERTICAL FIN

	1	2	3	4	5
CLS(1)	= -0.95180E-02	-0.66284E-02	-0.32970E-02	-0.17546E-02	-0.95422E-03
CLS(2)	= -0.95180E-02	-0.66284E-02	-0.32970E-02	-0.17546E-02	-0.95422E-03
CLSF(1)	= 0.0	0.0	0.0	0.0	0.0

LIFT COEFF. ON VERTICAL FIN CL = -0.17144E-02

PRESSURE DISTRIBUTION ON BODY INCLUDING VERTICAL FIN EFFECT

NO	CPU	NO	CPB	NO	CPB	NO	CPB	NO	CPA
1	-0.28648E-01	2	-0.28564E-01	3	-0.16171E-01	4	0.16171E-01	5	0.28564E-01
7	-0.33031E-01	8	-0.42001E-01	9	-0.43528E-01	10	0.43528E-01	11	0.42001E-01
11	-0.35865E-01	14	-0.51168E-01	15	-0.10534E-01	16	0.10535E-01	17	0.51168E-01
19	-0.32598E-01	20	-0.47580E-01	21	-0.13215E-01	22	0.13215E-01	23	0.47580E-01
25	-0.41138E-01	26	-0.58172E-01	27	-0.11446E-01	28	0.11446E-01	29	0.58172E-01
31	-0.37766E-01	32	-0.46533E-01	33	-0.88968E-01	34	0.68968E-01	35	0.46533E-01
37	-0.25734E-01	38	-0.27038E-01	39	-0.32431E-01	40	0.33431E-01	41	0.27038E-01
43	-0.17665E-01	44	-0.16974E-01	45	-0.94928E-02	46	0.94927E-02	47	0.16974E-01
49	-0.13010E-01	50	-0.11029E-01	51	-0.49603E-02	52	0.49603E-02	53	0.11029E-01
55	-0.83002E-02	56	-0.64432E-02	57	-0.25989E-02	58	0.25989E-02	59	0.64432E-02

TABLE 5. LIST OF COMPUTER PROGRAM

Reproduced from
best available copy.

FORTRAN IV G LEVEL	MAIN	DATE • 76132	14/11/76	PAGE 0001
C CALCULATION OF AERODYNAMIC PERFORMANCE OF FIN-BODY COMBINATION				
0001	COMMON /B1/MB/NB/NB1/B2/NUB/B3/PSA(155)/B4/BREF(5)/U6/XDV(155)/ \$B7/YV(155)/WH(155)*WLMD(155)*BL1/NBF*NBM*HUB*FDL*HDL/BY1/ALFAB/BY2/ \$AHW(155)/BY3/JRAU			
0002	CUMUN /C1/BC/C2/ARLAB(96)/C3/XW/C5/UBDY(72)/C6/VN(72)/C7/QL(72)/ \$C9/V(172)/CASEF/CLORD/ASYM/CL1551			
0003	CO-NON /D1/BCL/D2/H1/F1/NFLP/FL2/NT/FL3/VNW/FL4/AFLAP/NAME/IRPT/ \$P4/TG/P5/P1/Y2*Y3*Y4*Y5*Y6/P2/M*N/P3/XM*ALFAF/			
0004	COMMON /P1/XJ/Y1*Y2*Y3*Y4*Y5*Y6/XC1(551)*XC2(51)*XC3(51) \$T5(172)/T5/XD(1271)*YD(1271),2D(1271)/T6/XV(1551)*YV(1551)*WH(1551)			
0005	COMMON /U1/Y1(111)/U2/RFAREA*XAX/U2/DT/VL1/INC/W1/DX(961)/W2/CLS(151), \$CLSD(151),CLSF(151)/W3/CLDS(151)/W4/CLWING,CLFIN,CLBODY,TOTCL			
0006	STLND(155)			
0007	COMMON /C1/GA3M/Q2/XCP/Q8/ABV(172*551)*ABW(172*551)/R1/XL1/ \$U1/R3/XREF			
0008	COMMON /S1/UTUT/Y12/XG(551)*YG(551)*ZG(551)/T3/XS(721)*YS(721)* \$TS(721)/T5/XD(1271)*YD(1271),2D(1271)/T6/XV(1551)*YV(1551)*ZV(1551)			
0009	SCLS(151)			
0010	WRITEL6,9001			
0011	900 FORMAT//*3X,*COMPUTATION FOR SURFACE PRESSURE DISTRIBUTION ON FIN *-*BOUY COMBINATION AT SUBSONIC SPEEDS*,//			
0012	PI=3.14159			
0013	READING FIN-BODY GEOMETRY READ(5,101) X1,Y1,X2,Y2,X3,Y3,X4,Y4,X5,Y5,X6,Y6			
0014	10 FORMATTED10.51			
0015	C READING DIVISION NUMBER READ(5,151) M,N,NFLP			
0016	15 FORMAT(31I0)			
0017	C READING BODY PANEL NUMBER READ(5,171) MB,NBF,NBM,NBF,FDL,BDL			
0018	17 FORMAT(4I10,2F10.5)			
0019	NB=NMB			
0020	NT=14+NFLP			
0021	NU=NBT			
0022	NB=NBT+NBM+NBB			
0023	HUB=HB*HB			
0024	HTUT=0+HUB			
0025	C READING AERODYNAMIC INPUT READ(5,201) AM,ALFAF,ALFAB,AFLAP,ASYN,ASYM			
0026	20 FORMATTED10.51 WHITE16,S021			
0027	002 FORMAT//*3X,*FIN-BODY GEOMETRY			
0028	002 FORMAT//*3X,*FIN-BODY GEOMETRY			
0029	WHITE16,9041			
0030	904 FORMAT1H,9041*56*6X,*Y1*6X,*X2*6X,*Y2*6X,*X3*6X,*Y3*6X,*X4* \$6X,*Y4*6X,*X5*6X,*X6*6X,*Y6*)			
0031	WHITE16,Y061			
0032	906 FORMAT1H0,2X*12(F8.31)			
0033	WRITE16,907			
0034	FORMAT1/3X,*FIN-BODY PANEL NUMBER ******/			
0035	WRITE16,Y081,0*NFLP*NW,NO			
0036	908 FORMAT1H,2X*N = *12*2X*NFLP = *12*2X*NW = *12*2X*NFLP			

PORTMAN IV C LEVEL 21
 MAIN DATE = 76132 PAGE 0002
 14/11/16
 S,2X,*NO * 1,121
 WRITE(6,910) MB,NUF,NBM,NBB,NUR,FDL,BDL,NTOT
 910 FORMAT(1H0,2X,'MB' * '12,2X,'NUF' * '12,2X,'NBM' * '12,2X,'NBB' *
 \$,12,2X,'NB' * '12,2X,'NUB' * '13,3X,'FDL' * 'F5,2,2X,'BDL' * 'F5,2
 \$,5X,'TOTAL PANEL' * '13)
 WRITE(6,912) XM,ALFAF,ALFAF,AFLAP,ASYM,ASYF
 912 FORMAT(1H0,2A,'MAC1 NU' * 'F6,3,2X,'ANGLE OF INCIDENCE' * 'FS,2,1X
 \$,'IDEGL' * '2X,'FIN ANGLE OF ATTACK' * 'F5,2,1X,'(DEGL)' * '3X,'FLAP ANGL
 SE OF ATTACK' * 'F5,2,1A,'(DEGL)' * '2X,'FIN SYMMETRY' * 'F5,2,2X,'FLAP
 \$ SYMMETRY' * 'FS,2)
 UETA=SCI(11,-XM)*2
 SPNAY2
 N1=SPN1/2
 RAD1=Y1
 ITC=0
 JKAD=1
 IF (RAD1.LT.0.0001) JKAD=0
 IF (RAD1.EQ.0.0) GO TO 610
 CALL HGMY
 610 CALL GVS1
 0051 CALL CONP
 WRITE(6,914)
 914 FORMAT(1,3X,'REFERENCE CHORD *****')
 IF (RAD1.EQ.0.0) GO TO 612
 CALL GIV
 612 CALL GVS3
 0057 CALL XLC
 IF (RAD1.EQ.0.0) GO TO 614
 CALL BLLT
 CALL VBA
 WRITE(6,916)
 916 FORMAT(1H,3X,'UN BODY *****')
 WRITE(6,917)
 917 FORMAT(1H,18A,'1' * 13X,'2' * 13X,'3')
 WRITE(6,610) (REF(I),I=1,M1)
 610 FORMAT(1H,3X,'BHEF(I)' * '3IE12,5,2X))
 0067 614 WRITE(6,918)
 0068 918 FORMAT(1H,3X,'UN FIN *****')
 0069 WRITE(6,919)
 919 FORMAT(1H,19X,'1' * 13X,'2' * 13X,'4' * 13X,'5')
 0070 WRITE(6,603) (XL(I,J),J=1,M)
 0071 WRITE(6,601) (CLL(I,J),J=1,M)
 0072 WRITE(6,402) (XC1(I,J),J=1,M)
 0073 WRITE(6,404) (XC2(I,J),J=1,M)
 0074 WRITE(6,406) (XC3(I,J),J=1,M)
 0075 400 FORMAT(1H,3X,'XL(I)' * '5IE12,5,2X))
 0076 001 FORMAT(1H,3A,'CLL(I)' * '5IE12,5,2X))
 0077 402 FORMAT(1H,3X,'XC1(I)' * '5IE12,5,2X))
 0078 404 FORMAT(1H,3X,'XC2(I)' * '5IE12,5,2X))
 0079 406 FORMAT(1H,3X,'XC3(I)' * '5IE12,5,2X))
 0080 CALL AKUC
 0081 IF (RAD1.EQ.0.0) GO TO 616
 0082

```

0083      CALL PVMX
0084      CALL ARQO
0085      CALL ARQV
0086      CALL ARBF
0087      616  IRPT=1
0088      IF(IJRAD.EQ.0) GO TO 618
0089      1000  CONTINUE
0090      618  CALL BCF(BC,NO)
0091      CALL VUF(GAMM)
0092      CALL PBIXCP)
0093      CALL SLU
0094      CALL ALF( CL )
0095      CALL PMS(CMS)
0096      IF(IJRAD.EQ.0) GO TO 620
0097      CALL VLNB
0098      CALL BSS
0099      CALL BPD
0100      CALL BLUBCL)
0101
0102      CALL BSLO
0103      CALL WBS(XW,NUB,NO)
0104      IF(IRPT.LT.4) GO TO 2000
0105      WRITE(6,92C) IRPT
0106      920  FORMAT(7.3X,ITERATION = * .12* /)
0107      620  WRITE(6,922)
0108      922  FORMAT(7.3A,PRESSURE DISTRIBUTION ON PLANAR FIN * .12* /)
0109      WRITE(6,924)
0110      924  FORMAT(7.3A,NO=6X,*XV* .13X,*YV* .13X,*ZV* .13X,*XNR* .10X,*YNR* .10X
      * ,GAMA=.8A,ACP,. /)
0111      312  IJ=1,NO
0112      ANR=LAV(F,-AC1(IF))/CLL(IF)
0113      YR=YV(IF)/Y2
0114      WRITE(6,211) IF,XV(IF),YV(IF),ZV(IF),XNR,YNR,GAMM(IF),XCP(IF)
0115      311  FORMATT(1H,1.5*7(1A,E12.5))
0116      CO,TIGUE
0117      WRITE(6,926)
0118      926  FORMAT(7.3X,'SPANWISE LIFT AND MOMENT DISTRIBUTION * .12* /)
0119      WRITE(6,927)
0120      927  FORMATT(1H,0.2X,1*13X,2*13X,*3*13X,*4*13X,*5*1)
0121      WRITE(6,500) (CLS(JX),JX=1,M)
0122      WRITE(6,501) (CL5(JX),JX=1,M)
0123      WRITE(6,502) (CLSF(JX),JX=1,M)
0124      WRITE(6,503) (CMS(JX),JX=1,M)
0125      500  FORMATT(1H,0.3X,CLS(1)) = *5(E12.5,2X)
0126      502  FORMATT(1H,0.3X,CLSW(1)) = *5(E12.5,2X)
0127      504  FORMAT(1H,0.3X,CLSF(1)) = *5(E12.5,2X)
0128      506  FORMAT(1H,0.3X,CMS(1)) = *5(E12.5,2X)
0129      IF(IJRAD.EQ.0) GO TO 720
0130      WRITE(6,70) KFAKEA,CL
0131      700  FORMAT(7.2*F14.5,5X,'LIFT COEFF. = *E12.5*')
0132      CU TO 622
0133      720  CONTINUE

```

FORTRAN IV @ LEVEL 21

MAIN DATE = 76192 PAGE 0004

```

0134      WRITE(6,928)
0135      928 FORMAT(//,3X,'PRESSURE DISTRIBUTION ON BODY *****',/)

0136      WRITE(6,930)
0137      930 FORMAT(//,4X,'NO',6X,'XD',11X,'YD',11X,'ZD',11X,
     S 'VT',11X,'QL',11X,'CPB',/)
DO 850 I=1,NUB
 1B=1+NO
  WRITE(6,900) 1B,XD(1B),YD(1B),ZD(1B),VT(1),QL(1).

0140      3CPB(1)
0141      600 FORMAT(1H 15.0(1X+E12.5))
0142      650 CONTINUE
0143      WRITE(6,932)
0144      932 FORMAT(//,3X,'LOAD DISTRIBUTION ON BODY *****',/)

0145      DO 520 K1=1,NB
K2=(K1-1)*M1+
0146
0147      K3=K1*M1
      WRITE(6,910) (IB*CL(1B)*IB*K2,K3)
0148
0149      510 FORMAT(1H ,4(1I0,2X,E12.5))
0150      520 CONTINUE
0151      WRITE(6,934)
0152      934 FORMAT(//,3X,'SPANWISE LIFT DISTRIBUTION ON BODY *****',/)

0153      WRITE(6,950) (IX*CLBS(IX) *IX*1,M1)
0154      WRITE(6,954) (IX*CLBS(IX) *IX*1,M1)
0155      550 FORMAT(1H ,4(1I0,2X,E12.5))
0156      WRITE(6,560) XA,RAREA,CLWING,CLFIN,CLBODY,TOTCL
0157      560 FORMAT(//,3X,'MAX FIN CHORD = ',F8.3,SX,'REFERENCE AREA = ',E12.6/
     S/3X,'WING CL = ',E12.5,SX,'FIN CL = ',E12.5,SX,'BODY CL = ',E12.5/)

0158      2000 CONTINUE
0159      IF(IRPT.EQ.4) GO TO 1500
0160      IRPT=IRPT+1
0161      GO TO 1000
0162      1500
CONTINUE
C
0163      COMPUTE AERODYNAMIC COEFFICIENT ON VERTICAL FIN
0164      WRITE(6,936)
0165      936 FORMAT(//,3X,'PRESSURE DISTRIBUTION ON VERTICAL FIN *****',/)

0166      DO 60 I=1,NUB
 60  ASV11,J1=ABU11,J1
  IRC=1
 0167      DO 30 J=1,NO
 30  2D11,J1=TF1
  CALL PVAX
 0174      0175      CALL ARBF
 0169      DO 34 I=1,NO
 0170      TF1=YD(1)
 0171      TF2=ZD(1)
 0172      YD(1)=TF2
 0173      30 2D11,J1=TF1
 0174      CALL PVAX
 0175      CALL ARBF
 0176      DO 34 I=1,NO
 0177      SUM1=0.
 0178      DO 32 J=1,NO
 0179      32  SUM1=SUM1+ABV11,J1*GAMM(J)
 0180      SUM2=0.

```

FORTRAN IV C LEVEL 21

MAIN PAGE 0005

DATE = 76132

14/11/16

```

0181      DO 33 J=1,NUB
0182      33 SUM2=SUM2+AFN(I,J,1)*QL(J)
0183      34 BC(I)=ISUM1+SUM2
0184      CALL DINVR(R,BC,NC)
0185      DO 36 I=1,NO
0186      36 GAMM(I)=BC(I)
0187      CALL PDB(XCP)
0188      CALL SLD
0189      CALL XLF(CL)
0190      WRITE(6,950)
0191      WRITE(6,951)
0192      DO 37 J=1,NT
0193      I1=(J-1)*M-1
0194      I2=I1+N-1
0195      37 WRITE(6,210) (1,XCP(I)),I=I1,I2)
0196      WRITE(6,952)
0197      WRITE(6,953)
0198      WRITE(6,220) (CLS(I),I=1,M)
0199      WRITE(6,222) (CLSW(I),I=1,M)
0200      WRITE(6,224) (CLSF(I),I=1,M)
0201      WRITE(6,954) LL
0202      950 FORMAT(//,3X,'LOAD DISTRIBUTION ON VERTICAL FIN',*1)
0203      951 FORMAT(1H,*5(3X,'NO',7A,*XCP',4A))
0204      210 FORMAT(1H,*5(15,2X,E12.5))
0205      952 FORMAT(1H/*3X*'SPANWISE LIFT DISTRIBUTION ON VERTICAL FIN',*1)
0206      953 FORMAT(1H,2UX,1,13X,2,13X,3,13X,4,13X,5,1
0207      220 FORMAT(1H,3X,'CLS(I)',*5(E12.5,2X))
0208      222 FORMAT(1H,3X,'CLSW(I)',*5(E12.5,2X))
0209      224 FORMAT(1H,3X,'CLSF(I)',*5(E12.5,2X))
0210      954 FORMAT(//,3X,'LIFT COEFF. ON VERTICAL FIN CL = ',E12.5,/,1
0211      INC2
0212      WRITE(6,956)
0213      956 FORMAT(1H,3A,'PRESSURE DISTRIBUTION ON BODY INCLUDING VERTICAL FI
0214      SH EFFECT',*,1)
0215      958 FORMAT(1H,6(3X,'P',6X,'CPB',4X))
0216      DO 40 I=1,NUB
0217      SUM1=0.
0218      DO 38 J=1,NO
0219      38 SUM1=SUM1+ASV(I,J)*GAMM(I,J)
0220      40 UBDY(I)=SUM1
0221      DO 50 NX=1,NB
0222      51=MB*(NX-1)+1
0223      12=I1+MB-1
0224      DO 45 MX=1,MB
0225      1=MB*(NX-1)+MX
0226      IX=I+MI
0227      I1=M1*(2*N4-1)+1
0228      IF(I1.GT.I1) IX=I-M1
0229      ACPB=-2.*UBDY(IX)*BETA**2
0230      45 CPB(I)=CPB(I)+ACPB
0231      50 WRITE(6,242) (1,CPB(I)),I=I1,I2)

```

FORTRAN IV G LEVEL 21 **MAIN** **DATE = 76132** **PAGE 0006**
14/11/76

```
0232      240 FORMAT(1H,06(19.0X,E12.0))  
0233      622 CONTINUE  
0234      STOP  
0235      END
```

SUBROUTINE BGMY

DEFINE SOURCE POSITION ON BODY

```

0002      C
0003      C
0004      C
0005      C
0006      C
0007      C
0008      C
0009      C
0010      C
0011      C
0012      C
0013      C
0014      C
0015      C
0016      C
0017      C
0018      C
0019      C
0020      C
0021      C
0022      C
0023      C
0024      C
0025      C
0026      C
0027      C
0028      C
0029      C
0030      C
0031      C
0032      C
0033      C
0034      C
0035      C
0036      C
0037      C
0038      C
0039      C
0040      C
0041      C
0042      C
0043      C
0044      C
0045      C
0046      C
0047      C
0048      C
0049      C

0002      DIMENSION XN(117)
COMMON /T3/XS(72),YS(72),ZS(72)
COMMON /T4/TS(72)
COMMON /C2/AREAB(96)
COMMON /h1/DX(96)
COMMON /P1/X1,Y1,X2,Y2,X3,Y3,X4,Y4,X5,Y5,X6,Y6
COMMON /PL/NU
COMMON /PS/P1
COMMON /B1/MB,NB
COMMON /B12/NBF,NBM,NBB,FDL,BDL
COMMON /B2/NUB
COMMON /A1/RAU1
COMMON /U3/DT
DT=P1/E1
C=1.
NX=NBF-1
NB1=NEF+1,NEF+1
XP=X1-FDL*ABS(X3-X1)
A21=P1/(12.*NBF)
A22=P1*C/(12.*NBM)
A23=P1/(12.*NBB)
XN(1)=XP
DO 10 J1=1,NX
10  XN(J1+1)=XP+ABS(X1-XP)*SIN(AZ1+J1)
XN(EF+1)=X1
NY=NBM-1
DO 20 J2=1,NY
20  XN(BF+J2+1)=X1+ABS(X3-X1)*(1.-COS(AZ2+J2))/C
XN(NB1)=X3
N2=1,B3=1
X0=X3+BDL*AUS(X3-X1)
DO 30 J3=1,N2
30  XN(INB2+J3)=X3+ABS(X0-X3)*(1.-COS(AZ3+J3))
XN((IB+1))=X0
DO 100 JJ=1,NB
PP1=(XN(JJ)+XN(JJ+1))/2.
PP2=ABS(XN(JJ+1)-XN(JJ))
DO 100 JB=1,NB
XS(JB+(JJ-2)*NBM)≈PP1
DX(JB+(JJ-1)*NBM)≈PP2
100  CONTINUE
DO 120 I=1,NUB
120  AREAB(I)=RAD1*DT*DX(I)
N1=NBM-1
DO 200 IB=1,MB
200  TS(IB)=DT*(IB-5)
DO 190 JJ=1,N1
TS(IB+JJ*NBM)=TS(IF)

```

FORTRAN IV G LEVEL 21

DATE = 76114

10/33/50

PAGE 0002

```
0050      150 CONTINUE
0051      200 CONTINUE
0052          DU 300 1d=1•NJB
          YSLIBI   "RAD1*SINITS((IB))
          ZSLIBI   "RAD1*COSITS((IB))
0053      300 CONTINUE
          RETURN
          END
```

PAGE 0001

FORTRAN IV G LEVEL 21

SUBROUTINE GVS1

DATE = 76114

10/33/50

C CONTROL POINT DEFINITION

```

0001      C
          C
          C
0002      DIMENSION DK(115)
COMMON  /U1/YF(11)
COMMON  /T2/XG(55)*YG(55)+2G(55)
COMMON  /T6/XV(55)*YV(55)+2V(55)
COMMON  /P1/X1*Y1*X2*Y2,X3*Y3*X4*Y4*X5*Y5
COMMON  /P2/M*N
COMMON  AP3/XM,ALFAF
COMMON  SP4/NO
COMMON  /P5/P1
COMMON  /FL1/NFLP
COMMON  /FL2/NT
COMMON  /FL3/NW
NT1=LT-1
YF(1)=Y1
DO 20 JC=1,M
YF(JC+1)=Y1+(Y2-Y1)*(1.-COS(JC*PT/M))/2.
YF(JC)=(YF(JC)+YF(JC+1))/2.
WH(JC)=(YF(JC+2)-YF(JC))/2.
DO 10 JJ=1,NT1
Y(GJC+JJM)=YG(JC)
WH(JC+JJ*M)=WH(JC)
10 CONTINUE
20 CONTINUE
DO 30 JJ=1,NO
YV(JJ)=YF(JJ)
ZG(JJ)=0.
2V(JJ)=0.
20 CONTINUE
30 CONTINUE
THW=PI/N
THW1=THW/2.
N1=N-1
N2=N+1
DK(1)=0.
DK(42)=1.
DU 37 K=1,N1
XX=K
DK(K+1)=1.-COS(THW1*KK)
37 CONTINUE
C CONTROL POINT ON WING
DU 50 K=1,N
DO 40 J=1,M
J2=(K-1)*M+J
XG(J2)=X1+(X3-X1)*(UK(K)+3.*DK(K+1)*(X4-X2)/4.+((X4-X2)*(DK(K)+3.*DK(K+2))
$1/4.+((X3-X1)*(DK(K)+3.*DK(K+1)*(X2-X1)*(YV(J1)-Y1)/(Y2-Y1)
TLMD(J2)=(X4-X2)*(3.*DK(K)+DK(K+1)*(X3-X1)/4.+((X3-X1)*(3.*DK(K+DK(K+1)))
$/4.+X2-X1)/(Y2-Y1)
XV(J2)=X1+(X3-X1)*(3.*DK(K)+DK(K+1)*(X4-X2)*(YV(J1)-Y1)+(YV(J2)-Y1)*TLMD(J2)
40 CONTINUE

```

PAGE 0002 FOR TRAN IV 5 LEVEL 21 DATE = 761114 10/31/80 GVS1

三

21

```

0047      50 CONTINUE
0048      IF(NFLP.EQ.0) GO TO 80
0049      THF=P/NFLP
0050      THF1=THF/2.
0051      N3=NFLP-1
0052      I44=NFLP+1
0053      DKIN=1.
0054      DO 60 K=1,N3
0055      XK=K
0056      DKIK+1)=1.-COS(THF1*XK)
0057      60 CONTINUE
0058      C   CONTROL POINT ON CONTROL FIN
0059      DO 70 K=1,NFLP
0060      DO 65 J1=1,M
0061      J2=(K-1)*M+J1
0062      XG(J2+NW)=X3+(X5-X3)*(DKIK)*3.*DK(K+1)+3.*DK(
0063      SK+1)*1./4.-((X5-X3)*(DKIK+2)*DK(K+1))/4.+X4-X3)*(YV(J1)-Y3)/(Y4-Y3)
0064      TLMD(J2+NW)=((X6-X4)*(13.*ADKIK)+DK(K+2))/4.-(X5-X3)*13.*DK(K)+DK(K)+
0065      $11)/4.+X4-X3)/(Y4-Y3)
0066      XVL(J2+NW)=X3+(X5-X3)*(13.*DKIK+DK(K+1))/4.+(YV(J1)-Y3)*TLMD(J2+NW)
0067      65 CONTINUE
0068      70 CONTINUE
0069      80 CONTINUE
0070      RETURN

```

FORTRAN IV G LEVEL 21

DATE = 76114

PAGE 0001

CONP

SUBROUTINE CONP

```
      C
      COMMON /T2/XG(155)*YG(155)*ZG(155)
      COMMON /T3/XS(172)*YS(172)*ZS(172)
      COMMON /TS/XD(127)*YD(127)*ZD(127)
      COMMON /P4/NO
      COMMON /T1/NOT
      COMMON /BY3/JRAD
      N1=NTOT
      IF(JRAD.EQ.0) N1=NO
      DO 10 JC=1,N1
      IF(JC.GT.NO) GO TO 5
      XD(JC)=XG(JC)
      YD(JC)=YG(JC)
      ZD(JC)=ZG(JC)
      GO TO 10
      5  XD(JC)=XS(JC-NO)
      YD(JC)=YS(JC-NO)
      ZD(JC)=ZS(JC-NO)
      10 CONTINUE
      RETURN
      END
```

FORTRAN IV G LEVEL 21

DATE = 76114

PAGE 0001

10/33/50

GIV

PAGE 0001

SUBROUTINE GIV

C

```
COMMON /B7/YV1(55),WH1(55),TLMD(55)
COMMON /T6/XV(55),YV(55),WM(55),TLMD(55)
COMMON /P4/RD
COMMON /A1/RADI
DO 10 II=1,NO
YV(II)=RADI**2*(1.0/(YV(II))-WH(II))+1.0/(YV(II)+WH(II))/2.
WH(II)=RADI**2*(1.0/(YV(II))-WH(II))-1.0/(YV(II)+WH(II))/2.
TLMD(II)=TLMD(II)*WH(II)/WH(II)
10 CONTINUE
RETURN
END
```

FORTRAN IV G LEVEL 21

GVS3

PAGE 0001

0001 SUBROUTINE GVS3

C COMPUTE PANEL SURFACE AREA

```
0002      COMMON /B3/PSA(55)
0003      COMMON /B6/XDV(55)
0004      COMMON /T2/XG(55),Y6(55)*2G(55)
0005      COMMON /T6/XV(55),YV(55)*2V(55)*WH(55)*WLMD(55)
0006      COMMON /P4/NO
0007      COMMON /P6/BETA
0008      COMMON /P1/X1,Y1,X2,Y2,X3,Y3,X4,Y4,X5,Y5,X6,Y6
0009      COMMON /U2/RAREA,XAX
0010      XAX=X6-X1+Y1*(X2-Y1)/(Y2-Y1)-Y6*(X6-X5)/(Y6-Y5)
0011      RAREA=(XAX+X6-X2)*Y6
0012      DO 10 II=1,NO
0013      XDV(II)=XG(II)-XV(II)
0014      PSA(II)=4.*BETA*WH(II)*XDV(II)
0015      10 CONTINUE
0016      RETURN
0017      END
```

FORTRAN IV G-LEVEL 21

PAGE 0001

DATE 10/33/50

PAGE 0001

XLC

SUBROUTINE XLC

C

COMPUTE LOCAL CHORD LENGTH OF FIN

C

```

0002      DIMENSION XREF(10),XREF(5),XLFL(5)
0003      COMMON /PT1/XC1(5),XC2(5),XC3(5)
0004      COMMON /R1/XL1(10)
0005      COMMON /T2/XG(55),YG(55),ZG(55)
0006      COMMON /T6/XV(55),YV(55),ZV(55),WH(55),WLMD(55)
0007      COMMON /CHORD/CLL(55)
0008      COMMON /P1/X1,Y1,X2,Y2,X3,Y3,X4,Y4,X5,Y5,X6,Y6
0009      COMMON /P2/M,1
0010      COMMON /R3/AREF
0011      COMMON /FL2/HF
0012      N1=11-1
0013      DO 10 JL=1,N
0014      XC1(JL)=X1+(X2-X1)*(YG(JL)-Y1)/(Y2-Y1)
0015      XC2(JL)=X3+(X4-X3)*(YG(JL)-Y3)/(Y4-Y3)
0016      XC3(JL)=X5+(X6-X5)*(YG(JL)-Y5)/(Y6-Y5)
0017      XL(JL)=X2(JL)-XC1(JL)
0018      XLF(JL)=XC3(JL)-XC2(JL)
0019      XREF(JL)=XC1(JL)+XL(JL)/4.
0020      XREF(JL)=XC2(JL)+XL(JL)/4.
0021      CLL(JL)=XC3(JL)-XC1(JL)
0022      DO 5 J=1+N
0023      I=J+9N
0024      XC1(I)=XC1(JL)
0025      CLL(I)=CLL(JL)
0026      10 CONTINUE
0027      RETURN
0028      END

```

FORTRAN IV G LEVEL 21

0001

BLIT

PAGE 0001

DATE = 7611.0

PAGE 0001

```
0002      C      SUBROUTINE BLIT
COMMON /D4/DK,F(5)
COMMON /T3/X5(172),YS(172),ZS(172)
COMMON /D2/M1
COMMON /P1/X1,Y1,X2,Y2,X3,Y3,X4,Y4,X5,Y5,X6,Y6
DO 10 LH=1,M1
     B1=X1+(X2-X1)*(YS((IB1-Y1)/(Y2-Y1)
     B2=X6-Y5*(IB1))*(X6-X5)/(Y6-Y5)
 10  BREFI IB1=B2-Y1
      RETURN
END
0011
```

PAGE 0001

DATE = 76/14
10/33/50

FORTRAN IV G LEVEL 21
0001 C SUBROUTINE VBIA
C
C VELOCITY ON FIN INDUCED BY BODY INCIDENCE ANGLE
C
0002 COMMON /BY2/XBW(55)
0003 COMMON /T2/XG(55),YG(55),ZG(55)
0004 COMMON /BY1/ALFAB
0005 COMMON /P4/NO
0006 COMMON /A1/RADI
0007 COMMON /PS/PI
0008 ALB=ALFAB*PI/180.
0009 DU 10 J=1,NO
0010 XBW(J)=ALB*RADI**2/YG(J)**2
0011 RETURN
0012 END

COMPUTE AERODYNAMIC MATRIX

```

0002      COMMON /AH1/AR(56,56)
0003      COMMON /T6/XV(55),YV(55),ZV(55),WH(55),TLMD(55)
0004      COMMON /B7/YV(55),WH(55),TLMD(55)
0005      COMMON /TR1/TX,TY,TZ,TW,TM
0006      COMMON /UB/JS
0007      COMMON /PB/1,J
0008      COMMON /O9/PSN
0009      COMMON /P4/RU
0010      COMMON /CASEh/ASYN
0011      COMMON /CASEF/ASYF
0012      COMMON /L3/iw
0013      COMMON /BY3/JRAD
0014      NR=4
0015      IF JRAD.EU.0) NN=2
0016      DO 30 I=1,NO
0017      DO 20 J=1,NO
0018      IF (J.LE.iw) ASYN=ASYN
0019      IF (J.GT.NW) ASYN=ASYF
0020      TA=AV(J)
0021      T2=2V(J)
0022      DO 10 JS=1,NN
0023      IF (JS.LE.2) GO TO 15
0024      TY=YV(J)
0025      TW=WH(J)
0026      TM=TLMD(J)
0027      GO TO 16
0028      15  TY=YV(J)
0029      TW=WH(J)
0030      TM=TLMD(J)
0031      16  CONTINUE
0032      IF (JS.EQ.1.OR.JS.EQ.3) PSP=1.
0033      IF (JS.EQ.2.OR.JS.EQ.4) PSP=-1.
0034      CALL PVB(UB,VB,NB)
0035      CALL PV(PUP,VP,NP)
0036      CALL PV(SUS,VS,WS)
0037      XAR=XH*WP+WS
0038      IF (JS.EQ.1) SAR=XAR
0039      IF (JS.EQ.2) PAR=XAR
0040      IF (JS.EQ.3) SIAH=XAR
0041      IF (JS.EQ.4) PIAR=XAR
0042      10  CONTINUE
0043      IF (JRAD.NE.0) GO TO 50
0044      SIAR=0.
0045      PIAR=0.
50  AR(1,J)=SAR+ASYN*PAR+SIAR+ASYN*PIAR
0046      20  CONTINUE
0047      30  CONTINUE
0048      RETURN
0049

```

FORTRAN IV G LEVEL 21

0050

END

ARDC

DATE = 76114

PAGE 0002

FORTRAN IV G LEVEL 21

PAGE 0001 DATE = 76114 10/30/50

PVB

SUBROUTINE PVH(UB,VB,WB)

C COMPUTE PERTURBATION VELOCITY COMPONENTS INDUCED BY BOUND VORTEX

```
0002      COMMON /TS/XD(127),YD(127),ZD(127)
0003      COMMON /TR1/TX,TY,TZ,TW,TM
0004      COMMON /P3/XW,ALFAF
0005      COMMON /P5/P1
0006      COMMON /P6/BETA
0007      COMMON /P7/SPN
0008      COMMON /P8/I,J
0009      COMMON /P9/PSP
0010      COMMON /HB/J5
0011      CALL GVS2(SX,SY,TMU)
0012      A=SORT((XD(I)-SX)**2+BETA**2*(SY-PSP*YD(I))**2)
0013      B=BETA*(SY-TY+TW)
0014      C=SX-TX +BETA*TW+TMU
0015      D=BETA*(IY+TW-SY)
0016      E=TX +BETA*TW *TMU-SX
0017      Z=HETA*(TZ -ZD(I))
0018      A22=A**2+Z**2
0019      BC2=B**2+C**2
0020      DE2=D**2+E**2
0021      CF=U=1./SORT(I+TMU**2)
0022      SMU=CMU+TMU
0023      IF(SY.GT.TY-TW) PP1=1.
0024      IF(SY.LT.TY-TW) PP1=-1.
0025      CG=PP1*SCRT1(BC2)/SORT(AZ2+BC2)
0026      IF(SY.GT.TY+TW) PP2=-1.
0027      IF(SY.LT.TY+TW) PP2=1.
0028      CF=PP2*SORT(DE2)/SORT(AZ2+DE2)
0029      SCC=SPN*(CG+CF)/(2.*P1)
      COMPUTE INDUCED VELOCITY COMPONENTS FOR UNIT FREE STREAM VELOCITY AND
      UNIT VORTICITY STRENGTH
      UB=-SCC*Z*CMU/AZ2
      VB=SCC*Z*SMU/AZ2
      IF(XD(I).GT.SX) PP3=-1.
      IF(XD(I).LT.SX) PP3=1.
      WB=PP3*SCC*A/AZ2
      RETURN
      END
```

Revised 4/1/81
Reproduced 10/20/81

FORTRAN IV G LEVEL 21

0001 SUBROUTINE PVP(UP,VP,WP)

PAGE 0001

DATE = 76114

PVP

10/31/50

```
C COMPUTE PERTURBATION VELOCITY COMPONENTS INDUCED BY PORT SIDE VORTEX
C
COMMON /TS/XD(127),YD(127),ZD(127)
COMMON /TR1/TX,TY,TZ,TW,TM
COMMON /P5/PI
COMMON /P6/BETA
COMMON /P7/SPN
COMMON /P8/I,J
COMMON /P9/PSP
COMMON /BB/J,S
COMMON GVS2(SX,SY,TMU)
G=BETA*(PSP*YD(I1-TY+TW)
Z=BETA*(TZ -ZD(I1))
GZ2=G*2+Z**2
XH=XD(I1)-TX +BETA*TW*TMU
GZH2=GZ2+XH**2
CK=XH/SORT(GZH2)
SCK=SPN*(I1+CK)/(I2.*P1)
UP=0.
VP=-SCK*Z/GZ2
WP=-SCK*G/GZ2
RETURN
END
```

FORTRAN IV G LEVEL 21

PVS

PAGE 0001

DATE = 76114

10/33/50

0001 SUBROUTINE PVSUS(VS,WS)

0002 C COMPUTE PERTURBATION VELOCITY COMPONENTS INDUCED BY STARBOARD SIDE VORTEX

```
0003 COMMON /TS/XD(127),YD(127),ZD(127)
C
0004 COMMON /B8/JS
0005 COMMON /TR1/TX,TY,TZ,TW,TM
0006 COMMON /P5/P1
0007 COMMON /P6/BETA
0008 COMMON /P7/SPN
0009 COMMON /P9/PSP
0010 CALL GVS2(SX,SY,TMU)
0011 X=HETA*(TY+TW
0012 Z=BETA*(TZ
0013 -ZD(I))
0014 ZI2=Z**2+XI**2
0015 XI=XD(I)-TX
0016 ZIJ2=ZI2+XJ**2
0017 CS=X/J5QRT(ZIJ2)
0018 SCS=SPN*(I.+CS)/(I.*PI)
0019 US=0.
0020 VS=SCS*Z/ZI2
0021 WS=-SCS*X1/ZI2
0022 RETURN
END
```

PAGE 0001

10/33/50

DATE = 76114

GVS2

FORTNAM IV 6 LEVEL 21

SUBROUTINE GVS2(SX,SY,TMU)

```
0001      C COMPUTE INTERCEPT POINT OF BOUND VORTEX
          C
          C COMMON /T5/XU(127),YD(127),ZD(127)
          C COMMON /P3/XM,ALFAF
          C COMMON /P6/BETA
          C COMMON /P8/I,J
          C COMMON /P9/PSP
          C COMMON /B8/J,S
          C COMMON /TR1/TX,TY,TZ,TW,TM
          TMU=TM/BETA
          SX=(TX+XD(I))*TMU**2+BETA*(PSP*YD(I)-TY
          SY=(BETA*(PSP*YD(I)+TY*TMU**2)+(XD(I)-TX
          SBETA
          RETURN
          END
          0012
          0013
```

FORTRAN IV G LEVEL 21

DATE = 76114

PAGE 0001

10/31/50

SUBROUTINE PVMX

```

      C COMMON /OB/ABU(172,55),ABV(172,55),ABN(172,55)
      C COMMON /T6/XVISS,YVISS),ZV(55),WH(55),TLMD(55)
      C COMMON /Y7/YVI(55),WH(55),TLMD(55)

0002      COMMON /TR1/TX,TY,TZ,TW,TM
0003      COMMON /P4/NO
0004      COMMON /B2/RW
0005      COMMON /B8/J5
0006      COMMON /P8/I,J
0007      COMMON /P4/NO
0008      COMMON /B2/RW
0009      COMMON /P9/PSP
0010      COMMON /CASEW/ASYN
0011      COMMON /CASEF/ASYF
0012      COMMON /FL3/RW
0013      COMMON /VL1/IRC
0014      COMMON /XV1/J
0015      K2=RUE;
0016      IF(IRC.EQ.1) N1=NO
0017      DO 30 KK=1,N1
0018      IF IO+KK
0019      IF(IRC.EQ.1) I=KR
0020      DO 20 J=1,NO
0021      IF(I.J.E.Q.W) ASYN=ASYN
0022      IF(I.J.GT.W) ASYN=ASYF
0023      T4=XV1(J)
0024      T2=ZV(J)
0025      DO 10 JS=1,4
0026      IF(JS.LE.2) GOTO 15
0027      TY=YVI(J)
0028      TW=WH(J)
0029      TH=TLMD1(J)
0030      GO TO 16
0031      15  TY=YVI(J)
0032      TW=WH(J)
0033      TH=TLMD1(J)
0034      16  CO,TIRUE
0035      IF(IJS.EQ.1.OR.JS.EQ.3) PSP=1.
0036      IF(IJS.EQ.2.OR.JS.EQ.4) PSP=1.
0037      CALL PVB(UB,VB,WB)
0038      CALL PVPLUP,VP,WP
0039      CALL PVSIUS,VS,WS
0040      RU=U3+UP+US
0041      HV=V3+VP+VS
0042      RW=WB+WP+WS
0043      IF(IJS.EQ.1) GO TO 1
0044      IF(IJS.EQ.2) GO TO 2
0045      IF(IJS.EQ.3) GO TO 3
0046      IF(IJS.EQ.4) GO TO 4
0047      1  SXU=RU
0048      SXV=RV
0049      SXW=RW
0050      GO TO 20
0051      2  PXU=RU

```

FORTRAN IV C LEVEL 21

DATE = 76114

PAGE 0002

10/33/50

PVMX

```
0052      PAV=RV  
          PXI=RW  
          GO TO 10  
10      3  SIXU=RU  
          SIXV=RV  
          SIXW=RW  
          GU TO 10  
        4  PIXU=RU  
          PIXV=RV  
          PIXW=RW  
10      CONTINUE  
          ABUIKK,J)=SXU+ASYN*PXU+SIXU+ASYN*PIXU  
          ABVIKK,J)=SXV+ASYN*PXV+SIXV+ASYN*PIXV  
          ABWIKK,J)=SXW+ASYN*PXW+SIXW+ASYN*PIXW  
20      CONTINUE  
30      CONTINUE  
        RETURN  
END
```

FORTRAN IV G LEVEL 21

DATE • 76114

PAGE 0001

10/33/50

AR00

0001 C SUBROUTINE AR00

```
COMMON /AR2/AU(72,72)
COMMON /T3/XS(72),YS(72),ZS(72)
COMMON /C2/AREAB(196)
COMMON /B2/NUB
COMMON /P4/NU
COMMON /P5/P1
COMMON /P6/BETA
DO 20 JB=1,NUB
  DO 20 JB=1,NUB
    DO 10 IS=1,2
      IF (IS.EQ.1) PSP=1.
      IF (IS.EQ.2) PSP=-1.
      IF (JB.EQ.AND.IS.EQ.1) GO TO 5
      RHO=SORT((XS(JB)-XS(JB))**2+BEТА**2*(PPSP*VS(1B)-YS(JB))**2+
$ (ZS(JB)-ZS(JB))**2)
      P=(AS(1B)-XS(JB))*BEТА*AREA(B(JB))/(4.*PI*RHO**3)
      IF (IS.EQ.1) P1=P
      IF (IS.EQ.2) P2=P
      GO TO 10
  5 PI=0.
  10 CONTINUE
  A(1B,JB)=P1+P2
  20 CONTINUE
  RETURN
END
```

FORTRAN IV G LEVEL 21

PAGE 0001

DATE = 76114

10/33/50

AROV

PAGE 0001

SUBROUTINE AROV

C

```

0002      COMMON /AR3/ASV(72,72)
0003      COMMON /T3/XS(72),YS(72),TS(72)
0004      COMMON /T4/TS(72)
0005      COMMON /C2/AREAB(196)
0006      COMMON /B2/NUB
0007      COMMON /P4/NU
0008      COMMON /P5/P1
0009      COMMON /P6/BETA
0010      COMMON /A1/RADI
0011      DO 20 IB=1,NUB
0012      DO 20 JB=1,NUB
0013      DO 10 IS=1,2
0014      IF (IS.EQ.1) PSP=1.
0015      IF (IS.EQ.2) PSP=-1.
0016      IF (IB.EQ.JB.AND.IS.EQ.1) GO TO 5
0017      CIJ=1.-COS(PSP*TS(1IB)-TS(JB))
0018      RHO=SQRT((XS(1IB)-XS(JB))**2+BEТА**2*RAD**2*2.+)
0019      PC=CIJ*BETA**2*RAD*AREAB(JB)/(2.*P1*RHO**3)
0020      IF (IS.EQ.1) PC1=PC
0021      IF (IS.EQ.2) PC2=PC
0022      GO TO 10
0023      PC1=0.
0024      10 CONTINUE
0025      ASV(1B,JB)=PC1+PC2
0026      20 CONTINUE
0027      RETURN
0028      END

```

FORTRAN IV C LEVEL 21

ARBF

PAGE 0001

10/33/50

```

0001      SUBROUTINE ARBF
C
0002      COMMON /ARA/AFN(72*55)
0003      COMMON /T5/XD(127)*YD(127),ZD(127)
0004      COMMON /C2/AREAB(96)
0005      COMMON /B2/RHUB
0006      COMMON /P4/NU
0007      COMMON /PS/PI
0008      COMMON /P6/BETA
0009      DO 20 J=1,NO
N1=NUB
0010      DO 20 I=1,N1
0011      IB=IC+1
0012      DO 10 IS=1,2
0013      IF(IIS.EQ.1) HSP=.1.
0014      IF(IIS.EQ.2) HSP=-.1.
0015      RHO=SOR((XD(1B))-XD(J))**2+(ZD(1B)-ZD(J))**2+(2D(
$IB)-ZD(J))**2)
0016      PU=BETA**2*(ZD(J)-ZD(1B))*AREAB(1)/(4.*PI*RHO**3)
0017      IF(IIS.EQ.1) PD1=PD
0018      IF(IIS.EQ.2) PD2=PD
0019      10 CONTINUE
0020      AFNL1+J)=PD1+PD2
0021      20 CONTINUE
0022      RETURN
0023
0024      END

```

FORTAN IV G LEVEL 21

VDF

PAGE 0001

0001 C SUBROUTINE VDF(GAMM)

C COMPUTE VORTEX DISTRIBUTION ON FIN

```
0002      C      DIMENSION GAMM(95)
0003      C      DIMENSION XB(56)
0004      C      COMMON /ARI/AR(56,56)
0005      C      COMMON /C1/XB
0006      C      COMMON /P4/NO
0007      C      CALL DINVAR(XB,NO)
0008      DO 10 I=1,NO
0009      10 GAMM(I)=XB(I)
0010      RETURN
0011      END
```

FORTRAN IV G LEVEL 21

BCF

DATE = 76114

PAGE 0001

0001 SUBROUTINE BCF(XR,N3)

C COMPUTE BOUNDARY CONDITION ON FIN

```
0002      DIMENSION XB(56),XW(56),AL(56)
0003      COMMON /BY2/XBW(55)
0004      COMMON /C3/XN
0005      COMMON /NAME/IRPT
0006      COMMON /P3/ALFAF
0007      COMMON /PS/P1
0008      COMMON /P6/BETA
0009      COMMON /BY3/JRAD
0010      COMMON /BL3/NW
0011      COMMON /FL4/AFLAP
0012      DU 5 1=1,3
0013      IF(1.GT.NW) GO TO 2
0014      AL(1)=ALFAF*P/180.
0015      GU TU 5
0016      2 AL(1)=AFLAP*P/180.
0017      3 CONTINUE
0018      DO 10 I1=1,N3
0019      IF(IRPT.EQ.1) XW(I1)=0.
0020      IF(JRAD.EQ.0) XBW(I1)=0.
0021      XBW(I1)=BETA(AL(I1))*XBW(I1)-XW(I1)
0022      10 CONTINUE
0023      RETURN
0024      END
```

FORTRAN IV C LEVEL 21
 DINV
 SUBROUTINE DINVID.E.N
 C
 DIMENSION D(56,56),E(56),XL(56,56)
 NX=N+1
 DO 1 I=1,NX
 DO 1 J=1,NX
 XL(I,J)=U.
 XL(I,I)=1.
 1 CONTINUE
 DO 2 I=1,N
 IX=I+1
 XL(I,IX)=D(I,I).
 2 CONTINUE
 XL(2,1)=D(2,1)/XL(1,2)
 DO 3 J=2,N
 J1=J-1
 DO 4 K=J,N
 A=U.
 KA=K+1
 DO 3 I=1,J1
 A=A+XL(I,J1)*XL(I,KX)
 3 CONTINUE
 XL(J,KX)=D(J,K)-A
 4 CONTINUE
 J2=J+1
 IF (-J2-N) 8,8,9
 8 XL(J2,1)=D(J2,1)/XL(1,2)
 DO 6 K=2,J
 K1=K-1
 A=0.
 DO 5 I=1,K1
 A=A+XL(I,J2,1)*XL(I,K+1)
 5 CONTINUE
 XL(J2,K1)=(D(J2,K)-A)/XL(K,K+1)
 6 CONTINUE
 7 CONTINUE
 9 CONTINUE
 DO 15 I=1,N
 IF (ABS(XL(I,I+1))>E*0.000001) GO TO 15
 WRITE(6,100)
 CALL EXIT
 15 CONTINUE
 100 FORMAT("//3X,22HILL-CONDITIONED MATRIX//")
 DO 10 I=2,N
 I1=I-1
 A=U.
 DO 11 J=1,I1
 A=A+XL(I,J)*E(J)
 11 CONTINUE
 E(I,I)=A
 10 CONTINUE
 XL(N,N)=E(N)/XL(M,N+1)

DATE = 76114

PAGE 0001

10/33/50

FORTRAN IV G LEVEL

DATE # 76114

PAGE 0002

DINV

```
      N1=N-1
  0052  DO 13 I=1,N1
  0053    I1=N-I+1
  0054    L=N-I
  0055    A=0.
  0056    DO 12 J=1,I,N
  0057      A=A+XL(I,J)*JXL(INK,J)
  0058  12 CONTINUE
  0059    XL(I,N-L)=(I1(L)-A)/XL(I,L+1)
  0060
  0061  13 CONTINUE
  0062    DO 16 I=1,N
  0063      L1=XL(INK,I)
  0064    16 CONTINUE
  0065    RETURN
  0066  END
```

o
Reproduced from
best available copy.

FORTRAN IV G LEVEL 21

PDB

PAGE 0001

10/33/50

DATE = 76114

0001 SUBROUTINE PDB(XCP)

 C COMPUTE PRESSURE DISTRIBUTION ON FIN

```
      C
      0002      DIMENSION XCP(55)
      0003      LIMNSION GAMM(55)
      0004      COMMON /B6/XDV(55)
      0005      COMMON /P6/BETA
      0006      COMMON /P7/SPN
      0007      COMMON /P4/NO
      0008      COMMON /Q1/GAMM
      0009      DO 10 J=1,NO
      0010      XCP(J)=2.*SPN*GAMM(J)/BETA**2/XDV(J)
 10  CONTINUE
      RETURN
      END
```

PAGE 0001

DATE = 76114

10/31/80

FC - G LEVEL 21

SLD

0001 C SUBROUTINE SLD

C COMPUTE SPANNWISE LIFT DISTRIBUTION

C DIMENSION GAMM(55)

COMMON /B2/CLS1,CLS1B,CLSFB

COMMON /CHORD/CLLSS

COMMON /P2/M,"

COMMON /P6/DETA

COMMON /P7/SPN

COMMON /Q1/GAMM

COMMON /FL2/NT

A1=4 *SPN?BETA**2

DO 20 JC=1,M

SUMW=0.

SUMF=0.

DO 10 JJ=1,NT

JP=JC+(JJ-1)*N

IF (JJ.GT.N) GO TO 5

SUMW=SUMW+GAMM(JP)

GO TO 10

5 SUMF=SUMF+GAMM(JP)

10 CONTINUE

CLSW(JC)=A1+SUMW/CLL(JC)

CLSF(JC)=A1+SUMF/CLL(JC)

CLSI(JC)=CLSW(JC)+CLSF(JC)

20 CONTINUE

RETURN

END

PAGE 0001

DATE = 76114 10/23/50

FORTRAN IV G LEVEL 21

0001 SUBROUTINE XLF(CL)

```
C COMPUTE LIFT COEFFICIENT OF FIN
C
DIMENSION XCP(55)
COMMON /B3/PSA(55)
COMMON /P6/BETA
COMMON /U2/RFAREA,XMAX
COMMON /P4/NU
COMMON /Q2/ XCP
SUM1=0.0
DO 10 JX=1,NO
  SUM1=SUM1+PSA(JX)*XCP(JX)
  CL=SUM1/BETA/RFAREA
  RETURN
END
10
0002
0003
0004
0005
0006
0007
0008
0009
0010
0011
0012
0013
```

FORTRAN IV LEVEL 21

DATE 8/76

SAGE 8881

SUBROUTINE PMSICH

COMPUTE SPANNISH DOCUMENT DISTRIBUTION

```

C
0002 DIMENSION CMS(110)
0003 DIMENSION GAM(55)
0004 DIMENSION XREF(10)
0005 COMMON /CHURD/CLL(55)
0006 COMMON /T6/XV(55),YV(55),ZV(55),WH(55),TLMD(55)
0007 COMMON /P2/M,N
0008 COMMON /FL2/NT
0009 COMMON /P6/BETA
0010 COMMON /P7/SPN
0011 COMMON /U1/GAMM
0012 COMMON /R3/XREF
0013 COMMON /U2/RFAREA,XAX
0014 DO 10 JC=1,M
0015 SUM=0.
0016 DO 5 JU=1,NT
0017   JP=JC+(JU-1)*M
0018   SUM=SUM+GAMM(JP)*(XREF(JC)-XV(JP))
0019 10 CMS(JC)=-4.*SPN*SUM/CLL(JC)/XAX/BETA**2
0020 END

```

FORTRAN IV C LEVEL 21

PAGE 0001

10/33/50

VLNB

SUBROUTINE VLNB

```
C      DIMENSION GAM(155)
C      COMMON /CS/VBDY(72)
C      COMMON /C6/VN(72)
C      COMMON /C9/VT(72)
C      COMMON /T4/T5(72)
C      COMMON /QB/ABU(72,55),ABV(72,55)
C      COMMON /B2/NUB
C      COMMON /P4/NO
C      COMMON /Q1/GAMM
C      DO 20 J=1,NUB
C      SUM1=0.
C      SUM2=J.
C      SUM3=0.
C      DO 10 J=1,NO
C      SUM1=SUM1+ABU(I,J)*GAMM(J)
C      SUM2=SUM2+ABV(I,J)*GAMM(J)
C      SUM3=SUM3+ABn(I,J)*GAMM(J)
C 10  CONTINUE
C      UBDY(I)=SUM1
C      VBDY=SUM2
C      NBDY=SUM3
C      SNS=SIN(VT(I))
C      CS=COS(VT(I))
C      VT(I)=VBDY*SNS+WBDY*CSS
C      VT(I)=VBDY*CSS-WBDY*SNS
C 20  CONTINUE
C      RETURN
C      END
```


FORTRAN IV G LEVEL 21

BPD

PAGE 0001

0001 SUBROUTINE BPD

C

C BULY PRESSURE DISTRIBUTION

```
0002 COMMON /AR2/A0(172,72)
C003  C7/UL(172)
C004  A2/CPB(172)
C005  CS/UBDY(172)
C006  COMMU /B2/NUB
C007  COMMU /P6/HETA
DO 20 I=1,NUB
C008  SUM=0.
C009
C010 DO 10 J=1,NUB
      SUM=SUM+AQ(I,J)*QL(J)
10 CONTINUE
C012  CP9(I)=2.*UBDY(I)+SUM)/BETA**2
C013
C014
C015  RETURN
C016  END
```

FORTRAN IV G LEVEL 21

BLD

PAGE 0001

DATE = 76114

10/13/50

0001 C SUBROUTINE BLD(BCL)

C BODY LIFT DISTRIBUTION

```
0002      DIMENSION BCL(36)
0003      COMMON /A2/CPB(172)
0004      COMMON /B1/NB,MN
0005      COMMON /D2/M1
0006      DU 50 K1=1,NB
0007      DO 40 I1=1,M1
0008      BCL(I1(K1-1)+M1+I1)=CPB((MN+K1-I1+1)*NB+I1)
0009      40 CONTINUE
0010      50 CONTINUE
0011      RETURN
0012      END
```

FORTRAN IV 61/EVEI 21

DATE - 2000

卷二

200

THE JOURNAL OF CLIMATE

四

```

0001      SUBROUTINE HSLD
0002      C BODY SPANWISE LIFT DISTRIBUTION
0003      DIMENSION BCL(36)
0004      COMMON /W3/CLBS(5)
0005      COMMON /B4/HREF(5)
0006      COMMON /W1/DX(96)
0007      COMMON /D1/UCL
0008      COMMON /D2/M1
0009      COMMON /B1/MB,NB
0010      DU 20  J=1,M1
0011      SUM=0.
0012      I=JJ+(KK-1)*M1
0013      SUM=SUM+BCL(I)*DX(I)
0014      CONTINUE
0015      CLBS(I,JJ)=SUM/BREF(I,JJ)
0016      CONTINUE
0017      RETURN
0018      END

```

FORTRAN IV G LEVEL 21
0001 SUBROUTINE WBS(XW,N1,N2)

PAGE 0001

DATE = 76114
10/33/50

C

C VELOCITY ON FIN INDUCED BY BODY SOURCE

C

0002 DIMENSION XW(16)

0003 COMMON /C7/QL(72)

0004 COMMON /AK6/AFN(172+65)

0005 DO 20 J=1,N2

0006 SUM=0.

0007 DO 10 I=1,N1

0008 SUM=SUM+AFN(I,J)*QL(I)

0009 10 CONTINUE

0010 XW(J)=SUM

0011 20 CONTINUE

0012 RETURN

0013 END

FORTRAN IV G LEVEL 21

XLIFT

PAGE 0001

0001 C SUBROUTINE XLIFT

C LIFT COEFFICIENT OF FIN-BODY COMBINATION

```
      0002      COMMON /W2/CL(15),CLSW(15),CLSF(15)
      0003      COMMON /CHORD/CLL(55)
      0004      COMMON /U1/Y1(11)
      0005      COMMON /W3/CLBS(15)
      0006      COMMON /B4/BHEF(15)
      0007      COMMON /W4/CLWING,CLFIN,CLBODY,TOTCL
      0008      COMMON /D2/N1
      0009      COMMON /N2/M,N
      0010      COMMON /U3/DT
      0011      COMMON /U2/RFAREA,XAX
      0012      COMMON /A1/RAD1
      0013      SUMIN=0.
      0014      SUMF=0.
      0015      DO 5 JF=1,N
      0016      WD=YF(JF+1)-YF(JF)
      0017      SUMW=SUMIN+CLSW(JF)*CLL(JF)*WD
      0018      5 SUMF=SUMF+CLSF(JF)*CLL(JF)*WD
      0019      CLWING=SUMW/RFAREA
      0020      CLFIN=SUMF/RFAREA
      0021      SUMB=0.
      0022      DO 10 JB=1,M1
      0023      10 SUMB=SUMB+CLBS(JB)*BREF(JB)*COS(DT*TJB-0.57)
      0024      CLBODY=DT*RADI*SUMB/RFAREA
      0025      TOTCL=CLWING+CLFIN+CLBODY
      0026      RETURN
      0027      END
```